Safe exploration of an aerodynamic field by a mini drone

Gabriele Perozzi

N° d'ordre : 362

CENTRALE LILLE

THESE

Présentée en vue
d'obtenir le grade de

DOCTEUR

En

Spécialité: Automatique, Génie Informatique, Traitement du Signal et Image

PAR

Gabriele PEROZZI

DOCTORAT DELIVRE PAR CENTRALE LILLE

Titre de la thèse :

"Exploration sécurisée d'un champ aérodynamique par un mini drone"

"Safe exploration of an aerodynamic field by a mini drone"

Soutenu le 13 Novembre 2018 devant le jury d'examen :

Rapporteur:	Clara-Mihaela IONESCU, Professor, Ghent University.
Rapporteur:	Franck PLESTAN, Professor, EC-IRCCyN Nantes.
Président:	Jean-Pierre BARBOT, Professor, ENSEA University.
Directeur de thèse:	Denis EFIMOV, Researcher HDR, Inria - Lille.
Co-Directeur de thèse:	Jean-Marc BIANNIC, Professor, ONERA - Toulouse.
Encadrant ONERA:	Laurent PLANCKAERT, Engineer, ONERA - Lille.

Thèse préparée dans les laboratoires:

- ONERA: The French Aerospace Lab.
- Ecole Doctorale SPI 072 (Lille I, Lille III, Artois, ULCO, UVHC, Centrale Lille).

Région Hauts-de-France

Dedicated

to both my parents,

the most important people in my life.

Funding, acknowledgments and personal notes

Funding

This scientific research was possible thanks to the Région Hauts-de-France and to ONERA: The French Aerospace Lab, that have contributed equally to fund my studies. Without these funds, I could never have enrolled for my PhD course.

Acknowledgments and personal notes on the research activity

I want to use this small section to thank the people that helped me, to give the right acknowledgments, and to describe my PhD experience. I want to start with Denis at Inria-Lille (Non-A team). I was very lucky to have had a wonderful PhD supervisor like him. He was my main mentor for all the three years, being a very respectful person and teacher and, as his student, my main focus was to try to reach his level. This personal target helped me to win two awards for the best student paper in one European conference and for the creativity prize at "Fédération de Recherche CNRS Transports Terrestres & Mobilité" 2018. In particular, I still remember the days when I could go the late evening to Inria to meet him. He was always ready to wait me in his office while other his colleagues were already at home. He also helped me to get one position as teaching assistant at the ISEN University. Then, I want to thank my PhD co-supervisor Jean-Marc Biannic at ONERA-Toulouse. I spent in Toulouse only 4 days, and in these days he was always very kind and able to find my weaknesses, checking my difficulties, and to explain me very clearly the control methodology. He was also available to help me in finding solutions to technical problems on my research by phone and by email during my permanence at Lille. It is a pity that I couldn't finish his part because of lack of time. My other acknowledgments go to Jean-Pierre Richard at Inria. He helped me to get one position as teaching assistant at University of Lille 1. Then, I want to thank Gang Zheng at Inria. More than three years ago he was so kind to inform me about this PhD position with Denis. He shared with me this position without any obligation, and I appreciate very much this fact. Then, there is Corinne Jamroz. She was the team assistant at Inria, a very gentle and efficient person. Definitely, she was the perfect team assistant that any researcher can desire. She was always ready to solve any kind of problem, by the Inria side. Then, there is all the Non-A team at Inria. I found a very friendly environment, full of young researchers and students. It is a perfect place to feel at home and be always motivated. The Non-A team was full of people with whom I could always spend nice time eating and speaking together, but there was the time for fun and the time for hard work and I absolutely loved this attitude. My regret is that I didn't have the possibility to spend more time together with them taking part in the numerous days dedicated to group activities. I have met a perfect and wonderful place where I always was free to study for my project, to check the articles in literature thanks to the numerous international journal subscriptions, and to propose new ideas for the controllers. It was a vibrant and dynamic working environment, where it was possible to establish many external contacts, in particular I met the Professor Leonid Fridman from Mexico, a wonderful person who was ready to study with me new advanced nonlinear algorithms and apply them in drones. I recognize that I still have very much to learn in control theory but the time that I spent at Inria has contributed very much to my personal and professional growth. Last but not least, there are my parents. They were always by my side when I encountered any problem during my PhD.

In conclusion, I managed to finish my PhD especially thanks to my supervisor Denis, who helped me very much. I am happy because I have successfully finished my PhD. However, I am also very sad because I have to leave the Non-A team at Inria and I have to leave my supervisor Denis in order to expand my professional network. For my future, I hope to gain more experiences in different research labs expanding my knowledge, which has been always

my biggest aspiration, and to become a Researcher at the same level of my supervisor Denis to whom I will be eternally grateful.

Résumé Général long (in french)

Contexte

Au cours des dernières décennies, les petits véhicules aériens sans pilote, tant pour des applications militaires que commerciales, ont suscité un intérêt croissant en raison de leur coût réduit, de leur taille qui leur permet de fonctionner plus près des points d'intérêt et de leur relative discrétion acoustique. Les avantages incluent la possibilité de rester en vol stationnaire, de voler à haute et basse vitesse, de se déplacer dans toutes les directions et de décoller et atterrir verticalement. Les quadricoptères sont particulièrement utiles dans les zones urbaines ou à proximité des bâtiments, dans les zones dangereuses, pour des missions de sauvetage lors de catastrophes naturelles telles que les tremblements de terre. Ces machines doivent souvent se déplacer dans des environnements inconnus en termes de géographie et de conditions aérologiques. De plus, la faible masse de ces engins (comparée aux forces générées par les perturbations de l'air) réduit considérablement le domaine du vol stable. Des contraintes supplémentaires concernant la vitesse du vent doivent donc être prises en compte dans la conception des lois de commande. Des études ont prouvé que les estimations de la vitesse et de la direction du vent basées sur des mesures effectuées à l'aide des sondes Pitot et d'un système de navigation par satellite (GPS), montés sur des drones de type avion, peuvent approcher les caractéristiques réelles du vent. Cependant, pour les quadricoptères, les problèmes principaux restent la limitation de la charge utile et l'interaction avec le flux d'air généré par les rotors. Ainsi, si les quadricoptères doivent fonctionner dans des environnements urbains, dans des flux d'air turbulents pour lesquels une prévision précise est impossible a priori avec des ressources embarquées limitées, l'accent doit être mis sur des modèles aérodynamiques détaillés, des algorithmes d'estimation et des lois de contrôle avancées.

Motivation de la thèse

Cette thèse s'inscrit dans le cadre du projet "Petits drones dans le vent" porté par le centre ONERA de Lille. Ce projet vise à utiliser le drone comme "capteur du vent" et une prédiction du champ de vent pour gérer un UAV dans des conditions aérologiques perturbées. Grâce à l'estimation temps réel du vent à bord il deviendrait possible de mettre à jour une cartographie du vent et le quadricoptère pourrait planifier une trajectoire évitant les zones dangereuses. Les résultats de la thèse, qui consistent à trouver une estimation instantanée du vent tout en assurant un comportement du drone en vol acceptable, seront fusionnés avec une autre étude portant sur la prévision des champs de vent et la planification des trajectoires. Un problème clé pour parvenir à ces résultats est de trouver un modèle de quadricoptère suffisamment représentatif pour construire un bon capteur de vent et ensuite adapter les gains de contrôle afin de garantir performances et robustesse. Ces travaux de recherche s'inscrivent donc dans un cadre pluridisciplinaire, associant l'aérodynamique, la théorie du contrôle et la théorie de l'estimation. La partie contrôle porte principalement son attention sur le contrôleur par mode glissant (SMC), dont les propriétés de robustesse aux incertitudes paramétriques et aux perturbations ont été démontrées pour une large classe de systèmes non linéaires. Dans la partie estimation on s'intéresse à la conception d'estimateurs du vent en temps fini par rapport au bruit des capteurs et aux incertitudes affectant les coefficients aérodynamiques identifiés. Cette thèse est le résultat d'une collaboration entre l'Inria, pour la conception des algorithmes de contrôle non linéaire et d'estimation, et l'ONERA, pour la modélisation et la validation expérimentale sur un quadricoptère. Par conséquent, les principales contributions de cette recherche comprennent:

- Plusieurs méthodes de contrôles non linéaire pour stabiliser un quadricoptère et suivre un chemin en présence

d'incertitude sur le vent en tenant compte d'un modèle de mécanique du vol détaillé du drone;

- Des algorithmes d'estimation de la vitesse du vent basés sur un modèle aérodynamique représentatif d'un quadricoptère réaliste;
- Des contrôleurs qui utilisent les estimations obtenues de la vitesse du vent afin d'ajuster les gains de lois de contrôle en fournissant un effort de contrôle raisonnable sur les rotors;
- Une étude basée sur la simulation des performances et de la robustesse des solutions de contrôle et d'estimation proposées (une boîte à outil a été conçue);
- Une validation expérimentale partielle de ces résultats au laboratoire de vol de l'ONERA-Lille.

Résultats de la thèse

Les résultats de la thèse peuvent être résumés comme suit:

- Afin de mieux représenter l'impact du champ de vent sur les mini-drones, les coefficients aérodynamiques sont calculés en utilisant la théorie des moments des éléments de pale pour les hélicoptères en prenant en compte l'influence du vent. Ensuite, le modèle dynamique complet du quadricoptère est présenté, à partir des expressions des forces et moments externes et en considérant les coefficients aérodynamiques. Les équations résultantes sont fortement non linéaires et leur application directe pour la synthèse des algorithmes de contrôle et d'estimation est délicate. Pour surmonter ce problème, certaines simplifications acceptables sont utilisées, basées sur des tests. Les équations d'état globales décrivant l'action des commandes et l'influence du vent sur le quadricoptère sont finalement établies. Cette représentation d'état servira de base aux développements des algorithmes de contrôle et d'estimation.
- Après la modélisation du quadricoptère, la thèse met l'accent sur la conception d'algorithmes de régulation et l'étude des propriétés de robustesse du système rebouclé sur des lois "SMC" utilisant la vitesse du vent comme entrée. Les limites supérieures des perturbations induites par le vent sont caractérisées, ce qui permet d'appliquer une technique SMC avec des propriétés de convergence garanties. La particularité du cas considéré est que les limites supérieures de la perturbation dépendent de l'amplitude de contrôle d'une manière non linéaire, ce qui conduit à une nouvelle procédure pour la synthèse des lois de commande. Ensuite, l'analyse et la réduction du phénomène de battement haute fréquence au voisinage de la surface de glissement (chattering effect), ainsi que l'étude des problèmes induits par la dynamique du rotor sont étudiés. Deux SMC à gains variables sont proposés, utilisant des conceptions de premier ordre et quasi-continu. Les résultats montrent que le contrôle quasi-continu présente un niveau de performance supérieur.
- On s'intéresse ensuite aux algorithmes d'estimation du vent. Plusieurs estimateurs de la vitesse du vent sont proposés et analysés du point de vue de la précision obtenue. Une décomposition auxiliaire des équations dynamiques est effectuée dans des termes connus et inconnus à estimer. Trois algorithmes d'estimation de paramètres variant dans le temps sont introduits, comparés et finalement fusionnés. Cette méthodologie tire profit d'un modèle de dynamique de vol UAV détaillé, utilisant des coefficients aérodynamiques non linéaires identifiés. Les résultats montrent que les algorithmes rejettent efficacement le bruit du capteur, mais sont fortement influencés par les incertitudes de modèle découlant du processus d'identification. Les algorithmes d'estimation sont moins précis sur la dynamique verticale en utilisant le modèle quadricoptère non linéaire complet.

- En addition, une boîte à outils, qui consiste en un groupe de bibliothèques Simulink pour simuler un quadricoptère en présence de vent, a été conçue pour effectuer des simulations préliminaires et valider les algorithmes SMC et d'estimation étudiés avant de réaliser des expériences en laboratoire.

Problèmes ouverts

D'autres études peuvent être menées pour améliorer les résultats de cette thèse:

- En ce qui concerne la partie du modèle de quadricoptère, la formulation du modèle peut encore être améliorée en ajoutant des termes négligés liés à des phénomènes physiques pour lesquels il n'existe pas encore de formulation adéquate. En particulier pendant le vol, il existe des influences aérodynamiques entre les rotors avant et arrière, et entre le corps et les rotors. De plus, les quatre moteurs entraînant les quatre rotors présentent des différences liés au processus de production. Les composants mécaniques et électriques ne sont jamais rigoureusement identiques d'une production à l'autre, même avec des spécifications similaires. Ces études supplémentaires pourraient améliorer l'estimation du vent.

- En ce qui concerne la partie commande, le SMC peut encore être améliorée. La conception SMC quasi-continu permet d'appliquer des simplifications sur les limites supérieures des perturbations. Certaines constantes sont sélectionnées pour être supérieures aux dérivées des perturbations, produisant une surestimation des gains. Sur le plan analytique, il n'est pas possible de calculer exactement les limites supérieures, mais des identifications supplémentaires peuvent résoudre ce problème. Les algorithmes SMC à gain variable sont conçus en utilisant un modèle de traînée qui relie la perturbation aérodynamique à la vitesse du vent. Puisque le but de cette recherche est de trouver une estimation fiable du vent, le contrôleur a été conçu pour prendre en compte directement la vitesse du vent. Cependant, un axe d'amélioration de la robustesse du SMC consisterait à considérer comme entrée une estimation de la perturbation liée au vent plutôt que la vitesse du vent. D'autres améliorations consisteraient à optimiser la dynamique du mode glissant en tenant compte des contraintes de performance, ainsi que de produire un maillage de tous les paramètres, trajectoires, profils de vent et d'optimiser directement un ensemble de gains plutôt que de procéder à des réglages séparés comme c'est actuellement le cas.

- Le contrôleur H_∞, introduit en annexe, constitue une alternative aux stratégies non linéaires "SMC" mises en œuvre dans cette thèse. Faute de temps, cette stratégie n'a pas pu être implémentée. L'idée est de démarrer avec une solution classique, fournie par un contrôleur PID déjà existant et fonctionnant en régime nominal. Plus précisément, on reprend la synthèse des gains PID avec une technique H_∞ structurée, en analysant les fonctions de transfert obtenues par le contrôleur initial pour déduire les fonctions de pondération. Ensuite, la flexibilité du cadre de synthèse H_∞ peut être utilisée pour améliorer les propriétés de la solution de base.

- En ce qui concerne la partie "estimation du vent", les algorithmes peuvent être améliorés en évitant les simplifications supplémentaires au niveau de la dynamique de rotation du quadricoptère. Les résultats obtenus avec un modèle non linéaire complet de quadricoptère montrent que l'estimation est précise selon les axes x, y, mais beaucoup moins selon l'axe z. Pour cette raison, un processus d'identification supplémentaire peut être effectué pour améliorer les performances des algorithmes.

Contents

List of Symbols

Roman Symbols

A	m^2	Rotor area
a	$-$	Lift curve slope of the blade section
a_0, a_1, b_1	$-$	Coefficients of the blade flapping equation
b	$-$	Time constant of the rotors transfer function
C_{Di}	$-$	Induced drag coefficient of the blade section
C_{D0}	$-$	Drag coefficient of the blade section
C_H	$-$	Hub force coefficient
c_j, s_j	$-$	Cosines and Sines of the angles in the quadrotor configuration
C_Q	$-$	Rotor drag moment coefficient
C_{Rm}	$-$	Rotor rolling moment coefficient
C_T	$-$	Thrust coefficient
C_x, C_y, C_z, C_ϕ, C_θ, C_ψ	$-$	Coefficients proportional to conventional sliding mode controllers
D_x, D_y, D_z	m/s^2	Maximum wind speeds
d_x, d_y, d_z	$-$	Computed disturbance for the quadrotor in body frame
d_{xe}, d_{ye}, d_{ze}	$-$	Computed disturbance for the quadrotor in earth frame
d_ϕ, d_θ, d_ψ	$-$	Computed disturbance for the quadrotor around ϕ, , θ, ψ angles
F_{Xaero}, F_{Yaero}, F_{Zaero}	N	External aerodynamic forces acting on the quadrotor in body frame
F_{Xj}, F_{Yj}, F_{Zj}	N	External aerodynamic forces acting on each rotor
g	m/s^2	Gravity acceleration
h	m	Distance between rotors plane and the CoG of the quadrotor
$\mathbf{I}$	$kg.m^2$	Inertia matrix of the quadrotor
i_{rot}	A	Current in the electrical circuit of the rotor
I_{xx}, I_{yy}, I_{zz}	$kg.m^2$	Inertia of the quadrotor
l	m	Arm length of the quadrotor
j subscript	$-$	j^{th} rotor
J_{rot}	$kg.m^2$	Rotor moment of inertia
K_D	$-$	Identified coefficient for the quadrotor in C_H equation
K_z	$-$	Identified coefficient for the quadrotor in λ and C_T equations
L_{aero}, M_{aero}, N_{aero}	$N.m$	External aerodynamic moments acting on the quadrotor in body frame
L_j, M_j, N_j	$N.m$	Aerodynamic moments for each rotor
L_{rot}	H	Rotor inductance
m	kg	Mass of the quadrotor
p, q, r	deg/s	Angular velocities of the quadrotor
$\mathbf{R}$	$-$	Rotational Matrix
R	m	Rotor radius
R_{rot}	Ohm	Rotor internal resistance
stat subscript	$-$	In stationary flight (hover operating point)
u, v, w	m/s	Linear velocities of the quadrotor in body frame
u_j, v_j, w_j	m/s	Linear velocities of each rotor in body frame

u_w, v_w, w_w	m/s	Wind velocities with respect to the earth and in body frame
U_x, U_y, U_z, U_ϕ, U_θ, U_ψ	N; $N.m$	Control inputs
x, y, z	m	Position of the quadrotor in earth frame

Greek Symbols

α_x, α_y, α_z, α_ϕ, α_θ, α_ψ	–	Coefficients for the sliding surfaces
γ	–	Operating point limit of the quadrotor
γ_a, α_a	–	Parameters for wind estimator based on linear dynamics
γ_g, ℓ_g	–	Parameters for wind estimator based on angular dynamics
γ'_g, α'_g, ℓ'_g	–	Parameters for wind estimator based on angular dynamics under-the hypotheses of varying wind and sensor's noises
ε	deg	Angle for the quadrotor configuration
θ_{tw}	deg	Twist angle of the blades
θ_0	deg	Angle of attack of the root profile of the blades
λ	–	Inflow ratio
μ	–	Advance ratio
ξ_x, ξ_y, ξ_z, ξ_ϕ, ξ_θ, ξ_ψ	–	Coefficients in the first order SMC to avoid the chattering
ρ	kg/m^3	Air density
ϱ_x, ϱ_y, ϱ_z, ϱ_ϕ, ϱ_θ, ϱ_ψ	–	Coefficients in quasi-continuous SMC to avoid the chattering
σ	–	Rotor solidity ratio
τ_d	$N.m$	Rotor load
τ_r	$N.m$	Rotor torque
ϕ, θ, ψ	deg	Angles of the quadrotor
ω	rad/s	Rotor angular speed
Ω_r	deg/s	Propeller angular rate
ϖ_x, ϖ_y, ϖ_z, ϖ_ϕ, ϖ_θ, ϖ_ψ	–	Coefficients to compensate the upper bounds of the disturbances-that are not easy to compute analytically

List of Abbreviations

algorithm-lin	Wind estimation algorithm using linear quadrotor dynamics
algorithm-rot	Wind estimation algorithm using rotational quadrotor dynamics
algorithm-rot-2	Wind estimation algorithm using rotational quadrotor dynamics, wind derivative and- sensor's noise hypotheses
BEMT	Blade Element Momentum Theory
conv-SMC	Conventional Sliding Mode Control
GNSS	Global Navigation Satellite System
GPS	Global Position System
IMU	Inertial Measurement Unit
Inria	Institut National de Recherche en Informatique et en Automatique
ONERA	Office National d'Études et de Recherches Aérospatiales
PID	Proportional Integral Derivative
qc-SMC	Quasi-Continuous Sliding Mode Control (Designed in this Thesis)
SMC	Sliding Mode Control
UAV	Unmanned Aerial Vehicle
1-SMC	First Order Sliding Mode Control (Designed in this Thesis)

List of Figures

List of Tables

Chapter 1

Introduction

Contents

1.1 Context

In the last decades there has been a growing interest for small unmanned aerial vehicles (UAVs) both for military and commercial applications because of their reduced costs, their size which enables them to operate closer to point of interest and their relative acoustic discretion. Two conventional types, fixed-wing UAV and Vertical Takeoff and Landing (VTOL) UAV, are the most popular. Each type has its own limitations on flexibility, payload, flight range, cruising speed, takeoff and landing requirements and endurance. However, recently a new type of UAV is getting popularity and interests, named hybrid UAV [Saeed *et al.* 2018], that integrates the beneficial features of both conventional ones. Another VTOL type of aircraft with an important and significant potential is the Quadrotor [Shraim *et al.* 2018, Norouzi Ghazbi *et al.* 2016, Lee & Kim 2017], that is considered by most research studies as a very promising UAV. Advantages include the possibility to hover in a fixed position, to fly at high and low speeds, to move in any direction and to take off and land vertically. As a result, many surveys in disparate applications are coming out: remote control using brain computer interface [Nourmohammadi *et al.* 2018]; civil applications related to remote sensing, spraying of liquids, and logistics [González-Jorge *et al.* 2017]; network cooperation between unmanned aerial and aquatic vehicle [Sánchez-García *et al.* 2018]; combinations of aerial vehicles and manipulators [Bonyan Khamseh *et al.* 2018]; entertainment with the emerging technology of Augmented and Virtual Reality (AVR) [Kim *et al.* 2018]; vision based controls without human interaction [Kanellakis & Nikolakopoulos 2017]; formation control of multiple quadrotors [Hou *et al.* 2017].

Quadrotors are particularly useful in urban areas or nearby buildings and dangerous interiors, for rescue missions in natural calamities such as earthquakes [Nedjati *et al.* 2016, Michael *et al.* 2014, Qi *et al.* 2015]. Since these machines are often required to move in unfamiliar environments in terms of geography and in terms of

aerological conditions, many works can be found studying this issue: autonomous explorations for UAVs in unknown urban environment using on-board Inertial Measurement Unit (IMU) and Global Position System (GPS) sensors [Shim *et al.* 2005, Song *et al.* 2015]; how long the micro UAV can continue to follow a pre-calculated flight path in absence of GPS signals [Ireland & Anderson 2012], which can often happen in closed environments and nearby buildings; automatic detection and avoidance of obstacles using optical flow velocities [Eresen *et al.* 2012]; study of the dynamic response of a UAV operating in turbulent conditions in urban environment [Murray *et al.* 2014], which can cause dangerous sharp-edged wind gusts; autonomous position control for quadrotors in wind gusts generated by urban building [Raza & Etele 2016, Raza *et al.* 2017, Raza *et al.* 2018]; modeling of the urban wind gust environment and its application to autonomous flight [Galway *et al.* 2008]; wind field estimation and quadrotor flight in urban canopy layer [Ware & Roy 2016, Ware 2016]. In addition, the low mass of such units (comparing to the forces generated by the air disturbances) reduces significantly the domain of stable flight, then additional constraints, regarding the wind speed, have to be considered in the control design. Studies have proven that estimates of wind speed and wind direction based on measurements carried out using the Pitot tubes and Global Navigation Satellite System (GNSS) receivers, mounted on consumer-grade UAVs, may accurately approximate true wind parameters [Niedzielski *et al.* 2017]. However, for mini quadrotors the main issue is the limitation of the payload and interaction with the inflow of rotors. Thus, if the mini quadrotors must operate in urban environments, inside turbulent air flow patterns for which accurate prediction is not possible *a priori* with limited on-board resources, the focus must be on detailed aerodynamic models, estimation algorithms and sophisticated control laws.

1.2 Motivation of the thesis

Models with different grade of complexity are computed to be used in different problems. In particular, many control techniques are studied and applied to quadrotors, and many works are presented using the drone itself as forces, moments, and wind estimator with or without airflow sensors to reconstruct the wind field nearby physical objects and predict optimal and safe trajectories in urban environment. It is obvious that this topic has a key-role in the research on quadrotors nowadays. For this reason, ONERA started the project "Small drones in the wind" at Lille center, which aims to minimize the impact of the aerodynamics field on mini drone, adapting the behavior of the UAV in real time via guidance and optimal control laws using a prediction of the wind field. It means that using the real-time on-board wind estimation and adapting properly the control gains, the UAV can compute an optimal path planning and trajectory based on an existent geometric map of the environment and knowing the aerodynamic behavior of the airflow in the flight domain and updated by the UAV flow measurements, to smartly avoid dangerous areas, as in Fig.1.1.

This thesis is a part of the mentioned ONERA's project and it was possible thanks to a collaboration between Inria, for the design of the control and estimation algorithms, and ONERA, for the experimental validation on a quadrotor. The thesis result, which is to find an *instant* wind estimation and control, will be merged with another study dealing with wind field *prediction* and path planning. The main problem in the realization of such a research, is to find a representative enough quadrotor model, to build a good wind software sensor and then adapt the control gains avoiding their overestimation in order to have a robust system and keep good performances. As a consequence, this research has a multidisciplinary domain: the aerodynamics, the control theory, and the estimation theory. The control part mainly focuses its attention on sliding mode controller (SMC), which is an excellent control for nonlinear systems affected by incertitude and perturbations. Design of $\mathcal{H}_\infty$ regulator, which is a control that uses linearized systems, is also provided in the appendix. The estimation part must provide a finite-time wind estimates against the sensors' noise and the incertitude of the identified aerodynamic coefficients. The detailed state of the art descriptions

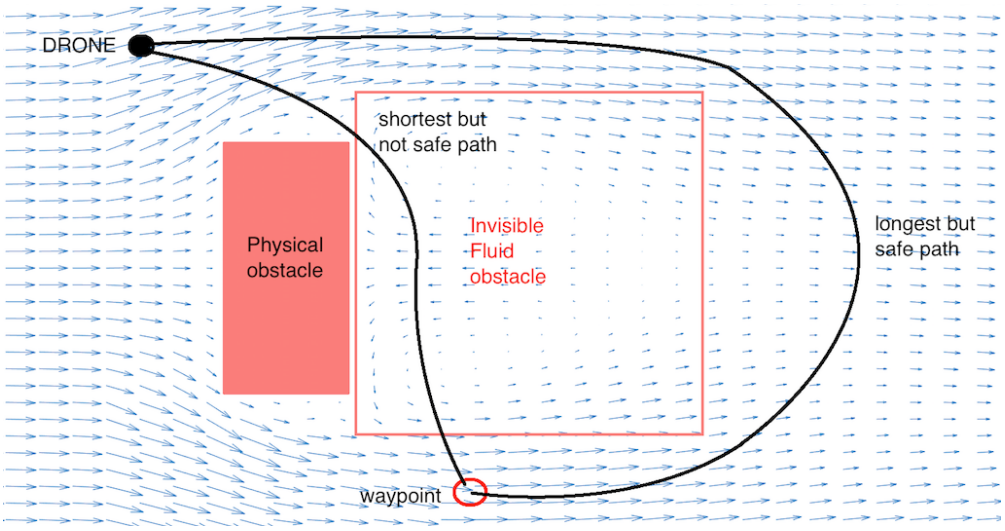

Figure 1.1: Example of an optimal longest but safe trajectory of the UAV close to the building and under wind perturbations.

of control and estimation tools for quadrotors, as well as the motivations for using the selected approaches, are given below in the corresponding chapters.

Therefore, the main contributions of the thesis include:

- Several new control methods for stabilization of a quadrotor and path following in the presence of wind by taking into account a detailed flight model of the drone;
- Three estimation algorithms of wind velocities based on a realistic model of a quadrotor;
- A combined regulator of a quadrotor that uses the obtained estimates of the wind speed in order to adjust the control gains providing a reasonable control effort on the rotors;
- Intensive simulation based investigation of performance and robustness of the proposed control and estimation solutions (a Simulink toolbox has been developed);
- Experimental validation of these results at ONERA lab.

1.3 Organization of the thesis

The chapter 2 is entirely devoted to the formulation of a quadrotor model. In order to better represent the impact of the wind field on mini drones, aerodynamic coefficients influenced by wind components, are computed in body frame using the blade element momentum theory (BEMT) for helicopters. Then, the whole dynamics model of the quadrotor is presented, finding the external equilibrium forces and moments and considering the nonlinear aerodynamic coefficients influenced by the wind velocity. Last, the quadrotor physical model is rewritten in the state-space form to show the influence of the control signals and of the wind velocities on the system state of the quadrotor. Using this state-space representation, control laws and estimation algorithms are computed in the next two chapters.

The chapter 3 deals with the design of regulation algorithms and the study of the system robustness property applying SMC having wind velocity as input. The upper bounds of wind-induced disturbances are characterized, which allow a SMC technique to be applied with guaranteed convergence properties. The peculiarity of the considered case is that the disturbance upper bounds depend on the control amplitude itself, which leads to a new procedure for the control tuning. Then the analysis and reduction of chattering effects, as well as investigation of rotor dynamics issues are studied. Initial study and design of $\mathcal{H}_\infty$ control have been also performed and presented in the appendix C.

The chapter 4 presents several estimators of wind velocity and a study about the wind estimates precision. Three time-varying parameter estimation algorithms are introduced, compared and finally merged. In this context, the interest for such algorithms is twofold. First, the need for an accurate real-time estimation of the wind is essential to improve the flight safety of small drones in a perturbing environment. Second, with the help of an accurate model, including nonlinearities, the proposed algorithms can be used to model the wind-field accurately, thus transforming the UAV into a wind sensor. To this end, first, a quadrotor flight dynamics model is given, which takes into account wind influence. Second, an auxiliary decomposition of dynamical equations is performed in known and unknown terms to be estimated, and several estimation schemes are proposed. An algorithm for fusion of these estimates is also computed. This methodology takes the advantage of a detailed UAV flight dynamics model, using identified nonlinear aerodynamic coefficients.

The chapter 5 presents simulations and partial experiments and it is organized as follows. First, the identification process of the aerodynamic coefficients is explained and the Parrot and X4-MaG quadrotors parameters are provided. Second, wind estimation algorithms are studied enlightening the influence of the aerodynamic coefficients incertitude, the influence of the sensors' noise and the influence of the characteristics of the wind profile. Then, simulations regarding the designed SMCs robustness against the model incertitude and the influence of the varying wind velocity are shown, and practical ideas are given on how to tune the SMC gains with some example experiments, in comparison with PID control results, to prepare the experiment in free flight. Last, the coupling between SMC and wind estimation is illustrated, showing the pros in having a wind estimates as input to the controller to mitigate the control effort on the rotors.

1.4 Used Materials

The production of this thesis has involved complementary study and practice in the following utilities.

1.4.1 Software

- Matlab (Matrix Laboratory), produced by MathWorks Inc.
- Simulink, produced by MathWorks Inc.
- RT-MaG (Real-Time Marseille Grenoble) open-source toolbox, extensively explained in [Manecy *et al.* 2014, Gipsa-Lab & of Mouvement-Sciences], can be used to directly design Linux-based real-time applications for Computer-On-Module (COM) using Matlab/Simulink software. Via Matlab and Simulink, RT-MaG provides a high-level of abstraction user interface making it possible to design robotic applications and giving access to classical robotic communication interfaces.
- Motive, produced by OptiTrack, is a 6 degrees of freedom tracker software for objects that characterizes the user's interface to communicate with Optitrack cams.

- NatNet SDK (Software Development Kit), produced by OptiTrack, is a kit for the communications between the software Motive and an existent application (e.g: Matlab) for real-time streaming, providing the necessary libraries.

1.4.2 Hardware

ONERA changed the drone during the PhD, for this reason two quadrotors are used and they are described below.

- Commercial Parrot Ar. Drone 2.0 (see Fig. 1.2(b)), produced by Parrot, is the drone used to identify the aerodynamic model studied in this thesis (experiments are carried out on this drone to estimate the aerodynamic coefficients and to build the quadrotor model). The control laws, the wind estimation algorithms, and the CW-Quad Toolbox (see Appendix D) are built and initially simulated respecting the constraints imposed by the identification of this quadrotor model. This drone is the first one used in the project to prove the applicability of the approaches proposed in this thesis to realistic UAV.

- X4-MaG drone (see Fig. 1.2(a)), introduced in [Manecy *et al.* 2015], is an open-hardware quadrotor platform, developed jointly by the ISM laboratory (Marseille, France) and the Gipsa-Lab (Grenoble, France), for academic and research applications. The drone is a small and low-cost open quadrotor which offers two levels of controllers providing a manual mode and an automatic mode thanks to Linux-based controller embedded on-board. The robot is equipped with a low-level autopilot based on a micro controller with its 6-axis IMU (NanoWii) and a high-level autopilot based on a Linux-based Computer-On-Module (Gumstix COM), which can be programmed directly via Simulink. The X4-MaG quadrotor is equipped with three different electronic boards: The NanoWii stabilizes the platform in the manual mode and sends sensors values to the high-level controller in the automatic mode. A Rotor Controller Board (RCB) controls in closed-loop the rotational speed of each propeller. A Gumstix Overo AirSTORM COM is the high level controller programmed via the RT-MaG toolbox. This drone is the final one used in the project.

- 4 OptiTrack cameras, produced by OptiTrack, are chosen, and they are 2 "Prime 13" and 2 "Prime 13W".

- Ground station using Simulink based monitoring.

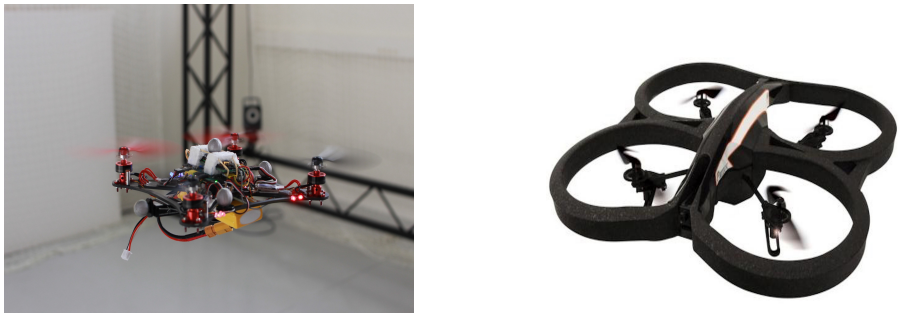

(a) (b)

Figure 1.2: Images of the: X4-MaG drone (a); Parrot Ar.Drone 2.0 (b)

1.4.3 Experimental setup

To carry out the experiments, it was possible to build and test a new experimental setup for drones at the B20 lab (see Fig. 1.3(b)) in the last month of this research, and it is composed by:

- Drone: The vehicle, which is used to perform experiments;
- Cams: The cameras track the position and the attitude of the quadrotor;
- Hub 1: This hub gathers the info from the cameras;
- PC server: The PC server, running Motive software, gets the info about the position, the attitude of the quadrotor and the cameras frames;
- Hub 2: This hub makes possible the communication between the PC running the tracking software (Motive), to the PC running the Simulink user interface;
- PC client: The ground station, running the Matlab/Simulink and the toolbox user interface, is used to check the quadrotor attitude, position and control, flying mode in case of emergency and transmit reference trajectory.
- Wi-Fi sender: The requested position, attitude and rotor velocities, imposed by the user or by the control law, are sent to the quadrotor;
- Wired connections: Wired connections with cables are represented by non-dashed arrows;
- Wireless connections: Wireless connections are present between the PC client and the quadrotor and between the quadrotor and the cameras. They are represented by the dashed arrows.

A radio control based flying mode, to quickly address an emergency situation, and a safety mode in case of data link failure are also present.

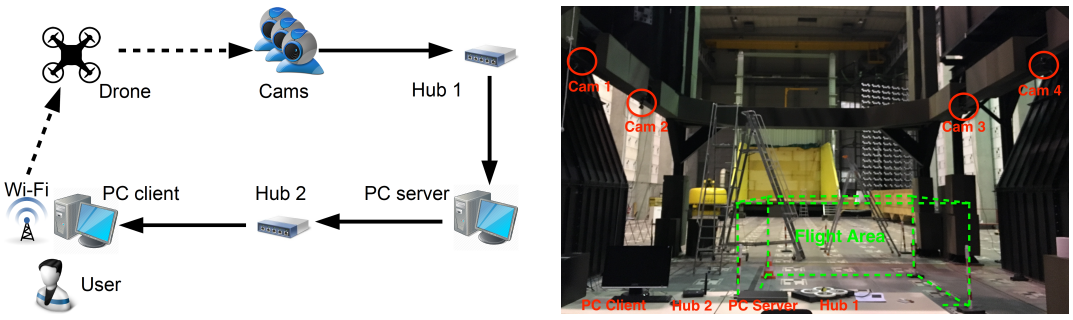

(a) (b)

Figure 1.3: Images of the: scheme of the experimental setup (a), experimental setup (b).

1.4.4 Facilities

The experiments are carried out at B20 lab and at L2 wind tunnel of ONERA-Lille center.

- The B20 Lab provides lateral and vertical wind gust generators to simulate the artificial wind. Gusts with sharp edges and with various amplitudes and shapes can be created, taking advantage of the possibility to parameterize the profile and the intensity of wind gusts generated along the flight (see Fig. 1.4(c)).
  - Lateral wind gust generator: The lateral wind gusts generator (see Fig. 1.4(a)) has the following characteristics: 6 m width of the airflow tube (y axis). 4.8 m max length of the airflow tube (x axis). 3.5 m height of the airflow tube (z axis). 5 m/s max flow velocity.
  - Vertical wind gust generator: Generation of ascending or descending wind gusts is achieved by the vertical gust generator (see Fig. 1.4(b)), which has the following characteristics: 3.5 m width of the airflow tube of (y axis). 4.8 m max length of the airflow tube (x axis). 5.3 m height of the airflow tube (z axis). 5 m/s maximal flow velocity.

  The effective area for flight tests is 4.74 m height, 4 m length, 2 m depth.

- The L2 wind tunnel allows to work in the target area of flight for the X4-MaG drone speeds, which is around 5 m/s. A balance is mounted at the top of the sting, allowing to measure the forces and the torques acting on the quadrotor. This sensor, called "Balance Φ12 n.6", is provided by ONERA. It can measures forces in the range of ±355 N, ±355 N, ±226 N respectively in x, y, z directions, and torques of ±8.5 $N.m$, ±8.5 $N.m$, ±10.6 $N.m$ respectively around the x, y, z axes. The quadrotor is mounted on top of this balance. This apparatus allows to identify in safe condition aerodynamic coefficients and to study complex phenomena such as rotor interactions.

(a) (b) (c)

Figure 1.4: Images of the lateral wind gust generator (a), vertical wind gust generator (b) in the B20 lab; and of the produced wind profile over the passage of the drone (c).

1.5 List of productions during the PhD

Peer-reviewed journal articles

- G. Perozzi, D. Efimov, J-M. Biannic, L. Planckaert. "Trajectory tracking for a quadrotor under wind perturbations: sliding mode control with state-dependent gains". *Journal of The Franklin Institute*. Vol. 355, n. 12. August 2018. DOI: 10.1016/j.jfranklin.2018.04.042.

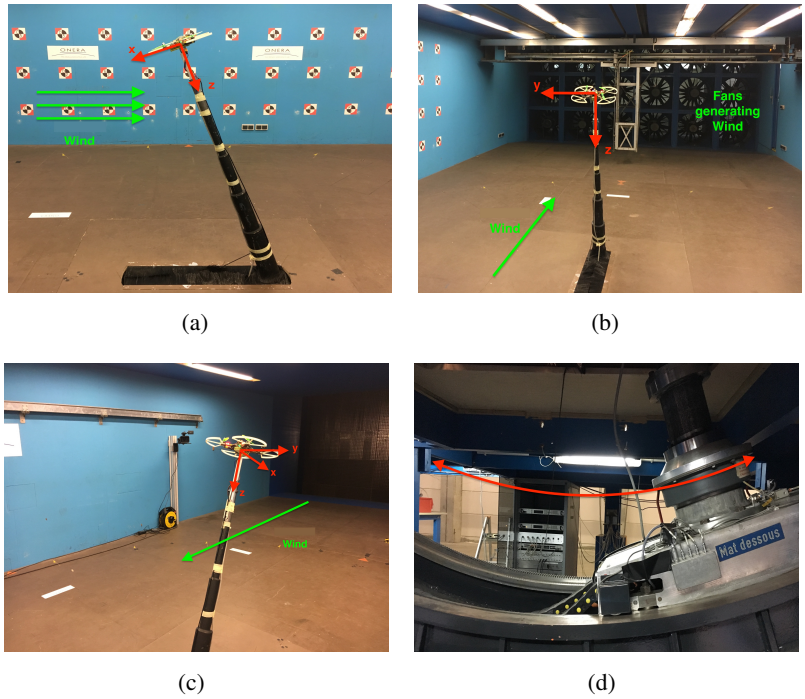

(a) (b)

(c) (d)

Figure 1.5: Images of the L2 wind tunnel in lateral view (a), frontal view (b), posterior view (c); and of the mechanism that allows the stick to move circularly (d).

Peer-reviewed proceedings articles

- G. Perozzi, D. Efimov, J-M. Biannic, L. Planckaert, P. Coton. "Wind estimation algorithm for quadrotors using detailed aerodynamic coefficients". In Proceedings of *American Control Conference, AIAA section*. Milwaukee, WI, USA. Jun, 2018.
- G. Perozzi, D. Efimov, J-M. Biannic, L. Planckaert, P. Coton. "On sliding mode control design for UAV using realistic aerodynamic coefficients". In Proceedings of *56th IEEE Conference on Decision and Control*. Melbourne, Australia. Dec, 2017. DOI: 10.1109/CDC.2017.8264459.
- G. Perozzi, D. Efimov, J-M. Biannic, L. Planckaert, P. Coton. "Wind rejection via quasi-continuous sliding mode technique to control safely a mini drone". In Proceedings of *7th European Conference for Aeronautics and Space Science*. Milan, Italy. Jul, 2017. DOI: 10.13009/EUCASS2017-329.

Peer-reviewed internal reports

- "ONERA Journée des doctorantes 3rd Year". *ONERA/DAAA/ELV*. Châtillon, France. Jan, 2018.
- "Deuxième année de thése Activités 2017". *ONERA/DAAA/ELV*. RT 2/25151 DAAA. Lille, France. Sep, 2017.
- "ONERA Journée des doctorantes 2nd Year". *ONERA/DAAP/ELV*. Châtillon, France. Jan, 2017.
- "Première année de thése Activités 2016". *ONERA/DAAP/ELV*. RT 1/25151 DAAP. Lille, France. Oct, 2016.

- "Admission to the 2nd PhD Year". *École Centrale de Lille.* Lille, France. Oct, 2016.
- "ONERA Journée des doctorantes 1st Year". *ONERA/DAAP/ELV*. Châtillon, France. Jan, 2016.

Reports

- "Optimization of the control effort for quadrotors using a varying-gain quasi-continuous sliding mode control influenced by a wind estimator". Apr, 2018. Available on: https://hal.inria.fr/hal-01758112.
- "A toolbox for quadrotors: from aerodynamic science to control theory". Jan, 2018. Available on: https://hal.inria.fr/hal-01696344.
- "CW-Quad Toolbox user's guide". Jan, 2018. Available on: https://hal.inria.fr/hal-01696347.

Software

- Simulink toolbox for Quadrotors. (see Appendix D)

Awards

- Creativity prize at Fédération de Recherche CNRS Transports Terrestres & Mobilité. 2018.
- Best student paper at EUCASS conference. 2017.

CHAPTER 2

Quadrotor model influenced by wind speed

Contents

2.1 Introduction

To estimate correctly the wind velocity and to stabilize the quadrotor in a wind field, a realistic quadrotor model taking into account the wind velocity must be considered. For this reason, this chapter is devoted to description of such a representative model accepted in the thesis work. The main difficulty in the model selection is to balance a very detailed model, representing the behavior of the quadrotor close to the reality, with a simplified model, which is useful to design the control and the estimation algorithms. Based on different tasks in literature, different assumptions are considered in quadrotor's modeling, [Ghazbi *et al.* 2016, Shraim *et al.* 2018, Zhang *et al.* 2014]. Modeling of aircraft based on the Euler-Lagrange and Newton-Euler formalism are presented in [Miller 2011, Kim *et al.* 2010, Elsamanty *et al.* 2013, Bresciani 2008]. Basic concepts of helicopter aerodynamics are illustrated in [Seddon & Newman 2011, Leishman 2006]. The aerodynamic coefficients of rotating blades are discussed in [Bouabdallah & Siegwart 2007b], and in hover the thrust and drag are assumed proportional to the square of the propellers' rotational speed in [Bouadi *et al.* 2011, Dikmen *et al.* 2009]. Due to the low translational and angular speeds, friction forces and moments are neglected, [Mian & Wang 2008, Freddi *et al.* 2009]. A model considering aerodynamic coefficients in forward and vertical flights is presented in [Orsag & Bogdan 2012] at higher speeds. Most of the works assume that the center of mass and the coordinate system origin coincide, as in [Mokhtari & Benallegue 2004], however there are also some works that consider this difference, as in [Mellinger *et al.* 2011]. In particular, [Mellinger *et al.* 2011] considers a model that takes into account the change of mass and the change of the center of mass position. Taking-off and landing cases in presence of obstacles and sloped terrains are considered in [Cabecinhas *et al.* 2012]. Blade flapping effect is investigated in [Pounds *et al.* 2010, Hoffmann *et al.* 2007, Pounds *et al.* 2004, Bouabdallah 2007, Madani & Benallegue 2007]. Gyroscopic effect of rotors is very small in comparison with the one caused by the aerodynamics torques. For this reason there are many studies that consider this effect, such as in [Bouabdallah & Siegwart 2005], while in other studies this effect is neglected, such as in [Das *et al.* 2009]. The mutual aerodynamic interaction between the rotors during the flight are studied in [Hwang *et al.* 2015].

Based on analysis and comparison of these models, the remaining part of this Chapter is devoted to introduction of a model accepted in the present thesis work. It is selected in order to better represents the features of quadrotor dynamics important for the considered applications.

2.2 Flight dynamics of the quadrotor

Quadrotors are vehicles that can fly in a 3D environment and, to be properly studied, two different frames must be considered. The Body frame of the quadrotor, and the Earth frame which is the inertial reference. Forces and moments acting on the quadrotor are computed in body frame, then they are transposed into the Earth frame thanks to the rotation matrix **R** (see Appendix B.1). Using the Earth frame, desired positions in 3D space can be imposed. For this reason, a relation between these frames must be defined.

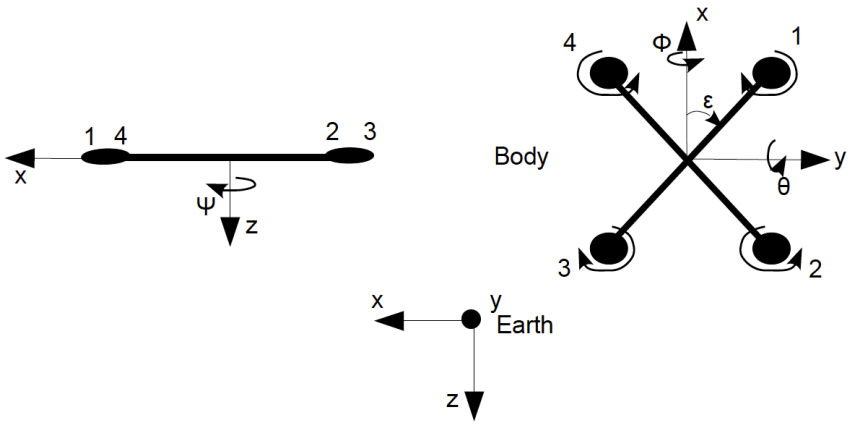

Figure 2.1: Quadrotor configuration with Earth and Body frames.

Quadrotors are underactuated systems, with 4 rotors corresponding to 4 controls, and 6 degrees of freedom. Fig. 2.1 shows the 3 translational directions (x, y, z corresponding to forward, lateral and altitude dynamics) and the 3 rotational directions (ϕ, θ, ψ corresponding to roll, pitch and yaw dynamics). The detailed model of the quadrotor dynamics, computed to control the drone and to estimate the wind velocity, is based on the quadrotor notation as in Fig. 2.1.

Then the translation dynamics of the drone in the body frame yield

$$m\begin{bmatrix}\dot{u}\\ \dot{v}\\ \dot{w}\end{bmatrix} + m\begin{bmatrix}p\\ q\\ r\end{bmatrix} \times \begin{bmatrix}u\\ v\\ w\end{bmatrix} = \begin{bmatrix}F_{Xaero}\\ F_{Yaero}\\ F_{Zaero}\end{bmatrix} + m\mathbf{R}^T\begin{bmatrix}0\\ 0\\ g\end{bmatrix}, \tag{2.1}$$

which can be represented in the earth frame

$$m\begin{bmatrix}\ddot{x}\\ \ddot{y}\\ \ddot{z}\end{bmatrix} = \mathbf{R}\begin{bmatrix}F_{Xaero}\\ F_{Yaero}\\ F_{Zaero}\end{bmatrix} + m\begin{bmatrix}0\\ 0\\ g\end{bmatrix}, \tag{2.2}$$

where m is the mass of the UAV, (u, v, w) are the linear velocities expressed in body frame, (p, q, r) are the angular velocities in body frame, (F_{Xaero}, F_{Yaero}, F_{Zaero}) are the external aerodynamic forces in body frame, g is the gravity acceleration in Earth frame.

The rotational dynamics of the drone with respect to Earth frame are

$$\mathbf{I}\begin{bmatrix}\dot{p}\\ \dot{q}\\ \dot{r}\end{bmatrix} = -\begin{bmatrix}p\\ q\\ r\end{bmatrix}\times\mathbf{I}\begin{bmatrix}p\\ q\\ r\end{bmatrix}+\begin{bmatrix}L_{aero}\\ M_{aero}\\ N_{aero}\end{bmatrix}+\begin{bmatrix}-J_{rot}q\Omega_r\\ J_{rot}p\Omega_r\\ -J_{rot}\dot{\Omega}_r\end{bmatrix} \tag{2.3}$$

where (L_{aero}, M_{aero}, N_{aero}) are the external aerodynamic moments in the body frame, Ω_r is the propeller angular rate, J_{rot} is the propeller inertia, and with the quadrotor inertia matrix

$$\mathbf{I} \approx \begin{bmatrix}I_{xx} & 0 & 0\\ 0 & I_{yy} & 0\\ 0 & 0 & I_{zz}\end{bmatrix},$$

where (I_{xx}, I_{yy}, I_{zz}) are the inertia of the drone around (x, y, z) axes respectively. The other components of this matrix are not considered since they are very small. These three inertia values are linked together by an approximate relation $I_{zz} \approx I_{xx} + I_{yy}$. According to the identification work in [Planckaert & Coton 2015] performed at moderate speeds in forward, lateral, and vertical directions of ± 5, $\pm 5 \pm 1\ m/s$ respectively, rotor gyroscopic effects and inertial counter torques can be neglected since they are rather small.

The relations between angular velocities and Euler angles (see Appendix B.2)

$$\begin{aligned}\dot{\phi} &= p + \tan\theta(q\sin\phi + r\cos\phi),\\ \dot{\theta} &= q\cos\phi - r\sin\phi,\\ \dot{\psi} &= \frac{q\sin\phi + r\cos\phi}{\cos\theta}\end{aligned} \tag{2.4}$$

are considered avoiding the singularity at $\theta = \frac{\pi}{2}$, which is a reasonable assumption in our case since the topic of the thesis is not to achieve extreme maneuvers.

Hence, the full model of the system is presented by the equations (2.2), (2.3), (2.4). The aerodynamic forces (F_{Xaero}, F_{Yaero}, F_{Zaero}), moments (L_{aero}, M_{aero}, N_{aero}), and related coefficients are derived below using ablade element momentum theory in helicopters (see Appendix A), well explained in [Bramwell *et al.* 2001, Johnson 2012, Leishman 2006].

Aerodynamic forces and moments for each rotor, where subscript j indicates the j^{th} rotor, are derived as

$$\begin{aligned}F_{Xj} &= -\rho A R^2 \frac{u_j - u_w}{\sqrt{(u_j-u_w)^2+(v_j-v_w)^2}} C_{Hj}\omega_j^2,\\ F_{Yj} &= -\rho A R^2 \frac{v_j - v_w}{\sqrt{(u_j-u_w)^2+(v_j-v_w)^2}} C_{Hj}\omega_j^2,\\ F_{Zj} &= -\rho A R^2 C_{Tj}\omega_j^2,\\ L_j &= -\operatorname{sign}(\omega_j)\rho A R^3 \frac{u_j - u_w}{\sqrt{(u_j-u_w)^2+(v_j-v_w)^2}} C_{Rmj}\omega_j^2,\\ M_j &= -\operatorname{sign}(\omega_j)\rho A R^3 \frac{v_j - v_w}{\sqrt{(u_j-u_w)^2+(v_j-v_w)^2}} C_{Rmj}\omega_j^2,\\ N_j &= -\operatorname{sign}(\omega_j)\rho A R^3 C_{Qj}\omega_j^2,\end{aligned}$$

where ρ is the air density, A is the rotor area, R is the rotor radius, $(u_w,\ v_w,\ w_w)$ are the wind velocities with respect to the Earth and in body frame respectively in $(x,\ y,\ z)$ directions, C_{Hj} is the hub force coefficient, C_{Tj} is the rotor thrust coefficient, ω_j is the rotor angular speed, C_{Qj} is the rotor drag moment coefficient, C_{Rmj} is the rotor rolling moment coefficient. The translational rotor velocities in body frame $(u_j,\ v_j,\ w_j)$ are computed as a function of the state in body frame:

$$\begin{bmatrix} u_j \\ v_j \\ w_j \end{bmatrix} = \begin{bmatrix} p \\ q \\ r \end{bmatrix} \times \begin{bmatrix} lc_j \\ ls_j \\ h \end{bmatrix} + \begin{bmatrix} u \\ v \\ w \end{bmatrix}, \tag{2.5}$$

with

$$\mathrm{c}_j = \cos\left(\frac{\pi}{2}(j-1) + \varepsilon\right), \quad \mathrm{s}_j = \sin\left(\frac{\pi}{2}(j-1) + \varepsilon\right),$$

where h is the distance between rotors plane and the center of gravity of the UAV, l is the arm length, and in our UAV configuration we have $\varepsilon = \frac{\pi}{4}$. Thus, for vectors c_j and s_j we have cosines and sines of the angles $[\frac{\pi}{4}, \frac{3}{4}\pi, \frac{5}{4}\pi, \frac{7}{4}\pi]$.

Total aerodynamic forces are

$$F_{Xaero} = \sum_{j=1}^{4} F_{Xj}, \quad F_{Yaero} = \sum_{j=1}^{4} F_{Yj}, \quad F_{Zaero} = \sum_{j=1}^{4} F_{Zj}. \tag{2.6}$$

Total aerodynamic moments are

$$\begin{aligned} L_{aero} &= \sum_{j=1}^{4} \left(L_j + F_{Zj} l \mathrm{s}_j - h F_{Yj}\right), \\ M_{aero} &= \sum_{j=1}^{4} \left(M_j - F_{Zj} l \mathrm{c}_j + h F_{Xj}\right), \\ N_{aero} &= \sum_{j=1}^{4} \left(N_j + F_{Yj} l \mathrm{c}_j - F_{Xj} l \mathrm{s}_j\right). \end{aligned} \tag{2.7}$$

Since the blades of the rotors may be flexible, they present a flapping effect during the angular revolution (see Appendix A.4).

2.2.1 Rotors dynamics

The rotors are driven by DC-motors, which bind together the electrical and the mechanical quantities. As in [Bouabdallah & Siegwart 2005, Bouabdallah & Siegwart 2007a], rotors can be represented as in Fig. 2.2, and described by the following dynamic equations

$$L_{rot}\frac{di_{rot}}{dt} = u_{rot} - R_{rot} i_{rot} - K_e \omega, \quad J_{rot}\frac{d\omega}{dt} = \tau_m - \tau_d,$$

where u_{rot} is the rotor input, R_{rot} is the rotor internal resistance, L_{rot} is the rotor inductance, K_e is the rotor back EMF (ElectroMagnetic Force) constant, τ_r is the rotor torque, ω is the rotor angular speed, τ_d is the rotor load, J_{rot} is the rotor moment of inertia, i_{rot} is the current.

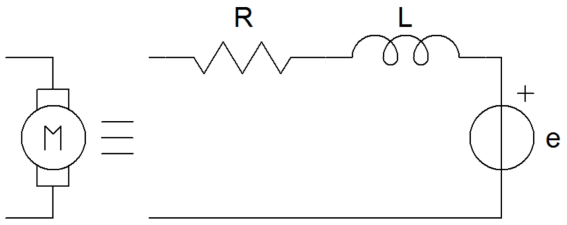

Figure 2.2: Rotor model

Considering small motors with very low inductance, the given system can be simplified and approximated by linearization around an operating point ω_0, then the system takes the form of $\dot{\omega} = -A\omega + Bu_{mot} + C$, where A, B, C are rotors parameters, and it can be further described by a transfer function

$$G(s) = \frac{1}{bs+1}, \tag{2.8}$$

where b is the time constant of the rotors to be identified. The value of the parameter b is small for small rotors having small time-delay, and *vice-versa*.

2.3 Nonlinear dependance by the wind

The aerodynamic coefficients (C_T coefficient of the thrust, C_{Rm} coefficient of the rolling moment, C_H coefficient of the hub force, C_Q coefficient of the drag moment, μ advance ratio, λ inflow ratio) are computed as follows, using blade element momentum theory and under the hypothesis that the induced velocity is uniform over the rotor.

$$\begin{aligned}
C_{Rmj} &= \sigma a\left(\frac{\mu_j}{8}\left(\lambda_j - \frac{4}{3}\theta_0 + \theta_{tw}\right) + \frac{b_1}{16}\left(1 - \frac{\mu_j^2}{2}\right)\right),\\
C_{Tj} &= \sigma a\left(\left(1 + \frac{3}{2}\mu_j^2\right)\frac{\theta_0}{6} - \left(1+\mu_j^2\right)\frac{\theta_{tw}}{8} - \frac{\lambda_j}{4}\right),\\
\lambda_j &= \sigma a\frac{\left(1+\frac{3}{2}\mu_j^2\right)\frac{\theta_0}{6} - \left(1+\mu_j^2\right)\frac{\theta_{tw}}{8} - \frac{\lambda_j}{4}}{2\sqrt{\mu_j^2+\lambda_j^2}} + \frac{w_w - w_j + qlc_j - pls_j}{R|\omega_j|},\\
\mu_j &= \frac{1}{R|\omega_j|}\sqrt{\left(u_j - u_w\right)^2 + \left(v_j - v_w\right)^2},\\
C_{Qj} &= C_{QPj} + C_{Qij},\\
\frac{C_{QPj}}{\sigma} &= \frac{1}{8}\left(C_{D0} + C_{Di}\theta_0^2\right)\left(1+\mu_j^2\right) - C_{Di}\theta_0\theta_{tw}\left(\frac{1}{5} + \frac{\mu_j^2}{6}\right) + C_{Di}\theta_{tw}^2\left(\frac{1}{12} + \frac{\mu_j^2}{16}\right) - C_{Di}\lambda_j\\
&\quad\times\left(\frac{\theta_0}{3} - \frac{\theta_{tw}}{4}\right) + C_{Di}\left(\frac{\mu_j^2}{8}\left(a_0^2 + \frac{a_1^2}{4} + \frac{3b_1^2}{4}\right) + \frac{1}{16}\left(a_1^2+b_1^2\right) + \frac{\lambda_j^2}{4} + \frac{\mu_j}{6}a_0a_1 - \frac{\lambda_j\mu_j}{4}b_1\right),\\
\frac{C_{Qij}}{\sigma a} &= \lambda_j\left(\frac{\theta_0}{6} - \frac{\theta_{tw}}{8} - \frac{\lambda_j}{4}\right) - \frac{\mu_j^2}{8}\left(a_0^2 + \frac{a_1^2}{4} + \frac{3b_1^2}{4}\right) - \frac{1}{16}\left(a_1^2+b_1^2\right) - \frac{\mu_j}{6}a_0a_1 + \frac{\lambda_j\mu_j}{4}b_1,
\end{aligned}$$

$$
\begin{aligned}
C_{Hj} &= C_{HPj} + C_{Hij},\\
\frac{C_{HPj}}{\sigma} &= \frac{\mu_j}{4}\left(C_{D0} + C_{Di}\theta_0^2\right) + C_{Di}\Big(\frac{\mu_j}{24}\left(3\theta_{tw}^2 - 8\theta_0\theta_{tw}\right) + \frac{\theta_0}{24}\left(3\mu_j^2 b_1 - 12\lambda_j\mu_j - 4b_1\right)\\
&\quad - \frac{\theta_{tw}}{16}\left(\mu_j^2 b_1 - 4\lambda_j\mu_j - 2b_1\right) + \frac{\mu_j^2}{8}a_0 a_1 + \frac{\mu_j}{16}\left(a_1^2 - b_1^2\right) + \frac{1}{4}\lambda_j b_1\Big),\\
\frac{C_{Hij}}{\sigma a} &= \frac{\theta_0}{4}\left(\lambda_j\mu_j + \frac{2}{3}b_1\right) - \frac{\theta_{tw}}{8}\left(\lambda_j\mu_j + b_1\right) + \frac{\mu_j}{8}\left(a_0^2 + b_1^2\right) - \frac{3}{8}\lambda_j b_1 + \frac{1}{12}a_0 a_1,
\end{aligned}
\tag{2.9}
$$

where $(u_w,\ v_w,\ w_w)$ are the wind velocity components in body frame in $(x,\ y,\ z)$ directions, σ is the rotor solidity ratio (see eq. (A.5)), a is the lift curve slope of the blade section, C_{D0} is the drag coefficient of the blade section, C_{Di} is the induced drag coefficient of the blade section, θ_0 is the angle of attack of the root profile, θ_{tw} is the twist attack of the blades, $a_0,\ a_1,\ b_1$ are the coefficients of the blade flapping equation. The shape of above UAV coefficients can be explained recalling aerodynamics: the thrust is the resultant of the vertical forces acting on all the blade elements:

$$T_j = C_{T\,j}\rho A\left(\omega_j R\right)^2$$

The inflow ratio is the ratio between the component of UAV velocity perpendicular to the rotor disk with respect to the blade tip speed. The advance ratio indicates the component of the UAV velocity parallel to the rotor disk with respect to the blade tip speed. The rolling moment of a propeller exists in forward flight when the advancing blade is producing more lift than the retreating one and it is the integration over the entire rotor of the lift of each section acting at a given radius:

$$R_{m\,j} = C_{Rm\,j}\rho A\left(\omega_j R\right)^2 R$$

The hub force is the resultant of the horizontal forces acting on all the blade elements:

$$H_j = C_{H\,j}\rho A\left(\omega_j R\right)^2$$

The drag moment about the rotor shaft is caused by the aerodynamic forces acting on the blade elements, the horizontal forces acting on the rotor are multiplied by the moment arm and integrated over the rotor:

$$Q_j = C_{Q\,j}\rho A\left(\omega_j R\right)^2 R$$

As noticed, the full quadrotor model is complex to be studied effectively in control and estimation theories, and this complexity comes from the relation between the inflow ratio λ_j and the advance ratio μ_j. For this reason, some simplifications must be applied. Identification results thanks to indoor experiments on Parrot drone at low/moderate velocity, validates the previous UAV model and allows more simplifications to be accepted:

- $a_0,\ a_1,\ b_1 = 0$, considering that in our case the blade flapping dynamics is characterized by a quick response and that the rotor's blades are stiff enough, the flapping effect is neglected;
- $\theta_{tw} = 0$;
- $C_{Di} = 0$;

- $\lambda_j = \lambda_{stat} - \frac{4}{\sigma a} K_z \frac{w_j - w_w}{R|\omega_j|},\ K_z,\ \lambda_{stat} \geq 0$, where K_z (as by [Planckaert & Coton 2015]) comes from the approximation of the λ equation in vertical ascending flight, subscript *stat* indicates the value in stationary flight. $C_{T\,j} = C_{T\,stat} + K_z \frac{w_j - w_w}{R|\omega_j|},\ C_{T\,stat} \geq 0$, such models of λ_j and $C_{T\,j}$ are rather precise in the climbing phase, but less accurate in descent phase, since the model tends to slightly overestimate the propulsion in the descent phase;

- $C_{H\,j} = K_D \mu_j,\ K_D \geq 0$, the UAV drag is modeled as $\rho A R^2 \sum C_{H\,j} \omega_j^2$, corresponding to the rotors at low UAV speed, otherwise at higher speed we need to add the body drag effect since it depends on square of velocity. However the constant K_D, (as by [Planckaert & Coton 2015]) has been identified for the forward velocity less than $5\,m/s$ taking into account the interactions between the rear and the front rotors, and considering the whole UAV body and rotors. This term captures effects that are not easily modeled (blade flapping, interaction of rotor wakes).

2.4 Disturbance influence on the quadrotor

Once the quadrotor model is presented in details, control and estimation theories can be applied. To this end, the physical model is rewritten in state-space model, useful to enlighten the disturbance influence on the quadrotor. Substituting the equations (2.9), (2.6) and (2.7) in (2.1), (2.3), and performing calculations with the indicated simplifications, the control inputs are selected to be proportional to the terms with ω_j^2. Thus, expanding (2.1) and (2.3), the other terms dependent linearly on ω_j and wind velocities are considered as disturbances (see system (2.10)). Since we do not know in advance the wind perturbations, but we know only the quadrotor velocity affecting the forces and moments, then we cannot use these terms in controls. Such a decomposition of thrust (which is proportional to ω_j and ω_j^2) and selection of disturbances are almost exact in the hover flight, where we have $(p,\ q,\ r) \approx (\dot{\phi},\ \dot{\theta},\ \dot{\psi})$. The resultant compact state-space form is

$$\dot{\mathbf{X}} = f(\mathbf{X},\ \mathbf{U},\ \mathbf{d}) = \begin{cases} \dot{\mathbf{X}}(1) = \mathbf{X}(4) \\ \dot{\mathbf{X}}(2) = \mathbf{X}(5) \\ \dot{\mathbf{X}}(3) = \mathbf{X}(6) \\ \dot{\mathbf{X}}(4) = U_x \frac{U_z}{m} - d_{xe} \\ \dot{\mathbf{X}}(5) = U_y \frac{U_z}{m} - d_{ye} \\ \dot{\mathbf{X}}(6) = g - \cos \mathbf{X}(7) \cos \mathbf{X}(8) \frac{1}{m}(U_z + d_{ze}) \\ \dot{\mathbf{X}}(7) = \mathbf{X}(10) \\ \dot{\mathbf{X}}(8) = \mathbf{X}(11) \\ \dot{\mathbf{X}}(9) = \mathbf{X}(12) \\ \dot{\mathbf{X}}(10) = \mathbf{X}(11)\mathbf{X}(12) \frac{I_{yy} - I_{zz}}{I_{xx}} + \frac{1}{I_{xx}}(U_\phi + d_\phi) \\ \dot{\mathbf{X}}(11) = \mathbf{X}(10)\mathbf{X}(12) \frac{I_{zz} - I_{xx}}{I_{yy}} + \frac{1}{I_{yy}}(U_\theta + d_\theta) \\ \dot{\mathbf{X}}(12) = \mathbf{X}(10)\mathbf{X}(11) \frac{I_{xx} - I_{yy}}{I_{zz}} + \frac{1}{I_{zz}}(U_\psi + d_\psi) \end{cases} . \tag{2.10}$$

The state vector $\mathbf{X}$ is chosen as

$$\mathbf{X} = [x \quad y \quad z \quad \dot{x} \quad \dot{y} \quad \dot{z} \quad \phi \quad \theta \quad \psi \quad p \quad q \quad r]^T .$$

The control input vector and its relation with the rotor velocities are defined as

$$\mathbf{U} = \begin{bmatrix} U_z \\ U_\theta \\ U_\phi \\ U_\psi \end{bmatrix} \approx \begin{bmatrix} K_f & K_f & K_f & K_f \\ K_f l \mathrm{c}_j & K_f l \mathrm{c}_j & K_f l \mathrm{c}_j & K_f l \mathrm{c}_j \\ -K_f l \mathrm{s}_j & -K_f l \mathrm{s}_j & -K_f l \mathrm{s}_j & -K_f l \mathrm{s}_j \\ K_m & -K_m & K_m & -K_m \end{bmatrix} \begin{bmatrix} \omega_1^2 \\ \omega_2^2 \\ \omega_3^2 \\ \omega_4^2 \end{bmatrix},$$

with $\omega_{min} \leq \omega_j \leq \omega_{max}$ (if $\omega_j < \omega_{min}$ the rotor will stall, and ω_{max} is given by the limitation of the rotors power), and where $K_f = \rho A R^2 C_{T\,stat}$ and $K_m = \rho A R^3 \left(\frac{\sigma C_{D0}}{8} + \lambda_{stat} \sigma a \left(\frac{\theta_0}{6} - \frac{\lambda_{stat}}{4}\right)\right)$. The virtual controllers are defined as

$$\begin{aligned} U_x &= \sin \mathbf{X}(7) \sin \mathbf{X}(9) + \cos \mathbf{X}(9) \sin \mathbf{X}(8) \cos \mathbf{X}(7), \\ U_y &= \sin \mathbf{X}(9) \sin \mathbf{X}(8) \cos \mathbf{X}(8) - \cos \mathbf{X}(9) \sin \mathbf{X}(7). \end{aligned}$$

Using the mentioned simplifications, the disturbance $\mathbf{d} = [d_{xe}, d_{ye}, d_{ze}, d_\phi, d_\theta, d_\psi]$ is represented by the following remaining terms

$$d_x = \sum_{j=1}^{4} -\rho A R K_D \left(u_j - u_w\right) |\omega_j|, \tag{2.11}$$

$$d_y = \sum_{j=1}^{4} -\rho A R K_D \left(v_j - v_w\right) |\omega_j|, \tag{2.12}$$

$$d_z = \sum_{j=1}^{4} -\rho A R K_z \left(w_j - w_w\right) |\omega_j|, \tag{2.13}$$

$$\begin{aligned} d_\phi = \sum_{j=1}^{4} \Bigg(& \omega_j \rho A R^2 \left(u_j - u_w\right) \frac{\sigma a}{2} \left(\frac{\theta_0}{3} - \frac{\lambda_{stat}}{4}\right) + |\omega_j| \rho A R \left(h K_D \left(v_j - v_w\right) - l K_z \left(w_j - w_w\right) \mathrm{s}_j\right) \\ & + \mathrm{sign}\left(\omega_j\right) \frac{1}{2} \rho A R K_z \left(u_j - u_w\right) \left(w_j - w_w\right) \Bigg), \end{aligned} \tag{2.14}$$

$$\begin{aligned} d_\theta = \sum_{j=1}^{4} \Bigg(& \omega_j \rho A R^2 \left(v_j - v_w\right) \frac{\sigma a}{2} \left(\frac{\theta_0}{3} - \frac{\lambda_{stat}}{4}\right) + |\omega_j| \rho A R \left(-h K_D \left(u_j - u_w\right) + l K_z \left(w_j - w_w\right) \mathrm{c}_j\right) \\ & + \mathrm{sign}\left(\omega_j\right) \frac{1}{2} \rho A R K_z \left(v_j - v_w\right) \left(w_j - w_w\right) \Bigg), \end{aligned} \tag{2.15}$$

$$\begin{aligned} d_\psi = \sum_{j=1}^{4} \Bigg(& \omega_j \rho A R^2 K_z \left(w_j - w_w\right) \left(\frac{2\theta_0}{3} - 2\lambda_{stat}\right) - |\omega_j| \rho l A R K_D \left(\left(v_j - v_w\right) \mathrm{c}_j - \left(u_j - u_w\right) \mathrm{s}_j\right) \\ & - \mathrm{sign}\left(\omega_j\right) \rho A R \left(\frac{\sigma C_{D0}}{8} \left(\left(u_j - u_w\right)^2 + \left(v_j - v_w\right)^2\right) - \frac{4}{\sigma a} K_z^2 \left(w_j - w_w\right)^2\right) \Bigg). \end{aligned} \tag{2.16}$$

The disturbances in Earth frame are computed using the rotation matrix as

$$\mathbf{d_{earth}} = \begin{bmatrix} d_{xe} \\ d_{ye} \\ d_{ze} \end{bmatrix} = \mathbf{R} \cdot \begin{bmatrix} d_x \\ d_y \\ d_z \end{bmatrix} = \begin{bmatrix} c_\psi c_\theta d_x + (c_\psi c_\theta c_\phi - s_\psi c_\phi) d_y + (s_\phi s_\psi + c_\psi s_\theta c_\phi) d_z \\ s_\psi c_\theta d_x + (c_\psi c_\phi + s_\psi s_\theta s_\phi) d_y + (s_\psi s_\theta c_\phi - c_\psi s_\phi) d_z \\ -s_\theta d_x + c_\theta s_\phi d_y + c_\theta c_\phi d_z \end{bmatrix},$$

where $c_\psi = \cos(\psi)$, $s_\psi = \sin(\psi)$ and similar for the other angles.

2.5 Conclusion

In this chapter, flight dynamics and aerodynamic coefficients are derived using a combination of momentum and blade element theories. The resultant equations are highly nonlinear and thus their direct application for synthesis of control and estimation algorithms is complicated. To overcome this problem, some acceptable simplifications are used which are based on previous in-door experiments. For simplicity of presentation, in the following manuscript, two notations are used: simplified quadrotor model, which uses the nonlinear aerodynamic coefficients and the identification work; full control model, which uses the aerodynamic coefficients together with the identification work except of λ and C_T nonlinear equations. Last, the overall quadrotor system is rewritten in state-space form to show the controls and wind influences on the quadrotor. Using this state-space representation, control laws and estimation algorithms are computed in the next two chapters.

CHAPTER 3

Control laws influenced by the wind

Contents

3.1 Introduction

Starting from the state-space representation, control laws can be computed ensuring a stable and efficient navigation of the small drone under unpredictable wind perturbations. There exist many control design techniques to counteract the effects of wind perturbations on flight, among which SMC play a keyrole, and they are extensively illustrated in this Chapter. Since quadrotors are physical objects then smooth trajectories are desired. In literature many articles are presented to generate desired admissible trajectories to the system dynamics applied to quadrotors, such as the minimum snap trajectory [Mellinger & Kumar 2011] allowing to generate smooth trajectories to limit the feed-forward control. This research uses a simple method which can take into account UAV physical constraints (see Appendix B.3), which have to be synthesized considering their physical limitations (see Appendix B.5).

Many SMC methods have been proposed in the literature and some principal SMCs with their relative sliding surfaces and Lyapunov functions are illustrated in [Bernuau *et al.* 2014, Polyakov & Fridman 2014]. Sliding mode algorithms are extensively applied to dynamic systems and optimal algorithms are discussed in the Special Issue [Basin *et al.* 2012]. Their insensitivity to the model errors, parametric uncertainties and other disturbances and their ability to globally stabilize the underactuated systems are two advantages, [Xu & Özgüner 2008], for this reason they are applied extensively in quadrotors [Xu *et al.* 2017]. Dozens of articles have applied SMC methodology to quadrotors in order to solve the position and the attitude tracking problems ensuring robustness against external disturbances. [L'Afflitto *et al.* 2018] introduces the nonlinear SMC applied to quadrotors, [Kwon *et al.* 2017] estimates the quadrotor attitude using the extended Kalman filter and uses it in SMC design, [Promkajin & Parnichkun 2018] presents the attitude SMC design for nonidentical rotor quadrotors. A SMC is proposed to stabilize a class of cascaded under-actuated systems, in which the UAV system is divided, in [Xu & Ozguner 2006]. They have been compared extensively with respect to other controls and in-door experiments in [Bouabdallah & Siegwart 2005] where SMC is compared with backstepping control for micro quadrotor, and applied in out-door environments in [Muñoz *et al.* 2017]. Navigation experiments are carried out also in [Mercado *et al.* 2018] using monocular vision. A SMC to provide robust position and attitude of the vehicle while relying only on knowledge of

the limits of the disturbances is proposed in [Besnard *et al.* 2012]. Variants of adaptive SMCs are presented in [Chang & Shi 2017, Mofid & Mobayen 2018, Li *et al.* 2016, Islam *et al.* 2017], and the trajectory tracking of uncertain underactuated nonlinear dynamic systems is tackled by an adaptive fuzzy hierarchical sliding-mode control in [Hwang *et al.* 2014]. Terminal SMC is illustrated in [Cheng *et al.* 2017, Xiong & Zhang 2017], and in the work [Xiong & Zheng 2014] the controller of the fully actuated subsystem using a robust terminal sliding mode control algorithm is designed. Integral SMCs are shown in [Jia *et al.* 2017, Mu *et al.* 2017], and in the paper [Ramirez-Rodriguez *et al.* 2014] a robust backstepping-based controller is proposed that induces integral sliding modes for the Newton–Euler underactuated dynamic model of a quadrotor subject to smooth bounded disturbances. Chattering-free SMC is proposed in [González *et al.* 2014] by replacing a sign function with a high-slope saturation function. In [Sumantri *et al.* 2016] the energy saving effect because of chattering reduction is also evaluated. Second order SMC is used in [Zheng *et al.* 2014] where two different sliding manifolds are defined for fully actuated and underactuated subsystems. Famous super-twisting algorithms, which are able to ensure robustness with respect to bounded external disturbances, are discussed in [Derafa *et al.* 2012, Gonzalez-Hernandez *et al.* 2017]. Continuous SMCs are proposed in [Rios *et al.* 2018, Ríos *et al.* 2017]. Last, SMC techniques are used also as observers estimators of the effect of the external disturbances such as wind and noise, and the whole observer–estimator–control system is presented in [Benallegue *et al.* 2008, Alizadeh & Ghasemi 2015].

It is necessary to highlight that these works do not consider such a realistic model including wind perturbation as in the present thesis. Additional dependence of the perturbations on controls and state variables, as in our case, has not been considered previously. All these differences are principal and they impact significantly the design and the stability analysis, which are presented below. For synthesis of control laws, two robust nonlinear SMC law design are described, which consider realistic assumptions on external disturbances of quadrotors.

3.2 Disturbance upper bounds

In the literature, it is often assumed that each component of the disturbance input vector d admits a fixed upper bound, which means $|d| \le D$ for some known $D \ge 0$. Unfortunately, it is a rather conservative hypothesis, and that is why the varying state-dependent bounds will be considered in our case for d. However, we will assume boundedness of the wind velocities: $|u_w| \le D_x$, $|v_w| \le D_y$, $|w_w| \le D_z$, for some known $D_x \ge 0$, $D_y \ge 0$, $D_z \ge 0$, which is a reasonable restriction. To design a control, which is able to compensate the disturbances, we have to evaluate the upper bounds for them.

For x dynamics, the upper bound in body frame is computed from eq. (2.11)

$$|d_x| = |\tilde{K}_D \sum_{j=1}^{4} \left(u_j - u_w\right) \omega_j| \le \tilde{K}_D \sum_{j=1}^{4} |u_j - u_w||\omega_j \le \tilde{K}_D \sum_{j=1}^{4} \left(|u_j| + |u_w|\right)|\omega_j| \le \tilde{K}_D (\max_j |u_j| + |u_w|) \sum_{j=1}^{4} |\omega_j|,$$

where $\tilde{K}_D = \rho A R K_D$. Using the control $U_z = K_f \sum_{j=1}^{4} \omega_j^2$ and applying the Jensen's inequality, an upper estimate can be obtained

$$\sum_{j=1}^{4} |\omega_j| \le K \sqrt{|U_z|}, \qquad K = \frac{2}{\sqrt{K_f}}. \tag{3.1}$$

An upper bound of the disturbance becomes

$$|d_x| \le \bar{K}_D \left(|X| + D_x\right) \sqrt{|U_z|} = d_{xx}, \tag{3.2}$$

where $\bar{K}_D = K\tilde{K}_D$. In the earth frame using the rotation matrix (B.1) and the upper bound for the disturbances (3.2), (3.3), (3.4) it becomes

$$|d_{xe}| = |c_\psi c_\theta d_x + (c_\psi c_\theta c_\phi - s_\psi c_\phi)d_y + (s_\phi s_\psi + c_\psi s_\theta c_\phi)d_z| \leq d_{xx} + 2d_{yy} + 2d_{zz},$$

where d_y, d_z, d_{yy} and d_{zz} are derived below. For the disturbances d_{ye} and d_{ze} the computations are similar to the previous ones, therefore only final expressions are given next.

For y dynamics, the upper bounds in body and earth frames respectively are computed from the eq. (2.12)

$$\begin{aligned} |d_y| &\leq \bar{K}_D\left(|X| + D_y\right)\sqrt{|U_z|} = d_{yy}, \\ |d_{ye}| &\leq d_{xx} + 2d_{yy} + 2d_{zz}. \end{aligned} \tag{3.3}$$

For z dynamics, the upper bounds in body and earth frames respectively are computed from the eq. (2.13)

$$|d_z| \leq \bar{K}_z\left(|X| + D_z\right)\sqrt{|U_z|} = d_{zz}, \tag{3.4}$$

$$|d_{ze}| \leq \left(f_{ze}\left(|X|\right) + D_{ze}\right)\sqrt{|U_z|}. \tag{3.5}$$

where $\bar{K}_z = K\rho ARK_z$, $f_{ze}(|X|) = \bar{K}_z \max_j |w_j| + \bar{K}_D \max_j |u_j| + \bar{K}_D \max_j |v_j|$, $D_{ze} = \bar{K}_z D_z + \bar{K}_D(D_x + D_y)$.

For roll dynamics, the upper bound estimate is computed from the equations (2.14) and (3.1)

$$|d_\phi| \leq \tilde{K}_\phi\left(f_{\phi 1}\left(X\right) + D_{\phi 1}\right)\sqrt{|U_z|} + \bar{K}_\phi\left(f_{\phi 2}\left(X\right) + D_{\phi 2}\right) \tag{3.6}$$

where $K_{\phi 1} = \rho AR^2\frac{\sigma a}{2}(\frac{\theta_0}{3} - \frac{\lambda_{stat}}{4})$, $K_{\phi 2} = \rho ARhK_D$, $K_{\phi 3} = lK_z\rho AR$, $\tilde{K}_\phi = K$, $f_{\phi 1}(X) = K_{\phi 1}\max_j |u_j| + K_{\phi 2}\max_j |v_j| + K_{\phi 3}\max_j |w_j \mathrm{s}_j|$, $D_{\phi 1} = K_{\phi 1}D_x + K_{\phi 2}D_y + K_{\phi 3}D_z \max_j |\mathrm{s}_j|$, $\bar{K}_\phi = \frac{1}{2}\rho ARK_z$, $f_{\phi 2}(X) = \max_j |u_j|^2 + \max_j |w_j|^2$, $D_{\phi 2} = D_x^2 + D_z^2$.

For pitch dynamics, the upper bound estimate is computed from the equations (2.15) and (3.1)

$$|d_\theta| \leq \tilde{K}_\theta\left(f_{\theta 1}\left(X\right) + D_{\theta 1}\right)\sqrt{|U_z|} + \bar{K}_\theta\left(f_{\theta 2}\left(X\right) + D_{\theta 2}\right)$$

where $K_{\theta 1} = \rho AR^2\frac{\sigma a}{2}(\frac{\theta_0}{3} - \frac{\lambda_{stat}}{4})$, $K_{\theta 2} = \rho ARhK_D$, $K_{\theta 3} = lK_z\rho AR$, $\tilde{K}_\theta = K$, $f_{\theta 1}(X) = K_{\theta 1}\max_j |v_j| + K_{\theta 2}\max_j |u_j| + K_{\theta 3}\max_j |w_j \mathrm{c}_j|$, $D_{\theta 1} = K_{\theta 1}D_y + K_{\theta 2}D_x + K_{\theta 3}D_z \max_j |\mathrm{c}_j|$, $\bar{K}_\theta = \frac{1}{2}\rho ARK_z$, $f_{\theta 2}(X) = \max_j |v_j|^2 + \max_j |w_j|^2$, $D_{\theta 2} = D_y^2 + D_z^2$.

For yaw dynamics, the upper bound estimate is computed from the equations (2.16) and (3.1)

$$|d_\psi| \leq \tilde{K}_\psi\left(f_{\psi 1}\left(X\right) + D_{\psi 1}\right)\sqrt{|U_z|} + \bar{K}_\psi\left(f_{\psi 2}\left(X\right) + D_{\psi 2}\right)$$

where $K_{\psi 1} = \rho AR^2K_z(\frac{2\theta_0}{3} - 2\lambda_{stat})$, $K_{\psi 2} = \rho ARlK_D$, $K_{\psi 3} = \rho ARlK_D$, $\tilde{K}_\psi = K$, $f_{\psi 1}(X) = K_{\psi 1}\max_j |w_j| + K_{\psi 2}\max_j |v_j \mathrm{c}_j| + K_{\psi 3}\max_j |u_j \mathrm{s}_j|$, $D_{\psi 1} = K_{\psi 1}D_z + K_{\psi 2}D_y \max_j |\mathrm{c}_j|$
$+ K_{\psi 3}D_x \max_j |\mathrm{s}_j|$, $\bar{K}_\psi = \rho AR$, $f_{\psi 2}(X) = \frac{\sigma C_{D0}}{8}(\max_j |u_j|^2 + \max_j |v_j|^2) + \frac{4}{\sigma a}\max_j |w_j|^2$, $D_{\psi 2} = \frac{\sigma C_{D0}}{8}(D_x^2 + D_y^2) + \frac{4}{\sigma a}D_z^2$.

3.3 First order control design

This control methodology takes into account and compensates the matched disturbances. The big issue for the considered problem is that the disturbance d depends on wind signals, the control itself, and state of the system, as shown in the previous Chapter. Thus, a mild development of SMC approach is needed. To this end, the sliding

surfaces in this work are selected proportional to the regulation errors e_i, in this way we are going to control the dynamics proportional to position and velocity

$$S_i = \dot{e}_i + \alpha_i e_i, \quad \alpha_i > 0, \tag{3.7}$$

where $i \in (x, y, z, \phi, \theta, \psi)$. The Lyapunov function is then chosen as

$$V_i = \frac{1}{2} S_i^2. \tag{3.8}$$

The dynamics of z can be rewritten in the earth frame

$$\ddot{z} = g - (\cos\phi \cos\theta) \frac{1}{m}(U_z + d_{ze}). \tag{3.9}$$

In hover state we have $\cos\theta\cos\phi \approx 1$, thus with a rotation of the UAV, a reasonable assumption is that $|\cos\phi\cos\theta| \geq \gamma > 0$, where γ is our operating point limit. To build the altitude control, the regulation error has been chosen as

$$e_z = z - z_{des}, \tag{3.10}$$

where z_{des} is the desired altitude for UAV. Thus, using eq. (3.10) and its derivative in eq. (3.7), the derivative of the sliding surface can be written as follows

$$\dot{S}_z = \ddot{z} - \ddot{z}_{des} + \alpha_z \dot{e}_z$$

and using eq. (3.9), it also equals to

$$\dot{S}_z = g - \frac{\cos\theta\cos\phi}{m}(U_z + d_{ze}) - \ddot{z}_{des} + \alpha_z \dot{e}_z. \tag{3.11}$$

The following expression of the control can be selected

$$U_z = \frac{m}{\cos\theta\cos\phi}\left(g - \tilde{u}_z - \ddot{z}_{des} + \alpha_z \dot{e}_z\right), \tag{3.12}$$

where $\tilde{u}_z$ is an auxiliary control defined later. After substitution of the control (3.12) in eq. (3.11) we obtain

$$\dot{S}_z = \tilde{u}_z + d_{ze}\frac{\cos\theta\cos\phi}{m}. \tag{3.13}$$

Using the Lyapunov function (3.8) with eq. (3.13), its derivative takes the form

$$\dot{V} = S_z\tilde{u}_z + S_z d_{ze}\frac{\cos\theta\cos\phi}{m} \leq S_z\tilde{u}_z + |S_z||d_{ze}\frac{1}{m}|.$$

Then, using eq. (3.5), the Lyapunov derivative becomes

$$\dot{V} \leq S_z\tilde{u}_z + |S_z|\frac{1}{m}\left(f_{ze}\left(|X|\right) + D_{ze}\right)\sqrt{|U_z|}.$$

From the expression (3.12) we can derive

$$|U_z| \leq \frac{m}{\gamma}(|g - \ddot{z}_{des} + \alpha_z \dot{e}_z| + |\tilde{u}_z|), \tag{3.14}$$

where $\gamma \leq |\cos\phi\cos\theta|$ and then, substituting in Lyapunov derivative, we obtain

$$\dot{V} \leq S_z\tilde{u}_z + |S_z|(\varrho(X, \ddot{z}_{des}, \dot{z}_{des}) + \nu(X)\sqrt{|\tilde{u}_z|}), \tag{3.15}$$

where

$$\varrho(X, \ddot{z}_{des}, \dot{z}_{des}) = \frac{1}{\sqrt{m\gamma}}\left(f_{ze}(|X|) + D_{ze}\right) \times \sqrt{|g + \alpha_z\dot{e}_z - \ddot{z}_{des}|}, \quad \nu(X) = \frac{1}{\sqrt{m\gamma}}\left(f_{ze}(|X|) + D_{ze}\right).$$

For simplicity of notation, in the following part we will denote $\varrho(X, \ddot{z}_{des}, \dot{z}_{des}) = \varrho(X)$. Let us look for the control in the form

$$\tilde{u}_z = -\beta(X)\text{sign}(S_z),$$

where $\beta(X)$ is a function to synthesize. Substituting this control in the obtained inequality (3.15) we get

$$\dot{V} \leq |S_z|(\varrho(X) + \nu(X)\sqrt{\beta(X)} - \beta(X))$$

and it is necessary to ensure by a choice of $\beta(X)$

$$\varrho(X) + \nu(X)\sqrt{\beta(X)} - \beta(X) = -\delta.$$

Solving this quadratic inequality with respect to $\beta(X)$ we found

$$\beta(X) = \frac{1}{2}(\nu(X)^2 + 2\varrho(X) + \nu(X)\sqrt{\nu^2(X) + 4\varrho(X)}) + \delta, \tag{3.16}$$

where $\delta > 0$ is a tuning parameter. Substituting eq. (3.16) in the inequality for $\dot{V}$ we get

$$\dot{V} < -\sqrt{2}\delta\sqrt{V},$$

consequently, the system state trajectory reaches and stays on the sliding surface S_z, which means asymptotic convergence of e_z to the origin. Moreover, finite-time stability with respect to S_z can be proved according to [Bernuau *et al.* 2014].

The dynamics of x can be rewritten in the earth frame as follows

$$\ddot{x} = (\sin\phi\sin\psi + \cos\psi\sin\theta\cos\phi)\frac{U_z}{m} - d_{xe}.$$

Since x dynamics cannot be directly controlled, a virtual control

$$U_x = \sin\phi\sin\psi + \cos\psi\sin\theta\cos\phi$$

is introduced, which will be used to find the desired Euler angles ϕ_{des}, θ_{des} that will be the inputs of attitude controller next. Then the dynamics of x takes the form

$$\ddot{x} = U_x\frac{U_z}{m} - d_{xe}.$$

In order to guarantee negativity of the time derivative of the Lyapunov function (3.8) the following expression of control in x is selected

$$U_x = \frac{m}{U_z}\left(\tilde{u}_x + \ddot{x}_{des} - \alpha_x\dot{e}_x\right), \tag{3.17}$$

where

$$\tilde{u}_x = -\left(d_{xx} + 2d_{yy} + 2d_{zz}\right) \text{sign} S_x$$

is an auxiliary SMC for x dynamics. Such a design is admissible since the control U_z is always separated with the zero and the discontinuous term in $\tilde{u}_x$, which leads to the chattering effect, is replaced with the continuous saturation approximation.

The y dynamics, by introducing the virtual control

$$U_y = \sin\psi \sin\theta \cos\phi - \cos\psi \sin\phi,$$

can be rewritten in the earth frame as follows

$$\ddot{y} = (\sin\psi \sin\theta \cos\phi - \cos\psi \sin\phi)\frac{U_z}{m} - d_{ye} = U_y \frac{U_z}{m} - d_{ye}.$$

Using similar arguments as for x, the auxiliary SMC for y dynamics takes the form

$$\tilde{u}_y = -\left(d_{xx} + 2d_{yy} + 2d_{zz}\right) \text{sign} S_y,$$

with the following expression of control in y

$$U_y = \frac{m}{U_z}\left(\tilde{u}_y + \ddot{y}_{des} - \alpha_y \dot{e}_y\right). \tag{3.18}$$

The dynamics of ϕ can be rewritten as

$$\dot{p} = qr\frac{I_{yy} - I_{zz}}{I_{xx}} + \frac{1}{I_{xx}}(U_\phi + d_\phi). \tag{3.19}$$

To build the roll control U_ϕ, the error has been chosen as

$$e_\phi = \phi - \phi_{des}. \tag{3.20}$$

Using eq. (3.20) and substituting its derivative in eq. (3.7), the derivative of the sliding surface can be calculated

$$\dot{S}_\phi = \dot{p} - \ddot{\phi}_{des} + \alpha_\phi \dot{e}_\phi,$$

which due to eq. (3.19) also equals to

$$\dot{S}_\phi = qr\frac{I_{yy} - I_{zz}}{I_{xx}} + \frac{1}{I_{xx}}(U_\phi + d_\phi) + \alpha_\phi \dot{e}_\phi - \ddot{\phi}_{des}. \tag{3.21}$$

The following expression of the control can be selected

$$U_\phi = I_{xx}\left(-qr\frac{I_{yy} - I_{zz}}{I_{xx}} + \tilde{u}_\phi - \alpha_\phi \dot{e}_\phi + \ddot{\phi}_{des}\right),$$

where $\tilde{u}_\phi$ is an auxiliary SMC. After substitution of this control in eq. (3.21), we obtain

$$\dot{S}_\phi = \tilde{u}_\phi + \frac{d_\phi}{I_{xx}}. \tag{3.22}$$

Using the Lyapunov function (3.8) with equations (3.22) and (3.6), its derivative becomes

$$\dot{V} = S_\phi \tilde{u}_\phi + S_\phi d_\phi \leq S_\phi \tilde{u}_\phi + |S_\phi||d_\phi \frac{1}{I_{xx}}| \leq S_\phi \tilde{u}_\phi + \frac{|S_\phi|}{I_{xx}}\Big(\tilde{K}_\phi(f_{\phi 1}(X) + D_{\phi 1})\sqrt{|U_z|} + \bar{K}_\phi(f_{\phi 2}(X) + D_{\phi 2})\Big). \quad (3.23)$$

To have eq. (3.23) negative, the auxiliary control for ϕ dynamics must be

$$\tilde{u}_\phi = -\frac{1}{I_{xx}}\text{sign}S_\phi\Big(\tilde{K}_\phi(f_{\phi 1}(X) + D_{\phi 1})\sqrt{|U_z|} + \bar{K}_\phi(f_{\phi 2}(X) + D_{\phi 2})\Big).$$

Pitch and yaw controls can be designed following computations similar to the roll one, so only final expressions are given below.

The dynamics of θ can be rewritten as

$$\dot{q} = pr\frac{I_{zz} - I_{xx}}{I_{yy}} + \frac{1}{I_{yy}}(U_\theta + d_\theta).$$

The auxiliary control for θ dynamics

$$\tilde{u}_\theta = -\frac{1}{I_{yy}}\text{sign}S_\theta\Big(\tilde{K}_\theta(f_{\theta 1}(X) + D_{\theta 1})\sqrt{|U_z|} + \bar{K}_\theta(f_{\theta 2}(X) + D_{\theta 2})\Big),$$

with the following expression of control

$$U_\theta = I_{yy}\left(-pr\frac{I_{zz} - I_{xx}}{I_{yy}} + \tilde{u}_\theta - \alpha_\theta \dot{e}_\theta + \ddot{\theta}_{des}\right).$$

The dynamics of ψ can be rewritten as

$$\dot{r} = pq\frac{I_{xx} - I_{yy}}{I_{zz}} + \frac{1}{I_{zz}}(U_\psi + d_\psi).$$

The auxiliary control for ψ dynamics

$$\tilde{u}_\psi = -\frac{1}{I_{zz}}\text{sign}S_\psi\Big(\tilde{K}_\psi(f_{\psi 1}(X) + D_{\psi 1})\sqrt{|U_z|} + \bar{K}_\psi(f_{\psi 2}(X) + D_{\psi 2})\Big),$$

with the following expression of control

$$U_\psi = I_{zz}\left(-pq\frac{I_{xx} - I_{yy}}{I_{zz}} + \tilde{u}_\psi - \alpha_\psi \dot{e}_\psi + \ddot{\psi}_{des}\right).$$

In the control design above it has been assumed that the rotors possess an immediate response on the desired values ω_j assigned to them by the control law. In reality they admit some dynamics, and for validation and comparison of the proposed control strategy, the transfer functions for the rotors have to be introduced in the realistic form as in eq. (2.8). However, it is a dynamics not considered during design, then it adds an undesired delay to the control.

Since a big shortage of SMC is the chattering (high frequency oscillations of a discontinuous control signal in the steady-state mode caused by imprecision of values of model parameters, digital and measurement noises), which can increase power consumption and ruin the rotors, then below several solutions for chattering reduction are compared. To this end, several modifications are introduced into the control algorithm for a comparison. In the

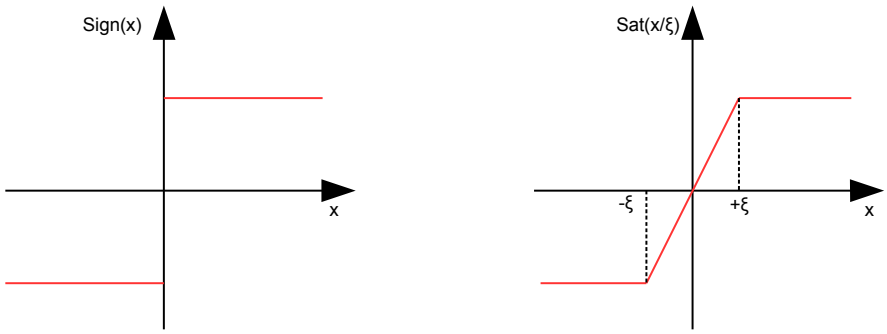

Figure 3.1: Approximation of sign using linear saturation function.

literature the problem of chattering reduction is a well-known issue discussed in many articles, see for an example [González *et al.* 2014]. Saturation functions are popular solutions used for chattering reduction in SMC that leads to a practical stability in the closed-loop system, as in Fig. .

Arc-tangent function replaces the function sign with a smooth function

$$\text{sat}_\xi(x) = \begin{cases} \text{sign}(x) & \text{if} \quad |x| \geq \xi \\ \frac{4}{\pi} \arctan\left(\frac{x}{\xi}\right) & \text{if} \quad |x| < \xi \end{cases}, \tag{3.24}$$

with the tunable gain $\xi > 0$. According to [Khalil 2002], for a sufficiently small ξ if for a sign function all trajectories converge in a finite time to an equilibrium, then with the saturation all trajectories will converge to a compact set around that equilibrium with the size proportional to the value of ξ. In practice ξ should be chosen small enough to find a trade-off between chattering reduction and minimal acceptable steady-state error. As result, the steady error is proportional to ξ, and even if a given formula in our specific problem is rather difficult to obtain, an intuition is provided in section 5.5.1, where two simulation examples are illustrated.

3.4 Quasi-continuous control design

Another way to reduce the chattering is to use a high order sliding mode control [Bernuau *et al.* 2014]. In this subsection for synthesis of a control law, a kind of high order sliding mode (HOSM) control called the quasi-continuous SMC [Ding *et al.* 2016] will be applied, which can be considered as an approximation of the sign on the plane.

Following [Ding *et al.* 2016], consider a double integrator system:

$$\ddot{x}(t) = g(t, X(t))\, u(t) + h(t, X(t)), \tag{3.25}$$

where $X(t) = [x(t), \dot{x}(t)]^T \in \mathbb{R}^2$ is the state vector, $u(t) \in \mathbb{R}$ is the control input, two functions $g : \mathbb{R}^3 \to \mathbb{R}$ and $h : \mathbb{R}^3 \to \mathbb{R}$ ensure forward existence and uniqueness of the system solutions at least locally. In addition, there are two known functions $\underline{g} : \mathbb{R}^3 \to \mathbb{R}$ and $\overline{h} : \mathbb{R}^3 \to \mathbb{R}$ such that for all $X \in \mathbb{R}^2$ and $t \geq 0$

$$g(t, X) \geq \underline{g}(t, X) > 0, \ |h(t, X)| \leq \overline{h}(t, X). \tag{3.26}$$

The following control for quasi-continuous SMC can be proposed for (3.25) (a more generic case is studied in [Ding *et al.* 2016] where bounded time-varying positive functions are considered in eq. (17) which leads to the

validity of the Theorem 4.5):

$$u(t,X) = -\frac{\overline{h}(t,X)+\alpha}{\underline{g}(t,X)}\frac{\lceil \dot{S} \rfloor^2 + \beta S}{|\dot{S}|^2 + \beta|S|}, \tag{3.27}$$

where $\lceil\cdot\rfloor^2 = |\cdot|^2\text{sign}(\cdot)$, $\alpha > 0$ and $\beta > 0$ are tuning parameters. In our nomenclature, $\alpha = \varpi_i$ with $i = x, y, z, \phi, \theta, \psi$. $\underline{g}$, $\overline{h}$ are respectively the computed lower and the upper-bounds. Note that the control (3.27) is continuous everywhere outside of the origin.

Theorem 1 *Consider the system in (3.25) and assume that the restrictions (3.26) are satisfied, then there exist $\alpha > 0$ sufficiently big and $\beta > 0$ such that the control (3.27) makes the system globally finite-time convergent.*

For this design the transfer functions for the rotors are taken into account in a generic and realistic form as previously in eq. (2.8), which leads to additional dynamics

$$b\,\dot{L}_j = U_j - L_j \quad j \in (z, \phi, \theta, \psi), \tag{3.28}$$

where L_j are the controls subjected by rotor dynamics.

Recall that for z dynamics, the second derivative of the position error, $e_z = z - z_{des}$, has the form

$$\ddot{e}_z = g - \frac{\cos\theta\cos\phi}{m}(L_z + d_{ze}) - \ddot{z}_{des},$$

where the control U_z is substituted by rotor dynamic output L_z from (3.28). The second derivative of the position error can be rewritten

$$\ddot{e}_z = -L_z\delta_z + \Delta_z,$$

where $\delta_z = (\cos\theta\cos\phi)/m$, $\Delta_z = g - \ddot{z}_{des} - (\cos\theta\cos\phi\, d_{ze})/m$. The first derivative of the sliding surface is obtained

$$\dot{S}_z = \ddot{e}_z + \alpha_z\dot{e}_z = -L_z\delta_z + \Delta_z + \alpha_z\dot{e}_z.$$

Using eq. (3.28), its second derivative is computed as

$$\ddot{S}_z = -\frac{U_z - L_z}{b}\delta_z + \dot{\delta}_z L_z + \dot{\Delta}_z + \alpha_z(-\delta_z L_z + \Delta_z) = -U_z\frac{\delta_z}{b} + \tilde{d}_z,$$

where $\tilde{d}_z = \dot{\Delta}_z + \alpha_z(-\delta_z L_z + \Delta_z) + (L_z\delta_z)/b + \dot{\delta}_z L_z$.

In the Theorem 1, it is stated that if the second order control is selected as

$$U_z = \frac{b}{\delta_z}\tilde{D}_z(t,X)\frac{\lceil \dot{S}_z \rfloor^2 + S_z}{|\dot{S}_z|^2 + |S_z|},$$

then the point $S_z = \dot{S}_z = 0$ is reached in a finite time provided that $\tilde{D}_z(t,X) > |\tilde{d}_z|$, using α_z which is inside $\tilde{D}_z(t,X)$ and S_z.

The position errors, $e_x = x - x_{des}$, $e_y = y - y_{des}$, have the dynamics

$$\ddot{e}_x = U_x\frac{U_z}{m} - d_{xe} - \ddot{x}_{des}, \quad \ddot{e}_y = U_y\frac{U_z}{m} - d_{ye} - \ddot{y}_{des}.$$

In [Ding *et al.* 2016] it is stated that if

$$\ddot{e}_x = -\tilde{D}_x(t,X)\frac{\lceil \dot{e}_x \rfloor^2 + \alpha_x e_x}{|\dot{e}_x|^2 + \alpha_x|e_y|}, \quad \ddot{e}_y = -\tilde{D}_y(t,X)\frac{\lceil \dot{e}_y \rfloor^2 + \alpha_y e_y}{|\dot{e}_y|^2 + \alpha_y|e_y|}, \tag{3.29}$$

then $e_i = \dot{e}_i = 0$, $i = x, y$ is reached in a finite time provided that $\tilde{D}_x(t, X) > |d_{xe} + \ddot{x}_{des}|$, $\tilde{D}_y(t, X) > |d_{ye} + \ddot{y}_{des}|$. x and y dynamics are not influenced directly by the rotors, hence their stability does not need the introduction of an auxiliary sliding surface. Then, the respective controls for x, y positions are

$$U_x = -\frac{m\,\tilde{D}_x(t,X)}{U_z}\frac{\lceil \dot{e}_x \rfloor^2 + \alpha_x e_x}{|\dot{e}_x|^2 + \alpha_x |e_x|}, \quad U_y = -\frac{m\,\tilde{D}_y(t,X)}{U_z}\frac{\lceil \dot{e}_y \rfloor^2 + \alpha_y e_y}{|\dot{e}_y|^2 + \alpha_y |e_y|}.$$

Such a design is admissible since the control U_z is always separated with the zero and U_x, U_y are always continuous by definition of the quasi-continuous control.

The controls for other dynamics can be designed following similar computations as for z, so only final expressions are given for roll, pitch and yaw, respectively. The second derivative of the position error, $e_\phi = \phi - \phi_{des}$, taking into account eq. (3.28), has the form

$$\ddot{e}_\phi = qr\frac{I_{yy} - I_{zz}}{I_{xx}} + \frac{1}{I_{xx}}\left(L_\phi + d_\phi\right) - \ddot{\phi}_{des},$$

The roll control is

$$U_\phi = -\frac{b}{\delta_\phi}\tilde{D}_\phi(t,X)\frac{\lceil \dot{S}_\phi \rfloor^2 + S_\phi}{|\dot{S}_\phi|^2 + |S_\phi|},$$

where $\tilde{d}_\phi = \dot{\Delta}_\phi + \alpha_\phi(\delta_\phi L_\phi + \Delta_\phi) - (L_\phi \delta_\phi)/b - \dot{\delta}_\phi L_\phi - \phi L_\phi$, $\delta_\phi = 1/I_{xx}$, $\Delta_\phi = qr(I_{yy} - I_{zz})/I_{xx} + d_\phi/I_{xx} - \ddot{\phi}_{des}$, with $\tilde{D}_\phi(t, X) > |\tilde{d}_\phi + \ddot{\phi}_{des}|$. The parameter α_ϕ is inside $\tilde{D}_\phi(t, X)$ and S_ϕ.

The second derivative of the position error, $e_\theta = \theta - \theta_{des}$, taking into account eq. (3.28), has the form

$$\ddot{e}_\theta = pr\frac{I_{zz} - I_{xx}}{I_{yy}} + \frac{1}{I_{yy}}\left(L_\theta + d_\theta\right) - \ddot{\theta}_{des},$$

The pitch control is

$$U_\theta = -\frac{b}{\delta_\theta}\tilde{D}_\theta(t,X)\frac{\lceil \dot{S}_\theta \rfloor^2 + S_\theta}{|\dot{S}_\theta|^2 + |S_\theta|},$$

where $\tilde{d}_\theta = \dot{\Delta}_\theta + \alpha_\theta(\delta_\theta L_\theta + \Delta_\theta) - (L_\theta \delta_\theta)/b - \dot{\delta}_\theta L_\theta - \theta L_\theta$, $\delta_\theta = 1/I_{yy}$, $\Delta_\theta = pr(I_{zz} - I_{xx})/I_{yy} + d_\theta/I_{yy} - \ddot{\theta}_{des}$, with $\tilde{D}_\theta(t, X) > |\tilde{d}_\theta + \ddot{\theta}_{des}|$. The parameter α_θ is inside $\tilde{D}_\theta(t, X)$ and S_θ

Recall that for ψ dynamics, the second derivative of the position error, $e_\psi = \psi - \psi_{des}$, has the form

$$\ddot{e}_\psi = pq\frac{I_{xx} - I_{yy}}{I_{zz}} + \frac{1}{I_{zz}}\left(L_\psi + d_\psi\right) - \ddot{\psi}_{des},$$

The yaw control is

$$U_\psi = -\frac{b}{\delta_\psi}\tilde{D}_\psi(t,X)\frac{\lceil \dot{S}_\psi \rfloor^2 + S_\psi}{|\dot{S}_\psi|^2 + |S_\psi|},$$

where $\tilde{d}_\psi = \dot{\Delta}_\psi + \alpha_\psi(\delta_\psi L_\psi + \Delta_\psi) - (L_\psi \delta_\psi)/b$, $\delta_\psi = 1/I_{zz}$, $\Delta_\psi = pq(I_{xx} - I_{yy})/I_{zz} + d_\psi/I_{zz} - \ddot{\psi}_{des}$, with $\tilde{D}_\psi(t, X) > |\tilde{d}_\psi + \ddot{\psi}_{des}|$. The parameter α_ψ which is inside $\tilde{D}_\psi(t, X)$ and S_ψ.

The proposed quasi-continuous SMC can be modified to counteract the chattering avoiding the saturation functions, and using the quasi-continuous function itself as an approximation of the sign on the plane, with a mild modification by adding a small constant $\varrho_i > 0$ in the denominator:

$$\frac{\lceil \dot{S}_i \rfloor^2 + S_i}{\varrho_i + |\dot{S}_i|^2 + |S_i|}, \quad \frac{\lceil \dot{e}_i \rfloor^2 + \alpha_i e_i}{\varrho_i + |\dot{e}_i|^2 + \alpha_i |e_i|}.$$

where ϱ_i is strictly related with accuracy. The smaller is ϱ_i the higher is the effort on the rotors, which results in a more accentuated oscillation of the control, but with a smaller convergence error, and *vice versa*. According to [Ding *et al.* 2016], a finite-time convergence of the system can be achieved in the ideal case, when $\varrho_i = 0$ and there is no measurement or implementation (digital) noises. In our case, since these restrictions are not satisfied, the convergence is assured with respect to a compact set around the desired trajectory. Then ϱ_i are tuned accordingly to achieve a trade-off between control oscillations and convergence error.

Concluding the previous preliminary study, the quasi-continuous control is suitable to be applied in quadrotor regulation taking into account rotor dynamics without modification of the sliding surfaces, which have been designed for the conventional SMC without the rotor dynamics (2.8). It means that the function sign can be approximated efficacely with quasi-continuous function in SMC for quadrotors, and its finite time stability is proven in [Ding *et al.* 2016], considering $\varrho_i = 0$. Then, considering the imposed quadrotor dynamics as in first order SMC design ($\dot{e}_i + \alpha_i e_i = 0$ for $i = x, y, z, \phi, \theta, \psi$), the final expressions of quasi-continuous SMC chosen for implementation and comparison are given below.

The control for z is given by

$$U_z = \frac{m}{\cos\theta\cos\phi}\Big(g - \ddot{z}_{des} + \alpha_z\dot{e}_z + \Big(\frac{1}{2}(\nu(X)^2 + 2\varrho(X) + \nu(X)\sqrt{\nu^2(X) + 4\varrho(X)}) + \frac{L_z}{b} - L_z\alpha_z + \varpi_z\Big)\frac{\lceil\dot{S}_z\rfloor^2 + S_z}{\varrho_z + |\dot{S}_z|^2 + |S_z|}\Big),$$

where $\varpi_z > |\dot{\Delta}_z + \dot{\delta}_z L_z|$ is a tuning parameter.

The controls for $i = x,\ y$ are given by

$$U_i = \frac{m}{U_z}\Big(-\Big(d_{xx} + 2d_{yy} + 2d_{zz} + \varpi_i\Big)\frac{\lceil\dot{e}_i\rfloor^2 + e_i}{\varrho_i + |\dot{e}_i|^2 + |e_i|} + \ddot{i}_{des} - \alpha_i\dot{e}_i\Big),$$

where $\varpi_i > 0$ is a tuning parameter with $\tilde{D}_i(t, X) > |d_{ie} + \ddot{i}_{des}|$.

The controls for roll, pitch and yaw respectively are given by

$$\begin{aligned}
U_\phi &= I_{xx}\left(-qr\frac{I_{yy} - I_{zz}}{I_{xx}} + \tilde{u}_\phi - \alpha_\phi\dot{e}_\phi + \ddot{\phi}_{des}\right),\\
U_\theta &= I_{yy}\left(-pr\frac{I_{zz} - I_{xx}}{I_{yy}} + \tilde{u}_\theta - \alpha_\theta\dot{e}_\theta + \ddot{\theta}_{des}\right),\\
U_\psi &= I_{zz}\left(-pq\frac{I_{xx} - I_{yy}}{I_{zz}} + \tilde{u}_\psi - \alpha_\psi\dot{e}_\psi + \ddot{\psi}_{des}\right),
\end{aligned}$$

where the auxiliary controls are defined as

$$\begin{aligned}
\tilde{u}_\phi &= -\frac{1}{I_{xx}}\frac{\lceil\dot{S}_\phi\rfloor^2 + S_\phi}{\varrho_\phi + |\dot{S}_\phi|^2 + |S_\phi|}\Big(\tilde{K}_\phi(f_{\phi1}(X) + D_{\phi1})\sqrt{|U_z|} + \bar{K}_\phi(f_{\phi2}(X) + D_{\phi2}) + \varpi_\phi + \alpha_\phi\delta_\phi L_\phi - \frac{\delta_\phi}{b}L_\phi\Big),\\
\tilde{u}_\theta &= -\frac{1}{I_{yy}}\frac{\lceil\dot{S}_\theta\rfloor^2 + S_\theta}{\varrho_\theta + |\dot{S}_\theta|^2 + |S_\theta|}\Big(\tilde{K}_\theta(f_{\theta1}(X) + D_{\theta1})\sqrt{|U_z|} + \bar{K}_\theta(f_{\theta2}(X) + D_{\theta2}) + \varpi_\theta + \alpha_\theta\delta_\theta L_\theta - \frac{\delta_\theta}{b}L_\theta\Big),\\
\tilde{u}_\psi &= -\frac{1}{I_{zz}}\frac{\lceil\dot{S}_\psi\rfloor^2 + S_\psi}{\varrho_\psi + |\dot{S}_\psi|^2 + |S_\psi|}\Big(\tilde{K}_\psi(f_{\psi1}(X) + D_{\psi1})\sqrt{|U_z|} + \bar{K}_\psi(f_{\psi2}(X) + D_{\psi2}) + \varpi_\psi + \alpha_\psi\delta_\psi L_\psi - \frac{\delta_\psi}{b}L_\psi\Big),
\end{aligned}$$

with $\varpi_i > |\dot{\Delta}_i - \dot{\delta}_i L_i|,\ i = \phi,\ \theta,\ \varpi_\psi > |\dot{\Delta}_\psi|$ tuning parameters.

Homogeneous differentiator [Perruquetti *et al.* 2008] (see the expression (B.1)) is used to estimate the value of the first derivative of the sliding surfaces $\dot{S}_i$.

3.5 Sliding mode control design summary

The generic scheme of hierarchical control algorithm presented above is given in Fig. 3.2. Desired angles are computed using the controls U_x, U_y (see Appendix B.4). Homogeneous differentiator (see Appendix B.6) is used to estimate the first and second derivatives of angles and the first derivative of the sliding surfaces. In the considered case the upper bound of matched disturbances depends non-linearly on the control itself, the system state vector and wind disturbances. The closed-loop system stability is ensured respecting the maximal value of ϕ, θ, D_x, D_y, D_z. The peculiarity of the proposed SMC approach design is that the control allows the UAV to remain stable even without any coupled external disturbance observer.

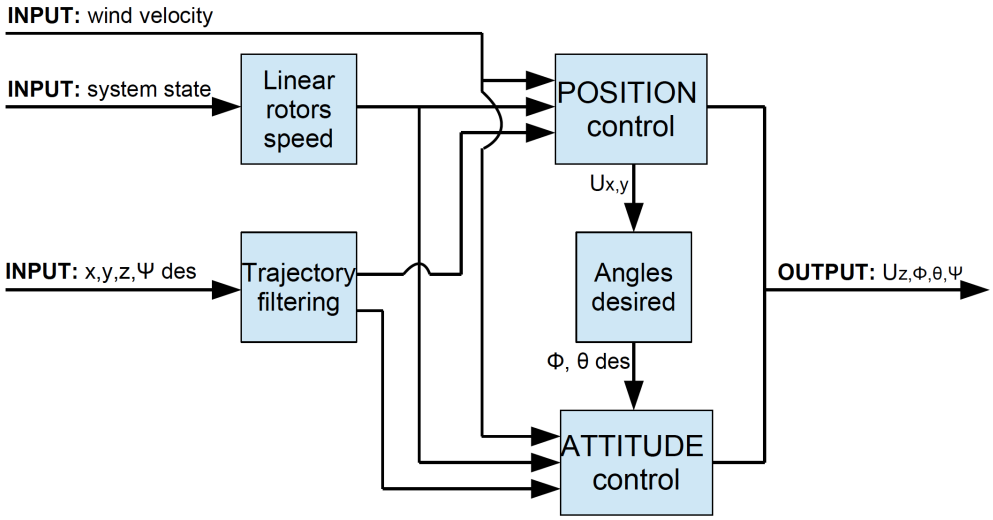

Figure 3.2: Hierachical SM control scheme

3.6 Conclusion

In this Chapter, robust sliding mode control approaches are used to stabilize a small quadrotor UAV under wind perturbations. Another approach is also introduced in Appendix C, where the H_∞ controller design is described, considering detailed quadrotor model influenced by wind speed. The main difference with SMC is that, H_∞ control is designed using linearized models of the nonlinear plant. Since these approaches are strictly related to the wind velocity, the coupling with a wind estimator, as in Fig. 3.3 is desired. In this way, by adapting the control amplitude, the regulator effort on the rotors can be reduced when it is possible. A good wind estimator is desired to reduce the uncertainty that will affect directly the performance of the proposed controllers, which is synthesized in the next Chapter 4. Extensive simulations, regarding also the control robustness against the model uncertainties and the influence of the varying wind velocity, are provided in Chapter 5.

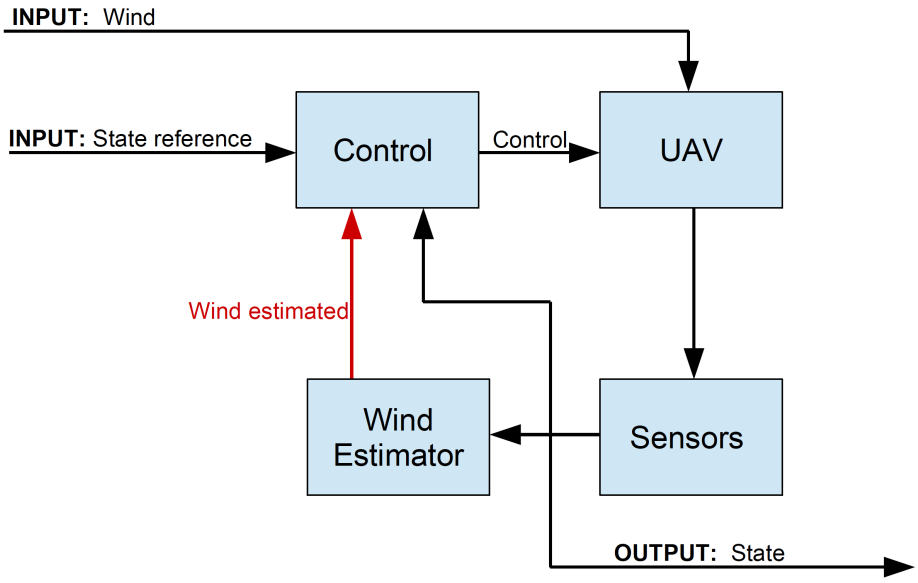

Figure 3.3: Control scheme having as input the wind estimates.

Chapter 4

Design of wind estimation algorithms

Contents

4.1 Introduction

A good control of a small UAV should have good robustness properties against unpredictable events such as wind perturbations and allow good flying performances. For this reason, wind estimates as input to the controllers designed in the previous Chapter could alleviate wind uncertainty constraints and leave more margin for performance aspects. The problem is that, the pressure sensors, such as aeroclinometer and Pitot tube, are not easily usable with rotary wing vehicles because inflow of the rotors interfere with atmospheric flow and light enough LIDAR based sensors were usually not available. Only recently, solutions to estimate the wind using new embedded wind sensors, mounted directly on-board on quadrotors, are studied in [Prudden *et al.* 2018, Palomaki *et al.* 2017]. However, the main drawback is that the on-board wind sensors use valuable payload that can be used for other scopes. Another approach to estimate the wind is related on an estimation software scheme (or an intelligent sensor), which has to be designed based on an adequate drone model and measurements available on quadrotors and on inertial tracking position system. According to the aerodynamic science, a nonlinear dependence of the UAV by the wind speeds u_w, v_w, w_w comes out (see Section 2.3), while the disturbances (external forces F_{Xaero}, F_{Yaero}, F_{Zaero} and moments L_{aero}, M_{aero}, N_{aero}) enter linearly in the drone equations. Hence, the problems of estimation of wind velocities and disturbances can be posed assuming them constant or slowly varying. To estimate constant and time-varying parameters, many algorithms were proposed recently in the literature, and two main groups can be identified:

1. The following works estimate the wind velocity and the disturbances using airspeed sensors. The work [Palanthandalam-Madapusi *et al.* 2008] develops an extension of the Kalman filter that provides an estimate of the unknown wind disturbance in micro-UAV scenario. The paper [Johansen *et al.* 2015] estimates the wind velocity, angle-of-attack and side-slip angle of a fixed-wing UAV using kinematic relationships with a Kalman Filter driven by a global navigation satellite system (GNSS) velocity measurement airspeed sensor, avoiding the need to know aerodynamic models or other aircraft parameters. The paper [Langelaan *et al.* 2011] describes a method for estimating wind velocity, rate of change of wind velocity, and wind gradient for small

and mini UAVs. In the work [Rysdyk 2006] an observer estimates wind data, which is used in the case where the UAV subjected to wind perturbation has to follow an object on the ground. [Qu *et al.* 2016a] uses airspeed sensor, roll angle, side-slip angle to estimate the wind speed for small fixed-wing UAV. [Rhudy *et al.* 2017] estimate the wind field based on four formulations, combining the data coming from the Pitot-static tube, the global position system (GPS), the inertial measurement unit (IMU) and the angle of attack and side-slip vanes. [Wenz & Johansen 2017] uses the IMU, the GNSS, and a Pitot-static tube, and other works are [Mondek & Hromčík 2015, Sun *et al.* 2018, Larrabee *et al.* 2014].

2. The following articles propose wind and disturbance estimations without the use of additional airspeed sensors. [Xing *et al.* 2017] estimates the shear wind vector at low altitude using IMU and GNSS module. [Pappu *et al.* 2017] uses a Kalman filter based gust identification technique for estimating wind gusts. The method described in [Lie & Gebre-Egziabher 2013] relies on measurements from GPS, an IMU, and a low-fidelity model of the aircraft's dynamics, which are fused using two cascaded extended Kalman filters. [Pendleton & Zhang 2017] estimate the wind using the drone model in hover flight. [Demitrit *et al.* 2017] addresses the problem of on-board wind estimation for a hovering vertical take-off and landing tail-sitter UAV. [Gonzalez-Rocha *et al.* 2017] use the kinematic particle model and dynamic particle model with identified motion model parameters. The article [Tomić & Haddadin 2014] presents a model-based method for external wrench estimation in flying robots based on proprioceptive sensors and the robot's dynamics model. [Tomić *et al.* 2016] describes two complementary methods using the estimation of the external wrench and the estimation of the propeller aerodynamic power. The paper [Yüksel *et al.* 2014] presents Lyapunov method for external forces and moments in flying robots. [Martínez-Vásquez *et al.* 2015] implements a linear observer with integral action for estimating the disturbance due a wind in hover flight mode. [Qu *et al.* 2016b] uses a decomposition of the hovering state equations to estimate the wind, and [Qu *et al.* 2017] extend the work using both IMU and a smoothing filter to reduce the effect of sensor noise. [Witte *et al.* 2016] uses a method based on on-board moving velocity sensors data such as five-hole and hot-wire probes. In [Benallegue *et al.* 2008], the high-order sliding mode observer is constructed as an estimator of the effect of the external disturbances in quadrotors such as wind and noise, using a differential global positioning system, a GPS, and a sonar altimeter. [Ali *et al.* 2016] uses the high order sliding mode differentiator to estimate the wind velocity for a fixed-wing UAV, using the rate of change of heading of the vehicle. Other works that use IMU and motion tracking system are [Rhudy *et al.* 2015, Sikkel *et al.* 2016, Xiang *et al.* 2016, Song *et al.* 2016, Waslander & Wang 2009, Neumann & Bartholmai 2015].

All the mentioned works perform the estimation using physical models with different assumptions based on the available sensors and valid in various projects. In our case, the objective is to develop an on-board algorithm for estimation of time-varying wind parameters by taking into account the detailed physical model described in the Chapter 2. Kalman Filter (KF) and Extended Kalman Filter (EKF) are both largely used in aerospace engineering community. However, they suffer of important issues. The optimality of KF is lost if there is any imperfection in the model, which is always the case in practical applications, and the current stability proofs for EKF are obtained under rather sever assumptions [Karvonen 2014]. The biggest problem is that they can only be used to assess the past steps filter stability, nothing determines if the filter will be stable in the future steps. Therefore, if the initial estimate is wrong, or if the process is modeled incorrectly, the filter may quickly diverge since there are not reliable stability conditions to check. In our case other methodologies are selected, designed specifically for the used quadrotor model representation. These sliding mode approaches provide stability conditions, that depend only on the dynamic and measurement model functions and the magnitude of noise terms, with a lower computational complexity than

the KFs. The design objectives include the time convergence optimization, robustness to measurement noises and aerodynamic coefficient uncertainties improvement, and in order to ensure a guaranteed convergence. It is supposed that the estimation algorithm can use IMU (accelerometer, gyroscope) sensors augmented with a motion tracking system and rotors rotational velocity sensors.

4.2 Decomposition in known and unknown terms

Accelerometers measure the external forces except gravity. So, quadrotor linear velocities (u, v, w) together with their derivatives (accelerations) are provided by the on-board accelerometer, which measures directly

$$\tilde{\Delta}_a(X) = \Delta_a(X) + \varepsilon_a,$$

where ε_a is a bounded measurement noise of the accelerometer, and

$$\Delta_a(X) = \begin{bmatrix} \Delta_{au}(X) \\ \Delta_{av}(X) \\ \Delta_{aw}(X) \end{bmatrix} = \begin{bmatrix} \dot{u} \\ \dot{v} \\ \dot{w} \end{bmatrix} + \begin{bmatrix} p \\ q \\ r \end{bmatrix} \times \begin{bmatrix} u \\ v \\ w \end{bmatrix} - \begin{bmatrix} -g \sin\theta \\ g \cos\theta \sin\phi \\ g \cos\theta \cos\phi \end{bmatrix}. \tag{4.1}$$

From the gyroscopes, which measure the rotational velocity in body frame with respect to the Earth, the other state coordinates are measured

$$\tilde{\Delta}_g(X) = \Delta_g(X) + \varepsilon_g, \quad \Delta_g(X) = \begin{bmatrix} p & q & r \end{bmatrix}^T,$$

where ε_g is the measurement noise generated by gyroscope. IMU sensor is augmented with ground based cameras, used to estimate $(u,\ v,\ w,\ \phi,\ \theta)$ in coupling with gyroscope and accelerometer and making the drone observable with respect to the inertial frame.

Following the structure of measured information, another decomposition can be performed by splitting the dynamic equations in two parts

$$\begin{bmatrix} \Delta_a(X) \\ \dot{\Delta}_g(X) \end{bmatrix} = f_0(X, U, \omega) + \Omega(\omega) d_w,$$

where f_0 is supposed to be known (its expression is detailed below), and Ω is a time-varying regressor matrix related to the wind speed d_w, which has to be estimated. In order to derive the expressions of f_0 and Ω, the translational rotor velocities in the body frame are computed from eq. (2.5).

Remark 1 *Nonlinear terms, which represent a small part of rotor rolling torque R_m for roll*

$$+sign\left(\omega_j\right) \frac{1}{2} \rho A R K_z \left(u_j - u_w\right)\left(w_j - w_w\right),$$

and for pitch

$$+sign\left(\omega_j\right) \frac{1}{2} \rho A R K_z \left(v_j - v_w\right)\left(w_j - w_w\right),$$

and a small part of rotor torque Q for yaw dynamics

$$-sign\omega_j \rho A R \left(\frac{\sigma C_{D0} \left(\left(u_j - u_w\right)^2 + \left(v_j - v_w\right)^2 \right)}{8} - \frac{4 K_z^2 \left(w_j - w_w\right)^2}{\sigma a} \right)$$

are neglected. These restrictions can be accepted for low UAV velocity and low wind velocity.

After these considerations, the system can be rewritten in element-wise form as

$$\begin{bmatrix} \Delta_{au}(X) \\ \Delta_{av}(X) \\ \Delta_{aw}(X) \\ \dot{p} \\ \dot{q} \\ \dot{r} \end{bmatrix} = \begin{bmatrix} f_{0u}(X,\omega) \\ f_{0v}(X,\omega) \\ f_{0w}(X,U,\omega) \\ f_{0p}(X,U,\omega) \\ f_{0q}(X,U,\omega) \\ f_{0r}(X,U,\omega) \end{bmatrix} + \begin{bmatrix} \Omega_u(\omega) \\ \Omega_v(\omega) \\ \Omega_w(\omega) \\ \Omega_p(\omega) \\ \Omega_q(\omega) \\ \Omega_r(\omega) \end{bmatrix} d_w, \tag{4.2}$$

where $f_0 : \mathbb{R}^{14} \to \mathbb{R}^6$ and $\Omega : \mathbb{R}^4 \to \mathbb{R}^{6\times 3}$.

In the following, the argument dependence of the functions f_0 and Ω is avoided to make the presentation more compact.

The u dynamics is rewritten as $\Delta_{au} = f_{0u} + \Omega_u d_w$, where

$$f_{0u} = -\frac{1}{m}\rho ARK_D \sum u_j|\omega_j|, \quad \Omega_u d_w = \frac{1}{m}\rho ARK_D u_w \sum |\omega_j|.$$

The v dynamics is rewritten as $\Delta_{av} = f_{0v} + \Omega_v d_w$, where

$$f_{0v} = -\frac{1}{m}\rho ARK_D \sum v_j|\omega_j|, \quad \Omega_v d_w = \frac{1}{m}\rho ARK_D v_w \sum |\omega_j|.$$

The w dynamics is rewritten as $\Delta_{aw} = f_{0w} + \Omega_w d_w$, where

$$f_{0w} = -\frac{U_w}{m} - \frac{1}{m}\rho ARK_z \sum w_j|\omega_j|, \quad \Omega_w d_w = \frac{1}{m}\rho ARK_z w_w \sum |\omega_j|.$$

The roll dynamics is rewritten as $\dot{p} = f_{0p} + \Omega_p d_w$, where

$$f_{0p} = \frac{I_{yy} - I_{zz}}{I_{xx}} qr + \frac{U_p}{I_{xx}} + \frac{1}{I_{xx}} \sum_{j=1}^{4} \left(\omega_j \rho AR^2 u_j \frac{\sigma a}{2} \left(\frac{\theta_0}{3} - \frac{\lambda_{stat}}{4} \right) + |\omega_j| \rho AR \left(hK_D v_j - lK_z w_j \mathrm{s}_j \right) \right),$$

$$\Omega_p d_w = \frac{1}{I_{xx}} \sum_{j=1}^{4} \left(-\omega_j \rho AR^2 u_w \frac{\sigma a}{2} \left(\frac{\theta_0}{3} - \frac{\lambda_{stat}}{4} \right) + |\omega_j| \rho AR \left(-hK_D v_w + lK_z w_w \mathrm{s}_j \right) \right).$$

The pitch dynamics is rewritten as $\dot{q} = f_{0q} + \Omega_q d_w$, where

$$f_{0q} = \frac{I_{zz} - I_{xx}}{I_{yy}} pr + \frac{U_q}{I_{yy}} + \frac{1}{I_{yy}} \sum_{j=1}^{4} \left(\omega_j \rho AR^2 v_j \frac{\sigma a}{2} \left(\frac{\theta_0}{3} - \frac{\lambda_{stat}}{4} \right) + |\omega_j| \rho AR \left(lK_z w_j \mathrm{c}_j - hK_D u_j \right) \right),$$

$$\Omega_q d_w = \frac{1}{I_{yy}} \sum_{j=1}^{4} \left(-\omega_j \rho AR^2 v_w \frac{\sigma a}{2} \left(\frac{\theta_0}{3} - \frac{\lambda_{stat}}{4} \right) + |\omega_j| \rho AR \left(hK_D u_w - lK_z w_w \mathrm{c}_j \right) \right).$$

The yaw dynamics is rewritten as $\dot{r} = f_{0r} + \Omega_r d_w$, where

$$f_{0r} = \frac{I_{xx} - I_{yy}}{I_{zz}} pq + \frac{U_r}{I_{zz}} + \frac{1}{I_{zz}} \sum_{j=1}^{4} \left(\omega_j \rho AR^2 K_z w_j \left(\frac{2\theta_0}{3} - 2\lambda_{stat} \right) - |\omega_j| \rho lARK_D \left(v_j \mathrm{c}_j - u_j \mathrm{s}_j \right) \right),$$

$$\Omega_r d_w = \frac{1}{I_{zz}} \sum_{j=1}^{4} \left(-\omega_j \rho AR^2 K_z w_w \left(\frac{2\theta_0}{3} - 2\lambda_{stat} \right) - |\omega_j| \rho lARK_D \left(-v_w \mathrm{c}_j + u_w \mathrm{s}_j \right) \right).$$

Using the provided UAV model, it is possible to estimate the wind with three linear dynamics and a simple inversion, since $(\dot{u}, \dot{v}, \dot{w})$ are linearly dependent on wind and we already have terms proportional to (θ, ϕ) that consider the rotational behavior of the UAV subjected to external wind. The estimation with the three rotational dynamics adds redundant equations which can be used in the following fusion algorithm to improve the estimation and to reduce the bound of the incertitude. However, the rotational dynamics include the inertia matrix which is rather complicated to precisely estimate, so the measurements are subjected to a low accuracy.

To design the algorithm let us consider the following system

$$\begin{cases} \begin{bmatrix} \Delta_a \\ \dot{\Delta}_g \end{bmatrix} = \begin{bmatrix} f_{0a} \\ f_{0g} \end{bmatrix} + \begin{bmatrix} \Omega_a \\ \Omega_g \end{bmatrix} d_w \\ \begin{bmatrix} \tilde{\Delta}_a \\ \tilde{\Delta}_g \end{bmatrix} = \begin{bmatrix} \Delta_a + \varepsilon_a \\ \Delta_g + \varepsilon_g \end{bmatrix} \end{cases},$$

where the variables $\tilde{\Delta}_a$ and $\tilde{\Delta}_g$ are available for measurements, $f_{0a} = [f_{0u}\ f_{0v}\ f_{0w}]^T$, $f_{0g} = [f_{0p}\ f_{0q}\ f_{0r}]^T$, $\Omega_a = [\Omega_u\ \Omega_v\ \Omega_w]^T$ and $\Omega_g = [\Omega_p\ \Omega_q\ \Omega_r]^T$ are the vector and matrix variables, whose values are functions of measured variables X, U and ω.

The simplest estimation problem is to find an unknown input from the state measurements, where the input and the state are related by a first order differential equation using various differentiation schemes, as illustrated in [Stotsky & Kolmanovsky 2001]. However, to avoid unnecessary state differentiation, three sub-algorithms can be considered: one suitable for linear dynamics given by the accelerometer, the others for rotational dynamics given by the gyroscope.

The following algorithms are designed assuming the availability of the estimation of (u, v, w) from eq. (4.1), and (ϕ, θ) with their derivatives. For simplicity, in theoretical analysis we supposed that these values are reconstructed exactly, but for simulation a state measurement noise has been added modeling this effect. The algorithms are based on the following hypothesis (we will switch between them depending on the applied approach):

Assumption 1 *The measurement noises are absent ($\varepsilon_a = 0$ and $\varepsilon_g = 0$) and the wind velocity is constant ($\dot{d}_w = 0$).*

Assumption 2 *The measurement noises ε_a, ε_g and the wind acceleration $\dot{d}_w$ are bounded signals*

$$\sup_{t\geq 0} \max\{|\varepsilon_a(t)|, |\varepsilon_g(t)|\} \leq \bar{\varepsilon}, \quad \sup_{t\geq 0} |\dot{d}_w(t)| \leq \bar{\dot{d}}_w,$$

for some $\bar{\varepsilon} > 0$ and $\bar{\dot{d}}_w > 0$.

Assumption 3 *The matrix Ω_g is bounded and persistently excited (PE) for all $t \geq 0$ (see [Rios et al. 2017] for a definition of this property [1]).*

4.3 Estimation based on translational dynamics

Define the predicted acceleration:

$$\hat{\Delta}_a = f_{0a} + \Omega_a \hat{d}_w,$$

[1] The Lebesgue measurable and square integrable matrix function $R : \mathbb{R} \to \mathbb{R}^{m\times n}$ is PE if there are $\ell > 0$, $\xi > 0$ such that $\int_t^{t+\ell} R(s)R(s)^T ds \geq \xi I_m$ for all $t \geq 0$, where I_m is an identity square matrix of dimension m.

which is based on the estimate $\hat{d}_w$ of the wind velocity derived below; and introduce the error between the measured state acceleration $\tilde{\Delta}_a$ and the predicted one as follows

$$e_a = \tilde{\Delta}_a - \hat{\Delta}_a = \Omega_a(d_w - \hat{d}_w) + \varepsilon_a,$$

where ε_a is the bounded sensors noise for the accelerometers. According to [Rios *et al.* 2017], the following finite-time estimation algorithm can be introduced

$$\dot{\hat{d}}_w = \gamma_a \, \Omega_a^T \lceil e_a \rfloor^{\alpha_a}, \quad 0 < \alpha_a < 1, \, \gamma_a \gg 0, \tag{4.3}$$

where $\lceil \cdot \rfloor^{\alpha_a} = |\cdot|^{\alpha_a} \text{sign}(\cdot)$ is understood element-wise. The Lyapunov function for this estimation algorithm can be selected in the following form

$$V = \frac{1}{2\gamma_a} |d_w - \hat{d}_w|^2,$$

and, with (4.3), its first derivative is:

$$\begin{aligned} \dot{V} =& \frac{1}{\gamma_a}(d_w - \hat{d}_w)^T(\dot{d}_w - \dot{\hat{d}}_w) = -(d_w - \hat{d}_w)^T \Omega_a^T \lceil e_a \rfloor^{\alpha_a} + \frac{1}{\gamma_a}(d_w - \hat{d}_w)^T \dot{d}_w \\ =& -(d_w - \hat{d}_w)^T \Omega_a^T \lceil \Omega_a(d_w - \hat{d}_w) + \varepsilon_a \rfloor^{\alpha_a} + \frac{1}{\gamma_a}(d_w - \hat{d}_w)^T \dot{d}_w. \end{aligned}$$

From the simplified quadrotor dynamics

$$\Omega_a = \frac{1}{m} \rho A R \sum |\omega_j| \begin{bmatrix} K_D & 0 & 0 \\ 0 & K_D & 0 \\ 0 & 0 & K_z \end{bmatrix},$$

thus, since for a flying drone $\sum |\omega_j| > 0$, this is an invertible matrix, and according to [Rios *et al.* 2017] there exist two constants $\nu_{a1} > 0$, $\nu_{a2} > 0$ such that

$$\dot{V} \leq -\nu_{a1} V^{\frac{\alpha_a + 1}{2}}, \quad \forall |d_w - \hat{d}_w| > \nu_{a2} \max\{\bar{\dot{d}}_w, \bar{\varepsilon}\}.$$

The following results have been proven:

Theorem 2 *Let Assumption 1 be satisfied, then the value d_w can be estimated in a finite time by (4.3).*

Theorem 3 *Let Assumption 2 be satisfied, then for (4.3) there exist $T(\bar{\dot{d}}_w, \bar{\varepsilon}) > 0$ and $\nu_{a2} > 0$ such that*

$$|d_w(t) - \hat{d}_w(t)| \leq \nu_{a2} \max\{\bar{\dot{d}}_w, \bar{\varepsilon}\} \quad \forall t \geq T(\bar{\dot{d}}_w, \bar{\varepsilon}).$$

Therefore, the system (4.3) is globally finite-time stable, and the parameter identification error converges to a neighborhood of the origin that depends on the upper bound of the noise $\bar{\varepsilon}$, maximal amplitude of acceleration of the wind $\bar{\dot{d}}_w$, the choice of the gain γ_a and the parameter α_a.

4.4 Estimation based on angular dynamics

Wind estimation problem for rotational dynamics is slightly different from the linear one because the state vector is measured and not its derivative is provided by the sensor, hence an adaptive observer, which estimates the state and the wind simultaneously, has to be also designed. To this end, first, the adaptive observer equations can be written as follows

$$\begin{aligned}\dot{\hat{\Delta}}_g &= f_{0g} + \Omega_g \hat{d}_w + \ell_g \text{sign}(\tilde{\Delta}_g - \hat{\Delta}_g),\\ \dot{\hat{d}}_w &= \gamma_g \Omega_g^T (\tilde{\Delta}_g - \hat{\Delta}_g),\end{aligned} \tag{4.4}$$

where $\hat{\Delta}_g$ is an estimate of the state vector Δ_g, $\hat{d}_w$ is again an estimate of the vector of wind velocities d_w; $\ell_g > 0$ and $\gamma_g \gg 0$ are tuning parameters. For this observer let us consider the following Lyapunov function

$$V = \frac{1}{2}\left(|\Delta_g - \hat{\Delta}_g|^2 + \frac{1}{\gamma_g}|d_w - \hat{d}_w|^2\right),$$

which for (4.4), and under Assumption 1, admits the following derivative in time

$$\dot{V} = -\ell_g |\Delta_g - \hat{\Delta}_g|.$$

Consequently, using the standard arguments (see [Rios *et al.* 2017]), the function V is bounded for all $t \geq 0$ and the state estimation error $\Delta_g - \hat{\Delta}_g$ converges asymptotically to the origin. The wind estimation error $d_w - \hat{d}_w$ converges to the origin due persistence of excitation in Ω_g. Moreover, let us consider an auxiliary Lyapunov function

$$W = \frac{1}{2}|\Delta_g - \hat{\Delta}_g|^2,$$

whose derivative admits an upper bound estimate

$$\dot{W} \leq |\Delta_g - \hat{\Delta}_g|\left(|\Omega_g(d_w - \hat{d}_w)| - \ell_g\right),$$

thus, if ℓ_g is selected sufficiently big and $|\Omega_g(d_w - \hat{d}_w)| - \ell_g < -\nu_g$ for some $\nu_g > 0$ (as it was shown above the signal $\Omega_g(d_w - \hat{d}_w)$ is bounded), then

$$\dot{W} \leq -\nu_g \sqrt{2W}$$

and the state estimation error $\Delta_g - \hat{\Delta}_g$ has a finite-time rate of convergence, and the error $d_w - \hat{d}_w$ inherits the same property. The following result has been obtained (the induced norm of a matrix Ω_g is denoted by $\|\Omega_g\|_2$):

Theorem 4 *Let assumptions 1 and 3 be satisfied, and there is a known bound $\bar{d}_w > 0$ such that $|d_w| \leq \bar{d}_w$, then for $\ell_g > 2\|\Omega_g\|_2 \bar{d}_w$ the estimate $\hat{d}_w$ in (4.4) converges to the value of d_w in a finite time.*

The main issue with the algorithm (4.4) is hidden in rather strong restrictions imposed in Assumption 1, which we need to substantiate the convergence. Another algorithm based on less restrictive hypothesis can be obtained by the price of an augmented computational complexity as the following one:

$$\begin{aligned}\dot{\hat{\Delta}}_g &= f_{0g} + \Omega_g \hat{d}_w + \ell'_g(\tilde{\Delta}_g - \hat{\Delta}_g) + \Xi \dot{\hat{d}}_w,\\ \dot{\Xi} &= -\ell'_g \Xi + \Omega_g,\\ \dot{\hat{d}}_w &= \gamma'_g \Xi^T \left\lceil \tilde{\Delta}_g - \hat{\Delta}_g \right\rfloor^{\alpha'_g},\end{aligned} \tag{4.5}$$

where $\hat{\Delta}_g$ and $\hat{d}_w$ as before are the estimates of Δ_g and d_w, respectively; $\ell'_g > 0$, $\alpha'_g \in (0,1)$ and $\gamma'_g \gg 0$ are design parameters; Ξ is an auxiliary matrix variable having the dimension of Ω_g (obviously it is always bounded for bounded Ω_g and $\ell'_g > 0$). In order to clarify the stability and robustness properties of this estimation scheme let us introduce three estimation errors

$$e_\Delta = \Delta_g - \hat{\Delta}_g, \quad e_d = d_w - \hat{d}_w, \quad \delta = e_\Delta - \Xi e_d,$$

which have the following dynamics:

$$\begin{aligned}
\dot{e}_\Delta &= -\ell'_g(e_\Delta + \varepsilon_g) + \Omega_g e_d - \gamma'_g \Xi\Xi^T \left\lceil e_\Delta + \varepsilon_g \right\rfloor^{\alpha'_g}, \\
\dot{\delta} &= -\ell'_g(\delta + \varepsilon_g) - \Xi\dot{d}_w, \\
\dot{e}_d &= -\gamma'_g \Xi^T \left\lceil \Xi e_d + \delta + \varepsilon_g \right\rfloor^{\alpha'_g} + \dot{d}_w.
\end{aligned}$$

Introduce the following additional hypothesis:

Assumption 4 *The minimum singular value of the matrix variable $\Xi(t) \in \mathbb{R}^{3\times 3}$ is bigger than σ_Ξ for all $t \geq 0$.*

The last condition on Ξ can be ensured by a proper initialization and the same property of Ω_g (Assumption 3). Under this assumption boundedness of all estimation errors can be proven analyzing consequently the independent Lyapunov functions $V(\delta)$, $V(e_d)$ and $V(e_\Delta)$, where

$$V(x) = 0.5x^T x.$$

Indeed under Assumption 2, first, let us analyze behavior of V for the dynamics of δ, where all inputs ($\dot{d}_w$ and ε_g) are bounded:

$$\dot{V} \leq -0.5\ell'_g \delta^T \delta + \frac{1}{2\ell'_g}|\Xi\dot{d}_w + \ell'_g\varepsilon_g|^2,$$

which implies boundedness of $\delta(t)$. Second, for the dynamics of e_d:

$$\dot{V} \leq -\gamma'_g e_d^T \Xi^T \left\lceil \Xi e_d + \delta + \varepsilon_g \right\rfloor^{\alpha'_g} + e_d^T \dot{d}_w,$$

and assume that $|\Xi e_d| > |\delta + \varepsilon_g|$ (which is true if $|e_d| > \sigma_\Xi^{-1}|\delta + \varepsilon_g|$) then

$$e_d^T \Xi^T \left\lceil \Xi e_d + \delta + \varepsilon_g \right\rfloor^{\alpha'_g} = \sum_{i=1}^{3} |(\Xi e_d)_i||(\Xi e_d)_i + \delta_i + \varepsilon_{gi}|^{\alpha'_g} \geq 2^{\alpha'_g - 1} \sum_{i=1}^{3} |(\Xi e_d)_i|^{\alpha'_g + 1} + |(\Xi e_d)_i||\delta_i + \varepsilon_{gi}|^{\alpha'_g},$$

$$e_d^T \dot{d}_w \leq \frac{1}{\alpha'_g + 1}|c\Xi e_d|^{\alpha'_g + 1} + \frac{\alpha'_g}{\alpha'_g + 1}|c^{-1}\Xi^{-1}\dot{d}_w|^{1+\alpha'^{-1}_g},$$

where $c = 2^{\alpha'^{-2}_g}\gamma'_g > 0$, and Jensen's and Young's inequalities have been used. Thus

$$\dot{V} \leq -2^{\alpha'^{-2}_g}\gamma'_g|\Xi e_d|^{\alpha'_g + 1} + \frac{\alpha'_g}{\alpha'_g + 1}|c^{-1}\Xi^{-1}\dot{d}_w|^{1+\alpha'^{-1}_g},$$

is satisfied for $|\Xi e_d| > |\delta + \varepsilon_g|$, or equivalently

$$\dot{V} \leq -2^{\alpha'^{-3}_g}\gamma'_g|\Xi e_d|^{\alpha'_g + 1} \leq -2^{\frac{\alpha'_g - 7}{2}}\gamma'_g \sigma_\Xi^{1+\alpha'_g} V^{\frac{\alpha'_g + 1}{2}},$$

provided that $|e_d| > \sigma_\Xi^{-1} \max\{|\delta + \varepsilon_g|, \sqrt[\alpha'_g+1]{\frac{2\alpha'_g}{\alpha'_g+1} c^{-2-\alpha'^{-1}_g} |\Xi^{-1}\dot{d}_w|^{1+\alpha'^{-1}_g}}\}$. Next, again boundedness of all inputs (δ, ε_g and $\dot{d}_w$) implies the same property for e_d. Finally, for the dynamics of e_Δ:

$$\dot{V} \leq -\ell'_g e_\Delta^T e_\Delta + e_\Delta^T(\Omega_g e_d + \ell'_g \varepsilon_g) - \gamma'_g e_\Delta^T \Xi\Xi^T \left\lceil e_\Delta + \varepsilon_g \right\rfloor^{\alpha'_g},$$

and assuming that $|e_\Delta| > \sigma_\Xi^{-1}|\varepsilon_g|$ we obtain

$$\dot{V} \leq -0.5\ell'_g e_\Delta^T e_\Delta + \frac{1}{2\ell'_g}|\Omega_g e_d + \ell'_g \varepsilon_g|^2 \quad \text{or equivalently} \quad \dot{V} \leq -0.25\ell'_g e_\Delta^T e_\Delta,$$

provided that $|e_\Delta| > \max\{\sigma_\Xi^{-1}|\varepsilon_g|, \frac{\sqrt{2}}{\ell'_g}|\Omega_g e_d + \ell'_g \varepsilon_g|\}$, therefore e_Δ is also bounded and the following result has been proven:

Theorem 5 *Let assumptions 2 and 4 be satisfied, then in (4.5) there exists $T > 0$ such that*

$$|e_d(t)| \leq \varrho(\bar{\varepsilon}, \bar{\dot{d}}_w), \quad |e_\Delta(t)| \leq \max\{\sigma_\Xi^{-1}\bar{\varepsilon}, \frac{\sqrt{2}}{\ell'_g}\left(\|\Omega_g\|_2 \varrho\left(\bar{\varepsilon}, \bar{\dot{d}}_w\right) + \ell'_g \bar{\varepsilon}\right)\},$$

for all $t \geq T$, where

$$\varrho(\bar{\varepsilon}, \bar{\dot{d}}_w) = \sigma_\Xi^{-1} \max\{\frac{2}{\ell'_g}\|\Xi\|_2 \bar{\dot{d}}_w + 3\bar{\varepsilon}, \sqrt[\alpha'_g+1]{c' \bar{\dot{d}}_w^{1+\alpha'^{-1}_g}}\}; \quad c' = \frac{2\alpha'_g}{\alpha'_g+1} c^{-2-\alpha'^{-1}_g} \sigma_\Xi^{-1-\alpha'^{-1}_g}.$$

If $\delta = \bar{\varepsilon} = \bar{\dot{d}}_w = 0$, then a finite-time convergence of $\hat{d}_w$ to d_w is substantiated.

4.5 Estimation based on fusion algorithm

As we can conclude, the restrictions used for the estimation algorithms are not the same. Algorithm (4.4) is obtained in the noise-free and constant wind conditions. Despite the theoretical result this algorithm also possesses some noise filtering abilities, however since the simulations show that a good estimation for varying wind velocities with high frequencies is not achieved, it is preferable to avoid it in the fusion algorithm. The estimation schemes (4.3), (4.5) assume both that the noise and wind derivative are bounded signals (note that the worst-case upper bounds on the estimation errors are also obtained for these algorithms). Thus, some fusion of these last solutions is desirable. To this end, let us define the estimates of d_w generated by the algorithms (4.3), and (4.5), as $\hat{d}_w^i$ for $i = 1, 2$ respectively. Denote the errors as $\upsilon_1(t) = e_a(t)$ for (4.3) and $\upsilon_2(t) = \tilde{\Delta}_g(t) - \hat{\Delta}_g(t)$ for (4.5). Then

$$\hat{d}_w^{\text{fusion}}(t) = \frac{\sum_{i=1}^2 e^{-\kappa_i \upsilon_i^2(t)} \hat{d}_w^i(t)}{\sum_{i=1}^2 e^{-\kappa_i \upsilon_i^2(t)}} \tag{4.6}$$

is the united estimate of d_w from all the estimation algorithms, and $\kappa_i > 0$ for $i = 1, 2$ are tuning parameters. Fusion algorithm has the estimation error, in the worst case, given by the maximum of the two estimation errors for the algorithms (4.3) and (4.5):

$$|e_d(t)| \leq \max\{\sigma_\Xi^{-1} \max\{\frac{2}{\ell'_g}\|\Xi\|_2 \bar{\dot{d}}_w + 3\bar{\varepsilon}_g, \sqrt[\alpha'_g+1]{\frac{2\alpha'_g}{\alpha'_g+1}(2^{\alpha'_g-2}\gamma'_g)^{-2-\alpha'^{-1}_g} \sigma_\Xi^{-1-\alpha'^{-1}_g} \bar{\dot{d}}_w^{1+\alpha'^{-1}_g}}\}, \nu_{a2} \max\{\bar{\dot{d}}_w, \bar{\varepsilon}_a\}\}.$$

4.6 Conclusion

This Chapter can be summarized as follow. First, the proposed wind estimation algorithms take the advantage of a detailed quadrotor aerodynamic model, and they are strictly related to the accuracy of the drone model representation and the identified aerodynamic coefficients. Second, the estimation accuracy is related to the different assumptions on the maximal amplitude of the sensors' noise and of the first derivative of the wind velocity.

The proposed estimation algorithms, (4.3), (4.4) and (4.5), require as input an estimate of (u, v, w, θ, ϕ), which are generally obtained fusing the accelerometric and gyroscopic measurements available on-board, and ground measurements such as camera tracking. The variables (u, v, w) can be obtained from the accelerometer in eq. (4.1). Fig. 4.1 shows the scheme of the proposed algorithms and how the translation to earth frame can be done.

The real-time estimation of the wind can be coupled with an advanced control, as in Fig. 3.3, to improve the flight safety of small drones in a perturbing environment. An extended study regarding the influence of the aerodynamic coefficients incertitude, the influence of the sensors' noise, and the influence of the characteristics of the wind profile is illustrated in the Chapter 5.

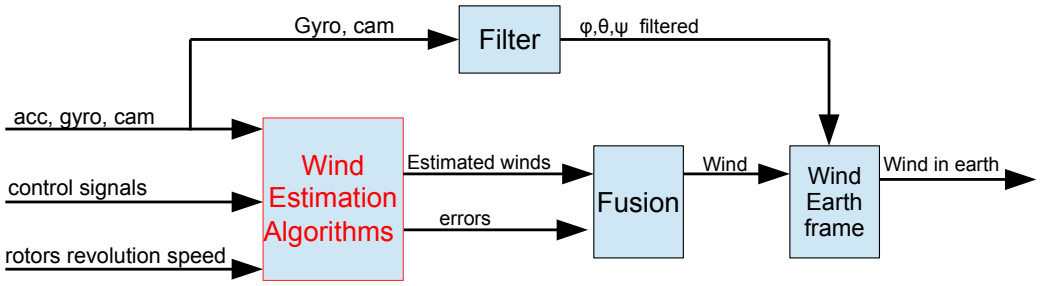

(a)

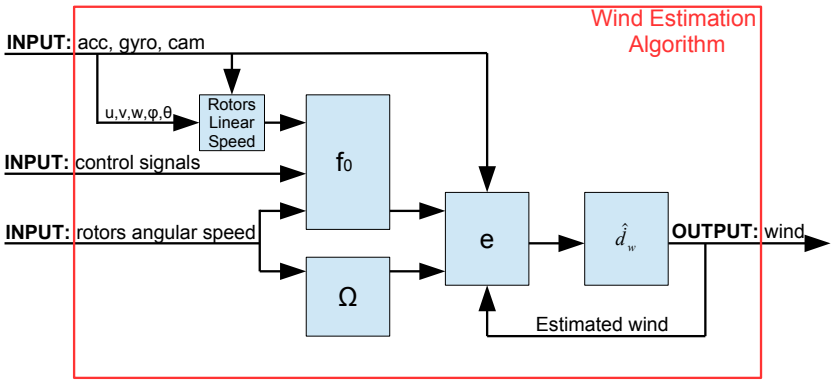

(b)

Figure 4.1: Conceptual scheme of: (a) translation of wind estimates to earth frame; (b) proposed wind estimation algorithm.

Chapter 5

Validation of the controllers and wind estimation

Contents

5.1 Introduction

Experimental validation was carried out at ONERA. The workstation, the lab and the drones are described in Section 1.4, and they were available from the last year. Then, after that the workstation was fully mounted, that the requested additional software was implemented and validated, it was possible to start partial in-door experiments. In particular, the experiments are 3D trajectory tracking using PID control (see Appendix B.7 for the mathematical formulation), and the response of quasi-continuous SMC, holding the UAV at non zero attitude from the reference hover position. The preliminary extensive simulations, using the built Simulink Toolbox (see Appendix D), are provided to prepare safely the full flight experimental stage. Since during this PhD research, 2 quadrotors were used: Parrot Ar Drone 2.0, and open-source X4-MaG Drone, simulations and experiments are divided between these two types of drones. Simulations on Parrot are used to illustrate the contributions of SMC techniques and estimation algorithms applied to realistic UAV. Then, the X4-MaG is used to partially validate these approaches.

The presentation is as follows. First, the set of parameters of the two quadrotors are introduced. Second, wind estimation algorithms are tested in simulations using a standard PID control. Then, the tuning process for the

SMC algorithms, using the results coming from the wind estimation experiments, is illustrated. Last, preliminary experiments and validations of the qc-SMC are described.

5.2 Characterization of the quadrotors

The quadrotor parameters are illustrated in Table 5.1 for the Parrot, and in Table 5.2 for the X4-MaG. The aerodynamic identification experiments were carried out at L2 wind tunnel for the X4-MaG. Tests are made changing the angle of attack, wind speed and rotor rotation rates. The drone was mounted on a sting through "Balance Φ12 n.6" in order to measure the resultant aerodynamic forces and moments acting on the quadrotor. Forces and moments were measured and simplified aerodynamics can be identified together with their coefficients. The identification process is described in internal reports at ONERA and partially illustrated in [Planckaert & Coton 2015]. As recall, from Chapter 2, quadrotor model with two different levels of detail are used. The simpler quadrotor model coming from the identification work, to build the algorithms; and the full quadrotor model, coming from the complete aerodynamic equations in eq. (2.9).

Table 5.1: Parrot drone parameters

Par.	R	l	h	g	θ_0	m	I_{xx}
Val.	0.1	0.185	−0.025	9.81	23.9	0.472	0.00356
Unit	m	m	m	m/s^2	deg	Kg	$Kg.m^2$
Par.	I_{yy}	I_{zz}	ρ	σ	a	C_{D0}	λ_{stat}
Val.	0.00402	0.00712	1.25	0.111	4.6542	2.15	0.1056
Unit	$Kg.m^2$	$Kg.m^2$	Kg/m^3				
Par.	$C_{T\,stat}$	K_D	K_z	b			
Val.	0.0223	0.06	0.09	0.1			
Unit							

Table 5.2: X4-MaG drone parameters

Par.	R	l	h	g	θ_0	m	I_{xx}
Val.	0.0635	0.1	−0.0303	9.81	10	0.362	0.0015
Unit	m	m	m	m/s^2	deg	Kg	$Kg.m^2$
Par.	I_{yy}	I_{zz}	ρ	σ	a	C_{D0}	λ_{stat}
Val.	0.0015	0.003	1.25	0.1604	4.1778	0.2	0.0524
Unit	$Kg.m^2$	$Kg.m^2$	Kg/m^3				
Par.	$C_{T\,stat}$	K_D	K_z	b			
Val.	0.0055	0.034	0.09	0.02			
Unit							

5.3 Objectives and general constraints

Designed control and estimation algorithms are tuned based on the following objectives, constraints, and hypotheses. The objectives are:

- Stability of the quadrotor;
- The position error must be bounded for sinusoid trajectories having limited maximal frequency;
- Estimation algorithms must be as much accurate as possible.

The constraint is:

- Control inputs and state vector are bounded signals.

The hypothesis is:

- Wind speed and its first derivative are bounded signals.

For the constraints, state vector and control input saturation can be deduced as in Tables 5.3, 5.4.

Table 5.3: Constraints on angles, position and rotors velocity.

Par.	ϕ_{max}	θ_{max}	ψ_{max}	ϕ_{min}	θ_{min}	ψ_{min}	$\dot{\phi}_{max}$	$\dot{\theta}_{max}$
Val.	40	40	180	−40	−40	−180	40	40
Unit	deg	deg	deg	deg	deg	deg	deg $/s$	deg $/s$
Par.	$\dot{\psi}_{max}$	$\dot{\phi}_{min}$	$\dot{\theta}_{min}$	$\dot{\psi}_{min}$	x_{max}	y_{max}	z_{max}	x_{min}
Val.	10	−40	−40	−10	100	100	−100	0
Unit	deg $/s$	deg $/s$	deg $/s$	deg $/s$	m	m	m	m
Par.	y_{min}	z_{min}	$\dot{x}_{max}$	$\dot{y}_{max}$	$\dot{z}_{max}$	$\dot{x}_{min}$	$\dot{y}_{min}$	$\dot{z}_{min}$
Val.	0	0	5	5	−1	−5	−5	1
Unit	m	m	m/s	m/s	m/s	m/s	m/s	m/s
Par.	ω_{max}	ω_{min}						
Val.	400	200						
Unit	rad/s	rad/s						

Table 5.4: Constraints on control inputs.

	$U_z\,(N)$	$U_\phi\,(Nm)$	$U_\theta\,(Nm)$	$U_\psi\,(Nm)$
min.	1.4	−0.14	−0.14	−0.30
max.	5.6	0.14	0.14	0.30

5.4 Wind estimators

The behavior of the UAV is strongly dependent on the speed relative to the wind. The main component of the wind has a low frequency spectrum but UAV may experience sharp edge gust while passing from downwind side of a

building to upwind side. Wind estimation algorithms are subjected to some objectives, which are the robustness against the sensor's noises, the fast frequency estimation, and the reduction of the estimation incertitude in order to update the wind speed map and reduce the control effort. Wind speeds must have sinusoidal dynamics with $2m/s$, $2m/s$, $0.2m/s$ maximal values and $0.3\,rad/s$ maximal frequency. They are simulated as sinusoids since the gust generator at the B20 lab allows to create a sinusoidal wind gust profile, hence the sinusoid wind effect over time is correlated to the motion of the drone through the turbulent area. In this section, to show the performance of the proposed estimation algorithms, Parrot Drone set of parameters are used, Gaussian noises with 2.5 deg $/s$, and $0.052\,m/s^2$ standard deviations for gyroscope and accelerometer respectively, are added to simulate the augmented-IMU sensors noise. Additional Gaussian noises of $1\,cm/s$ standard deviation for linear velocities, and 1 deg standard deviation for angles are added because state measurement (u, v, w, ϕ, θ) are not reconstructed exactly. These values come from the available cameras in the lab. Since control and estimation algorithms are typically separated, a simple stationary PID control is used. Simpler identified quadrotor model is considered, however, a more extended study is presented in the following section 5.4.3 taking into account all the neglected nonlinearities. For simplicity of presentation some notations are used: algorithm-lin, algorithm-rot, algorithm-rot-2 respectively for algorithms that use linear quadrotor dynamics in eq. (4.3), rotational quadrotor dynamics in eq. (4.4), rotational quadrotor dynamics with wind derivative and sensor noises hypotheses in eq. (4.5).

5.4.1 Convergence of the estimations

Accuracy and convergence of estimation algorithms are the most important problem which must be studied carefully. A good algorithm must perform the estimation in very short time to be useful in quadrotor domain. Acceptable trade-off between accuracy and filtering are observed with the tuned parameters in Table 5.5, which are used for all the following simulations. This trial and error tuning process is illustrated with some examples as follows, enlightening the relation between the convergence time, the accuracy and the filtering effect. Fig. 5.1(a) shows a comparison for the algorithm-lin. Fig. 5.1(b) shows a comparison for the algorithm-rot-2, which presents an undesired overshoot in case of fast response. Simulations have demonstrated that more filtering ability can be obtained at the price of less accuracy in estimation and *vice-versa*. Based on this preliminary study, the best algorithm is the algorithm-lin having acceptable filtering ability and fast enough response.

Table 5.5: Wind estimators parameters

Par.	γ_a	α_a	γ_g	ℓ_g	γ'_g	α'_g	ℓ'_g
Val.	70	0.9	100	30	90	0.001	30

Fig. 5.2 is a comparison between all the proposed algorithms, showing their response to an input unitary step. Algorithm-rot is the worst because it is very slow and it is subjected to the highest incertitude. As a recall, algorithms are designed to estimate the wind with some estimation error. Fusion algorithm has the estimation error, in the worst case, given by the maximum of the two algorithm-lin and algorithm-rot-2 estimation errors. Because of this characteristics, the error of the fusion algorithm is always equal or bigger than the one in algorithm-lin. The error for algorithm-lin is given by

$$|e_d(t)| = \nu_{a2}\max\{\bar{\dot{d}}_w,\, \bar{\varepsilon}\}, \quad \nu_{a2} > 0.$$

The parameter ν_{a2} can be tuned small enough to ensure the convergence of the estimation against the maximum between the amplitude of the wind speed first derivative, which depends on the particular wind profile, and on the sensor noises. In this context, simulations are provided in section 5.4.3 where the algorithm must estimate the

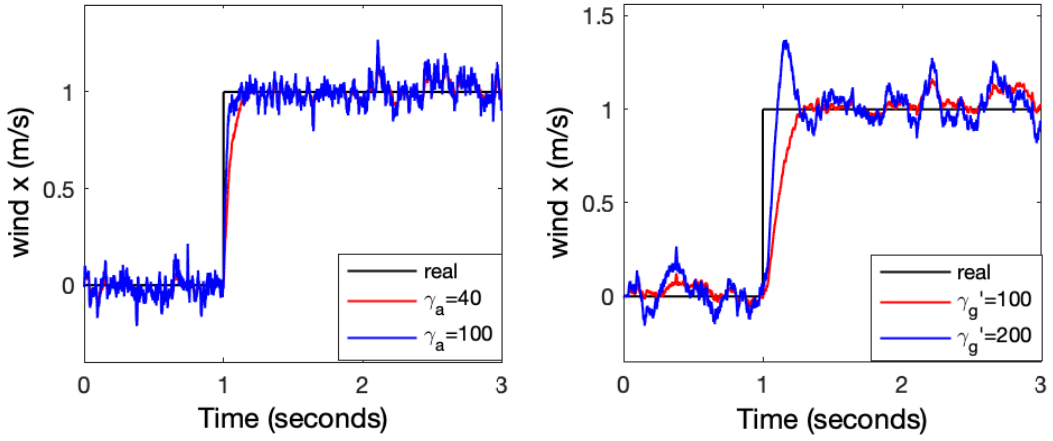

(a) (b)

Figure 5.1: Tuning process comparisons for algorithm-lin in (a), and for algorithm-rot-2 in (b).

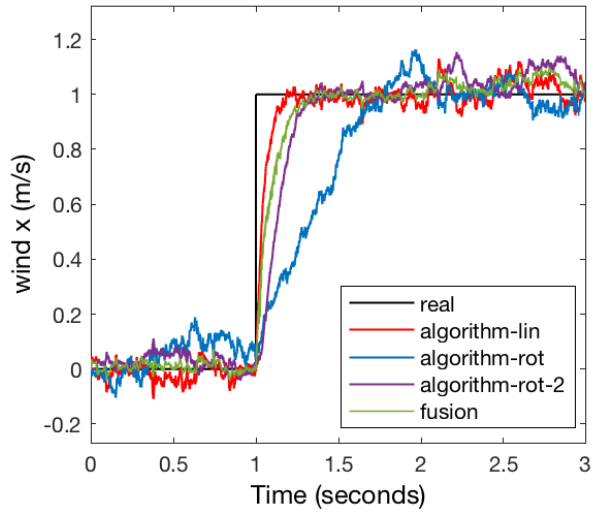

Figure 5.2: Unitary step response comparison between the designed estimation algorithms.

wind against more wind steps with different amplitude and considering the incertitude coming from the identified aerodynamic coefficients.

In this section, it is shown that the proposed algorithms can achieve a good estimation in short time even if the wind speed changes very much in amplitude, as an example in the worst ideal case the reference wind speeds are considered as steps. It means that, the estimation algorithms can achieve estimation in shorter time in a realistic case, where the changes of the wind speeds are smoother.

5.4.2 Conceptual validation

In simulations we are going to compare the wind velocities in the earth frame, using a stationary PID controller. The wind estimates $\hat{d}_w$ in the body frame, are then transposed to the earth frame thanks to the rotation matrix and filtered angles. Wind signals in earth frame are simulated as sinusoids having maximal amplitude of $2\,m/s$, $2\,m/s$, $0.2\,m/s$ and frequencies of $0.3\,rad/s$, $0.25\,rad/s$, $0.2\,rad/s$, since the quadrotor identification work by [Planckaert & Coton 2015] is valid for $\approx \pm 5$, ± 5, ± 1 translational velocities respectively in x, y, z axes (such identification is rather precise in the climbing phase, but less accurate in descent phase, since the model tends to slightly overestimate the propulsion in the descent phase). For simplicity of demonstration, the simpler identified quadrotor system is considered together with rotors dynamics, however, a more extended study is presented in the following section 5.4.3 taking into account all the neglected nonlinearities. Algorithm-rot and algorithm-rot-2 cannot estimate correctly the z component of the wind because w_w (wind velocity along z axis in body frame) is not present in the equations of moments. Fig. 5.3(a) shows the performance of the algorithm-lin. Wind is well estimated and filtered. Fig. 5.3(b) shows the performance of the algorithm-rot. The assumed noise-free and constant wind velocity conditions influence very much the quality of the result. Fig. 5.3(c) demonstrates that the problem of these restrictive hypotheses is solved introducing the algorithm-rot-2. However, at higher wind velocity an estimation error is present due to the Remark 1 in page 34 (small components of the of rotor rolling torque and rotor torque are neglected for low wind and UAV velocities). Fig. 5.3(d) shows the performance of the fusion algorithm, which allows to estimate correctly the wind velocity using a fusion of algorithm-lin and algorithm-rot-2 along the x, y axes, and using only algorithm-lin for z axis. Having performed the wind estimation for such a reference wind signal, it is obvious that the algorithms can achieve the estimation of wind signals having frequencies lower than the considered case and having equal maximal amplitude.

5.4.3 Robustness of the estimation

Evaluation of the robustness is very important because the aerodynamic coefficients are always subjected to some incertitude during the identification process. Moreover, this study should provide an admissible incertitude coming from the quadrotor identification process. This incertitude is very useful during the SMC tuning process, as explained later. Algorithm-lin, which has the best performance based on the preliminary analysis, and fusion algorithm are used for two sets of tests. Nominal values of the aerodynamic coefficients are imposed in the estimator, then the maximal and minimal values of the coefficients incertitude are considered in the quadrotor model. Estimation algorithms are designed to work on the quadrotor model with nominal values of the identified aerodynamic coefficients. For this reason, to test their robustness, 32 simulations are illustrated considering the minimal and maximal values of the parameters $I_{xx} \approx \pm 10\%$, $I_{yy} \approx \pm 10\%$, $C_{T\,stat} \approx \pm 10\%$, $K_D \approx \pm 20\%$, $h \approx \pm 0.01m$. A Matlab script is created to perform these simulations. The results in Fig. 5.4 (16 simulation results corresponding to I_{yy}, $C_{T\,stat}$, K_D, h incertitudes), Fig. 5.5 (4 simulation results corresponding to $C_{T\,stat}$, K_D incertitudes) show a dependence between the amplitude of the wind speed and the incertitude of the estimation of the wind speed in x dynamics, because of the neglected nonlinear effects coming from the identification process, whose main objective was to provide a quadrotor model simple enough to be studied efficiently in control and estimation theories. The worst cases are more precise for smaller wind speeds, as an example $1\,m/s$. At higher speeds the worst cases become less accurate, as an example $2\,m/s$. From the figures of the simulations, we obtain admissible estimation errors which are around $0.7\,m/s$ for wind speed of $1\,m/s$, and estimation errors around $1.4\,m/s$ for wind speed of $2\,m/s$. Limitations of these algorithms is that the wind estimates are valid only for the considered quadrotor model using the nominal identified aerodynamic coefficients. Introducing an uncertainty in these coefficients, produce important estimation error.

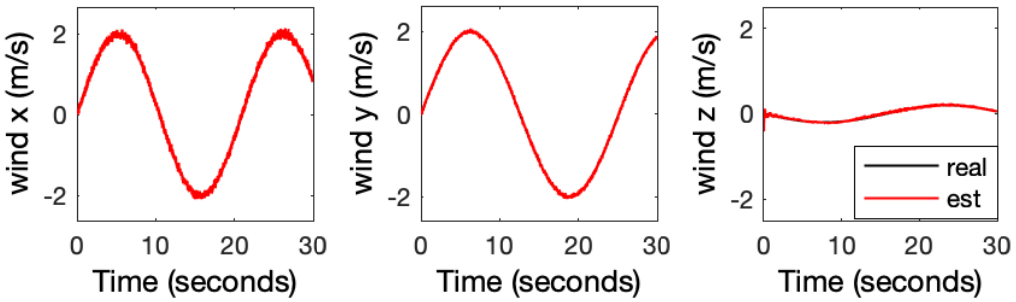

(a)

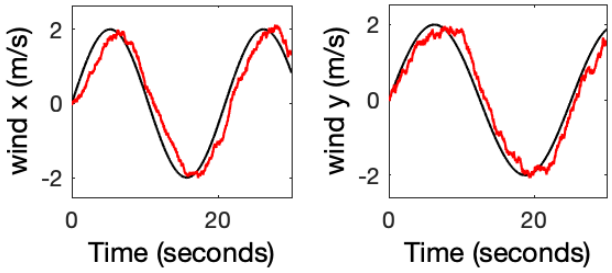

(b)

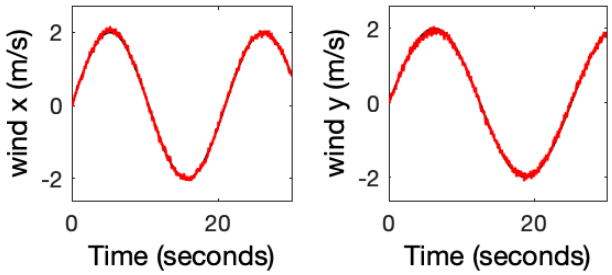

(c)

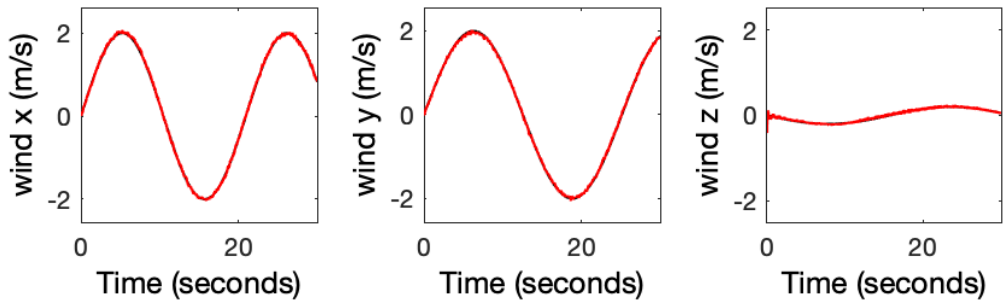

(d)

Figure 5.3: Wind estimation using algorithm-lin in (a), using algorithm-rot in (b), using algorithm-rot-2 in (c), using fusion algorithm in (d).

As a result, the estimation performance is highly affected by the incertitude of K_D. This issue is due to the identification process, where it is not possible to observe separately K_D and the wind speeds. Since the focus of this research was to estimate the wind speed, (u_w, v_w, w_w), we separated this vector from its coupling term K_D, however, the full product $K_D(u_w, v_w, w_w)$ can be used to design the controllers as further improvement. Fig. 5.6 shows the results testing the estimation algorithm on full quadrotor model. Wind signals in earth frame are simulated as sinusoids having maximal amplitude of $2\,m/s$, $2\,m/s$, $0.2\,m/s$ and frequencies of $0.3\,rad/s$, $0.25\,rad/s$, $0.2\,rad/s$. While in x, y dynamics the estimation is still acceptable, in z the estimation produces results which are not reliable. This important error comes from the identification of the coefficient of thrust C_T, which is quite a challenge to precisely estimate: the estimation algorithms are built using simpler quadrotor model, where C_T and K_D have been linearized to allow the design of the algorithms. K_D was identified to take into account dynamics that cannot be measured separately.

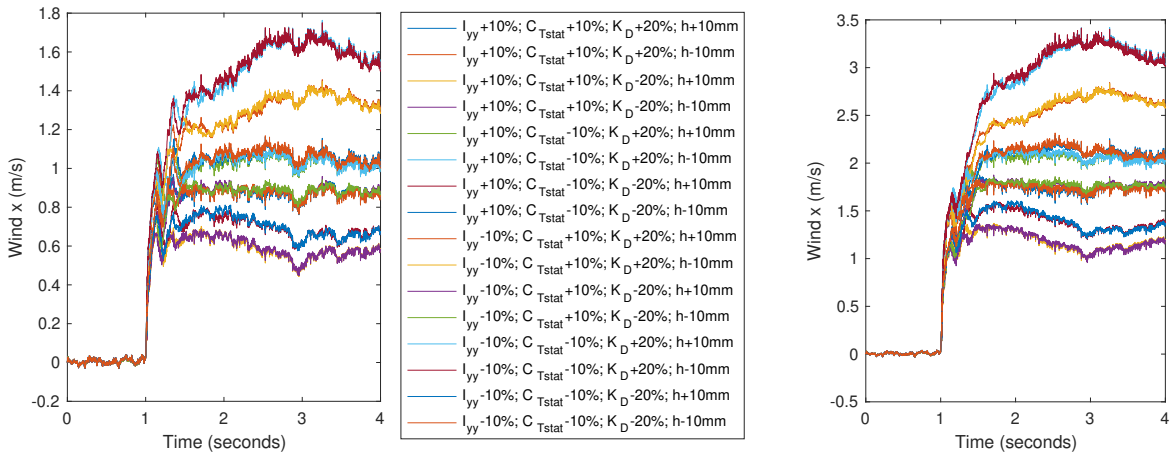

(a) (b)

Figure 5.4: Step responses for fusion algorithm to $1\,m/s$ wind speed in (a), to $2\,m/s$ in (b)

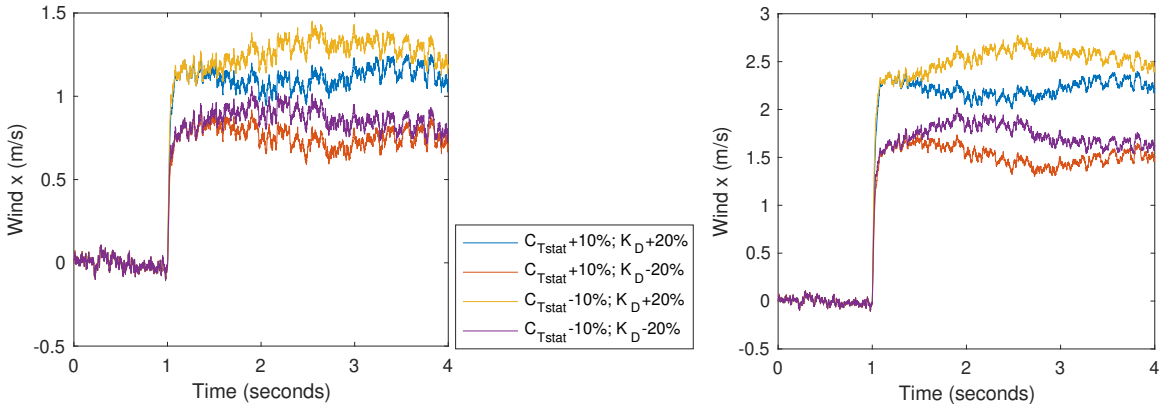

(a) (b)

Figure 5.5: Step responses for algorithm-lin to $1\,m/s$ wind speed in (a), to $2\,m/s$ in (b).

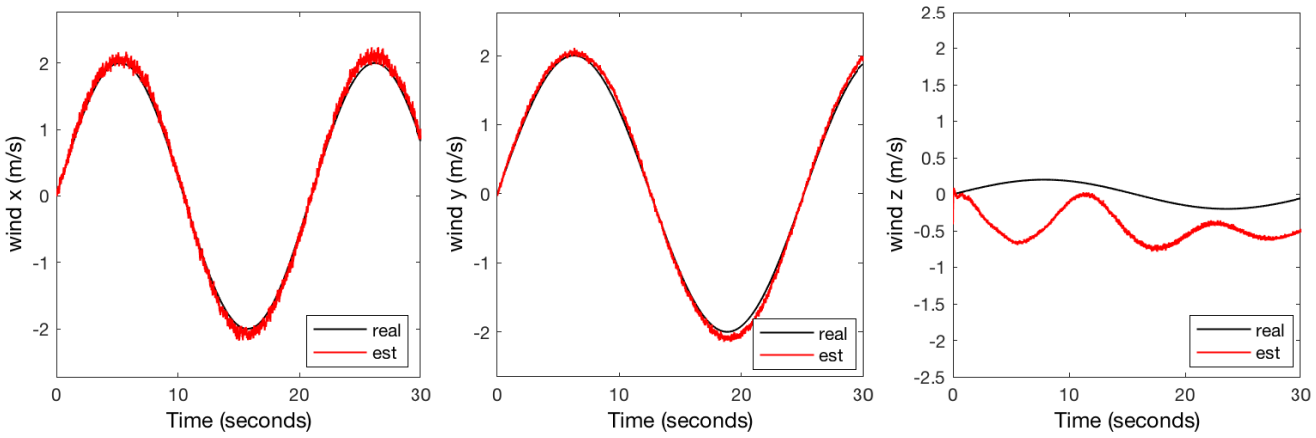

Figure 5.6: Wind estimation using full nonlinear quadrotor model.

5.5 Sliding Mode Controller

Control algorithms are also subjected to some objectives and constraints (see section 5.3). Controls must be robust to quadrotor model incertitude and to the incertitude coming from the wind estimator. They must take into account the dynamics of the planned trajectory and follow the desired trajectories with $10\,cm$ maximal error in x, y, z. They must be particularly robust to compensate the nominal wind profile, having maximal amplitude of $(2,\ 2,\ 0.2)\,m/s$ and frequencies of $(0.3,\ 0.25,\ 0.2)\,rad/s$, which has been tested to the estimation algorithms. The controllers should also adapt themselves to the experienced disturbances, varying the efforts on the rotors, they must compensate the chattering effect, which can ruin the rotors and drain the on-board battery very fast, and they must take into account the rotors dynamics.

Before to start the tuning process, there are some observations which can be made to facilitate the applicability of the sliding mode controls:

- Identify the quadrotor model parameters and b based on the rotors dynamics for Parrot drones, where b is the time-delay caused by the rotor dynamics and it is used to counteract the time-delay between the control signal and the effective rotor response.

- Choose $\gamma = 0.58$, which comes from the imposed operating point limit equal to ϕ_{max}, $\theta_{max} = 40$ deg, then γ provides the safe operating domain where the stability is assured based on the control designs.

- Choose D_i. Based on the theory $D_x \geq |u_w|,\ D_y \geq |v_w|,\ D_z \geq |w_w|$. Their values influence the amplitude of the gain function, and thus the control effort on the rotors. Values of D_i are chosen as the maximal amplitude of the wind and augmented by $(1,\ 1,\ 0.1)$ in $(x,\ y,\ z)$ to have additional margin of stability.

- Impose the control dynamics using the sliding surface. SMCs require to make a choise of the sliding surface *a priori*. Using linear control PID as in [Mellinger & Kumar 2011, Mellinger 2012], it can be shown that the angular bandwidth $(\phi,\ \theta)$ should be about 10 times bigger than position bandwidth $(x,\ y,\ z)$. Sliding surfaces are influenced by α_i parameters and they can be chosen such that for example $\alpha_\theta \approx 10\,\alpha_x$. In particular α_x, α_y, α_z are equally influenced by the mass, whilst α_ϕ, α_θ, α_ψ are influenced respectively by the inertia

I_{xx}, I_{yy}, I_{zz}. Moreover, α_ϕ, α_θ must be chosen in accordance with α_y, α_x respectively. Yaw bandwidth (ψ) should also be about 5 times bigger than position bandwidth.

As an example to illustrate how these parameters influence the results and to show the coupling effect between rotational and linear dynamics, Fig. 5.7 compares two cases: case 1 with $\alpha_x = 1$, $\alpha_\theta = 10$, case 2 with $\alpha_x = 1$, $\alpha_\theta = 5$.

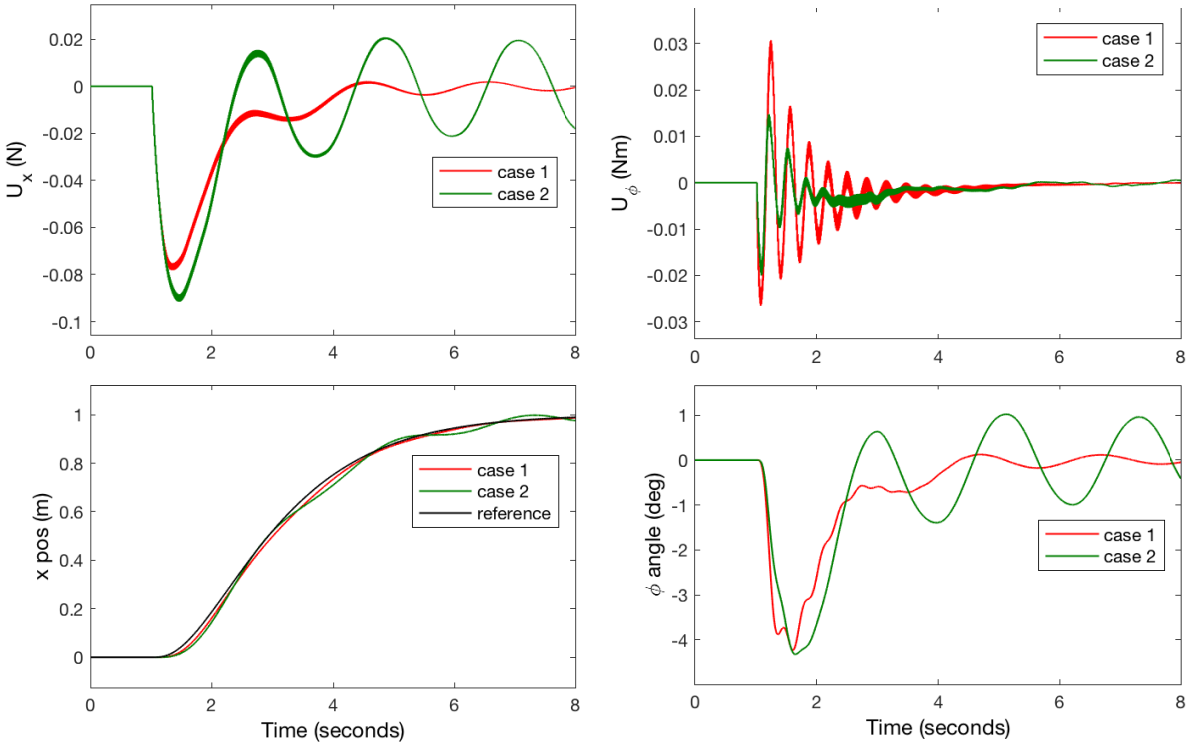

Figure 5.7: Influence of α_i parameter of qc-SMC for x and θ quadrotor dynamics.

5.5.1 Tuning steps for the controller

Under the hypotheses of Tables 5.1, 5.4, 5.3 where $\dot{z}_{max}$, z_{max} are with negative signs because z axis is taken with the positive direction towards down as in Fig. 2.1, the following process is used to tune carefully the gains for the sliding mode controllers. It must take into account all the coupling interactions (e.g. the same result can be obtained with different set of parameters), the influence of these parameters on the results (only some set of parameters ensure the stability of the system), the imposed constraints and objectives in our problem (maximal trajectory tracking error, avoidance of the chattering effect and of control inputs saturation, robust to wind speeds).

The tuning of parameters is sophisticated because there is not a unique rule, however, below a schematic list of steps is illustrated, which can help in understanding this process. Since the parameters of nonlinear controllers are characterized by an highly coupling influence, it is quite difficult to check their main influence in complex trajectories. For simplicity of presentation, the results are provided in simple step reference case, with no wind profile, and checking the results in comparison with the final tuned parameters.

The main steps are:

1. Choose one trajectory, using step references. As example the trajectory used in section 5.5.2 for SMCs comparisons;

2. Choose one admissible wind profile with the constraints coming from the section of the estimation algorithm. As example the wind profile chosen to test the estimation algorithms in section 5.4.2;

3. Tune the other parameters respecting the maximal trajectory tracking error, avoiding as much as possible the chattering and the controls saturation. This is the most important and delicate trade-off. Since the nonlinear controller have strong interactions between the parameters, it means that two or more sets of parameters can achieve the same performance, however some choices are better than others based on our problem. All the following parameters must be tuned accordingly together since they have very strong interactions:

   - Tune the parameters β_i. Based on the standard qc-SMC formulation, this parameter influences the time of convergence. As first step, the attitude-altitude quadrotor model without the rotors dynamics and in hover conditions was used. In this case the standard qc-SMC could achieve the reference and the stability was maintained. The typical chattering activity of SMCs was counteracted. As second step, the rotors dynamics and the non-hover conditions were introduced, but very important oscillations on the control inputs appeared. For this reason, many values of β were tested (0.0001, 0.001, 0.01, 0.1, 1, 2, 3, 4, 5, 10, 50, 100, 200), however in all these cases the controller produced oscillations that destabilized the system, and the results didn't produce any improvements to lead the tuning process in one precise direction. For this reason, the standard qc-SMC formulation was modified and additional ϱ_i were inserted. With the introduction of auxiliary ϱ_i the tuning process was facilitate since the system was stable. The varying function gain was then reformulated including the rotors dynamics to minimize the position error. Many simulations were then performed again adopting the same ϱ_i and changing $\beta_i = 1, 2, 3, 4, 100$. The stability were always achieved but the results didn't change very much and almost the same performance was observed in all the cases. For this reason, $\beta = 1$ is finally chosen arbitrary to ensure the stability of the system.
   - The values ϖ_x, ϖ_y, ϖ_z, ϖ_ϕ, ϖ_θ, ϖ_ψ replace first derivative upper bounds of the disturbances:

$$
\begin{aligned}
&\varpi_z \geq |\dot{\Delta}_z + \dot{\delta}_z L_z|,\\
&\varpi_x \geq 0 \text{ with } \tilde{D}_x(t, X) = |d_{xe} + \ddot{x}_{des} + \varpi_x| \text{ in eq. (3.29)},\\
&\varpi_y \geq 0 \text{ with } \tilde{D}_y(t, X) = |d_{ye} + \ddot{y}_{des} + \varpi_y| \text{ in eq. (3.29)},\\
&\varpi_\phi \geq |\dot{\Delta}_\phi|,\\
&\varpi_\theta \geq |\dot{\Delta}_\theta|,\\
&\varpi_\psi \geq |\dot{\Delta}_\psi|,
\end{aligned}
$$

     Choose ϖ_i in qc-SMC such that it is big enough to make the drone stable and having an acceptable position error. If this value is not properly tuned and it is too much high (or small), then the quadrotor position and angles can present undesired oscillations or quasi-chattering (or the system is unstable because the controller is not able to compensate the disturbance). For this reason, ϖ_i introduce an undesired overestimation of the gain function and their higher values correspond to better trajectory tracking. The adopted process in this thesis was to insert the nominal wind profile and increase ϖ until stability was obtained and tracking position max error was respected. Based on the theoretical control design, ϖ_x, ϖ_y could be easily chosen equal to 0, but they are both chosen equal to 3 in order to achieve

a better trajectory reference after many iterations. As an example, Fig. 5.8 compares two cases: case 1 with $\varpi_x = 3$, case 2 with $\varpi_x = 0$.

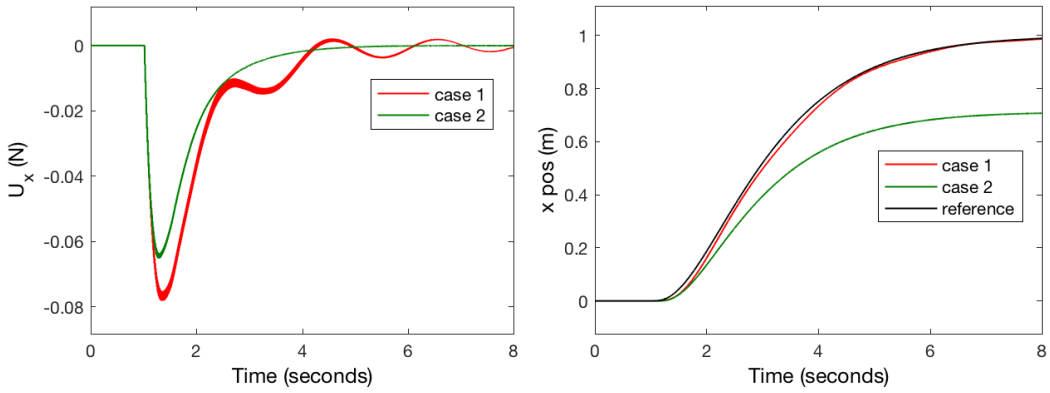

Figure 5.8: Influence of ϖ_i parameter of qc-SMC for x quadrotor dynamics.

- Choose ϱ_i (or ξ_i in case of 1-SMC) such that the quadrotor position and angles oscillation is reduced as much as possible. A good compromise between position and angles accuracy and control effort must be considered. The tuning of these two parameters is generally very sophisticated and it takes many iterations to achieve an acceptable result.

  The parameters ϱ_x, ϱ_y, ϱ_z, ϱ_ϕ, ϱ_θ, ϱ_ψ are the novel parameters inserted in this research to counteract the big control oscillation. Higher ϱ_i correspond to less oscillations but they produce a bigger position and angle errors. As an example, Fig. 5.9 compares two cases: case 1 with $\varrho_x = 0.1$, case 2 with $\varrho_x = 1$.

  The parameters ξ_x, ξ_y, ξ_z, ξ_ϕ, ξ_θ, ξ_ψ appear in the saturation function as an approximation for the function *sign* for the designed 1-SMC, such that for $\xi = 0$ the saturation function sat_ξ is equal to the *sign* function. They have the same role as ϱ_i in qc-SMC. Fig. 5.10 compares two cases: case 1 with $\xi_x = 1$, case 2 with $\xi_x = 0.01$. A trajectory tracking error appears which is proportional to the saturation parameter, but the typical chattering effect on the control input is avoided.

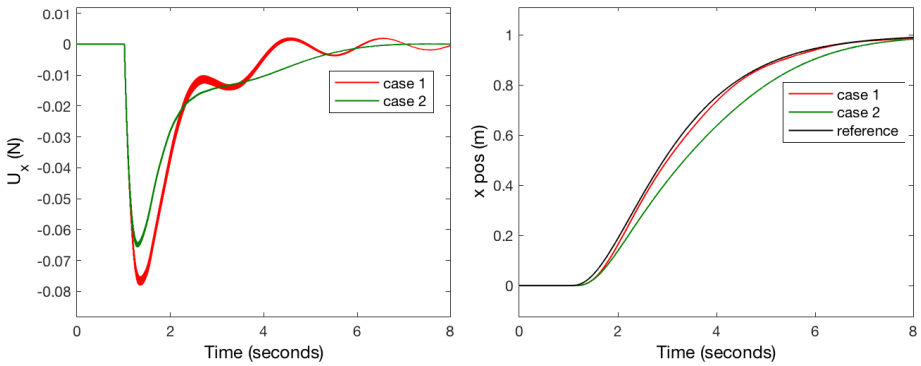

Figure 5.9: Influence of ϱ_i parameter of qc-SMC for x quadrotor dynamics.

4. Make other tests introducing quadrotor model incertitude (see section 5.5.3). If the stability, the maximal control efforts or maximal position errors are not completely satisfied, repeat the process from step 3.

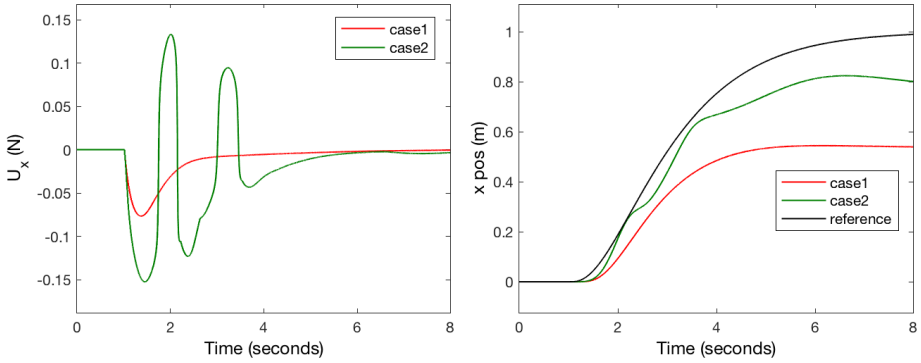

Figure 5.10: Influence of ξ_i parameter of 1-SMC for x quadrotor dynamics.

5. Make other tests introducing wind step disturbances (see section 5.5.3). If the stability, the maximal control efforts or maximal position errors are not completely satisfied, repeat the process from step 3.

6. Make another test using aggressive trajectory to check the quadrotor in its limit conditions (see section 5.5.3). If the stability, the maximal control efforts or maximal position errors are not completely satisfied, repeat the process from step 3.

5.5.2 Comparisons between the designed controllers

After the tuning process, final simulations are provided to compare the proposed quasi-continuous SMC (qc-SMC) and first order SMC (1-SMC), using full quadrotor model. The resulting set of parameters, used for the following conceptual validation of the SMCs algorithms, are listed in Table 5.6.

Table 5.6: Tuned sliding mode controls parameters for Parrot drone

Par.	α_x	α_y	α_z	α_ϕ	α_θ	α_ψ	ξ_x	ξ_y	ξ_z	ξ_ϕ	ξ_θ	ξ_ψ	ϱ_x
Val.	1	1	1	10	10	5	0.7	0.7	1	1	1	1	0.1
Par.	ϱ_y	ϱ_z	ϱ_ϕ	ϱ_θ	ϱ_ψ	ϖ_x	ϖ_y	ϖ_z	ϖ_ϕ	ϖ_θ	ϖ_ψ	D_x	D_y
Val.	0.1	1	0.5	0.5	0.5	3	3	1	9	9	12	3	3
Par.	D_z	C_x	C_y	C_z	C_ϕ	C_θ	C_ψ						
Val.	0.3	5.5	5.5	23	30	30	60						

For simplicity of demonstration (D_x, D_y, D_z) are selected as constant input to the controllers. One wind profile and one trajectory (which couples together forward, lateral and vertical flights, moving the quadrotor in x, y, z positions) are considered for this comparison, as in Fig. 5.11. Conventional SMC (conv-SMC) is built as $\tilde{u}_i = C_i \operatorname{sign} S_i$ for constant $C_i \geq \|d_i\|_\infty$, for $i = x, y, z, \phi, \theta, \psi$ and it is suitable under hypothesis that perturbations are bounded functions of time. In conv-SMC, as usual for implementation, the function sign is replaced by the approximation sat_ξ in eq. (3.24). Constant gains C_i are chosen to compensate the disturbances and taking their maximal values, only after checking the computed disturbances illustrated in Fig. 5.11. Unfortunately, 1-SMC and conv-SMC cannot achieve the same accuracy as the qc-SMC since they become unstable due to the high control oscillations if the convergence error is very small, as previously explained in the control tuning process for the saturation functions. For this reason, the same ξ is used for 1-SMC and conv-SMC, while more accuracy is achieved

for qc-SMC. Figures 5.12, 5.13, 5.14, 5.15, 5.16, 5.17 illustrate the positions and their control inputs, angles and their control inputs, and sliding surfaces.

First, the simulation clearly shows that using a varying-gain function instead of a constant gain improves the transients, because the SMCs using this function are subjected to less effort on the rotors. The main advantage is that, while the tuned gain for the conv-SMC has to be done only *a posteriori*, the varying-gain of 1-SMC and of qc-SMC can be tuned partially *a priori* making an hypothesis on maximal wind velocities. Second, as previously discussed in the tuning process, 1-SMC and conv-SMC tend to destabilize the system if better accuracy and more control effort are imposed. In this contest, qc-SMC can achieve the best accuracy. These points highlights the importance of tuning the varying-gains influenced by the wind velocity and by the state of the system.

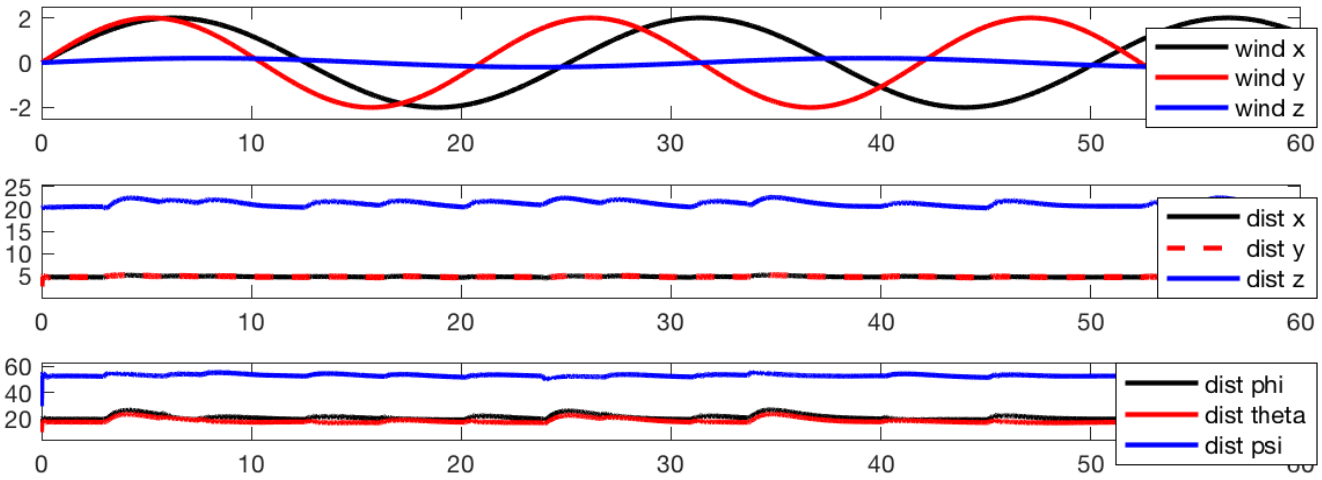

Figure 5.11: Wind speeds and computed disturbances from 1-SMC for comparisons of the designed SMCs.

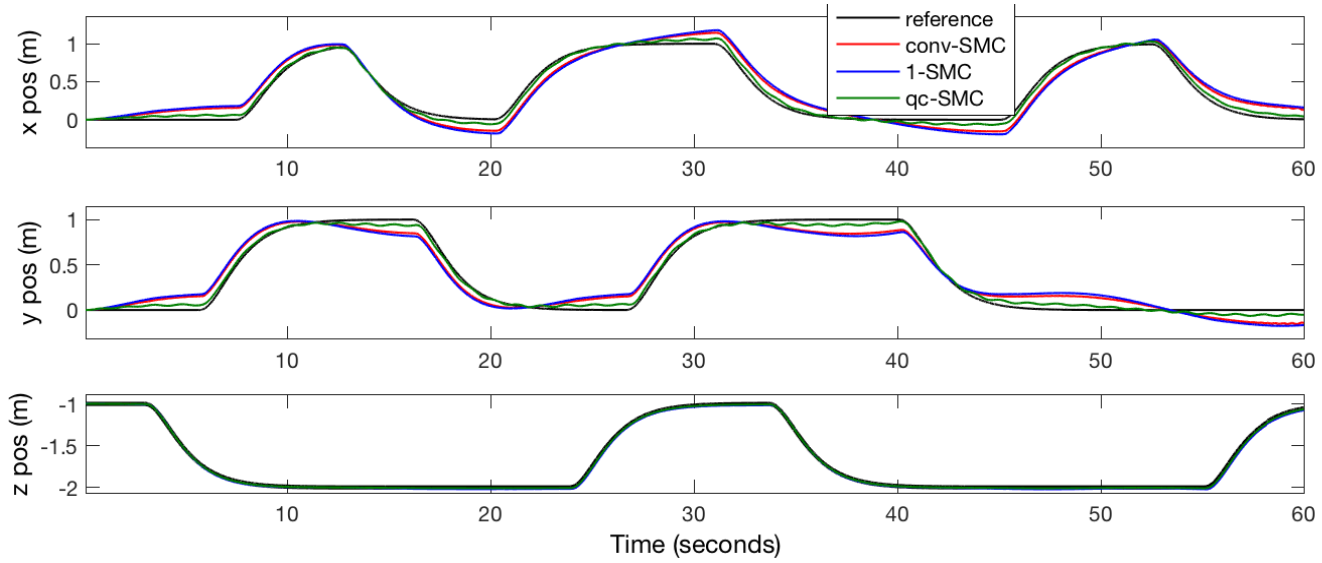

Figure 5.12: x, y, z positions using the designed SMCs.

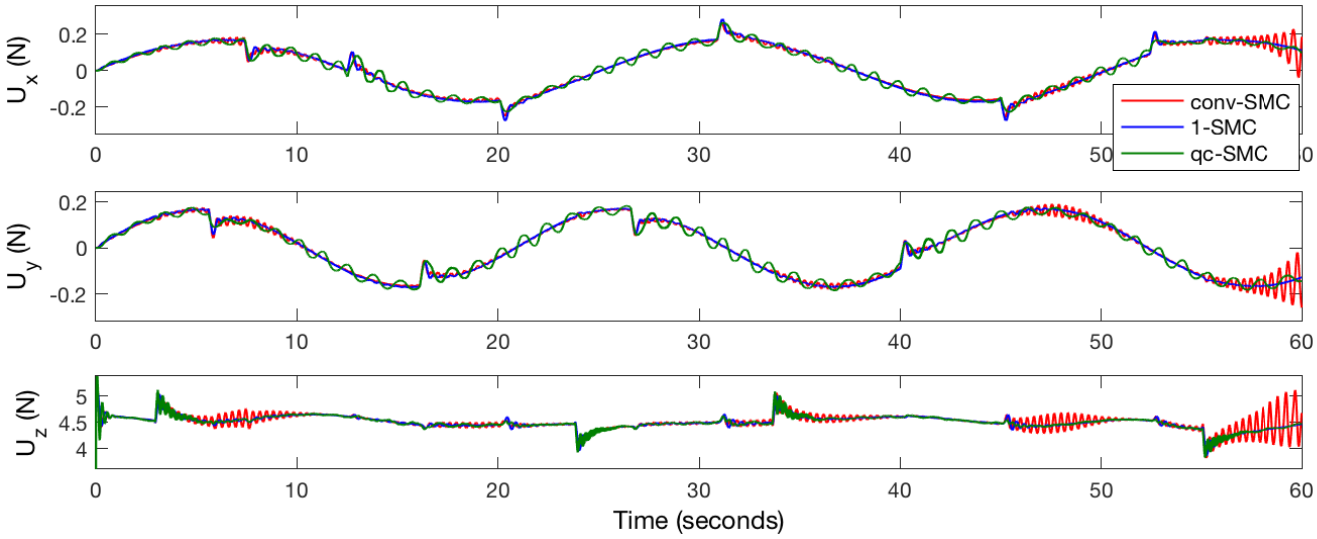

Figure 5.13: x, y, z controls using the designed SMCs.

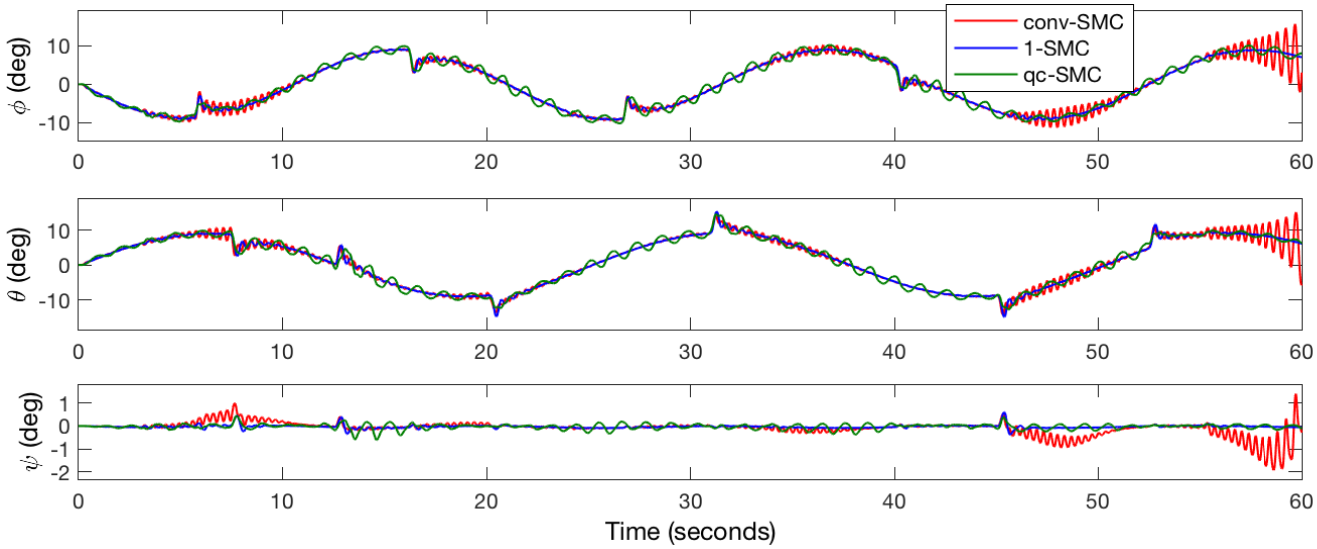

Figure 5.14: ϕ, θ, ψ angles using the designed SMCs.

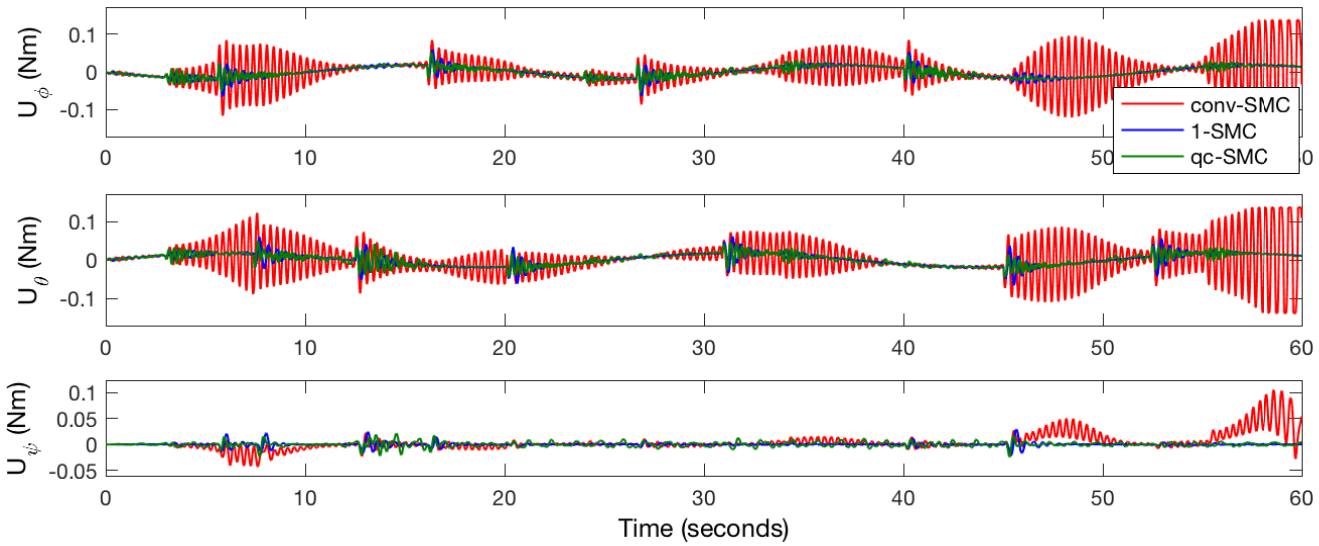

Figure 5.15: ϕ, θ, ψ controls using the designed SMCs.

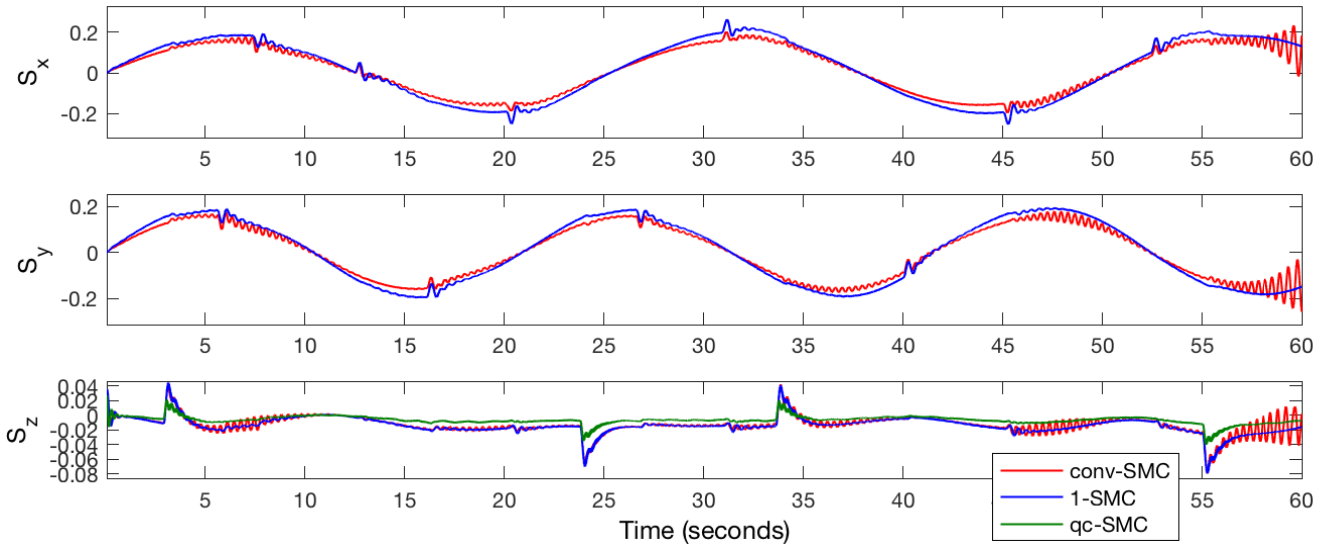

Figure 5.16: x, y, z sliding surfaces of the designed SMCs.

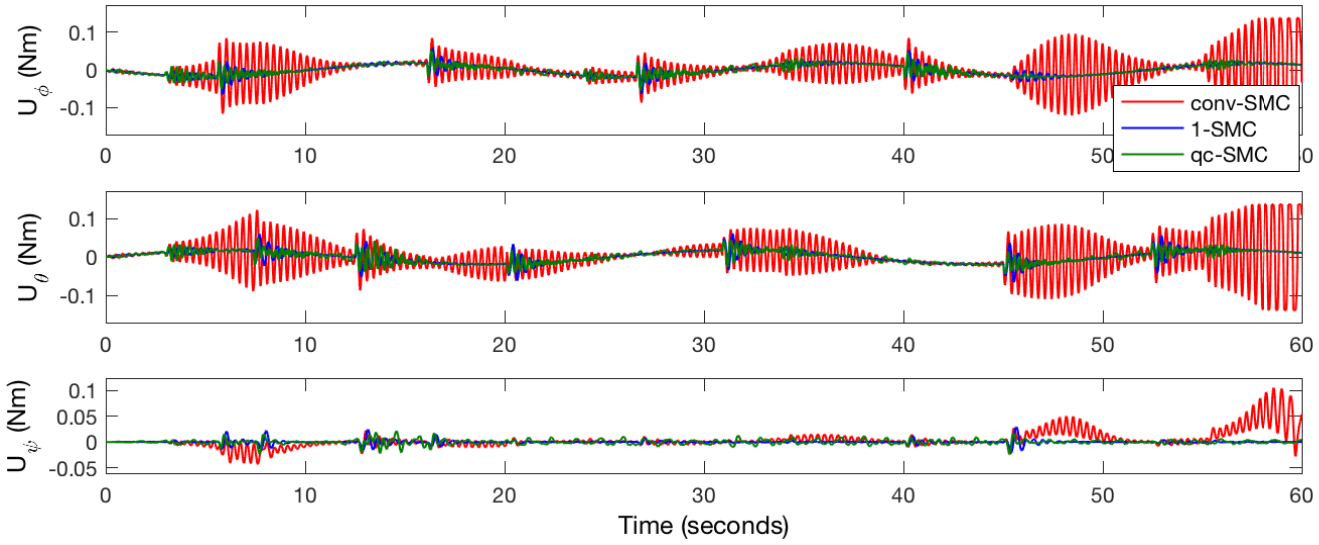

Figure 5.17: ϕ, θ, ψ sliding surfaces of the designed SMCs.

5.5.3 Control robustness

After that the SMCs were tested and compared, the qc-SMC was chosen since it has the best performance, based on the previous section. The designed qc-SMC algorithm is built in such a way to compensate the computed disturbances. These disturbances are influenced by the state of the system, which comes from the planned trajectory, and by the wind speed.

Robustness against the model incertitude and against fast varying wind speeds is studied as follows. Since the previous control simulations were tested and validated on full quadrotor system having nominal coefficient values, 128 simulations are carried out and they correspond to all the combinations of $I_{xx} \approx \pm 10\%$, $I_{yy} \approx \pm 10$, $h \approx \pm 0.01$, $C_{Tstat} \approx \pm 10\%$, $u_w = (-2, 2)$, $v_w = (-2, 2)$, $w_w = (-0.2, 0.2)$, and considering $I_{zz} \approx I_{xx} + I_{zz}$, $\lambda_{stat} = \sqrt{C_{Tstat}/2}$. The quadrotor is demanded to keep a steady position. The control has input $D_x = 3$, $D_y = 3$, $D_z = 0.3$. Nominal values of these coefficients are imposed in the control algorithm, then the maximal and minimal values of the coefficients incertitude are considered in the quadrotor and rotors models. As from the results in Fig. 5.18, the system is not stable for only 4 combinations of wind speeds and coefficient incertitude over the 128 possible cases. In all the other 124 cases, the system is stable and it reaches the requested error position constraints in under 1.5 seconds, even if the control input U_z is saturated at initial time steps. However, it is worth to note that the selected cases are the worst ideal cases when wind speeds are steps, in reality wind speeds have much smoother dynamics that can allow the control inputs to adapt properly and fast enough to maintain the quadrotor stable, as in Fig. 5.19 where wind speeds are selected as sinusoids having frequencies of $(0.3\,rad/s,\ 0.25\,rad/s,\ 0.2\,rad/s)$ and maximal amplitude of (2, 2, 0.2) in (x, y, z) directions. Another test is illustrated in Fig. 5.22, where the 128 simulations include wind speed steps of $u_w = v_w = (-1.8, 1.8)$, $w_w = (-0.2, 0.2)$, and the stability and trajectory tracking errors are respected in less than 1 second. Then, two other tests are made, considering only the combinations of quadrotor coefficients incertitude in Fig. 5.20, and only the combinations of wind speed steps in Fig. 5.21. The results demonstrate that, for wind speed steps higher than $1.8\,m/s$ in (x, y), the stability of the system and the trajectory tracking maximal error are always assured in the transition phase only if the wind speed steps and the coefficients incertitude are considered separately. This is due to the inner property of the SMCs which are fast controllers and they are suitable to compensate unpredictable and fast varying external disturbances.

In previous sections, only one trajectory was considered for simplicity of the presentation. However, the computed disturbances are influenced by wind speeds, and by the planned trajectory and quadrotor constraints (e.g. quadrotor linear and angular velocities). For this reason an additional study about the trajectory planning must be added. The dynamics of the planned trajectory can be freely chosen and the trajectory saturation is fixed. It means that the velocity of the quadrotor and the control inputs amplitudes have maximal values, for all the possible planned trajectory. Even if, this property helps very much to obtain a big domain of stability, there could also be present some aggressive trajectories having a strong coupling effect between the 6 quadrotor velocities and wind speeds first derivative, whose stability is impossible to study *a priori*. For this reason, an additional aggressive trajectory is checked testing the quadrotor in its limit conditions, using nominal quadrotor coefficients for both quadrotor model and control algorithms, and one sinusoid profile of wind having ($0.3\,rad/s$, $0.25\,rad/s$, $0.2\,rad/s$) frequencies, (2, 2, 0.2) maximal amplitude in (x, y, z), and using $D_x = 3$, $D_y = 3$, $D_z = 0.3$. Figures 5.23, 5.24 show that the stability is assured respecting the trajectory tracking error constraints, however fast oscillations are present on the 3 angular control inputs. This issue causes higher energy consumption of the on-board battery, but the rotors are still safe as in Fig. 5.25(b). In conclusion, the stability of the quadrotor system is influenced by the aerodynamic coefficients, the wind speeds, and by the trajectories. Some tests were carried out to check the robustness properties of the proposed qc-SMC and they are schematically illustrated in Fig. 5.26.

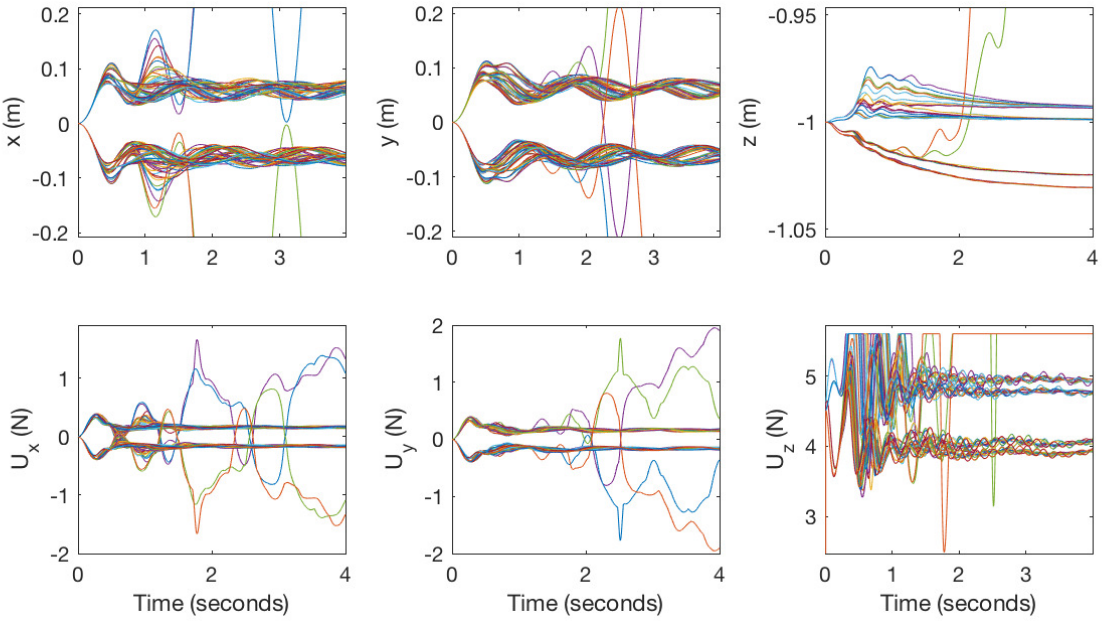

Figure 5.18: Positions (x, y, z) and their respective qc-SMC inputs considering fixed D_i, quadrotor model influenced by coefficients incertitude, and combinations of wind speed steps.

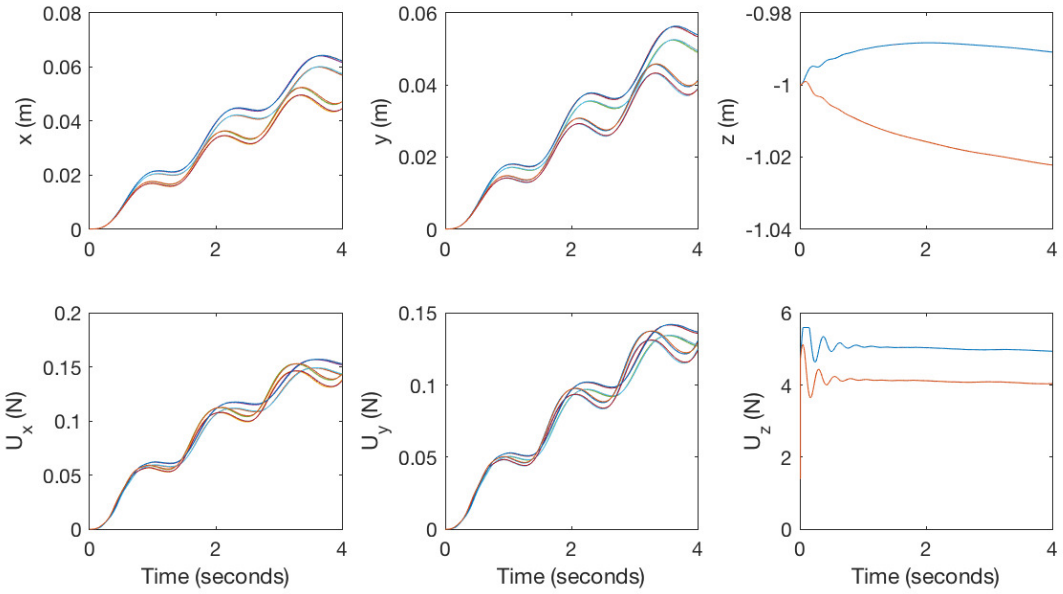

Figure 5.19: Positions (x, y, z) and their respective qc-SMC inputs considering fixed D_i, quadrotor model influenced by coefficients incertitude, and one profile of varying wind speed.

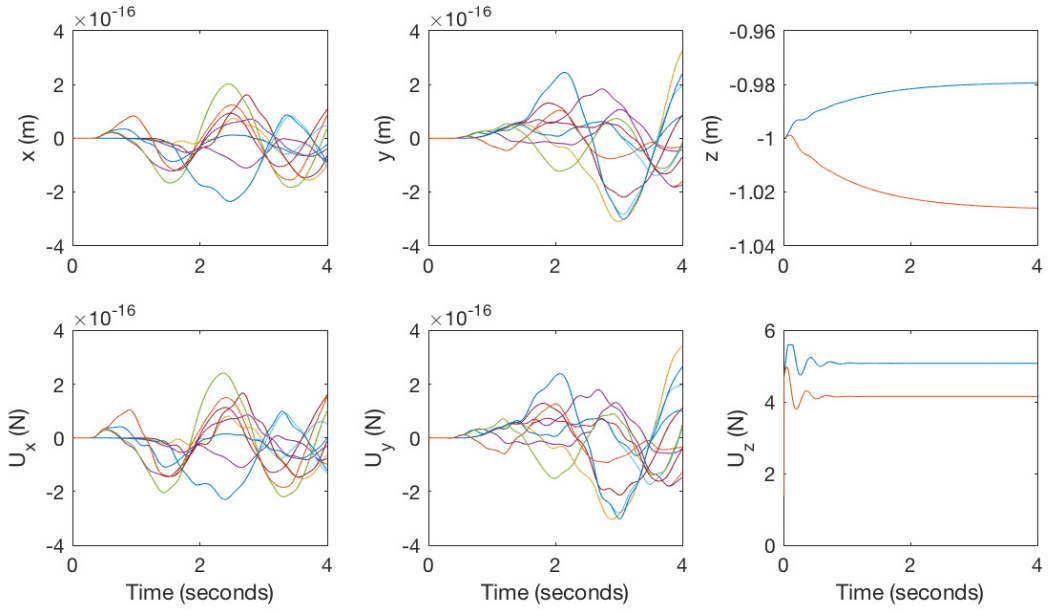

Figure 5.20: Positions (x, y, z) and their respective controls considering quadrotor model influenced by coefficients incertitude.

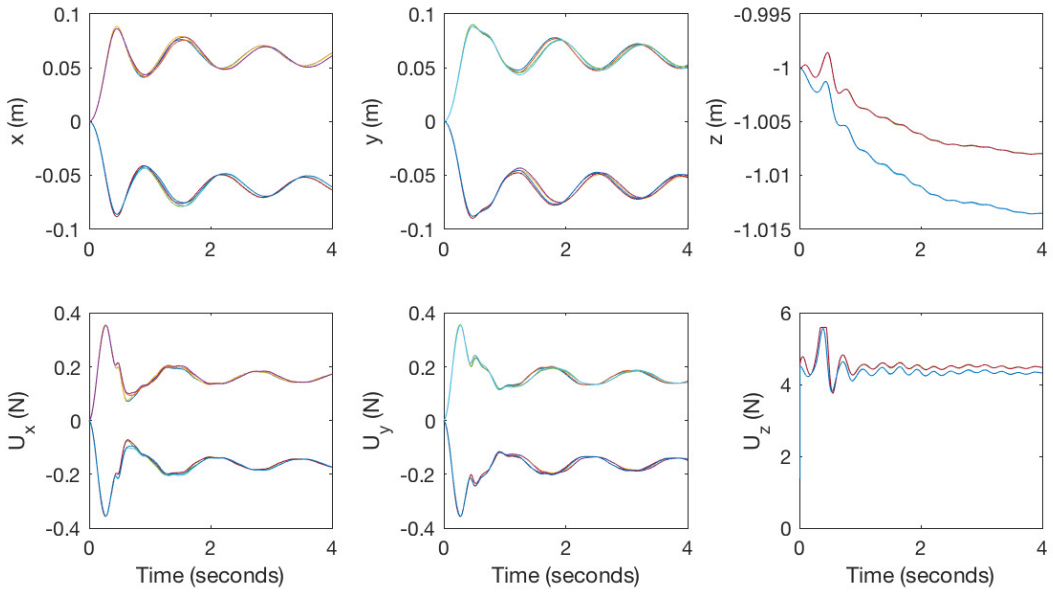

Figure 5.21: Positions (x, y, z) and their respective controls considering quadrotor model influenced by combinations of wind speed steps.

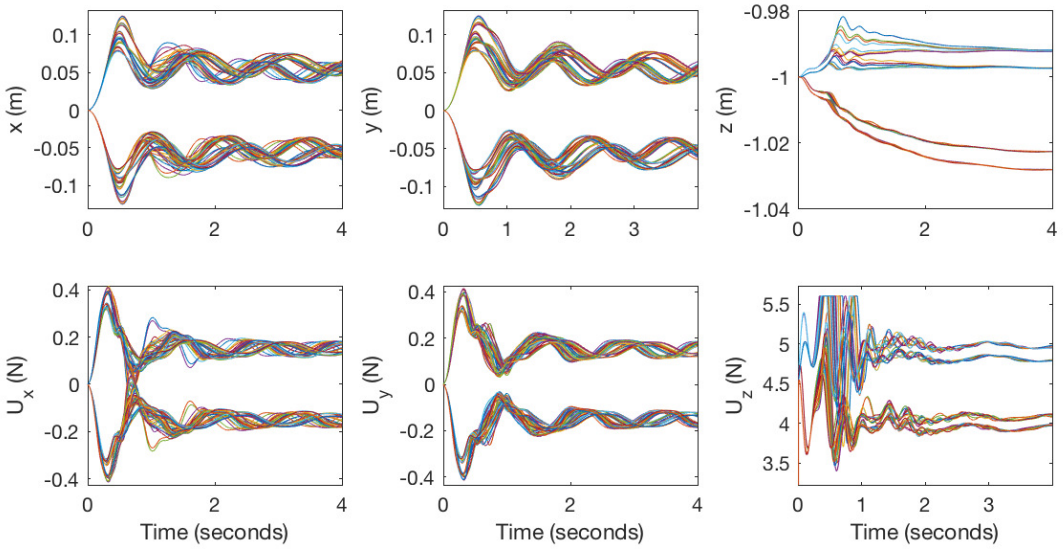

Figure 5.22: Positions (x, y, z) and their respective qc-SMC inputs considering fixed D_i, quadrotor model influenced by coefficients incertitude, and combinations of wind speed steps with reduced amplitude.

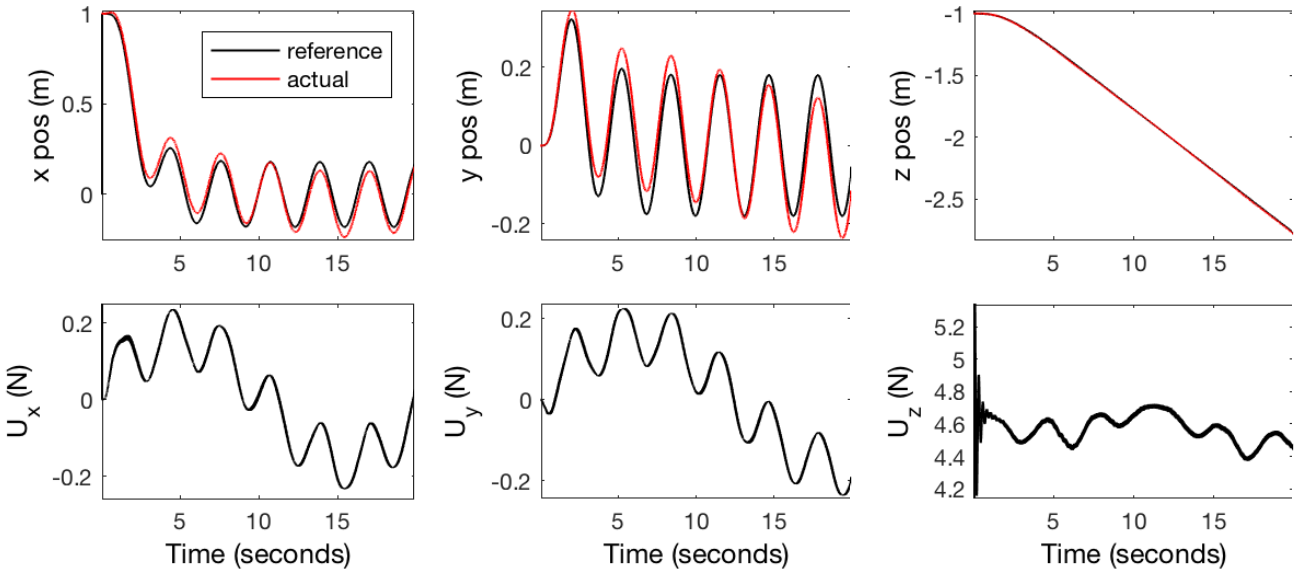

Figure 5.23: Test on aggressive trajectory: Positions (x, y, z) and their respective qc-SMC inputs considering fixed D_i.

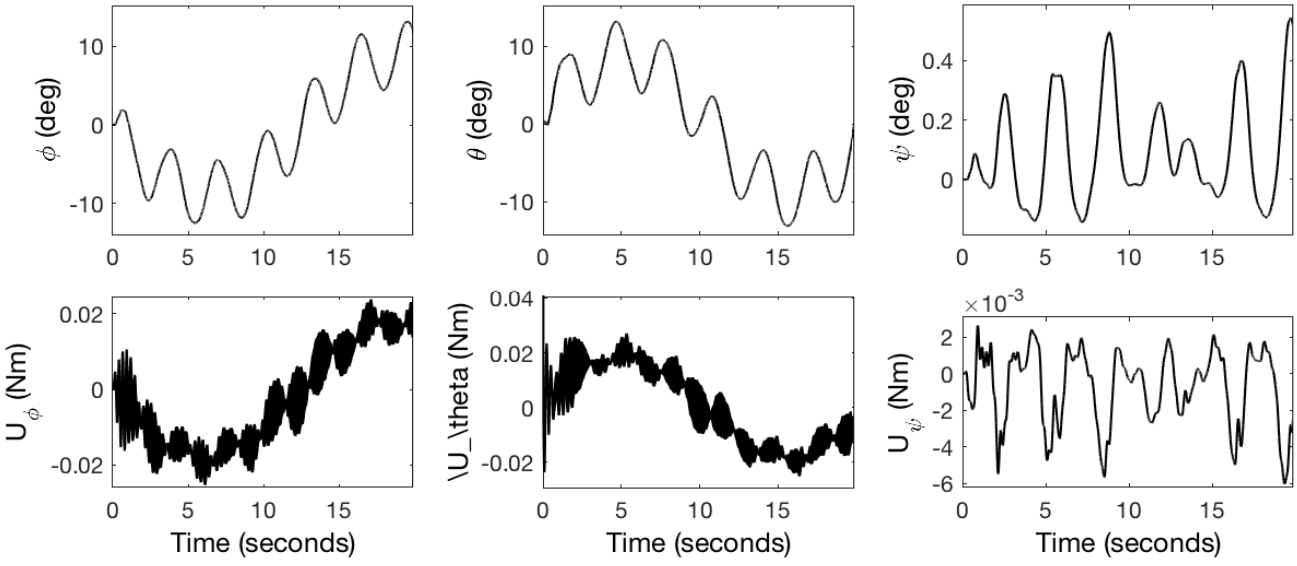

Figure 5.24: Test on aggressive trajectory: Angles and respective qc-SMC inputs considering fixed D_i.

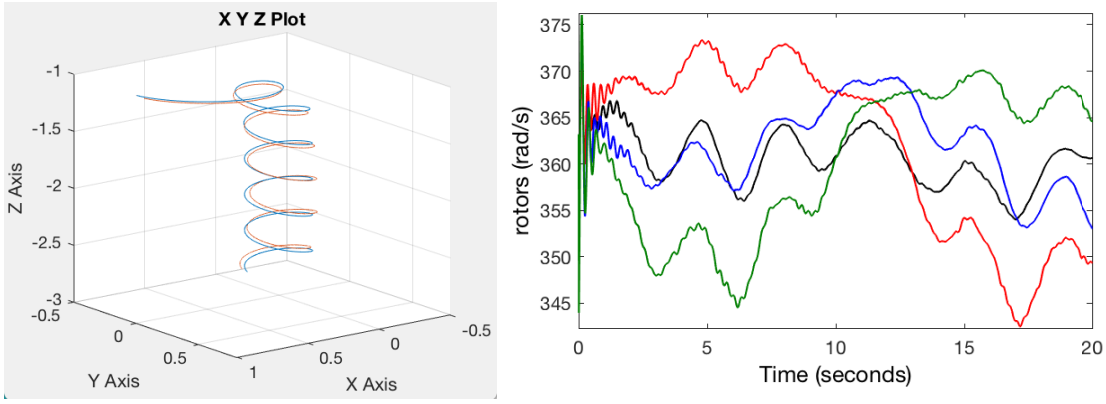

(a) (b)

Figure 5.25: Aggressive 3D trajectory: Positions (x, y, z) in (a), and rotors angular velocities in (b).

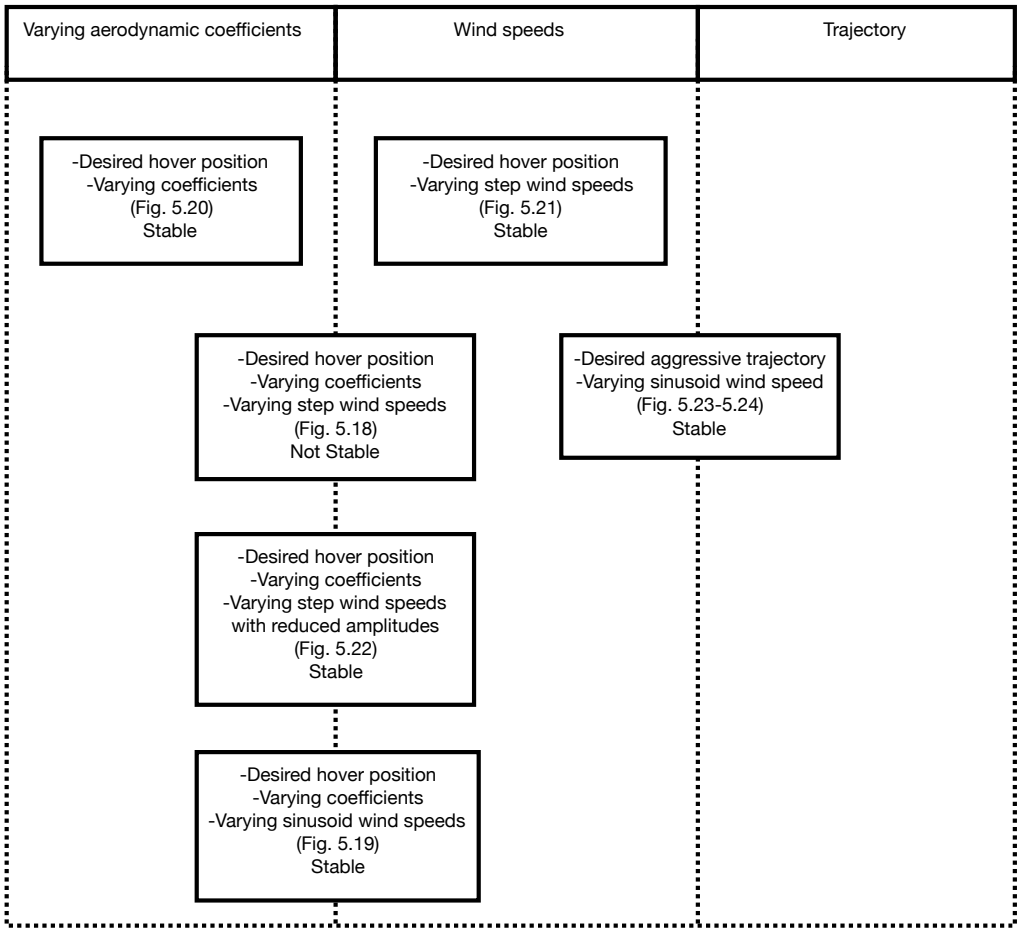

Figure 5.26: Visual organization of the tests to check the qc-SMC robustness.

5.5.4 Coupling of wind estimates and control algorithm

The main focus of the ONERA's project and the reason for this thesis was to find a good controller able to maintain the system stable but ensuring also a good wind estimation. This can be achieved with a good trade-off between control robustness and wind estimation accuracy. If the controller-quadrotor-estimator system is very robust against external perturbations, wind estimates are less precise. In opposite, if the system is less robust, its sensitivity to external disturbances is augmented and the wind estimates can be much more accurate.

The parameters of the designed control laws depends on the wind speeds. Thanks to these parameters, wind estimates and their incertitudes, coming from the estimation algorithms, can be used as input to the controllers and this coupling effect can be studied. In this way, by adapting the control amplitude, the regulator effort on the rotors can be reduced when it is possible, allowing to achieve a better performance with less control effort. Based on the imposed constraints, absolute values of the maximal wind speeds are $(2\,m/s,\ 2\,m/s,\ 0.2\,m/s)$ and frequencies are $(0.3\,rad/s,\ 0.25\,rad/s,\ 0.2\,rad/s)$ in $(x,\ y,\ z)$. Wind estimation on z is not well performed on the full quadrotor model. For this reason, only in z dynamics, the varying wind speed, does not come from the estimation algorithm but it is considered directly as external input simulation. Two qc-SMCs are compared: using varying wind estimation and constant maximal wind values.

- In the first case, the chosen parameters are directly $D_x = 3,\ D_y = 3,\ D_z = 0.3$.
- In the second case, nominal wind estimates are considered as input to the controller and their absolute values are augmented of $1\,m/s,\ 1\,m/s,\ 0.1\,m/s$, based on the tuning process to ensure better trajectory tracking and to have a sufficiently margin to remain in stable conditions.

Figures 5.27, 5.28 show respectively the $(x,\ y,\ z)$ actual and reference positions, quadrotor linear control inputs, $(\phi,\ \theta,\ \psi)$ actual angles, quadrotor angular control inputs. For a better comparison, control parameters, except for D_i, are kept equals in the two cases. Based on the results, the input varying wind velocity allows less control effort on the rotors (less chattering and smaller pitches) ensuring good trajectory tracking performance, due to the fact that the control gain is less overestimated in the second case. As a result, the controller with varying wind input presents a much smoother rotors behavior, even if undesired control input oscillations are still present. The only solution to avoid completely this issue is to "relax" the control inputs in order to have a bigger trajectory tracking error, but we must also respect the imposed trajectory tracking constraint of $0.1\,m$ maximal position error, so we must deal with this issue during the experimental stage.

After that the contribution in considering a varying wind speed as input to the controller is introduced, the stability must be studied. Robustness against the model incertitude and against fast varying wind speeds is studied again in all 128 cases corresponding to all the possible combinations, as in the previous section for $u_w = v_w = 2\,m/s$, but this time considering varying D_i, coming from the estimation algorithm. Fig. 5.29 shows that there still are 4 cases over 128 that do not provide a stability condition for the quadrotor.

In the previous part the influence of the wind estimates on the control algorithm is studied. It is shown that the control effort can be reduced when possible, but keeping stable the quadrotor. This influence has a significant impact on the control inputs producing less control oscillations. In this section, the influence of the control algorithm robustness on the wind estimates is studied. For this reason, two cases are illustrated. In both cases, the varying wind estimates in x, y are considered as inputs to the control algorithm and augmented by 1, the varying wind in z is directly considered as input to the controller and augmented by 0.1 since wind estimates are less accurate. Fig. 5.30 shows the case where the qc-SMC uses the nominal tuned parameters, which allows the overall control-quadrotor-estimator system to be very robust against external wind perturbations. Fig. 5.31 illustrates the case where the

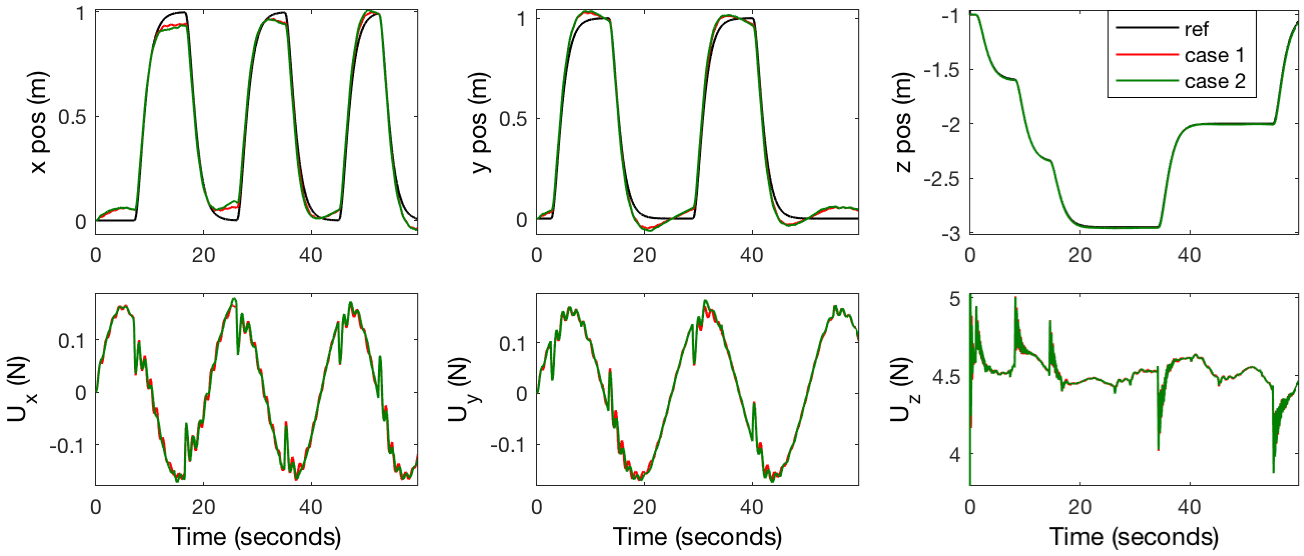

Figure 5.27: Quadrotor position: Comparison between constant gain D_i and wind estimates as input to qc-SMC.

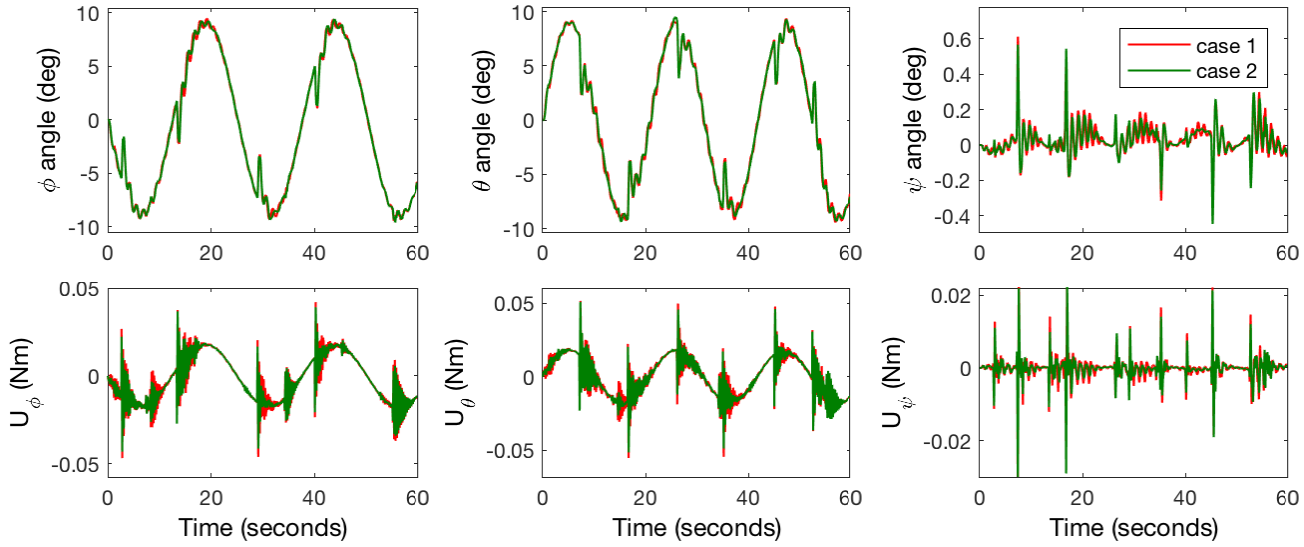

Figure 5.28: Quadrotor angles: Comparison between constant gain D_i and wind estimates as input to qc-SMC.

qc-SMC is "relaxed" using different values of $\varrho_x = 1$, $\varrho_y = 1$, $\varrho_z = 1.5$, $\varrho_\phi = 1.3$, $\varrho_\theta = 1.3$, $\varrho_\psi = 1.3$, which allows the overall system to be less robust against wind perturbation. Even if we can expect that the wind estimation in the first case is much less accurate producing an underestimation of the real wind speed, the results show that the wind estimates are exactly the same in both cases. The motivation can be that, because of some hidden dynamics, it is very difficult to obtain a quadrotor model representing totally the reality and that, outside the laboratory and using GPS, it is not possible to reconstruct the state with such a great precision. The mentioned issues cause a time-delay affecting the wind estimates, which is not considered in this research.

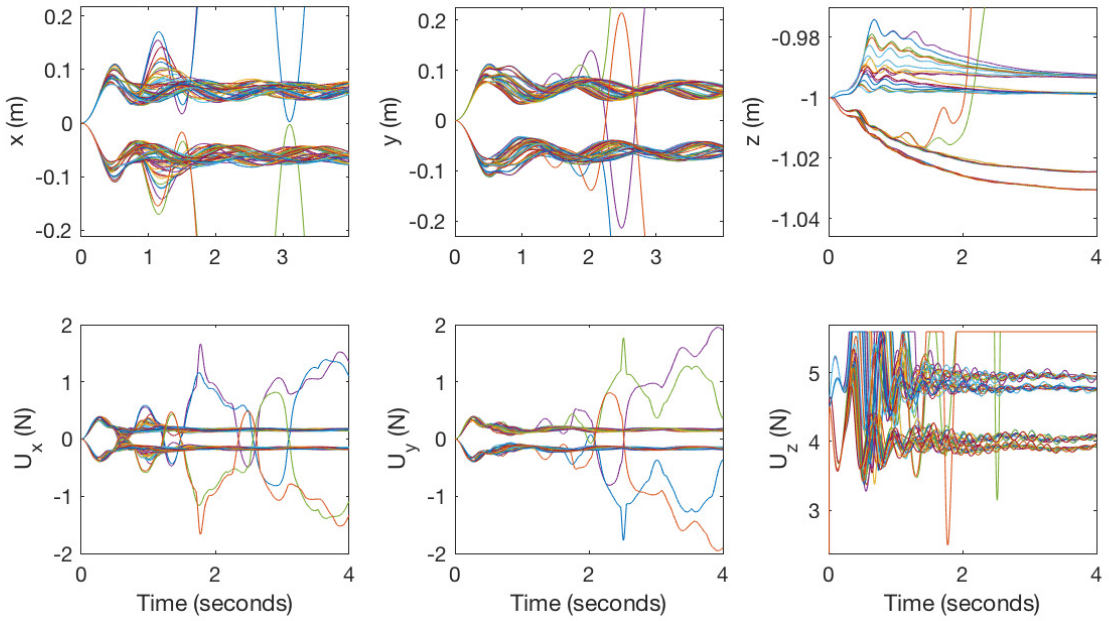

Figure 5.29: Positions (x, y, z) and their respective qc-SMC inputs considering wind step estimates, full quadrotor model influenced by coefficients incertitude and combinations of wind speed steps

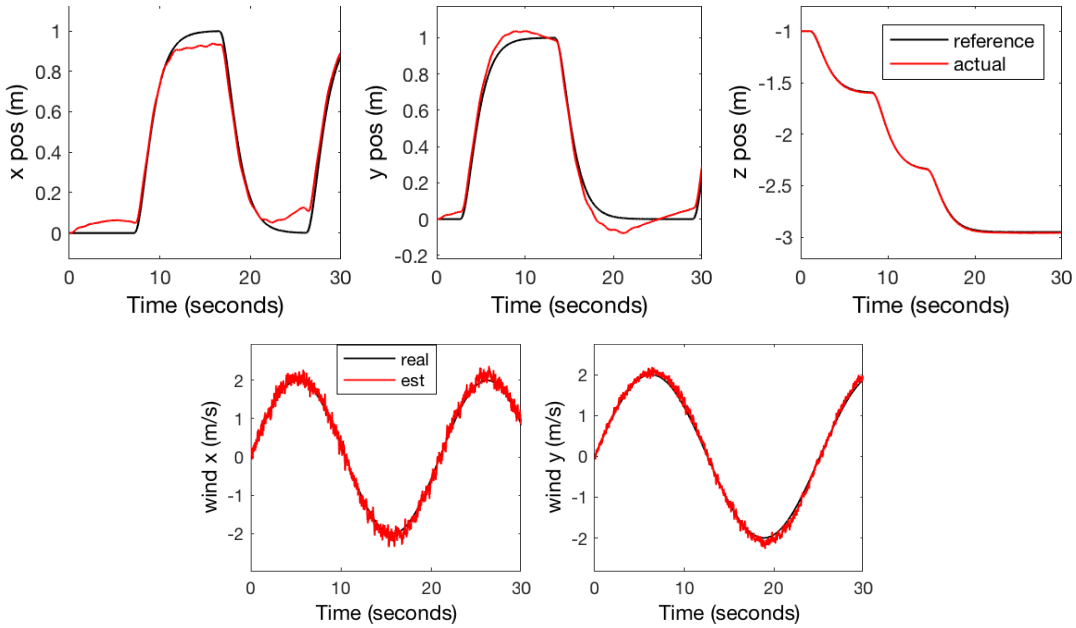

Figure 5.30: Positions (x, y, z) and wind estimates, using qc-SMC inputs considering wind estimates, full quadrotor model and tuned smaller values of ϱ_i.

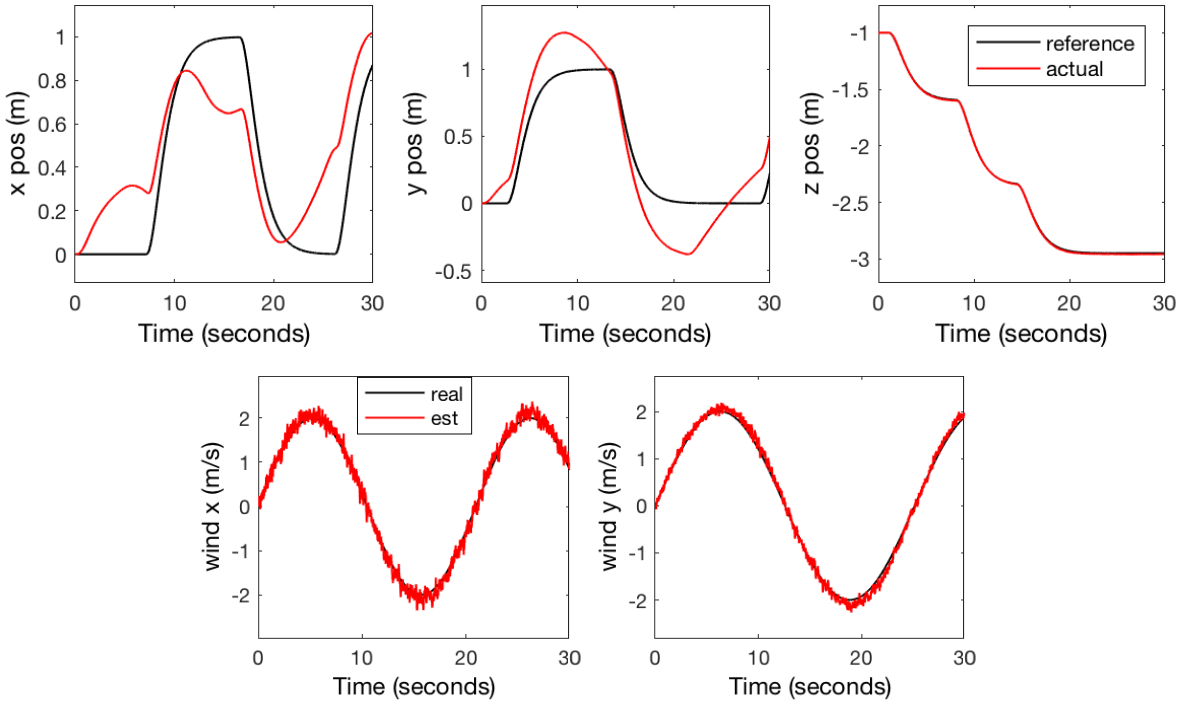

Figure 5.31: Positions (x, y, z) and wind estimates, using qc-SMC inputs considering wind estimates, full quadrotor model and higher values of ϱ_i.

In the previous control/estimation coupling study, the wind estimates are supposed to be exact without any additional error. In reality, wind estimates admit some estimation errors coming from the incertitude of the identified aerodynamic coefficients. As explained in section 5.4.3, these errors depends on the wind speed: we obtain admissible estimation errors which are around $0.7\,m/s$ for step wind speed of $1\,m/s$, and estimation errors around $1.4\,m/s$ for step wind speed of $2\,m/s$. One solution to include the estimation error to the control algorithm is to augment the nominal wind estimates of values depending on the estimation errors for that particular wind speed (more wind speeds can be tested *a priori* and their corresponding errors can be inserted in a table, then an interpolation can be found). In this way, the robustness of the control algorithms are still preserved. Then, the control algorithm takes as input $\bar{w} = \min\{|\hat{w}|, |\hat{w} + e_w|\}$ where $|\hat{w}|$ is the nominal wind estimate and $|\hat{w} + e_w|$ is the nominal wind estimate augmented by its estimation error.

5.5.5 Preliminary experiments

After that the control algorithm was validated in simulations, some preliminary experiments are carried out at ONERA. The following results can give an idea on how the gains influence the real experiments. X4-MaG drone is investigated in this section. Tuning process for X4-MaG is not explained because it follows the same steps and the same deductions made for the Parrot. First of all, the time-delay caused by the rotors dynamics can be obtained performing some preliminary tests, where desired rotor velocities are imposed as step references. Actual and reference rotors velocity in revolutions per minute (rpm) are illustrated in Fig. 5.32. Then the PID and the qc-SMC are tested. The quadrotor is demanded to keep the hover position and some external disturbances are added

(the drone is kept steady by hand, and then it is inclined with different angles to check the resulting forces and moments generated by the controllers). The following figures shows three values: Optitrack (the angles coming from the cameras), estimated (the angles estimated thanks to the quadrotor on-board sensors), desired (the desired angles that the quadrotor must keep). PID controller is tested and the results are shown in Fig. 5.33. Three cases are then presented to show the influence of the ϱ_i parameter on SMCs. The main disadvantage of sliding mode controllers is the chattering effect and the explanation on the methodology to avoid the chattering is extensively explained previously. Fig. 5.35 shows the qc-SMC with $\varrho_\phi = 10$; $\varrho_\theta = 10$; $\varrho_\psi = 5$, the SMC presents an accentuated quasi-chattering effect, which can drain very fast the on-board battery because of the numerous switching activities of the rotors. Fig. 5.35 shows the SMC with $\varrho_\phi = 40$; $\varrho_\theta = 40$; $\varrho_\psi = 35$. The quasi-chattering effect is attenuated, but the control inputs are still not comparable with the PID ones. For this reason, more experiments are needed to tune accordingly the SMC parameters. However, these results are very promising since they have proven that the chattering effect, which is the main drawback of SMCs in quadrotors problem, can be attenuated with a careful tuning of parameters and using the designed qc-SMC.

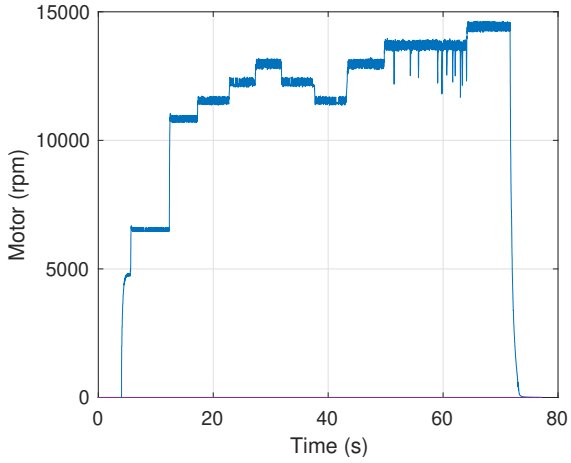

(a)

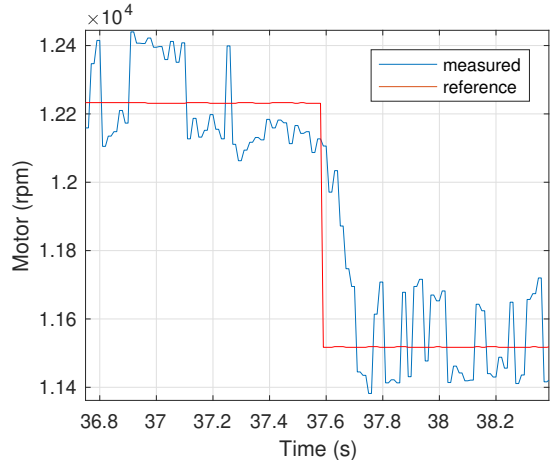

(b)

Figure 5.32: Steps response of the motors in (a), and its zoom in (b).

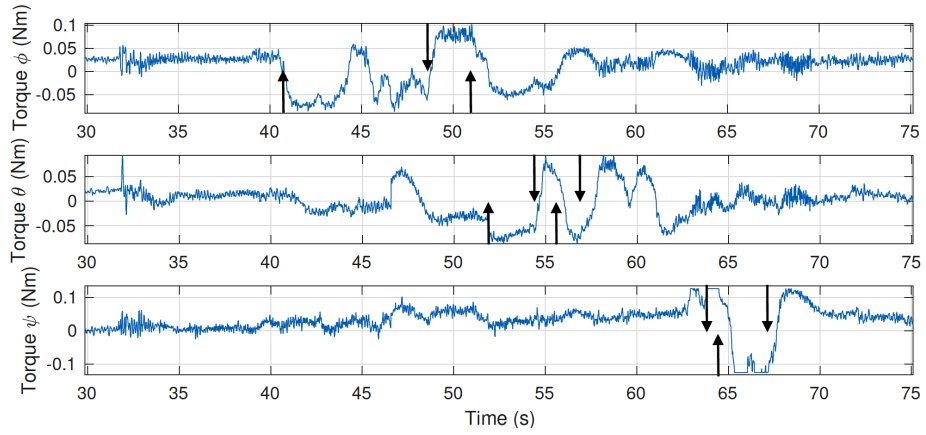

(a)

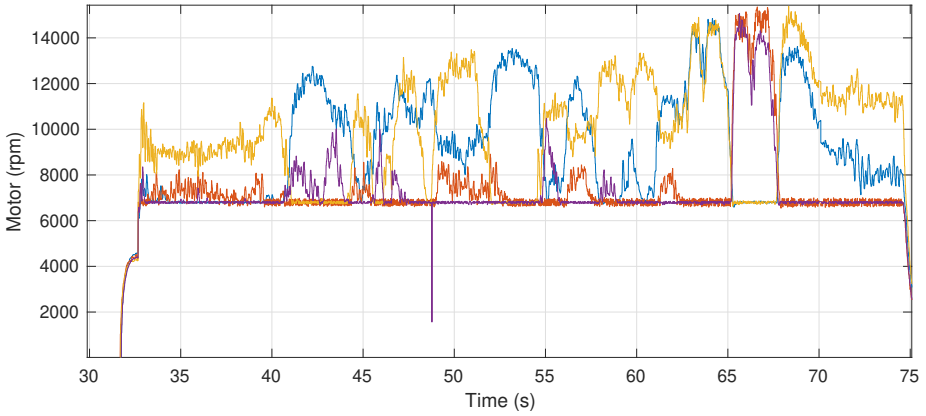

(b)

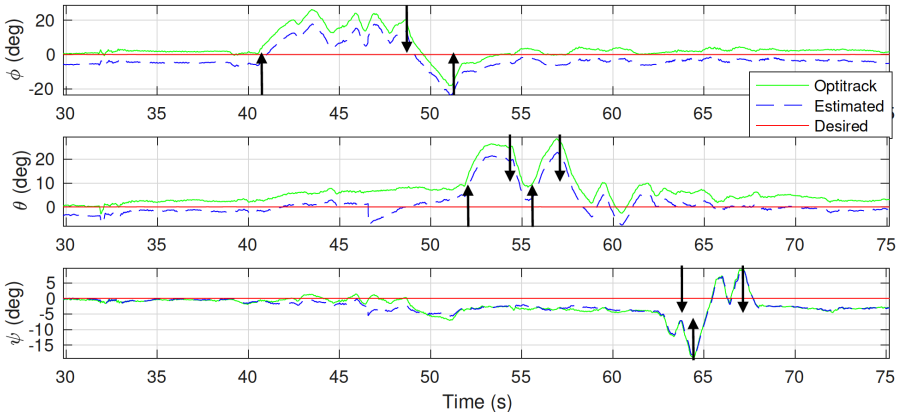

(c)

Figure 5.33: PID controller: Computed torques (a), motor velocities (b), desired and actual angles (c).

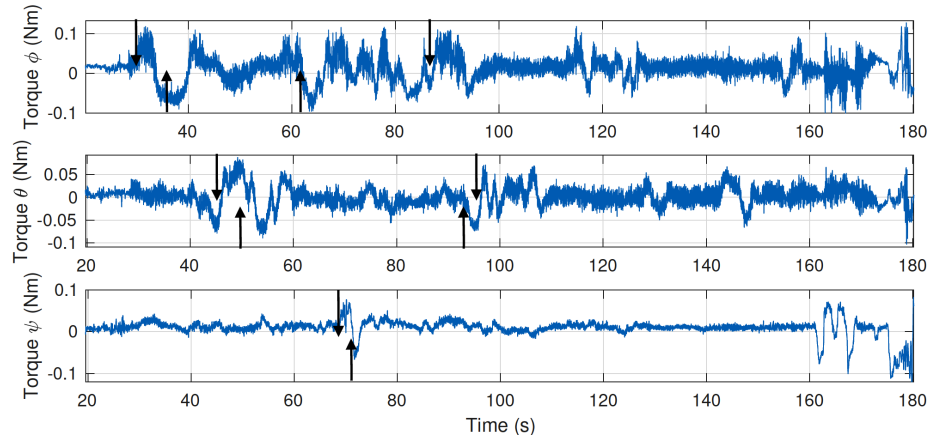

(a)

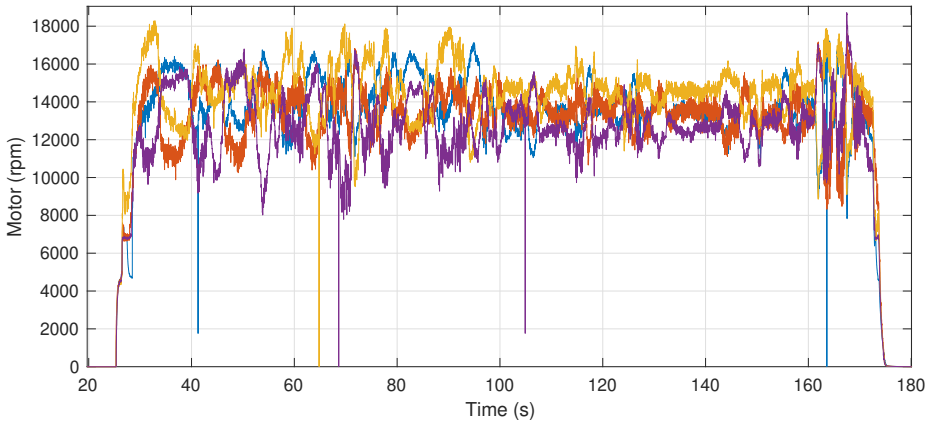

(b)

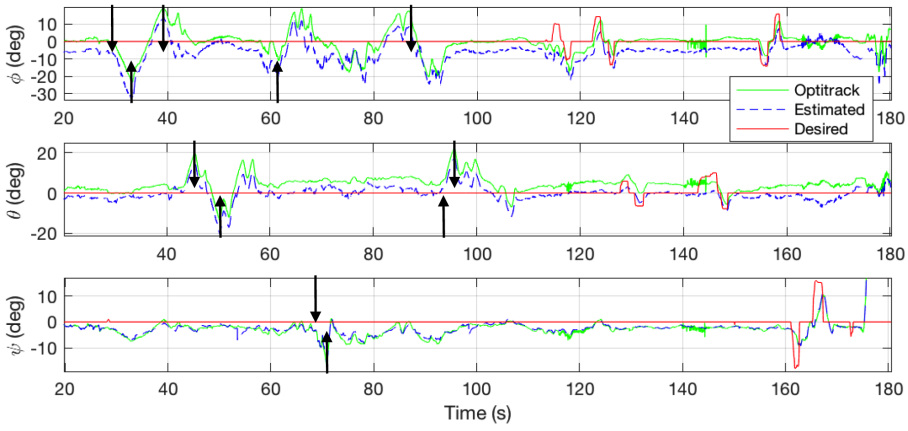

(c)

Figure 5.34: Exp 1 using qc-SMC: Computed torques (a), motor velocities (b), desired and actual angles (c).

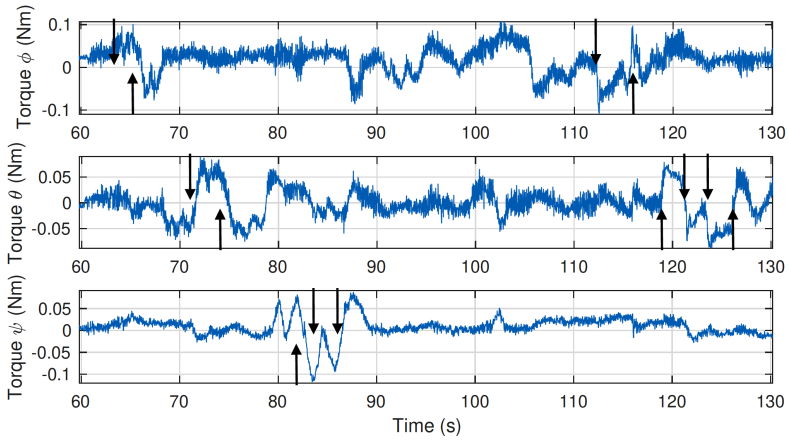

(a)

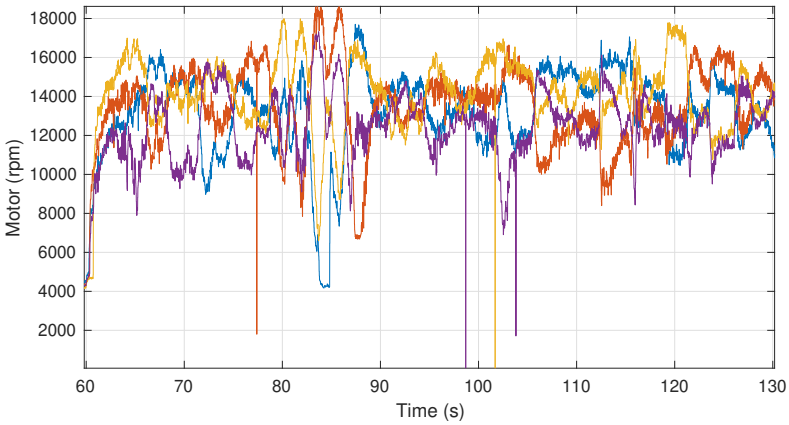

(b)

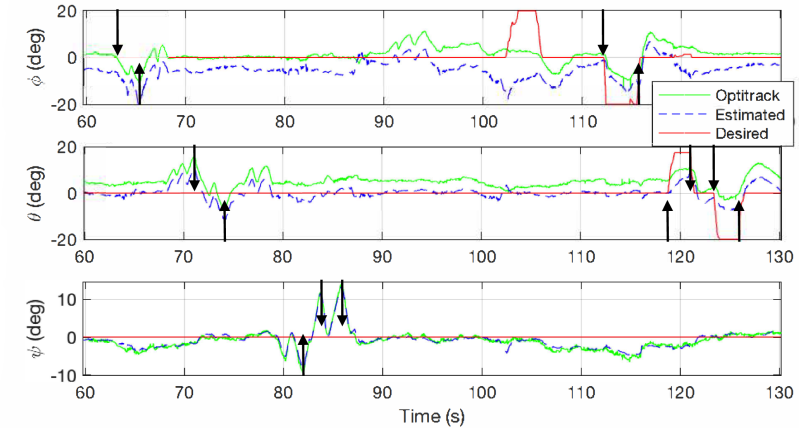

(c)

Figure 5.35: Exp 2 using qc-SMC: Computed torques (a), motor velocities (b), desired and actual angles (c).

5.6 Conclusion

This Chapter is entirely devoted to validation of the proposed control and estimation algorithms respecting given constraints:

First, four wind estimation algorithms are studied. Results validate the algorithms that perform well the estimation using the simpler quadrotor model. Simulations have also found that smaller convergence time can be obtained at the price of smaller filtering ability against noises. In this context, estimation algorithm based on linear quadrotor dynamics has the best results. Limit of the estimation robustness against the incertitude of aerodynamic coefficients, which are not considered in the algorithms design, and against wind speeds are also studied. It is shown that the considered worst cases (where the aerodynamic coefficients used in algorithms design differ very much from the ones used for test) have estimation errors which depend on the wind speeds. A final test with the full nonlinear quadrotor model show that the estimation is performed quite well for x, y directions, while in z the estimation produce result that is not acceptable. In conclusion, except for z dynamics, wind estimation algorithm can be applied respecting the imposed constraints: wind speeds having sinusoidal dynamics with $2m/s$, $2m/s$, $0.2m/s$ maximal values and $0.3\,rad/s$ maximal frequency, Gaussian noises with 2.5 deg$/s$, and $0.052\,m/s^2$ standard deviations for gyroscope and accelerometer respectively, additional Gaussian noises of $1\,cm/s$ standard deviation for linear velocities, and 1 deg standard deviation for angles because state measurement (u, v, w, ϕ, θ) are not reconstructed exactly. These values comes from the measurements in lab.

Then, SMCs are extensively studied. The tuning process is illustrated in detail. The contribution with respect to conventional first order sliding mode control is highlighted, and a recent quasi-continuous high order sliding mode control is also tested and discussed in simulations. Based on results of numerical experiments the qc-SMC has the best performance among all the designed SMCs. Then, its stability is extensively studied considering different wind speeds and quadrotor model incertitude, illustrating the main limitations and checking the domain of stability. Since this approach is strictly related to the wind estimation, the coupling with the estimator is also desired. In this context, simulations are provided showing the resulting improvement of the control effort. Last, the preliminary real experiments shows that qc-SMC has the ability to attenuate the chattering issue. In conclusion, qc-SMC can be applied to control a quadrotor respecting the given imposed constraints: trajectory tracking with $10\,cm$ maximal error in (x, y, z) in the worst condition (maximal wind speed equal to 2, m/s), adaptation of the effort on the rotors, attenuation of the chattering effect.

Chapter 6

Conclusion and Open Problems

Conclusion

The results of the thesis can be summarized as follows:

In order to better represent the impact of the wind field on mini drones, aerodynamic coefficients influenced by wind components are computed in body frame using the blade element momentum theory for helicopters. Then, the whole dynamics model of the quadrotor is presented, finding the external equilibrium forces and moments and considering the nonlinear aerodynamic coefficients influenced by the wind velocity. The resultant equations are highly nonlinear and thus their direct application for synthesis of control and estimation algorithms is complicated. To overcome this problem, some acceptable simplifications are used which are based on in-door experiments. The overall quadrotor system is then rewritten in state-space form to show the controls and wind influences on the quadrotor. Using this state-space representation, control laws and estimation algorithms are computed.

After the quadrotor modeling, the thesis focuses the attention on the design of regulation algorithms and the study of the system robustness property applying SMC having wind velocity as input. The upper bounds of wind-induced disturbances are characterized, which allow a SMC technique to be applied with guaranteed convergence properties. The peculiarity of the considered case is that the disturbance upper bounds depend on the control amplitude itself in a nonlinear fashion, which leads to a new procedure for the control tuning. Then the analysis and reduction of chattering effects, as well as investigation of rotor dynamics issues are studied. Two varying gain SMCs are proposed, using first-order and quasi-continuous designs. The results show that the quasi-continuous control has the best performance with respect to designed first-order and conventional SMCs.

After the controllers design, the thesis focuses the attention on the wind estimation algorithms, presenting several estimators of wind velocity and studying the wind estimates precision. An auxiliary decomposition of dynamical equations is performed in known and unknown terms to be estimated. Three time-varying parameter estimation algorithms are introduced, compared and finally merged. This methodology takes the advantage of a detailed UAV flight dynamics model, using identified nonlinear aerodynamic coefficients. Results shows that the sensor's noise are counteracted by the algorithms, however the algorithm is strongly affected by the model incertitude which comes from the identification process. The estimation algorithms are less reliable on z dynamics using the full non linear quadrotor model.

The CW-Quad Toolbox, which consists in a group of Simulink libraries to simulate a quadrotor under wind perturbation, is built to make preliminary simulations and validate the studied SMC and estimation algorithms before to perform experiments in lab. Fully configurable masks are provided to simulate quadrotors with different shapes and in different flight conditions. Only blocks provided with basic Simulink environment are used to ensure a better compatibility with most of Simulink versions, avoiding any other auxiliary toolbox which typically are sold separately. In this way, it is easier to take and/or modify each single model component to improve them or to use them in other projects without compromise the entire code. In opposite to use also Matlab code which allows to build the model faster, but not easily modifiable.

Open Problems

Further studies can be made to improve the results of this thesis:

Regarding the quadrotor model part, the model formulation can be further improved adding some neglected terms which are not tested and not validated in this research. In particular during the flight, there are aerodynamic influences between the front and the rear rotors, and between the body and the rotors [Hwang *et al.* 2015]. Moreover, the four motors, driving the four rotors, present some difference due to the production process. Mechanical and electrical components are never equal, even with the same specifics. These additional studies may improve the wind estimation.

Regarding the control part, SMC can be further improved. The quasi-continuous SMC design allows simplifications to be applied on the upper-bounds of the disturbances. Some constants are selected to be greater than these time-varying disturbances and derivative, producing the overestimation of the gains. Analytically it is not possible to compute exactly the upper-bounds, however additional identifications can solve this problem. The varying-gain SMC algorithms are designed using the identified K_D coefficient, which is strictly related to the wind speed. Since the focus of this research is to find the wind estimates, then the controller was built to consider as input directly the wind speed. However, an improvement for the SMC robustness would be to consider as input an estimation of the product $K_D(u_w,\, v_w,\, w_w)$. Other improvements would be to optimize the dynamics of the sliding mode taking into account the performance constraints, as for H_∞, and to create a grid of all the parameters, trajectories, wind profiles to tune an optimal set of gains together, which are tuned separately step by step in this research. $\mathcal{H}_\infty$ controller, introduced and explained in the Appendix C, can be further implemented and tested to validate the proposed controller strategy. Another missing step is to find optimal weighting transfer functions, which is often very tricky. The idea is to start with the baseline solution, given by the implemented working PID controller, and redesign the PID gains with a structured H_∞ design technique, analyzing the transfer functions that are achieved by the PID controller to deduce the weight functions. Next, the flexibility of the H_∞ design framework can be used to improve the properties of the baseline solution.

Regarding the wind estimation part, the algorithms can be improved avoiding the additional simplifications for the rotational quadrotor dynamics. Results with full nonlinear quadrotor model show that the estimation is performed quite well for x, y directions, while in z the estimation produces a less accurate result. For this reason, an additional identification process can be made to improve the algorithms performance.

After that control and estimation algorithms were developed and extensively studied, an experimental validation is expected to be carried out at ONERA-Lille. Even extensive simulations have some hidden errors that can be discovered only in the tests. Experiments are also very useful to modify accordingly the control and the wind estimation laws, tuning properly the gains and adding terms that are not considered in the design process.

Appendix A

Computation of the flight aerodynamics

Contents

The equations presented in this appendix are only a minimal part of the helicopter analysis theory, but they are useful to give the idea where the quadrotor flight dynamic equations come from.

A.1 Momentum theory

The momentum theory (MT) allows the prediction of the rotor thrust and power to be carried out based on airflow model (see Fig. A.1). The vehicle must operate in different flight cases: hover, climb, descent, and/or forward flight. These flight cases use the same scheme in Fig. A.1 but changing accordingly the vector directions of the velocities.

A.1.1 Hover flight

For hover phase, under the assumption that the flow is quasi-steady and by the principles of conservation of mass, the mass flow rate must be constant inside the boundaries of the rotor wake such as

$$\dot{m} = \iint_{\infty} \rho \vec{V} \cdot d\vec{S} = \iint_{2} \rho \vec{V} \cdot d\vec{S},$$

where V is the velocity of the airflow, S denotes the surface of the airflow volume, ρ is the air density, 0, 1, 2, ∞ denote respectively the first upper-stream circle of the airflow volume, the circle just up the rotor disk, the circle just down the rotor disk, and the last circle at the downstream. Assuming 1-D incompressible flow case

$$\dot{m} = \rho A_{\infty} w = \rho A_2 v_i = \rho A v_i,$$

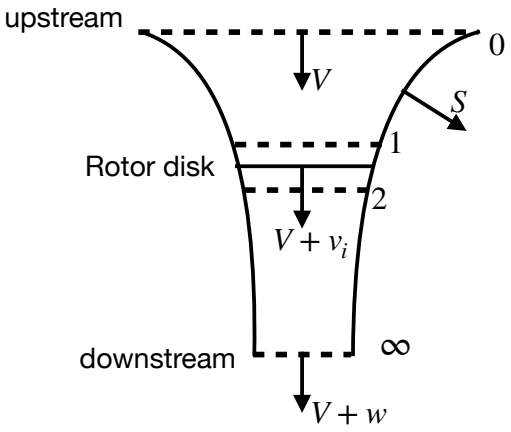

Figure A.1: Airflow model for momentum theory.

where w is the airflow at the downstream, v_i is the induced velocity through the rotor disk, and A denotes the area of the circle. The principle of conservation of fluid momentum gives

$$-\vec{F} = T = \iint_{\infty} \rho(\vec{V} \cdot d\vec{S})\vec{V} - \iint_{0} \rho(\vec{V} \cdot d\vec{S})\vec{V},$$

where F is the force caused by the gravity and the mass of the helicopter, and in hover flight the thrust becomes

$$T = \iint_{\infty} \rho(\vec{V} \cdot d\vec{S})\vec{V} = \dot{m}w. \tag{A.1}$$

From the principle of conservation of energy

$$Tv_i = \iint_{\infty} \frac{1}{2}\rho(\vec{V} \cdot d\vec{S})\vec{V}^2 - \iint_{0} \frac{1}{2}\rho(\vec{V} \cdot d\vec{S})\vec{V}^2,$$

which, in hover state, becomes

$$Tv_i = \iint_{\infty} \frac{1}{2}\rho(\vec{V} \cdot d\vec{S})\vec{V}^2 = \frac{1}{2}\dot{m}w^2. \tag{A.2}$$

Thus, from equations (A.1) and (A.2) we have that

$$v_i = \frac{1}{2}w,$$

and the thrust is finally obtained as

$$T = \dot{m}w = \dot{m}(2v_i) = 2(\rho A v_i)v_i = 2\rho A v_i^2, \tag{A.3}$$

which gives the induced velocity through the rotor in hover flight

$$v_h = v_i = \sqrt{\frac{T}{2\rho A}}.$$

The consequent power required to hover is

$$P = Tv_i = 2\dot{m}v_i^2 = 2(\rho A v_i)v_i^2 = 2\rho A v_i^3.$$

Finally, from eq. (A.3) the thrust coefficient is defined as

$$C_T = \frac{T}{\rho A V_{tip}^2} = \frac{T}{\rho A \omega^2 R^2},$$

where V_{tip} is the angular velocity at the tip of the blade. The induced inflow ratio, in hover flight, is defined as

$$\lambda_h = \lambda_i = \frac{v_i}{\omega R} = \frac{1}{\omega R}\sqrt{\frac{T}{2\rho A}} = \sqrt{\frac{T}{2\rho A \omega^2 R^2}} = \sqrt{\frac{C_T}{2}}.$$

In the same way the rotor power coefficient can be found

$$C_P = \frac{P}{\rho A V_{tip}^3} = \frac{P}{\rho A \omega^3 R^3}.$$

Based on momentum theory for hover flight, the power coefficient can be rewritten as

$$C_P = \frac{Tv_i}{\rho A(\omega R)^3} = \frac{T}{\rho A(\omega R)^2}\frac{v_i}{\omega R} = C_T\lambda_i = \frac{C_T^{\frac{3}{2}}}{\sqrt{2}}.$$

The rotor torque coefficient is defined as

$$C_Q = \frac{Q}{\rho A V_{tip}^2 R} = \frac{Q}{\rho A \omega^2 R^3}.$$

A.1.2 Axial climb flight

In axial climb phase, the three conservation laws can be applied considering the problem to be quasi 1-D, and at each cross section the flow properties are distributed uniformly. As before, by the conservation of mass

$$\dot{m} = \rho A_\infty(V_c + w) = \rho A(V_c + v_i),$$

and by conservation of momentum

$$T = \iint_\infty \rho(\vec{V}\cdot d\vec{S})\vec{V} - \iint_0 \rho(\vec{V}\cdot d\vec{S})\vec{V}.$$

In steady climb velocity the thrust is

$$T = \dot{m}(V - c + w) - \dot{m}V_c = \dot{m}w,$$

which leads to the work done by the climbing rotor

$$T(V_c + v_i) = \iint_\infty \frac{1}{2}\rho(\vec{V}\cdot d\vec{S})\vec{V}^2 - \iint_0 \frac{1}{2}\rho(\vec{V}\cdot d\vec{S})\vec{V}^2 = \frac{1}{2}\dot{m}(V_c + w)^2 - \frac{1}{2}\dot{m}V_c^2 = \frac{1}{2}\dot{m}w(2V_c + w).$$

The relation, between the induced velocity in climbing v_i and hovering phases v_h, is given by

$$\frac{v_i}{v_h} = -\left(\frac{V_c}{2v_h}\right) + \sqrt{\left(\frac{V_c}{2v_h}\right)^2 + 1}.$$

This is called *normal working state* of the rotor, in which hovering is the lowest limit. For a negative value of V_c just as the rotor begins to descent, this solution is physically invalid, because the called *vortex ring state* appears, as in Fig. A.2. It means that the power ratio for climb is valid only for $\frac{V_c}{v_h} \geq 0$ and it is

$$\frac{P}{P_h} = \frac{V_c}{2v_h} + \sqrt{\left(\frac{V_c}{2v_h}\right)^2 + 1}.$$

A.1.3 Axial descend flight

In axial descend phase, under the same assumptions as before, by the conservation of the mass

$$\dot{m} = \iint_{\infty} \rho \vec{V} \cdot d\vec{S} = \iint_{2} \rho \vec{V} \cdot d\vec{S},$$

which means

$$\dot{m} = \rho A_{\infty}(V_c + w) = \rho A(V_c + v_i),$$

and by the conservation of fluid momentum

$$T = -\iint_{\infty} \rho(\vec{V} \cdot d\vec{S})\vec{V} - \iint_{0} \rho(\vec{V} \cdot d\vec{S})\vec{V},$$

therefore, the thrust is

$$T = -\dot{m}(V_c + w) - (-\dot{m})V_c = -\dot{m}w.$$

The work done by the descent rotor is

$$T(v_i + V_c) = \iint_{0} \frac{1}{2}\rho(\vec{V} \cdot d\vec{S})\vec{V}^2 - \iint_{\infty} \frac{1}{2}\rho(\vec{V} \cdot d\vec{S})\vec{V}^2 = \frac{1}{2}\dot{m}(V_c)^2 - \frac{1}{2}\dot{m}(V_c + w)^2 = -\frac{1}{2}\dot{m}w(2V_c + w).$$

The relation, between the induced velocity in descend and hover phases, is

$$\frac{v_i}{v_h} = -\left(\frac{V_c}{2v_h}\right) - \sqrt{\left(\frac{V_c}{2v_h}\right)^2 - 1},$$

and the power ratio in descent phase is

$$\frac{P}{P_h} = \frac{V_c}{2v_h} - \sqrt{\left(\frac{V_c}{2v_h}\right)^2 - 1},$$

which are both valid only for $\frac{V_c}{v_h} \leq -2$, as in Fig A.2.

A.1.4 Forward flight

In forward phase, the mass flow rate through the rotor is defined as

$$\dot{m} = \rho A \sqrt{(V_\infty \cos\alpha)^2 + (V_\infty \sin\alpha + v_i)^2} = \rho A \sqrt{V_\infty^2 + 2V_\infty v_i \sin\alpha + v_i^2},$$

where α is the angle between the airflow direction V_∞ and the rotor disk area. By conservation of momentum, the thrust can be found as

$$T = \dot{m}(w + V_\infty \sin\alpha) - \dot{m}V_\infty \sin\alpha = \dot{m}w = 2\dot{m}v_i = 2\rho A v_i \sqrt{V_\infty^2 + 2V_\infty v_i \sin\alpha + v_i^2},$$

where the rate between the induced velocity in forward and in hover phases is denoted by

$$v_i = \frac{v_h^2}{(V_\infty \cos\alpha)^2 + (V_\infty \sin\alpha + v_i)^2}. \tag{A.4}$$

By the conservation of energy, the power is

$$P = T(v_i + V_\infty \sin\alpha) = \frac{1}{2}\dot{m}(V_\infty \sin\alpha + w)^2 - \frac{1}{2}\dot{m}V_\infty^2 \sin^2\alpha = \frac{1}{2}\dot{m}(2V_\infty w \sin\alpha + w^2).$$

Let define two parameters as respectively $\lambda = \frac{(V_\infty \sin\alpha + v_i)}{\omega R}$ the inflow ratio, and $\mu = \frac{V_\infty \cos\alpha}{\omega R}$ the advance ratio, then their relation is

$$\lambda = \frac{V_\infty \sin\alpha}{\omega R} + \frac{v_i}{\omega R} = \mu \tan\alpha + \lambda_i.$$

Considering eq. (A.4), λ can also be rewritten as

$$\lambda = \mu \tan\alpha + \frac{C_T}{2\sqrt{\mu^2 + \lambda^2}}.$$

Then, the ratio between the rotor power in forward and hover phases can be found as

$$\frac{P}{P_h} = \frac{P}{Tv_h} = \frac{T(V_\infty \sin\alpha + v_i)}{Tv_h} = \frac{V_\infty \sin\alpha + v_i}{v_h} = \frac{\lambda}{\lambda_h}.$$

A.1.5 Vortex ring state

The vortex ring state appears in the region $-2 \leq \frac{V_c}{v_h} \leq 0$ (see Fig. A.2, from [Leishman 2006]), here the momentum theory is invalid because the flow can take two possible equilibrium and a well defined slipstream doesn't exist, thus the control volume cannot be defined. Under these circumstances, a more turbulent and aperiodic flow pattern may exist at the rotor. However, an approximated curve can still be defined empirically on the basis of flight tests [Leishman *et al.* 2002, Taamallah 2010]. For example, a continuous approximation of the induced velocity curve is

$$\frac{v_i}{v_h} = k + k_1\left(\frac{V_c}{v_h}\right) + k_2\left(\frac{V_c}{v_h}\right)^2 + k_3\left(\frac{V_c}{v_h}\right)^3 + k_4\left(\frac{V_c}{v_h}\right)^4$$

where k is the measured induced power factor in hover, k_1, k_2, k_3, k_4. are negative values coming from experiments.

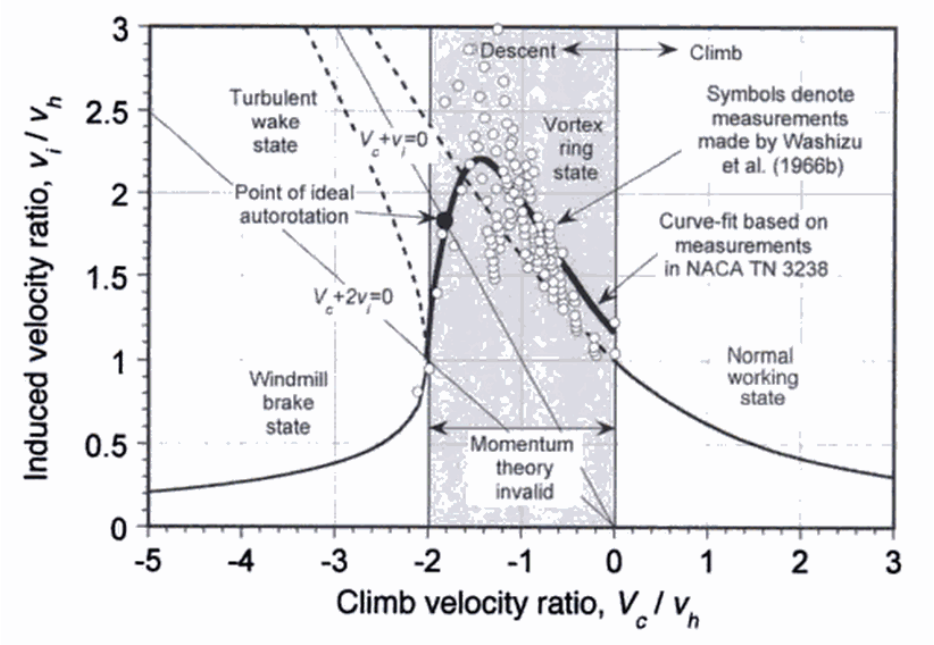

Figure A.2: Variation of induced velocity in vertical flight.

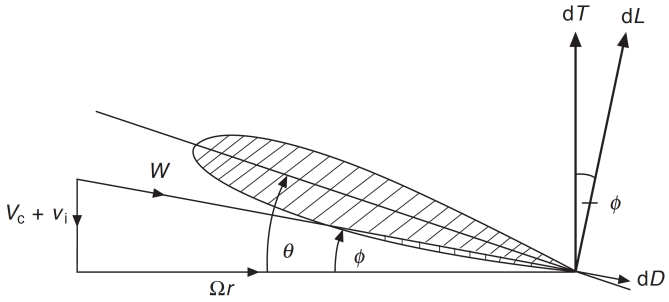

Figure A.3: Forces acting on the blade element.

A.2 Blade element theory

The Blade element theory (BET) assumes that each blade section acts as a quasi 2-D airfoil to produce aerodynamic forces and moments. Rotor performances can be obtained by integrating each blade element over the length of the blade and then over a rotor revolution.

Fig. A.3 shows the 2-D representation of a blade section where Ωr is blade tip speed, W is the resultant velocity, dL is the elementary lift, dD is the elementary drag, ϕ is the relative inflow angle, θ is the pitch angle. The elementary lift and drag are defined as

$$dL = \frac{1}{2}\rho W^2 c\, C_l dy, \quad dD = \frac{1}{2}\rho W^2 c\, C_d dy$$

where y is the distance between the center of the rotor disk and the blade chord c, C_l is the lift coefficient. The rotor

solidity is defined as

$$\sigma = \frac{N_b c}{\pi R} \tag{A.5}$$

where N_b is the blades number of the rotor. Proceeding with the analysis and some simplifications, dT the elementary thrust, dQ the elementary torque, dP the elementary power, dC_T the elementary thrust coefficient, dC_Q the elementary torque coefficient, dC_P the elementary power coefficient can be found

$$dT = N_b dL, \quad dQ = N_b(\phi dL + dD)y, \quad dP = N_b\Omega(\phi dL + dD)y,$$
$$dC_T = \frac{1}{2}\frac{N_b c}{\pi R}C_l r^2 dr, \quad dC_Q = \frac{1}{2}\sigma(\phi C_l + C_d)r^3 dr,$$

where α is the angle of attack, and C_l is lift coefficient. The issue of the BET is to model correctly the induced velocity on the rotor disk, for this reason BET (which considers the shape of the blades) is often coupled with MT (which considers the rotors as unique objects).

A.3 Blade element momentum theory

The Blade element momentum theory (BEMT) combines blade element and momentum theories, and it estimates the inflow distribution along the blade by using the conservation laws applied to an annulus of the rotor disk, having dy thickness and distant from the center y. With the same considerations made for the momentum theory, the mass flow rate and the incremental thrust can be found

$$d\dot{m} = \rho dA(V_c + v_i) = 2\pi\rho(V_c + v_i)y\,dy, \quad dT = 4\pi\rho(V_c + v_i)v_i y\,dy.$$

And, therefore, the incremental coefficients of the annulus are computed as

$$dC_T = \frac{dT}{\rho\pi R^2\omega^2 R^2} = \frac{2\rho(V_c + v_i)v_i dA}{\rho\pi R^2\omega^2 R^2} = 4\left(\frac{V_c + v_i}{\omega R}\right)\left(\frac{v_i}{\omega R}\right)\left(\frac{y}{R}\right)d\left(\frac{y}{R}\right) = 4\lambda\lambda_i r dr,$$
$$dC_{Pi} = \lambda dC_T,$$

where dr is the infinitesimal radius of the rotor disk, dC_{Pi} is the induced power coefficient consumed by the annulus. The total power and the thrust coefficients are found as

$$C_T = \int_{r=0}^{r=1} dC_T, \quad C_{Pi} = \int_{r=0}^{r=1} \lambda dC_T.$$

Integrating over the rotor and under some approximations, the coefficients of thrust and power can be found as

$$C_T = \frac{1}{2}\sigma C_{l\alpha}\int_0^1 (\theta r^2 - \lambda r)dr,$$
$$C_P = \frac{C_T^{\frac{3}{2}}}{\sqrt{2}} + \frac{1}{8}\sigma C_{d0},$$

where $C_{l\alpha}$ is the lift coefficient corresponding to the angle of attack (based on the 2-D lift curve slope of the airfoil section), and C_{d0} is a constant coefficient of drag. The radial inflow quadratic equation is denoted by

$$\lambda(r, \lambda_c) = \sqrt{\left(\frac{\sigma C_{l\alpha}}{16} - \frac{\lambda_c}{2}\right)^2 + \frac{\sigma C_{l\alpha}}{8}\theta r} - \frac{\sigma C_{l\alpha}}{16} - \frac{\lambda_c}{2}.$$

where in hover $\lambda_c = 0$. In practical applications the BEMT equations are numerically solved discretizing the blade into a series of small elements Δr.

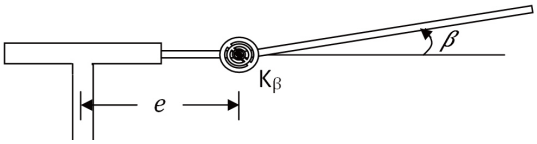

Figure A.4: Fictitious spring modeling the blade flapping.

A.4 Blade flapping

If the blade is not stiff enough, there exist some interaction between the structure dynamics and the aerodynamics of the blade. This interaction cause the blade flapping effect, which can be modeled as a fictious spring (see Fig. A.4). Under the hypothesis that β is small the equation of the blade motion is

$$I_x\ddot{\beta} + \omega^2\left(I_x + M_{blade}x_geR^2\right)\beta = M_a - k_\beta\beta,$$

where I_x is the moment of inertia of the blade, x_gR is the position of the center of gravity of the blade, M_{blade} is the mass of the blade, and M_a is the aerodynamic momentum of each element of the blade. The blade flapping equation can be expanded as

$$\begin{aligned}&\frac{d^2\beta}{d\psi^2} + \frac{1}{8}\gamma\left(1 + \frac{4}{3}\mu\sin\psi\right)\frac{d\beta}{d\psi} + \left((1+\delta) + \frac{1}{8}\gamma\left(\frac{4}{3}\mu\cos\psi + \mu^2\sin 2\psi\right)\right)\beta\\ &= -\frac{1}{8}\gamma\left(\theta_0\left(1 + \frac{8}{3}\mu\sin\psi + 2\mu^2\sin^2\psi\right) - \theta_{tw}\left(\frac{4}{5} + 2\mu\sin\psi + \frac{4}{3}\mu^2\sin^2\psi\right) - \frac{4}{3}\lambda - 2\mu\lambda\sin\psi\right),\end{aligned}$$

where ψ is the azimuth angle of the blade (see Fig. A.5).

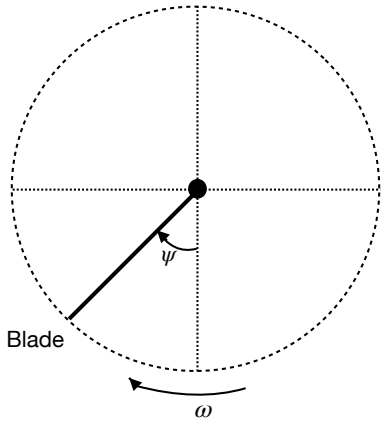

Figure A.5: Revolution of the blade's rotor.

Under the steady transition phase and periodic blade movement in ψ, the equation can be simplified as

$$\begin{aligned}\beta &= a_0 + a_1\sin\psi + b_1\cos\psi,\\ \dot{\beta} &= (a_1\cos\psi - b_1\sin\psi)\omega,\end{aligned} \tag{A.6}$$

with the following terms, where $\bar{c}$ is the average length of the blade chord, θ_{tw} and θ_0 are the twist angles at the tip and at the root of the blade profile,

$$a_0 = -\frac{\gamma}{8(1+\delta)}\left(\theta_0\left(1+\mu^2\right) - \theta_{tw}\left(\frac{4}{5}+\frac{2}{3}\mu^2\right) - \frac{4}{3}\lambda\right);\ \delta = \frac{M_{blade}x_g eR^2}{I_x};\ \gamma = \frac{\rho a \bar{c} R^4}{I_x};$$
$$\delta a_1 = -\frac{\gamma}{4}\mu\left(\frac{4}{3}\theta_0 - \theta_{tw} - \lambda\right) + \frac{\gamma}{8}b_1\left(1-\frac{\mu^2}{2}\right);\ \delta b_1 = -\frac{\gamma}{6}\mu a_0 - \frac{\gamma}{8}a_1\left(1+\frac{\mu^2}{2}\right).$$

A.5 Application of the BEMT

Once the the Blade Element Momentum Theory is introduced, as example the computation of the rotor's thrust is illustrated below. The other forces, moments and coefficients can be found with similar procedure.

A.5.1 Influence of apparent wind speed on blade elements

The first step is to find the equation of the wind speed acting on the blade element, as in Fig. A.6. The tangent

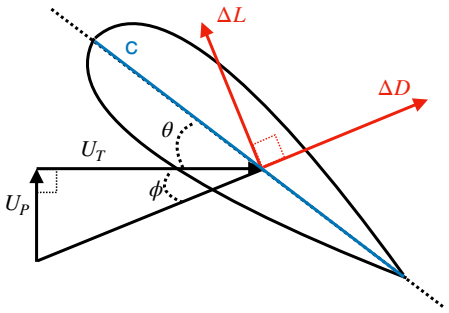

Figure A.6: Forces and wind speed acting on blade section.

component of the apparent wind speed on the blade is

$$U_T = \sqrt{(u-u_w)^2(v-v_w)^2}\sin\psi + \omega r,$$

and the perpendicular component is

$$U_P = \sqrt{(u-u_w)^2(v-v_w)^2}\beta\cos\psi + (w-w_w) + \dot{\beta}r - v_i + pl\sin\left(\frac{\pi}{2}(j-1)+\varepsilon\right) - ql\left(\frac{\pi}{2}(j-1)+\varepsilon\right).$$

A.5.2 Generated forces on the blade element

The resultant drag and lift of a blade section can be computed as

$$\Delta L \approx \frac{1}{2}\rho U_T^2 a\left(\theta_0 - \theta_{tw}\frac{r}{R} + \frac{U_P}{U_T}\right)c\Delta r,$$
$$\Delta D \approx \frac{1}{2}\rho U_T^2\left(C_{D0} + C_{Di}\left(\theta_0 - \theta_{tw}\frac{r}{R} + \frac{U_P}{U_T}\right)^2\right)c\Delta r,$$

assuming that $U_p \ll U_T$.

A.5.3 Computation of the total rotor's thrust

The thrust of each blade section ΔT can be found projecting ΔL and ΔD on the rotor axis

$$\Delta T = (\Delta L \cos\phi + \Delta D \sin\phi)\cos\beta.$$

Under the hypothesis that ϕ, β are small, we have that $\Delta T \approx \Delta L$ and the total thrust is

$$T = \frac{N_b}{2\pi}\int_0^{2\pi}\int_0^R \frac{\Delta L}{\Delta r} dr d\psi.$$

Under the hypothesis that β is an harmonic periodic function in ψ and considering only its first term, as in eq. (A.6), we obtain the total thrust

$$T = C_T \rho A R^2 \omega^2,$$

with

$$\begin{aligned}
C_T &= \sigma a\left(\left(1+\frac{3}{2}\mu^2\right)\frac{\theta_0}{6} - \left(1+\mu^2\right)\frac{\theta_{tw}}{8} - \frac{\lambda}{4}\right),\\
\mu &= \frac{1}{R|\omega|}\sqrt{(u-u_w)^2+(v-v_w)^2},\\
\lambda &= \frac{v_i + w_w - w + ql\cos\left(\frac{\pi}{2}(j-1)+\varepsilon\right) - pl\sin\left(\frac{\pi}{2}(j-1)+\varepsilon\right)}{R|\omega|}.
\end{aligned}$$

Appendix B

Auxiliary tools

Contents

B.1 Rotation matrix

The rotation of a rigid body in space can be represented using Euler angles or Quaternions. Choosing the Euler representation, 3 elementary rotations of $(\phi,\ \theta,\ \psi)$ angles around the $(x,\ y,\ z)$ axes respectively can be defined as

$$\mathbf{R}_{\mathbf{x}\phi} = \begin{bmatrix} 1 & 0 & 0 \\ 0 & \cos\phi & -\sin\phi \\ 0 & \sin\phi & \cos\phi \end{bmatrix},\ \mathbf{R}_{\mathbf{y}\theta} = \begin{bmatrix} \cos\theta & 0 & \sin\theta \\ 0 & 1 & 0 \\ -\sin\theta & 0 & \cos\theta \end{bmatrix},\ \mathbf{R}_{\mathbf{z}\psi} = \begin{bmatrix} \cos\psi & -\sin\psi & 0 \\ \sin\psi & \cos\psi & 0 \\ 0 & 0 & 1 \end{bmatrix},$$

And the total rotation matrix R is defined as

$$\mathbf{R} = \mathbf{R}_{\mathbf{x}\phi} \cdot \mathbf{R}_{\mathbf{y}\theta} \cdot \mathbf{R}_{\mathbf{z}\psi} = \begin{bmatrix} c_\psi c_\theta & -s_\psi c_\phi + c_\psi s_\theta s_\phi & s_\phi s_\psi + c_\psi s_\theta c_\phi \\ s_\psi c_\theta & c_\psi c_\phi + s_\psi s_\theta s_\phi & -c_\psi s_\phi + s_\psi s_\theta c_\phi \\ -s_\theta & c_\theta s_\phi & c_\theta c_\phi \end{bmatrix},$$

where $c_\psi = \cos(\psi)$, $s_\psi = \sin(\psi)$ and similar for the other angles. Then, the passage of a column vector $\mathbf{X}$ from the Earth frame $(\mathcal{R}_0)$ to the body one $(\mathcal{R})$ is defined as

$$[\mathbf{X}^T]_{\mathcal{R}} = [\mathbf{X}^T]_{\mathcal{R}_0}\mathbf{R}.$$

B.2 Angular rates

The time variations $(\dot\phi,\ \dot\theta,\ \dot\psi)$, which are a differentiation over time of the three angles $(\phi,\ \theta,\ \psi)$, are different from the quadrotor angular velocities $(p,\ q,\ r)$, which are physically measured by the gyroscope. The passage between the $(p,\ q,\ r)$ and the $(\dot\phi,\ \dot\theta,\ \dot\psi)$ is given by [Etkin & Reid 1996]:

$$\begin{bmatrix} p \\ q \\ r \end{bmatrix} = \begin{bmatrix} 1 & 0 & -\sin\theta \\ 0 & \cos\phi & \sin\phi\cos\theta \\ 0 & -\sin\phi & \cos\phi\cos\theta \end{bmatrix} \begin{bmatrix} \dot\phi \\ \dot\theta \\ \dot\psi \end{bmatrix}.$$

B.3 Trajectory generation

The desired step references for coordinates $(x,\ y,\ z)$ are filtered, using a third order filter (see Fig. B.1)

$$\frac{\xi_f}{\xi_{wp}} = \frac{1}{(1 + G_i s)^3},$$

to obtain smooth velocity and acceleration trajectories, where ξ_{wp} is the way-point step reference, $\xi_f = (x_{des},\ y_{des},\ z_{des})$ is the filtered signal, $G_i,\ i = 1,\ 2,\ 3$ are the arbitrarily weight to create the desired smooth trajectory.

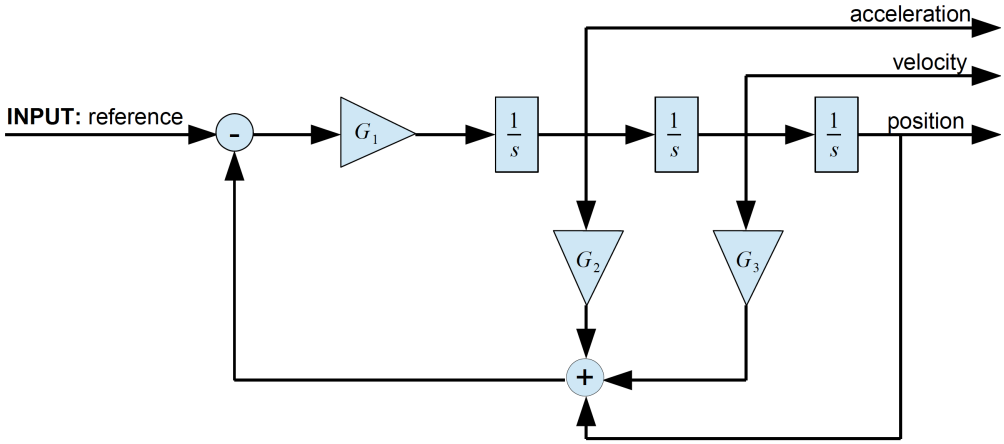

Figure B.1: Scheme for the third order filter.

B.4 Desired angles

The desired angles $(\phi_{des},\ \theta_{des})$ are derived from the expressions for the virtual controllers U_x and U_y, using the desired value of the yaw angle ψ:

$$\phi_{des} = \arcsin\left(U_x \sin\psi_{des} - U_y \cos\psi_{des}\right), \quad \theta_{des} = \arcsin\left(\frac{U_x \cos\psi_{des} + U_y \sin\psi_{des}}{\cos\phi_{des}}\right).$$

B.5 Quadrotor saturation

Quadrotors are physical objects and subjected to physical constraints, which correspond to their maximal linear and angular velocities and accelerations and controls. The limitations of the linear velocity and acceleration are

$$v_{min} = \begin{bmatrix} \dot{x}_{min} \\ \dot{y}_{min} \\ \dot{z}_{min} \end{bmatrix},\ v_{max} = \begin{bmatrix} \dot{x}_{max} \\ \dot{y}_{max} \\ \dot{z}_{max} \end{bmatrix};\ a_{min} = \begin{bmatrix} \ddot{x}_{min} = \frac{T_{min}}{m}\sin\theta_{min} \\ \ddot{y}_{min} = \frac{T_{min}}{m}\sin\phi_{min} \\ \ddot{z}_{min} = \frac{T_{min}}{m} - g \end{bmatrix},\ a_{max} = \begin{bmatrix} \ddot{x}_{max} = \frac{T_{max}}{m}\sin\theta_{max} \\ \ddot{y}_{max} = \frac{T_{max}}{m}\sin\phi_{max} \\ \ddot{z}_{max} = \frac{T_{max}}{m} - g \end{bmatrix};$$

where T_{max} is 90% of the maximal thrust achievable by the UAV to ensure that we still have some available thrust to proper control the drone in case of safe maneuvers, and T_{min} is the minimal thrust. The reference angles $(\phi_{des},\ \theta_{des})$

are saturated in an admissible range of (ϕ_{min}, θ_{min}) minimal values and (ϕ_{max}, θ_{max}) maximal values, to avoid the singularities.

The limitations of the angular velocity and acceleration and controls are

$$\Delta_{min} = \begin{bmatrix} \phi_{min} \\ \theta_{min} \\ \psi_{min} \end{bmatrix}, \quad \Delta_{max} = \begin{bmatrix} \phi_{max} \\ \theta_{max} \\ \psi_{max} \end{bmatrix}; \quad \Omega_{min} = \begin{bmatrix} \dot{\phi}_{min} \\ \dot{\theta}_{min} \\ \dot{\psi}_{min} \end{bmatrix}, \quad \Omega_{max} = \begin{bmatrix} \dot{\phi}_{max} \\ \dot{\theta}_{max} \\ \dot{\psi}_{max} \end{bmatrix};$$

$$U_{\phi,\theta,\psi min} = \begin{bmatrix} -l\rho AR^2 C_{T\,stat} \sin(\varepsilon)(\omega_{max}^2 - \omega_{min}^2) \\ -l\rho AR^2 C_{T\,stat} \cos(\varepsilon)(\omega_{max}^2 - \omega_{min}^2) \\ -2\rho AR^3 C_Q(\omega_{max}^2 - \omega_{min}^2) \end{bmatrix}, \quad U_{\phi,\theta,\psi max} = \begin{bmatrix} l\rho AR^2 C_{T\,stat} \sin(\varepsilon)(\omega_{max}^2 - \omega_{min}^2) \\ l\rho AR^2 C_{T\,stat} \cos(\varepsilon)(\omega_{max}^2 - \omega_{min}^2) \\ 2\rho AR^3 C_Q(\omega_{max}^2 - \omega_{min}^2) \end{bmatrix}.$$

B.6 Finite time differentiator

The homogeneous finite time differentiator, as in [Perruquetti *et al.* 2008], is defined by:

$$\begin{aligned} \dot{z}_1(t) &= -\lambda_1 \lceil z_1(t) - f(t) \rfloor^{\beta_1} + z_2(t), \\ \dot{z}_2(t) &= -\lambda_2 \lceil z_1(t) - f(t) \rfloor^{\beta_2} + z_3(t), \\ \dot{z}_3(t) &= -\lambda_3 \lceil z_1(t) - f(t) \rfloor^{\beta_3}, \end{aligned} \tag{B.1}$$

where $z \in \mathbb{R}^3$ is the differentiator state and $f(t)$ is the signal to be differentiated, $\beta_i = 1 - j\tau$ for $j = 1, 2, 3$ and any $\tau \in (-\frac{1}{3}, 0)$, while the parameters λ_1, λ_2, λ_3 are selected to ensure the Hurwitz property of the matrix

$$A = \begin{bmatrix} -\lambda_1 & 1 & 0 \\ -\lambda_2 & 0 & 1 \\ -\lambda_3 & 0 & 0 \end{bmatrix}.$$

Then the system (B.1) performs estimation of the first and second derivative of $f(t)$ in a finite time: $\hat{\dot{f}}(t) = z_2(t)$, $\hat{\ddot{f}}(t) = z_3(t)$. Increasing the smallest eigenvalue of A improves the rate of convergence. In this work $\tau < 0$ is sufficiently big, the eigenvalues of A are chosen by trial and error accordingly to the desired dynamics and in such a way to avoid undesired response delay.

B.7 PID controller

The Proportional Integrative Derivative (PID) controller, described below, is largely used in the literature and many works have provided experimental validation results. This controller is valid for linearized system around different flight conditions, such as in hover flight under the following hypothesis:

$$U_z = -mg, \ \cos\phi \approx 1, \ \cos\theta \approx 1, \ \sin\phi \approx \phi, \ \sin\theta \approx \theta, \ \dot{\phi} \approx p, \ \dot{\theta} \approx q, \ \dot{\psi} \approx r.$$

Since the x, y cannot be directly controlled, then auxiliary controls U_x, U_y are added, which are used to find the controlled angles. Position controller is structured as

$$\begin{aligned}
U_x =& K_{Px}(x_{des} - x) + K_{Ix}\int (x_{des} - x) + K_{Dx}(\dot{x}_{des} - \dot{x}) + \ddot{x}_{des},\\
U_y =& K_{Py}(y_{des} - y) + K_{Iy}\int (y_{des} - y) + K_{Dy}(\dot{y}_{des} - \dot{y}) + \ddot{y}_{des},\\
U_z =& g + K_{Pz}(z_{des} - z) + K_{Iz}\int (z_{des} - z) + K_{Dz}(\dot{z}_{des} - \dot{z}) + \ddot{z}_{des},
\end{aligned}$$

where K_{Pi}, K_{Ii}, K_{Di} for $i = x, y, z$ are the tuning parameters for proportional, integrative and derivative terms.

Attitude controller is structured as

$$\begin{aligned}
U_\phi =& I_{xx}\left(K_{P\phi}(\phi_c - \phi) + K_{I\phi}\int (\phi_c - \phi) - K_{D\phi}p\right),\\
U_\theta =& I_{yy}\left(K_{P\theta}(\theta_c - \theta) + K_{I\theta}\int (\theta_c - \theta) - K_{D\theta}q\right),\\
U_\psi =& I_{zz}\left(K_{P\psi}(\psi_{des} - \psi) + K_{I\psi}\int (\psi_{des} - \psi) - K_{D\psi}r\right),
\end{aligned}$$

where K_{Pi}, K_{Ii}, K_{Di} for $i = \phi, \theta, \psi$ are the tuning parameters. The controlled angles ϕ_c, θ_c are derived from U_x, U_y and using the desired value of ψ_{des}

$$\phi_c = -\frac{1}{g}\left(U_x \sin\psi_{des} - U_y \cos\psi_{des}\right), \quad \theta_c = -\frac{1}{g}\left(U_x \cos\psi_{des} + U_y \sin\psi_{des}\right).$$

The generic scheme of hierarchical control algorithm is given in Fig. 3.2, avoiding the use of the block *Linear rotors speed*.

Appendix C

H_∞ control

Contents

After that the nonlinear controls and estimation algorithms were studied in their totalities at Inria-Lille, there was still time for a new type of controller. In this Appendix, $\mathcal{H}_\infty$ control is introduced. Presentation is structured as follows: First, the quadrotor model is reduced to a fourth-order system (one state for the altitude and three states for the attitude). This order reduction facilitates the use of the H_∞ design approach while still allowing to consider the main four control inputs. The new reduced-order system is linearized around different operating points about which standard PID controllers are determined. Next, a reference model is obtained with the help of the above baseline controller and the H_∞ design problem is formulated. In this problem, additional constraints are considered such as the limitations of the trajectory reference and the control signals, using weighing functions. Last, a multi-model optimization problem is formulated, based on varying wind speed and improving the robustness. Practical considerations including the use of specialized algorithms such as the Matlab *hinfstruct* routine and the derivation of appropriate Simulink models.

C.1 Introduction to H_∞ control design

H_∞ controllers are now particularly used in aerospace applications, thanks to the recent development of efficient algorithms (based on nonsmooth optimization) that enables to design structured controllers such as PID gains. Its applications on quadrotors are well studied in many works and a systematic approach can be adopted using routines such as hinfstruct or systune [Apkarian & Noll 2006] that are implemented in the Matlab Control Toolbox. In the aerospace context useful adaptations and applications of such tools can be found in [Biannic *et al.* 2017, Biannic *et al.* 2016]. Based on the literature, three main groups can be identified:

- Some of recent works, using H_∞ control in quadrotor UAVs, are following listed. A Multi-channel fixed-order H_∞ synthesis is used with an *a priori* interpolation formula in [Niel *et al.* 2013]. The problem of designing an H_∞ control law in case of rotor failure in quadrotor vehicles is addressed in [Lanzon *et al.* 2014]. The paper [Gaitan & Bolea 2013] has proposed a H_∞ control approach for quadrotor based on parameters, which

allow obtaining linear models for different operation points by using black box identification techniques. Pitch and roll controls for the AR.Drone are tuned using H_∞ design in [Prayitno *et al.* 2016]. An H_∞ control is designed considering the coupling effect between longitudinal and lateral movements with roll and pitch motions in [Raffo *et al.* 2011]. Optimal H_∞ control design is also well explained for micro quadrotors in the recent Master's thesis [Chevallard 2017]. The robust H_∞ fault tolerant control of quadrotor attitude regulation is investigated in [Li *et al.* 2018]. A suboptimal H_∞ controller for a leader-follower formation problem of quadrotors with external disturbances and model parameter uncertainties is presented in [Jasim & Gu 2018]. A robust PID control strategy via affine parametrization is designed for an multivariable nonlinear UAV, and its robustness is assured by using the H_∞ norm of the weighted complementary sensitivity function in [García *et al.* 2012].

- H_∞ control is also particularly useful in coupling with other control techniques in quadrotor UAVs, as in the following papers. H_∞ is coupled with a model-based prediction control for longitudinal and lateral trajectories in [Chen & Huzmezan 2003]. A model-based predictive controller to track the reference trajectory and a nonlinear H_∞ controller to stabilize the rotational movements are coupled in [Raffo *et al.* 2008b]. The paper [Raffo *et al.* 2010] has proposed a hierarchical control structure consisting of a model predictive controller to track the reference trajectory together with a nonlinear H_∞ controller to stabilize the rotational movements. A robust mixed H_2/H_∞ static state feedback tracking controller with measurement noise and external disturbance robustness is presented for attitude tracking of a quadrotor in [Emam & Fakharian 2016]. A control structure is performed through a nonlinear H_∞ controller to stabilize the rotational movements and a control law based on backstepping approach to track the reference trajectory in [Raffo *et al.* 2008a]. The paper [Araar & Aouf 2014] has presented a controller which optimizes the L_∞ norm and designed using H_∞ control approach.

- H_∞ control is also coupled with different estimation algorithms, as in the following papers. Various sizes, configurations, payloads and propeller types of quadrotors are considered in [Ameho *et al.* 2013] using parameter estimation based on the Recursive Least Square algorithm. A disturbance observer for hybrid VTOL UAVs such as tail-sitters, is designed in frequency domain using H_∞ synthesis techniques in [Lyu *et al.* 2018]. The sliding mode disturbance estimator is coupled with the H_∞ controller in [Kerma *et al.* 2012]. The dynamic model of quadrotor UAV is decoupled into two subsystems, which are outer loop position control system and the inner loop angle control system, and by combining disturbance observer control with H_∞ control a composite tracking control is proposed in [Cheng *et al.* 2018].

It is necessary to highlight that these H_∞ controls design do not consider such a realistic model including wind perturbations as in the present thesis. External aerodynamic forces and moments enters linearly on the control design and they are typically considered as varying parameters coming from estimation algorithms. This difference is principal and it impacts the H_∞ design process, which is presented below.

C.2 Altitude and attitude subsystem

H_∞ controller can be used to achieve stabilization of systems with guaranteed performance. To stabilize a quadrotor system in a trim condition, 4 control inputs are important and they correspond to z, ϕ, θ, ψ dynamics. Hence, starting from the full system in eq. (2.10), we consider the following subsystem:

$$\dot{\mathbf{X}} = f(\mathbf{X},\, \mathbf{U},\, \mathbf{d}) = \begin{cases} \dot{\mathbf{X}}(3) = \mathbf{X}(6) \\ \dot{\mathbf{X}}(6) = g - \cos\mathbf{X}(7)\cos\mathbf{X}(8)\frac{1}{m}(U_z + d_{ze}) \\ \dot{\mathbf{X}}(7) = \mathbf{X}(10) \\ \dot{\mathbf{X}}(8) = \mathbf{X}(11) \\ \dot{\mathbf{X}}(9) = \mathbf{X}(12) \\ \dot{\mathbf{X}}(10) = \mathbf{X}(11)\mathbf{X}(12)\frac{I_{yy}-I_{zz}}{I_{xx}} + \frac{1}{I_{xx}}(U_\phi + d_\phi) \\ \dot{\mathbf{X}}(11) = \mathbf{X}(10)\mathbf{X}(12)\frac{I_{zz}-I_{xx}}{I_{yy}} + \frac{1}{I_{yy}}(U_\theta + d_\theta) \\ \dot{\mathbf{X}}(12) = \mathbf{X}(10)\mathbf{X}(11)\frac{I_{xx}-I_{yy}}{I_{zz}} + \frac{1}{I_{zz}}(U_\psi + d_\psi) \end{cases}. \tag{C.1}$$

with $\mathbf{X} = (x,\, y,\, z,\, \dot{x},\, \dot{y},\, \dot{z},\, \phi,\, \theta,\, \psi,\, p,\, q,\, r)$. The nonlinear model must be linearized around several trim conditions for different aerodynamic speed $(u - u_w,\, v - v_w,\, w - w_w)$. For each operating point, at a given aerodynamic speed, the system is described as

$$\begin{cases} \dot{X} = & AX + BU \\ Y = & CX + DU \end{cases}. \tag{C.2}$$

where X is the reduced-state for the altitude-attitude subsystem, and $U = (U_\phi,\, U_\theta,\, U_\psi,\, U_z)$ is the control input The standard structure of the control input consists of PID controllers on each dynamics so that only 12 gains have to be tuned. However, because of coupling effects, the tuning process is not trivial and must be performed globally.

$$\begin{aligned} U_\phi =& K_{P\phi}(\phi_c - \phi) + K_{I\phi}\int(\phi_c - \phi) - K_{D\phi}p, \\ U_\theta =& K_{P\theta}(\theta_c - \theta) + K_{I\theta}\int(\theta_c - \theta) - K_{D\theta}q, \\ U_\psi =& K_{P\psi}(\psi_{des} - \psi) + K_{I\psi}\int(\psi_{des} - \psi) - K_{D\psi}r, \\ U_z =& K_{Pz}(z_{des} - z) + K_{Iz}\int(z_{des} - z) + K_{Dz}(\dot{z}_{des} - \dot{z}) + \ddot{z}_{des} + g, \end{aligned}$$

C.3 Reference model selection

The reference model is introduced to enforce a desired performance of the closed-loop plant. Of course this model is chosen stable, but stability is not enforced by the reference model. Whatever the chosen model, the first objective of the H_∞ control technique is to provide an internally stabilizing controller. Poles are defined in the reference model, used to track the desired response to an external step input, such that

$$R(s) = \text{diag}\left(R_\phi(s), R_\theta(s), R_\psi(s), R_z(s)\right),$$

where

$$R_i(s) = \frac{\omega_i^2}{s^2 + 2\xi_i\omega_i s + \omega_i^2},\ i = \phi,\, \theta,\, \psi,\, z.$$

Damping parameters ξ_i and the natural pulsations ω_i are imposed according to specific requirements characterizing the Parrot quadrotor dynamics: $\xi_i = 0.7$, $\omega_\phi = \omega_\theta = 40$, $\omega_\psi = 20$, $\omega_z = 4$. ϕ, θ dynamics are faster than ψ dynamics and they are also 10 times faster than z dynamics. Fig. C.1 represents the desired response of each dynamics to an unitary step input.

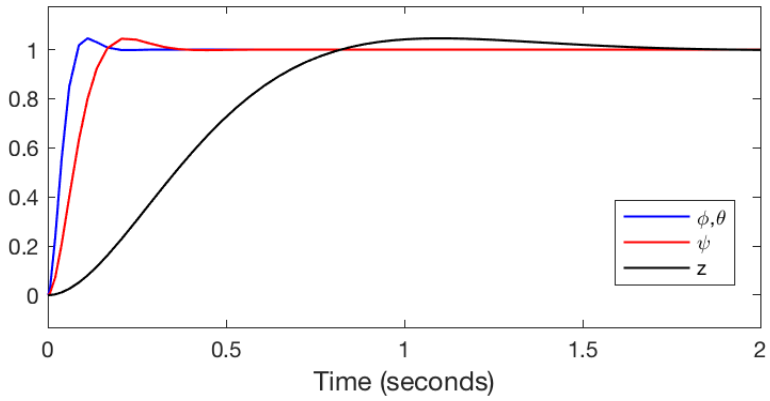

Figure C.1: Desired response of each dynamics to an unitary step input.

C.4 H_∞-based reference model matching

The controller tuning problem can be rewritten as a non-smooth and non-convex optimization problem that can be efficiently solved with the help of specialized algorithms implemented in Matlab. The objective is to find the best structured gain:

$$K = \begin{bmatrix} K_{P\phi} & 0 & 0 & 0 & K_{I\phi} & 0 & 0 & 0 & K_{D\phi} & 0 & 0 & 0 \\ 0 & K_{P\theta} & 0 & 0 & 0 & K_{I\theta} & 0 & 0 & 0 & K_{D\theta} & 0 & 0 \\ 0 & 0 & K_{P\psi} & 0 & 0 & 0 & K_{I\psi} & 0 & 0 & 0 & K_{D\psi} & 0 \\ 0 & 0 & 0 & K_{Pz} & 0 & 0 & 0 & K_{Iz} & 0 & 0 & 0 & K_{Dz} \end{bmatrix}$$

such that the error between the outputs of the closed-loop plant and the output of the reference model (z_p) is minimized. Simultaneously, the control signals (z_u) must be small as much as possible to limit the rotors and the on-board battery degradation. Fig. C.2 shows better these concepts in the closed-loop plant, which means to assure the best tracking to the desired dynamics response with the smallest allowed control. Signals z_u, z_p are evaluated

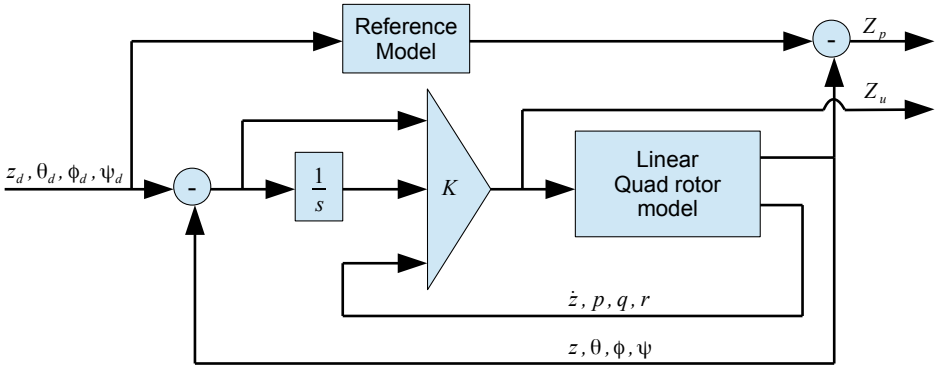

Figure C.2: H_∞ design using reference model and PID-structured controller.

through weighted $\mathcal{H}_\infty$ norms of the transfer functions $\mathcal{T}_{w\to z_p}(s)$ and $\mathcal{T}_{w\to z_u}(s)$

$$\|W_p(s).\mathcal{T}_{w\to z_p}(s)\|_\infty = \sup_{\omega\geq 0}\bar{\sigma}\left(W_{p1}(s).\mathcal{T}_{w\to z_{p1}}(j\omega)\right) = \sup_{w\in\mathcal{L}_2}\frac{\|\tilde{z}_{p1}\|_2}{\|w\|_2},$$
$$\|W_u(s).\mathcal{T}_{w\to z_u}(s)\|_\infty = \sup_{\omega\geq 0}\bar{\sigma}\left(W_u(s).\mathcal{T}_{w\to z_u}(j\omega)\right) = \sup_{w\in\mathcal{L}_2}\frac{\|\tilde{z}_u\|_2}{\|w\|_2},$$

where $W_p(s)$, $W_u(s)$ are the weight functions tuned by trial and error. It means that we are going to follow a reference, ensuring the minimal possible control. The weighting functions $W_p(s)$ and $W_u(s)$ are tuned to ensure a good tracking of the reference model $R(s)$ in the frequency domain of interest with a reasonable control activity. More precisely, $W_p(s)$ is typically a low-pass filter. The objective is to penalize the low-frequency domain, to make sure that the closed-loop plant follows correctly the reference model in the low frequency region. In opposite, $W_u(s)$ is a high-pass filter whose objective is to bound the fast variations of the control signal to avoid saturation. Figures C.3,**??**,**??** show the the bode diagram in frequency domain for the weight functions.

Then, the objective can be formulated as

$$\hat{K} = arg\min_K \|W_p(s).\mathcal{F}_l\left(P(s),K\right)_{w\to z_p}\|_\infty \quad s.t\,\|W_u(s).\mathcal{F}_l\left(P(s),K\right)_{w\to z_u}\|_\infty \leq c,$$

where the positive constant c is a tuned parameter according to the observed control reactions, $\mathcal{F}_l$ denoting the lower LFT transformation is the closed-loop transfer function of the system. Numerically, the resolution of the above problem is difficult since it describes a non-smooth and non-convex optimization problem. As is already clarified above, in the specific context of systems stabilization and H_∞ norm minimization, these two difficulties are now efficiently addressed by specialized algorithms which have been implemented in Matlab routines such as *hinstruct* or *systune*. The compact standard representation for H_∞ design is shown in Fig. C.4, where $P(s)$ is the model in a state-space format including the transfer functions to be minimized and the input/output to the controller.

C.5 Robustness improvement by multi-model optimization

The robustness properties of the initial PID gain must be improved in order to cope with the varying aerodynamic speed of the quadrotor. To this purpose, Linear-Fractional-Representation (LFR) is created by the polynomial interpolation of the linear models using an advanced technique [Roos *et al.* 2014], implemented in the SMAC toolbox [Biannic *et al.* 2016]. By this approach, a unique model is to be handled instead of a possibly huge family. Fig. C.5 shows this representation, where $G(s)$ includes all the linear plants $P(s)$.

C.6 Summary: steps to tune the structured-PID controller

Practical steps to implement the H_∞ design, starting from the complete nonlinear system, are:

1. Choose a group of aerodynamic speed (u_w, v_w, w_w).
2. Define the respective control inputs U_ϕ, U_θ, U_ψ, U_z.
3. Compute the linearized system P_i, corresponding to the given controls and speed.
4. In hover:

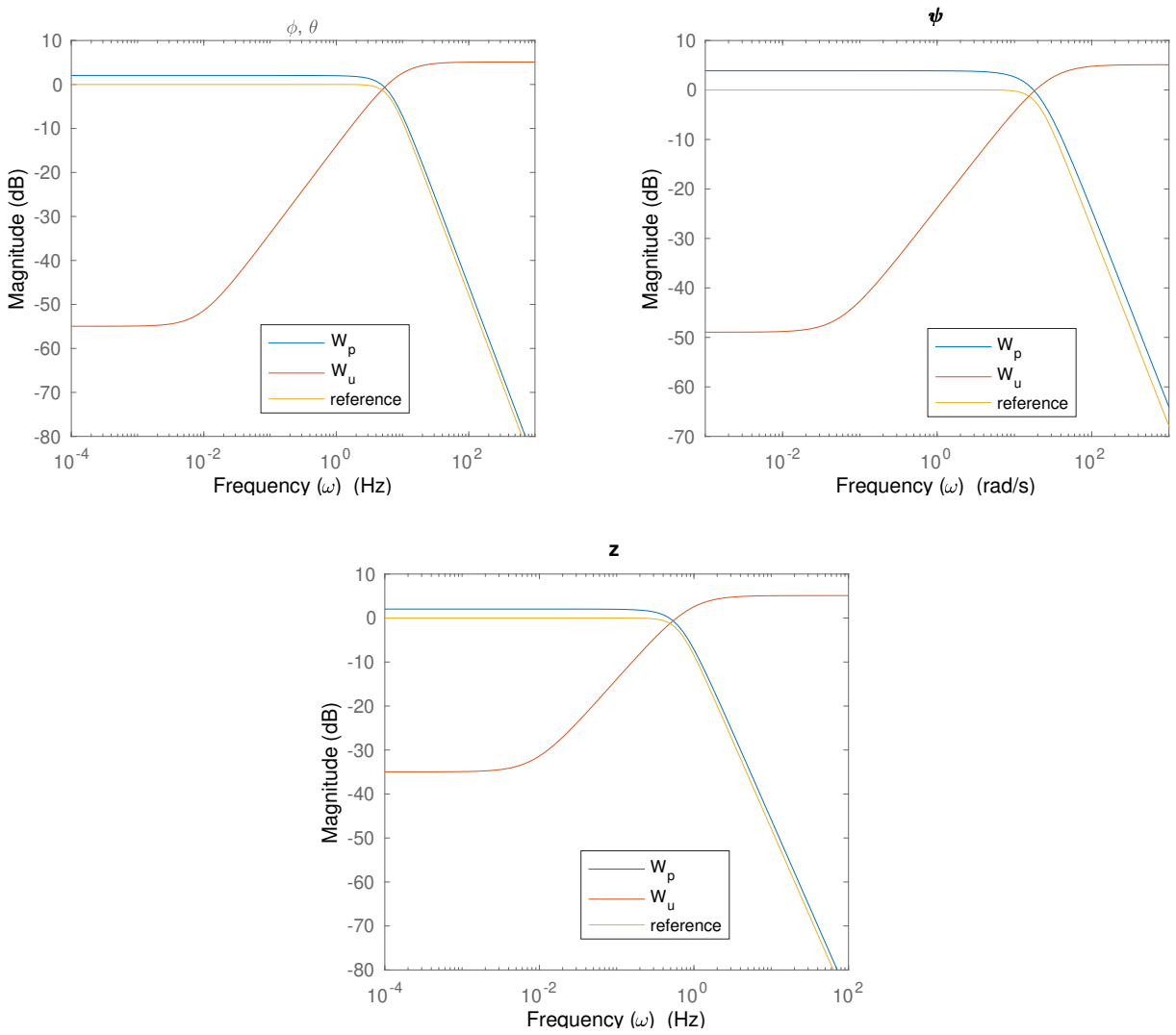

Figure C.3: Weighting functions of reference model.

(a) Find the state for the system P_i to check the hover condition.

(b) Compute the optimal structured-PID gain for the plant P_i in hover using the *hinf* routine in Matlab, the H_∞ design (see Fig. C.6), the imposed reference model, and the tuned weight functions.

(c) Test the controller in the closed-loop model (see Fig. C.7).

5. Create a list of the plants P_i corresponding to all the chosen speed.

6. Use the *hinf* routine in Matlab, giving as input the list of the plants and the weight functions, see [Biannic *et al.* 2017]. As option, an interpolation formula can be introduced inside the Matlab routine:
The parameter-varying controller $K(\Theta)$ is computed to stabilize the parameter-varying plant $P(s,\Theta)$ and minimize the transfer functions $\mathcal{T}_{w\to z_p}(s,\theta_i)$ for a set of values of $\Theta = \theta_1, \theta_2, \ldots \theta_n$ covering the operating

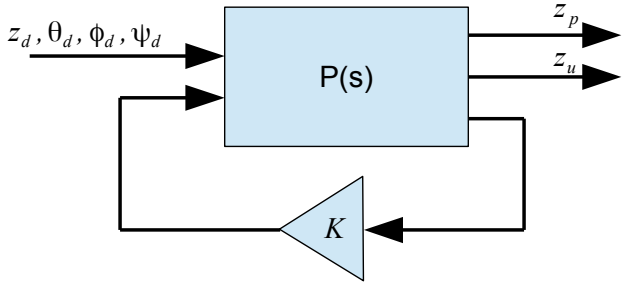

Figure C.4: Standard form for H_∞ design.

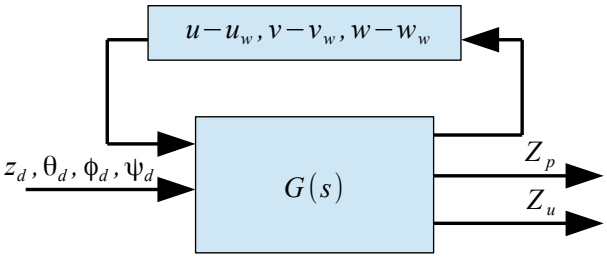

Figure C.5: Linear Fractional Representation of the quadrotor for varying aerodynamic speed.

domain. Then, as an example, the controller parametric dependency can be fixed *a priori*

$$K(\Theta) = K_0 + \Theta\, K_1 + \Theta^2\, K_2$$

The objective is then to solve the multi-objective problem to determine $K = K_0,\ K_1,\ K_2$ such that the H_∞ norm of the transfer function is minimized for each θ_i

$$\hat{K} = \operatorname{Arg}\min_{K} \max_{i=1\ldots n} \|\mathcal{T}_{w\to z_p}(s, \theta_i)\|_\infty,$$

where

$$\mathcal{T}_{w\to z_p}(s, \theta_i) = W_u(s)\mathcal{F}_l\left(P(s, \theta_i), K(\theta_i)\right) W_p(s),$$

and with

$$K(\theta_i) = K_0 + \theta_i\, K_1 + \theta_i^2\, K_2.$$

7. Interpolate the structured-PID gains found in the previous step (if the interpolation formula is not used).

C.7 H_∞ control Simulink/Matlab code

The Matlab code routine to compute the PID-structured gain is:

```
% Linearization of the nonlinear Simulink model in a given operating point
[aa,bb,cc,dd]=linmodv5('uav_model_alt_att');

% Selection of the linear subsystem
aaa=aa([8,7,9,12,4,5,6,3],[8,7,9,12,4,5,6,3]); %phi theta psi z p q r zdot
bbb=bb([8,7,9,12,4,5,6,3],[1,2,3,4,5,6,7]); %phi theta psi z p q r zdot - Up Uq Ur Uz ...
    uwx uwy uwz
ccc=cc([8,7,9,12,4,5,6,3],[8,7,9,12,4,5,6,3]); %phi theta psi z p q r
ddd=dd([8,7,9,12,4,5,6,3],[1,2,3,4,5,6,7]); %phi theta psi z p q r zdot - Up Uq Ur Uz ...
    uwx uwy uwz

% Creating the Plant from the Hinf design Simulink model
[a_m,b_m,c_m,d_m]=linmodv5('Hinf_design_alt_att');
P=ss(a_m,b_m,c_m,d_m);

% Declaration of the matrix gain dimension
no=4;
ni=12;

K0=ltiblock.gain('K0',no,ni);   % linear gain block init

CL0=lft(P,K0);   % unweighted closed-loop

%Tuning of the weight functions
Wperf1=tf(45^2,[1 2*45*0.7 40^2]);
Wperf2=tf(45^2,[1 2*45*0.7 40^2]);
Wperf3=tf(25^2,[1 2*25*0.7 20^2]);
Wperf4=tf(4.5^2,[1 2*4.5*0.7 4^2]);
Wrob1=tf([1.8 0.1],[1 2*40*0.7]);
Wrob2=tf([1.8 0.1],[1 2*40*0.7]);
Wrob3=tf([1.8 0.1],[1 2*20*0.7]);
Wrob4=tf([1.8 0.1],[1 2*4*0.7]);

CLW=blkdiag(Wperf1,Wperf2,Wperf3,Wperf4,Wrob1,Wrob2,Wrob3,Wrob4)*CL0;   % weighted ...
    closed-loop

% call to hinfstruct
opt=hinfstructOptions('Randomstart',3);
[CL,gam]=hinfstruct(CLW,opt);

K=ss(CL.Blocks.K0);    % Structured-PID gain for the given operating point
```

Fig. C.6 shows the Simulink model (*Hinf_design_alt_att.slx*) for the H_∞ design, Fig. C.7 shows the Simulink model for the closed-loop model.

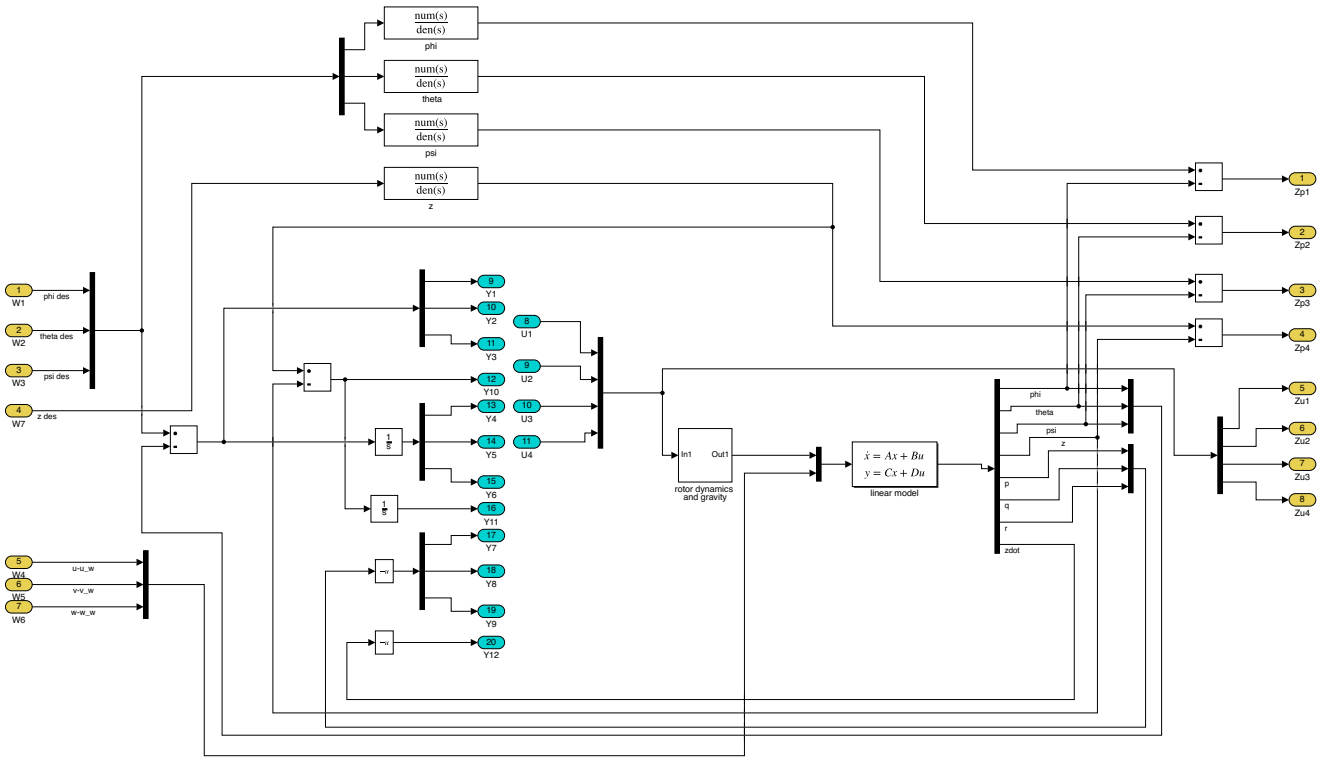

Figure C.6: H_∞ design in Simulink.

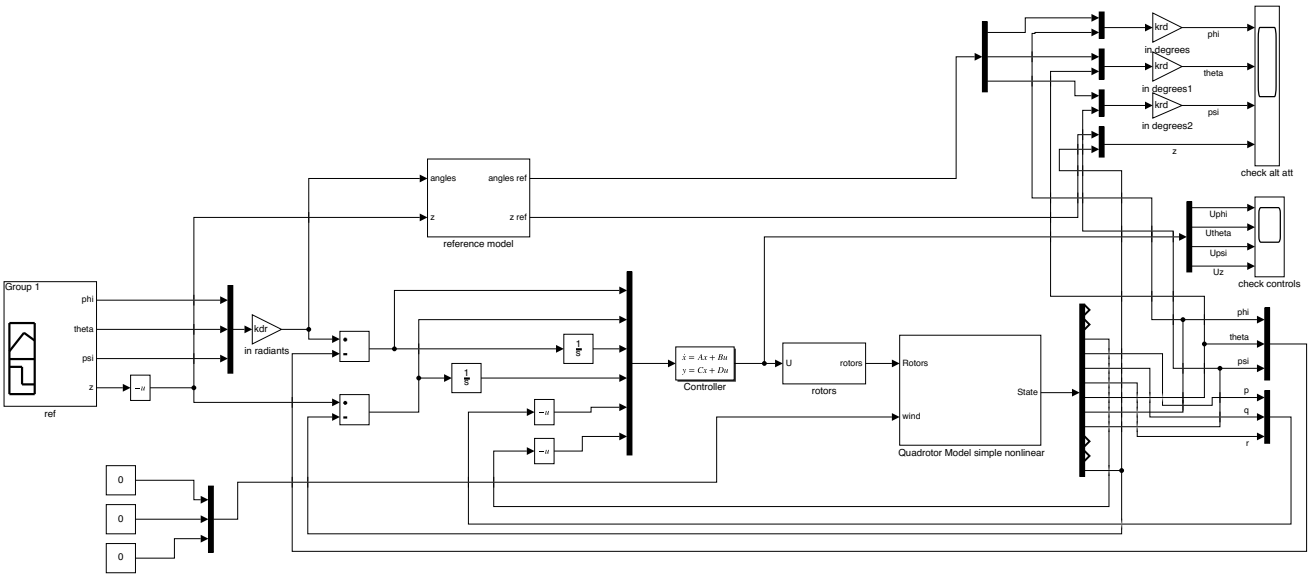

Figure C.7: Closed-loop model in Simulink to test the structured-PID controller.

Appendix D

CW-Quad simulation toolbox

CW-Quad Toolbox (**C**ontrols: Sliding mode control, PID control; **W**ind estimator for **Quad**rotors) consists in a group of Simulink libraries to simulate a quadrotor under wind perturbation. This toolbox was built during the first year of the project to make preliminary simulations and validate the studied controls and estimation algorithms, developed at Inria-Lille, before to perform experiments in lab at ONERA-Lille. It gathers control theory and aerodynamic science and frees the user to build his/her own environment. Fully configurable masks (see Fig. D.4 as example) are also provided to simulate quadrotors with different shapes and in different flight conditions.

As requested by ONERA-Lille, only blocks provided with basic Simulink environment are used (no Matlab scripts and no Matlab functions) to ensure a better compatibility with most of Simulink versions, to avoid any other auxiliary toolbox which are typically sold separately, and to have a better readability when used in other projects. The reason was that ONERA-Lille had license for basic Matlab/Simulink software and that RT-MaG Toolbox worked for a very old version of Matlab/Simulink.

This toolbox aims to help the user to study quadrotors in total: trajectories, controls (Sliding mode control, PID), state filtering and wind estimator, and it is structured as in Fig. D.2. A particular attention was given in building the *Controls, Rotors, Quadrotor, Sensors* blocks, avoiding Matlab code. In this way, it is easier to take and/or modify each single model component to improve them or to use them in other projects without compromise the entire code. In opposite to use also Matlab functions which allow to build the model faster, but not easy modifiable (see Fig. D.1). For example, Fig. D.3 shows the first sub-layer of the *Quadrotor* block, where the sub-models are well separated and linked thanks to input and output signals, improving the readability.

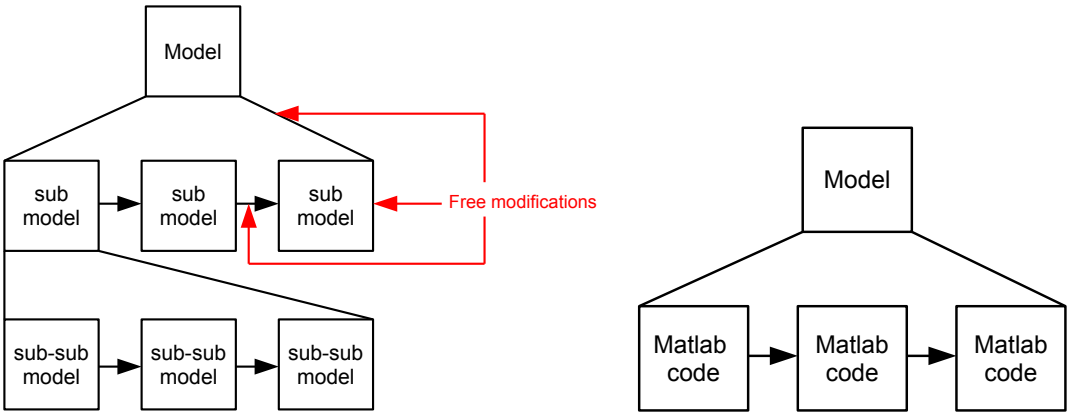

Figure D.1: Easy modifiable and readable (on the left) and hard modifiable (on the right) models.

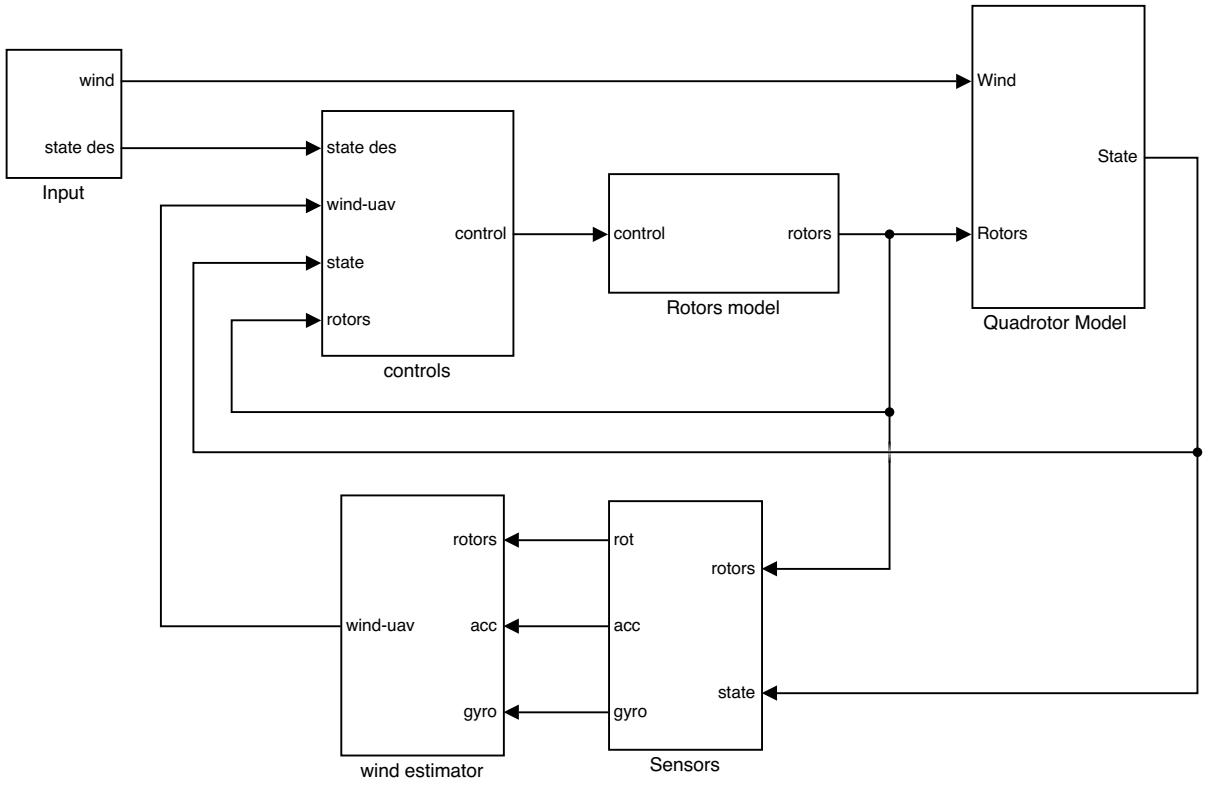

Figure D.2: Main layer of the Toolbox.

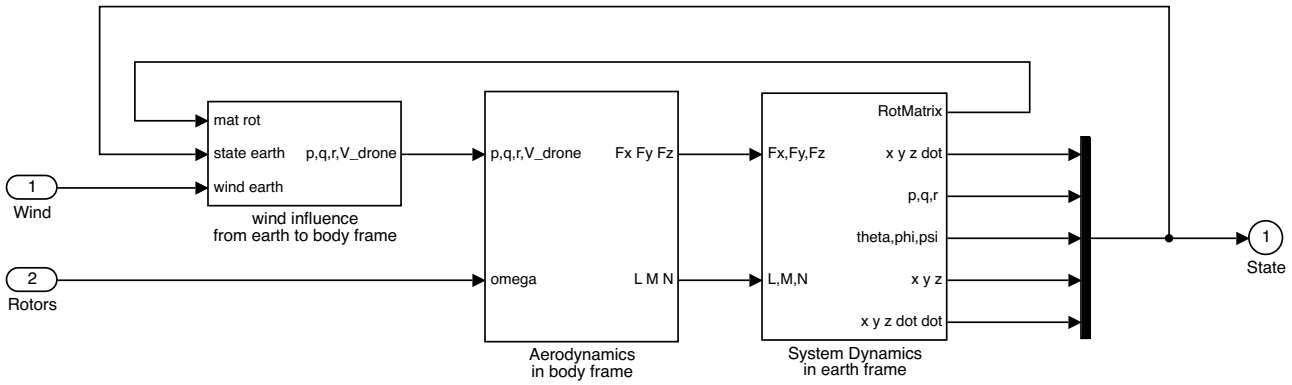

Figure D.3: Second layer of the quadrotor model.

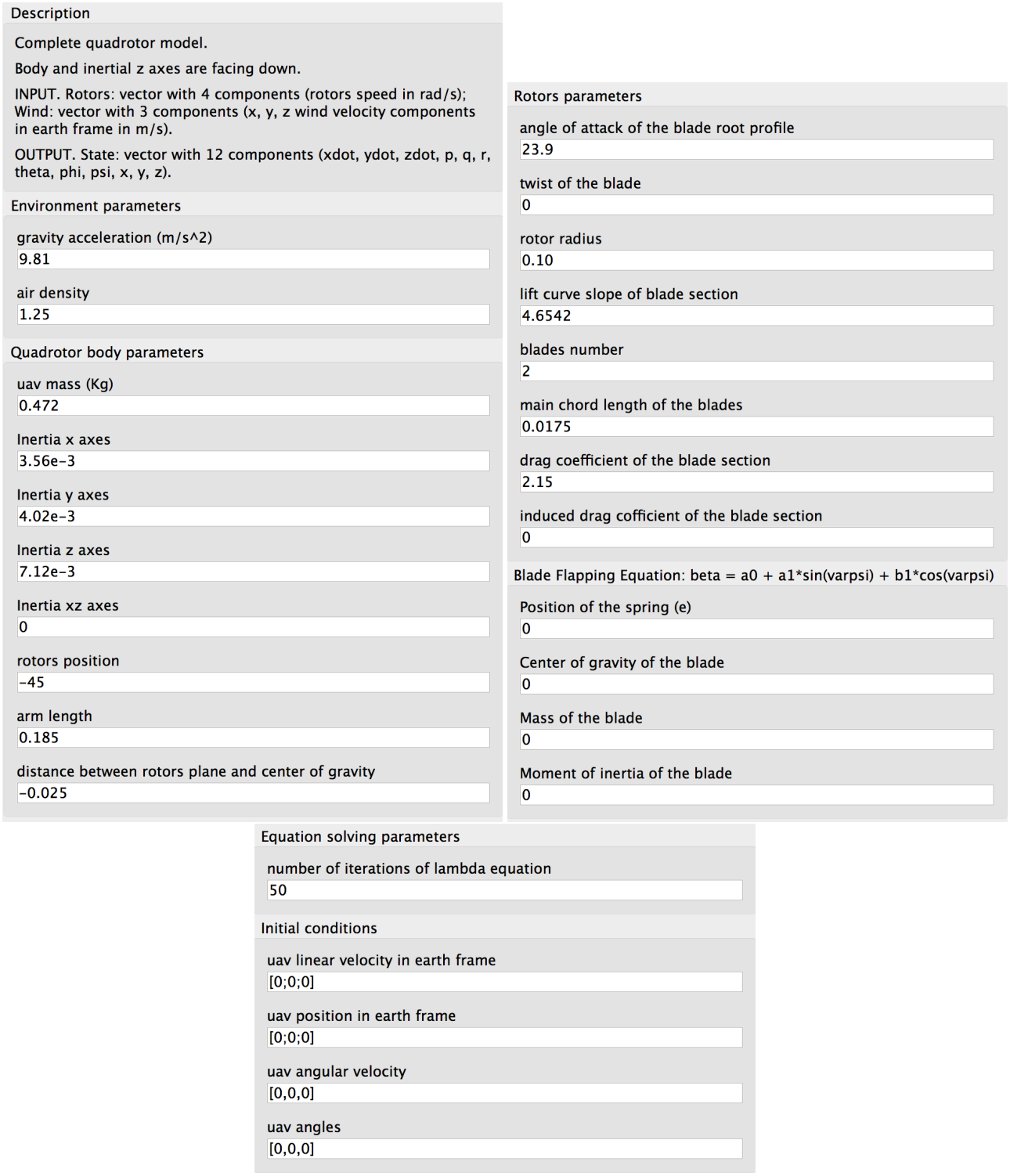

Figure D.4: Configurable mask for the quadrotor model.

Bibliography

[Ali *et al.* 2016] S. U. Ali, M. Z. Shah, R. Samar and A. Waseem. *Wind estimation for lateral path following of UAVs using higher order sliding mode*. In 2016 International Conference on Intelligent Systems Engineering (ICISE), pages 364–371, January 2016, DOI: 10.1109/INTELSE.2016.7475150. (Cited on page 33.)

[Alizadeh & Ghasemi 2015] G. Alizadeh and K. Ghasemi. *Control of Quadrotor Using Sliding Mode Disturbance Observer and Nonlinear H*. International Journal of Robotics, vol. 4, no. 1, pages 38–46, 2015. (Cited on page 20.)

[Ameho *et al.* 2013] Y. Ameho, F. Niel, F. Defaÿ, J. M. Biannic and C. Bérard. *Adaptive control for quadrotors*. In 2013 IEEE International Conference on Robotics and Automation, pages 5396–5401, May 2013, DOI: 10.1109/ICRA.2013.6631351. (Cited on page 90.)

[Apkarian & Noll 2006] Pierre Apkarian and Dominikus Noll. *Nonsmooth H_∞ Synthesis*. IEEE Transactions on Automatic Control, vol. 51, no. 1, pages 71–86, 2006, DOI: 10.1109/TAC.2005.860290. (Cited on page 89.)

[Araar & Aouf 2014] O. Araar and N. Aouf. *Full linear control of a quadrotor UAV, LQ vs H_∞*. In 2014 UKACC International Conference on Control (CONTROL), pages 133–138, July 2014, DOI: 10.1109/CONTROL.2014.6915128. (Cited on page 90.)

[Basin *et al.* 2012] Michael Basin, Leonid Fridman and Peng Shi. *Special Issue on Optimal sliding mode algorithms for dynamic systems*. Journal of the Franklin Institute, vol. 349, no. 4, pages 1317–1322, 2012, DOI: 10.1016/j.jfranklin.2012.02.013. (Cited on page 19.)

[Benallegue *et al.* 2008] A. Benallegue, A. Mokhtari and L. Fridman. *High-order sliding-mode observer for a quadrotor UAV*. International Journal of Robust and Nonlinear Control, vol. 18, no. 4-5, pages 427–440, March 2008, DOI: 10.1002/rnc.1225. (Cited on pages 20 and 33.)

[Bernuau *et al.* 2014] Emmanuel Bernuau, Denis Efimov, Wilfrid Perruquetti and Andrey Polyakov. *On homogeneity and its application in sliding mode control*. Journal of the Franklin Institute, vol. 351, no. 4, pages 1866–1901, April 2014, DOI: 10.1016/j.jfranklin.2014.01.007. (Cited on pages 19, 23 and 26.)

[Besnard *et al.* 2012] Lénaïck Besnard, Yuri B. Shtessel and Brian Landrum. *Quadrotor vehicle control via sliding mode controller driven by sliding mode disturbance observer*. Journal of the Franklin Institute, vol. 349, no. 2, pages 658–684, March 2012, DOI: 10.1016/j.jfranklin.2011.06.031. (Cited on page 20.)

[Biannic *et al.* 2016] J. M. Biannic, L. Burlion, G. Demourant, G. Hardier, T. Loquen and C. Roos. *The SMAC Toolbox*, 2016. http://w3.onera.fr/smac. (Cited on pages 89 and 93.)

[Biannic *et al.* 2017] Jean-Marc Biannic, Armin Taghizad, Lucie Dujols and Gabriele Perozzi. *A multi-objective H_∞ design framework for helicopter PID control tuning with handling qualities requirements*. In 7th European Conference for Aeronautics and Space Science (EUCASS), Milan, Italy, July 2017. DOI: 10.13009/EUCASS2017-51. (Cited on pages 89 and 94.)

[Bonyan Khamseh *et al.* 2018] Hossein Bonyan Khamseh, Farrokh Janabi-Sharifi and Abdelkader Abdessameud. *Aerial manipulation - A literature survey*. Robotics and Autonomous Systems, vol. 107, pages 221–235, September 2018, DOI: 10.1016/j.robot.2018.06.012. (Cited on page 1.)

[Bouabdallah & Siegwart 2005] S. Bouabdallah and R. Siegwart. *Backstepping and Sliding-mode Techniques Applied to an Indoor Micro Quadrotor*. In Proceedings of the 2005 IEEE International Conference on Robotics and Automation, pages 2247–2252, April 2005, DOI: 10.1109/ROBOT.2005.1570447. (Cited on pages 10, 13 and 19.)

[Bouabdallah & Siegwart 2007a] S. Bouabdallah and R. Siegwart. *Full control of a quadrotor*. In 2007 IEEE/RSJ International Conference on Intelligent Robots and Systems, pages 153–158, October 2007, DOI: 10.1109/IROS.2007.4399042. (Cited on page 13.)

[Bouabdallah & Siegwart 2007b] Samir Bouabdallah and Roland Siegwart. *Design and control of a miniature quadrotor*. In Advances in unmanned aerial vehicles, pages 171–210. Springer, 2007. (Cited on page 10.)

[Bouabdallah 2007] Samir Bouabdallah. *Design and control of quadrotors with application to autonomous flying*. PhD thesis, Ecole Polytechnique Federale de Lausanne, 2007, DOI: 10.5075/epfl-thesis-3727. (Cited on page 10.)

[Bouadi *et al.* 2011] H. Bouadi, S. Simoes Cunha, A. Drouin and F. Mora-Camino. *Adaptive sliding mode control for quadrotor attitude stabilization and altitude tracking*. In 2011 IEEE 12th International Symposium on Computational Intelligence and Informatics (CINTI), pages 449–455, November 2011, DOI: 10.1109/CINTI.2011.6108547. (Cited on page 10.)

[Bramwell *et al.* 2001] A. R. S. Bramwell, David Balmford and George Done. Bramwell's Helicopter Dynamics, second edition. Butterworth-Heinemann, April 2001. ch 2-7. (Cited on page 12.)

[Bresciani 2008] Tammaso Bresciani. *Modelling, identification and control of a quadrotor helicopter*. MSc Thesis, Lund University, 2008. (Cited on page 10.)

[Cabecinhas *et al.* 2012] D. Cabecinhas, R. Naldi, L. Marconi, C. Silvestre and R. Cunha. *Robust Take-Off for a Quadrotor Vehicle*. IEEE Transactions on Robotics, vol. 28, no. 3, pages 734–742, June 2012, DOI: 10.1109/TRO.2012.2187095. (Cited on page 10.)

[Chang & Shi 2017] S. Chang and W. Shi. *Adaptive fuzzy time-varying sliding mode control for quadrotor UAV attitude system with prescribed performance*. In 2017 29th Chinese Control And Decision Conference (CCDC), pages 4389–4394, May 2017, DOI: 10.1109/CCDC.2017.7979270. (Cited on page 20.)

[Chen & Huzmezan 2003] Ming Chen and Mihai Huzmezan. *A Combined MBPC/2 DOF H infinity Controller for a Quad Rotor UAV*. In AIAA Guidance, Navigation, and Control Conference and Exhibit, Guidance, Navigation, and Control and Co-located Conferences. American Institute of Aeronautics and Astronautics, August 2003, DOI: 10.2514/6.2003-5520. (Cited on page 90.)

[Cheng *et al.* 2017] Y. Cheng, T. Shao, F. Wu, Y. Guo and B. Xu. *Disturbance observer based control of quadrotors with SLFN*. In IECON 2017 - 43rd Annual Conference of the IEEE Industrial Electronics Society, pages 5774–5778, October 2017, DOI: 10.1109/IECON.2017.8217001. (Cited on page 20.)

[Cheng *et al.* 2018] Y. Cheng, L. Jiang, T. Li and L. Guo. *Robust tracking control for a quadrotor UAV via DOBC approach*. In 2018 Chinese Control And Decision Conference (CCDC), pages 559–563, June 2018, DOI: 10.1109/CCDC.2018.8407194. (Cited on page 90.)

[Chevallard 2017] Daniele Chevallard. Design, identification and control of a micro aerial vehicle. Master's thesis, Politecnico di Milano, July 2017. (Cited on page 90.)

[Das *et al.* 2009] Abhijit Das, Frank Lewis and Kamesh Subbarao. *Backstepping Approach for Controlling a Quadrotor Using Lagrange Form Dynamics*. Journal of Intelligent and Robotic Systems, vol. 56, no. 1-2, pages 127–151, September 2009, DOI: 10.1007/s10846-009-9331-0. (Cited on page 10.)

[Demitrit *et al.* 2017] Y. Demitrit, S. Verling, T. Stastny, A. Melzer and R. Siegwart. *Model-based wind estimation for a hovering VTOL tailsitter UAV*. In 2017 IEEE International Conference on Robotics and Automation (ICRA), pages 3945–3952, May 2017, DOI: 10.1109/ICRA.2017.7989455. (Cited on page 33.)

[Derafa *et al.* 2012] L. Derafa, A. Benallegue and L. Fridman. *Super twisting control algorithm for the attitude tracking of a four rotors UAV*. Journal of the Franklin Institute, vol. 349, no. 2, pages 685–699, March 2012, DOI: 10.1016/j.jfranklin.2011.10.011. (Cited on page 20.)

[Dikmen *et al.* 2009] I. C. Dikmen, A. Arisoy and H. Temeltas. *Attitude control of a quadrotor*. In 2009 4th International Conference on Recent Advances in Space Technologies, pages 722–727, June 2009, DOI: 10.1109/RAST.2009.5158286. (Cited on page 10.)

[Ding *et al.* 2016] Shihong Ding, Arie Levant and Shihua Li. *Simple homogeneous sliding-mode controller*. Automatica, vol. 67, pages 22–32, May 2016, DOI: 10.1016/j.automatica.2016.01.017. (Cited on pages 26, 27 and 29.)

[Elsamanty *et al.* 2013] M Elsamanty, A Khalifa, M Fanni, A Ramadan and A Abo-Ismail. *Methodology for identifying quadrotor parameters, attitude estimation and control*. In IEEE/ASME International Conference on Advanced Intelligent Mechatronics, pages 9–12, July 2013, DOI: 10.1109/AIM.2013.6584281. (Cited on page 10.)

[Emam & Fakharian 2016] M. Emam and A. Fakharian. *Attitude tracking of quadrotor UAV via mixed H2/H_∞ controller: An LMI based approach*. In 2016 24th Mediterranean Conference on Control and Automation (MED), pages 390–395, June 2016, DOI: 10.1109/MED.2016.7535919. (Cited on page 90.)

[Eresen *et al.* 2012] A. Eresen, N. Imamoglu and M.O. Efe. *Autonomous quadrotor flight with vision-based obstacle avoidance in virtual environment*. Expert Systems with Applications, vol. 39, no. 1, pages 894–905, January 2012, DOI: 10.1016/j.eswa.2011.07.087. (Cited on page 2.)

[Etkin & Reid 1996] Bernard Etkin and Lloyd Duff Reid. Dynamics of flight: stability and control. John Wiley and Sons, 1996. (Cited on page 85.)

[Freddi *et al.* 2009] A Freddi, S Longhi and A Monteriu. *A model-based fault diagnosis system for a mini-quadrotor*. In 7th workshop on Advanced Control and Diagnosis, pages 19–20, 2009. (Cited on page 10.)

[Gaitan & Bolea 2013] A. Torres Gaitan and Y. Bolea. *Modeling and robust attitude control of a quadrotor system*. In 2013 10th International Conference on Electrical Engineering, Computing Science and Automatic Control (CCE), pages 7–12, September 2013, DOI: 10.1109/ICEEE.2013.6676024. (Cited on page 89.)

[Galway *et al.* 2008] David Galway, Jason Etele and Giovanni Fusina. *Modeling of the Urban Gust Environment with Application to Autonomous Flight*. In AIAA Atmospheric Flight Mechanics Conference and Exhibit, Guidance, Navigation, and Control and Co-located Conferences. American Institute of Aeronautics and Astronautics, August 2008, DOI: 10.2514/6.2008-6565. (Cited on page 2.)

[García *et al.* 2012] R. A. García, F. R. Rubio and M. G. Ortega. *Robust PID Control of the Quadrotor Helicopter*. IFAC Proceedings Volumes, vol. 45, no. 3, pages 229–234, January 2012, DOI: 10.3182/20120328-3-IT-3014.00039. (Cited on page 90.)

[Ghazbi *et al.* 2016] S. Norouzi Ghazbi, Y. Aghli, M. Alimohammadi and A. A. Akbari. *QUADROTORS UNMANNED AERIAL VEHICLES: A REVIEW*. International Journal on Smart Sensing and Intelligent Systems, vol. 9, no. 1, pages 309–333, 2016, DOI: 10.21307/ijssis-2017-872. (Cited on page 10.)

[Gipsa-Lab & of Mouvement-Sciences] Gipsa-Lab and Institute of Mouvement-Sciences. *RT-MaG Project, an open-source toolbox for real-time robotic applications*. http://www.gipsa-lab.fr/projet/RT-MaG/index.php. (Cited on page 4.)

[Gonzalez-Hernandez *et al.* 2017] Ivan Gonzalez-Hernandez, Filiberto Munoz Palacios, Sergio Salazar Cruz, Eduardo Steed Espinoza Quesada and Rogelio Lozano Leal. *Real-time altitude control for a quadrotor helicopter using a super-twisting controller based on high-order sliding mode observer*. International Journal of Advanced Robotic Systems, vol. 14, no. 1, January 2017, DOI: 10.1177/1729881416687113. (Cited on page 20.)

[González-Jorge *et al.* 2017] Higinio González-Jorge, Joaquin Martínez-Sánchez, Martín Bueno and and Pedor Arias. *Unmanned Aerial Systems for Civil Applications: A Review*. Drones, vol. 1, no. 1, page 2, July 2017, DOI: 10.3390/drones1010002. (Cited on page 1.)

[Gonzalez-Rocha *et al.* 2017] Javier Gonzalez-Rocha, Craig A. Woolsey, Cornel Sultan, Stephan de Wekker and Nathan Rose. *Measuring Atmospheric Winds from Quadrotor Motion*. In AIAA Atmospheric Flight Mechanics Conference, AIAA SciTech Forum. American Institute of Aeronautics and Astronautics, January 2017, DOI: 10.2514/6.2017-1189. (Cited on page 33.)

[González *et al.* 2014] Iván González, Sergio Salazar and Rogelio Lozano. *Chattering-Free Sliding Mode Altitude Control for a Quad-Rotor Aircraft: Real-Time Application*. Journal of Intelligent & Robotic Systems, vol. 73, no. 1-4, pages 137–155, January 2014, DOI: 10.1007/s10846-013-9913-8. (Cited on pages 20 and 26.)

[Hoffmann *et al.* 2007] Gabriel Hoffmann, Haomiao Huang, Steven Waslander and Claire Tomlin. *Quadrotor Helicopter Flight Dynamics and Control: Theory and Experiment*. In AIAA Guidance, Navigation and Control Conference and Exhibit. American Institute of Aeronautics and Astronautics, August 2007, DOI: 10.2514/6.2007-6461. (Cited on page 10.)

[Hou *et al.* 2017] Z. Hou, W. Wang, G. Zhang and C. Han. *A survey on the formation control of multiple quadrotors*. In 2017 14th International Conference on Ubiquitous Robots and Ambient Intelligence (URAI), pages 219–225, June 2017, DOI: 10.1109/URAI.2017.7992717. (Cited on page 1.)

[Hwang *et al.* 2014] C. L. Hwang, C. C. Chiang and Y. W. Yeh. *Adaptive Fuzzy Hierarchical Sliding-Mode Control for the Trajectory Tracking of Uncertain Underactuated Nonlinear Dynamic Systems*. IEEE Transactions on

Fuzzy Systems, vol. 22, no. 2, pages 286–299, April 2014, DOI: 10.1109/TFUZZ.2013.2253106. (Cited on page 20.)

[Hwang *et al.* 2015] Je Young Hwang, Min Kyu Jung and Oh Joon Kwon. *Numerical Study of Aerodynamic Performance of a Multirotor Unmanned-Aerial-Vehicle Configuration*. Journal of Aircraft, vol. 52, no. 3, pages 839–846, 2015, DOI: 10.2514/1.C032828. (Cited on pages 10 and 74.)

[Ireland & Anderson 2012] M. Ireland and D. Anderson. *Development of Navigation Algorithms for Nap-of-the-Earth UAV Flight in a Constrained Urban Environment*. In 28th International congress of the aeronautical sciences, 2012. (Cited on page 2.)

[Islam *et al.* 2017] Shafiqul Islam, Peter X. Liu and Abdulmotaleb El Saddik. *Nonlinear robust adaptive sliding mode control design for miniature unmanned multirotor aerial vehicle*. International Journal of Control, Automation and Systems, vol. 15, no. 4, pages 1661–1668, August 2017, DOI: 10.1007/s12555-016-0013-y. (Cited on page 20.)

[Jasim & Gu 2018] W. Jasim and D. Gu. *Robust Team Formation Control for Quadrotors*. IEEE Transactions on Control Systems Technology, vol. 26, no. 4, pages 1516–1523, July 2018, DOI: 10.1109/TCST.2017.2705072. (Cited on page 90.)

[Jia *et al.* 2017] Zhenyue Jia, Jianqiao Yu, Yuesong Mei, Yongbo Chen, Yuanchuan Shen and Xiaolin Ai. *Integral backstepping sliding mode control for quadrotor helicopter under external uncertain disturbances*. Aerospace Science and Technology, vol. 68, pages 299–307, September 2017, DOI: 10.1016/j.ast.2017.05.022. (Cited on page 20.)

[Johansen *et al.* 2015] T. A. Johansen, A. Cristofaro, K. Sørensen, J. M. Hansen and T. I. Fossen. *On estimation of wind velocity, angle-of-attack and sideslip angle of small UAVs using standard sensors*. In 2015 International Conference on Unmanned Aircraft Systems (ICUAS), pages 510–519, June 2015, DOI: 10.1109/ICUAS.2015.7152330. (Cited on page 32.)

[Johnson 2012] Wayne Johnson. Helicopter Theory. Courier Corporation, March 2012. Chapters 2-5,9-13,15. (Cited on page 12.)

[Kanellakis & Nikolakopoulos 2017] Christoforos Kanellakis and George Nikolakopoulos. *Survey on Computer Vision for UAVs: Current Developments and Trends*. Journal of Intelligent & Robotic Systems, vol. 87, no. 1, pages 141–168, July 2017, DOI: 10.1007/s10846-017-0483-z. (Cited on page 1.)

[Karvonen 2014] Toni Karvonen. Stability of linear and non-linear Kalman filters. Master's thesis, University of Helsinki, 2014. (Cited on page 33.)

[Kerma *et al.* 2012] Mokhtar Kerma, Abdellah Mokhtari, Benallegue Abdelaziz and Yuri Orlov. *Nonlinear H_∞ control of a Quadrotor (UAV), using high order sliding mode disturbance estimator*. International Journal of Control, vol. 85, no. 12, pages 1876–1885, December 2012, DOI: 10.1080/00207179.2012.709656. (Cited on page 90.)

[Khalil 2002] Hassan K. Khalil. Nonlinear Systems. Prentice Hall, 2002. (Cited on page 26.)

[Kim *et al.* 2010] Jinhyun Kim, Min-Sung Kang and Sangdeok Park. *Accurate Modeling and Robust Hovering Control for a Quad-rotor VTOL Aircraft*. Journal of Intelligent & Robotic Systems, vol. 57, no. 1, pages 9–26, 2010, DOI: 10.1007/s10846-009-9369-z. (Cited on page 10.)

[Kim *et al.* 2018] Si Jung Kim, Yunhwan Jeong, Sujin Park, Kihyun Ryu and Gyuhwan Oh. *A Survey of Drone use for Entertainment and AVR (Augmented and Virtual Reality)*. In Augmented Reality and Virtual Reality, Progress in IS, pages 339–352. Springer, Cham, 2018, DOI: /10.1007/978-3-319-64027-3_23. (Cited on page 1.)

[Kwon *et al.* 2017] H. Kwon, K. Lee and K. You. *EKF based sliding mode control for a quadrotor attitude stabilization*. In 2017 International Conference on Intelligent Informatics and Biomedical Sciences (ICIIBMS), pages 101–104, November 2017, DOI: 10.1109/ICIIBMS.2017.8279718. (Cited on page 19.)

[L'Afflitto *et al.* 2018] A. L'Afflitto, R. B. Anderson and K. Mohammadi. *An Introduction to Nonlinear Robust Control for Unmanned Quadrotor Aircraft: How to Design Control Algorithms for Quadrotors Using Sliding Mode Control and Adaptive Control Techniques [Focus on Education]*. IEEE Control Systems, vol. 38, no. 3, pages 102–121, June 2018, DOI: 10.1109/MCS.2018.2810559. (Cited on page 19.)

[Langelaan *et al.* 2011] Jack W. Langelaan, Nicholas Alley and James Neidhoefer. *Wind Field Estimation for Small Unmanned Aerial Vehicles*. Journal of Guidance, Control, and Dynamics, vol. 34, no. 4 (2011), pages 1016–1030, July 2011, DOI: 10.2514/1.52532. (Cited on page 32.)

[Lanzon *et al.* 2014] Alexander Lanzon, Alessandro Freddi and Sauro Longhi. *Flight Control of a Quadrotor Vehicle Subsequent to a Rotor Failure*. Journal of Guidance, Control, and Dynamics, vol. 37, no. 2, pages 580–591, February 2014, DOI: 10.2514/1.59869. (Cited on page 89.)

[Larrabee *et al.* 2014] T. Larrabee, H. Chao, M. Rhudy, Y. Gu and M. R. Napolitano. *Wind field estimation in UAV formation flight*. In 2014 American Control Conference, pages 5408–5413, June 2014, DOI: 10.1109/ACC.2014.6859266. (Cited on page 33.)

[Lee & Kim 2017] Hyeonbeom Lee and H. Jin Kim. *Trajectory tracking control of multirotors from modelling to experiments: A survey*. International Journal of Control, Automation and Systems, vol. 15, no. 1, pages 281–292, February 2017, DOI: 10.1007/s12555-015-0289-3. (Cited on page 1.)

[Leishman *et al.* 2002] John Gordon Leishman, Mahendra J. Bhagwat and Shreyas Ananthan. *Free-Vortex Wake Predictions of the Vortex Ring State for Single-Rotor and Multi-Rotor Configurations*. In AHS International Forum 58, June 2002. (Cited on page 79.)

[Leishman 2006] Gordon J. Leishman. Principles of Helicopter Aerodynamics with CD Extra. Cambridge University Press, April 2006. ch 2-5. (Cited on pages 10, 12 and 79.)

[Li *et al.* 2016] Shushuai Li, Yaonan Wang, Jianhao Tan and Yan Zheng. *Adaptive RBFNNs/integral sliding mode control for a quadrotor aircraft*. Neurocomputing, vol. 216, pages 126–134, December 2016, DOI: 10.1016/j.neucom.2016.07.033. (Cited on page 20.)

[Li *et al.* 2018] Cong Li, Hui Jing, Jiading Bao, Shanlin Sun and Rongrong Wang. *Robust H_∞ fault tolerant control for quadrotor attitude regulation*. Proceedings of the Institution of Mechanical Engineers, Part I: Journal of Systems and Control Engineering, June 2018, DOI: 10.1177/0959651818780763. (Cited on page 90.)

[Lie & Gebre-Egziabher 2013] F. Adhika Pradipta Lie and Demoz Gebre-Egziabher. *Synthetic Air Data System*. Journal of Aircraft, vol. 50, no. 4, pages 1234–1249, May 2013, DOI: 10.2514/1.C032177. (Cited on page 33.)

[Lyu *et al.* 2018] X. Lyu, J. Zhou, H. Gu, Z. Li, S. Shen and F. Zhang. *Disturbance Observer Based Hovering Control of Quadrotor Tail-Sitter VTOL UAVs Using H_∞ Synthesis*. IEEE Robotics and Automation Letters, vol. 3, no. 4, pages 2910–2917, October 2018, DOI: 10.1109/LRA.2018.2847405. (Cited on page 90.)

[Madani & Benallegue 2007] Tarek Madani and Abdelaziz Benallegue. *Sliding mode observer and backstepping control for a quadrotor unmanned aerial vehicles*. In American Control Conference, 2007. ACC'07, pages 5887–5892, July 2007, DOI: 10.1109/ACC.2007.4282548. (Cited on page 10.)

[Manecy *et al.* 2014] A. Manecy, N. Marchand and S. Viollet. *RT-MaG: An open-source SIMULINK toolbox for Linux-based real-time robotic applications*. In 2014 IEEE International Conference on Robotics and Biomimetics (ROBIO 2014), pages 173–180, December 2014, DOI: 10.1109/ROBIO.2014.7090326. (Cited on page 4.)

[Manecy *et al.* 2015] Augustin Manecy, Nicolas Marchand, Franck Ruffier and Stéphane Viollet. *X4-MaG: A Low-Cost Open-Source Micro-Quadrotor and its Linux-Based Controller*. International Journal of Micro Air Vehicles, vol. 7, no. 2, pages 89–109, June 2015, DOI: 10.1260/1756-8293.7.2.89. (Cited on page 5.)

[Martínez-Vásquez *et al.* 2015] A. Martínez-Vásquez, A. Rodriguez-Mata, I. González-Hernández, S. Salazar, A. Montiel-Varela and R. Lozano. *Linear observer for estimating wind gust in UAV's*. In 2015 12th International Conference on Electrical Engineering, Computing Science and Automatic Control (CCE), October 2015, DOI: 10.1109/ICEEE.2015.7357983. (Cited on page 33.)

[Mellinger & Kumar 2011] D. Mellinger and V. Kumar. *Minimum snap trajectory generation and control for quadrotors*. In 2011 IEEE International Conference on Robotics and Automation, pages 2520–2525, May 2011, DOI: 10.1109/ICRA.2011.5980409. (Cited on pages 19 and 50.)

[Mellinger *et al.* 2011] D. Mellinger, Q. Lindsey, M. Shomin and V. Kumar. *Design, modeling, estimation and control for aerial grasping and manipulation*. In 2011 IEEE/RSJ International Conference on Intelligent Robots and Systems, pages 2668–2673, September 2011, DOI: 10.1109/IROS.2011.6094871. (Cited on page 10.)

[Mellinger 2012] Daniel Warren Mellinger. *Trajectory generation and control for quadrotors*. PhD thesis, University of Pennsylvania, USA, 2012. (Cited on page 50.)

[Mercado *et al.* 2018] Diego Mercado, Pedro Castillo and Rogelio Lozano. *Sliding mode collision-free navigation for quadrotors using monocular vision*. Robotica, pages 1–17, June 2018, DOI: 10.1017/S0263574718000516. (Cited on page 19.)

[Mian & Wang 2008] Ashfaq Ahmad Mian and Dao-bo Wang. *Dynamic modeling and nonlinear control strategy for an underactuated quad rotor rotorcraft*. Journal of Zhejiang University-SCIENCE A, vol. 9, no. 4, pages 539–545, April 2008, DOI: 10.1631/jzus.A071434. (Cited on page 10.)

[Michael *et al.* 2014] Nathan Michael, Shaojie Shen, Kartik Mohta, Vijay Kumar, Keiji Nagatani, Yoshito Okada, Seiga Kiribayashi, Kazuki Otake, Kazuya Yoshida, Kazunori Ohno, Eijiro Takeuchi and Satoshi Tadokoro.

Collaborative Mapping of an Earthquake Damaged Building via Ground and Aerial Robots. In Field and Service Robotics, Springer Tracts in Advanced Robotics, pages 33–47. Springer, Berlin, Heidelberg, 2014, DOI: 10.1007/978-3-642-40686-7_3. (Cited on page 1.)

[Miller 2011] Derek Miller. *Open Loop System Identificaiton of a Micro Quadrotor Helicopter from Closed Loop Data*. PhD thesis, University of Maryland, College Park, MD, USA, 2011. (Cited on page 10.)

[Mofid & Mobayen 2018] Omid Mofid and Saleh Mobayen. *Adaptive sliding mode control for finite-time stability of quad-rotor UAVs with parametric uncertainties*. ISA Transactions, vol. 72, pages 1–14, January 2018, DOI: 10.1016/j.isatra.2017.11.010. (Cited on page 20.)

[Mokhtari & Benallegue 2004] Abdellah Mokhtari and Abdelaziz Benallegue. *Dynamic feedback controller of Euler angles and wind parameters estimation for a quadrotor unmanned aerial vehicle*. In IEEE International Conference on Robotics and Automation, 2004., volume 3, pages 2359–2366, 2004. (Cited on page 10.)

[Mondek & Hromčík 2015] M. Mondek and M. Hromčík. *On-line on-board wind estimation system for small UAVs*. In 2015 20th International Conference on Process Control (PC), pages 369–374, June 2015, DOI: 10.1109/PC.2015.7169991. (Cited on page 33.)

[Mu *et al.* 2017] B. Mu, K. Zhang and Y. Shi. *Integral Sliding Mode Flight Controller Design for a Quadrotor and the Application in a Heterogeneous Multi-Agent System*. IEEE Transactions on Industrial Electronics, vol. 64, no. 12, pages 9389–9398, December 2017, DOI: 10.1109/TIE.2017.2711575. (Cited on page 20.)

[Murray *et al.* 2014] C. W. A. Murray, M. Ireland and D. Anderson. *On the response of an autonomous quadrotor operating in a turbulent urban environment*. In AUVSIs Unmanned Systems Conference, Orlando, FL, USA, May 2014. (Cited on page 2.)

[Muñoz *et al.* 2017] Filiberto Muñoz, Iván González-Hernández, Sergio Salazar, Eduardo S. Espinoza and Rogelio Lozano. *Second order sliding mode controllers for altitude control of a quadrotor UAS: Real-time implementation in outdoor environments*. Neurocomputing, vol. 233, pages 61–71, April 2017, DOI: 10.1016/j.neucom.2016.08.111. (Cited on page 19.)

[Nedjati *et al.* 2016] Arman Nedjati, Bela Vizvari and Gokhan Izbirak. *Post-earthquake response by small UAV helicopters*. Natural Hazards, vol. 80, no. 3, pages 1669–1688, February 2016, DOI: 10.1007/s11069-015-2046-6. (Cited on page 1.)

[Neumann & Bartholmai 2015] Patrick P. Neumann and Matthias Bartholmai. *Real-time wind estimation on a micro unmanned aerial vehicle using its inertial measurement unit*. Sensors and Actuators A: Physical, vol. 235, pages 300–310, November 2015, DOI: 10.1016/j.sna.2015.09.036. (Cited on page 33.)

[Niedzielski *et al.* 2017] Tomasz Niedzielski, Carsten Skjøth, Małgorzata Werner, Waldemar Spallek, Matylda Witek, Tymoteusz Sawiński, Anetta Drzeniecka-Osiadacz, Magdalena Korzystka-Muskała, Piotr Muskała, Piotr Modzel, Jakub Guzikowski and Maciej Kryza. *Are estimates of wind characteristics based on measurements with Pitot tubes and GNSS receivers mounted on consumer-grade unmanned aerial vehicles applicable in meteorological studies?* Environmental Monitoring and Assessment, vol. 189, no. 9, page 431, August 2017, DOI: 10.1007/s10661-017-6141-x. (Cited on page 2.)

[Niel *et al.* 2013] Fabien Niel, Yann Ameho, JeanMarc Biannic, François Defaÿ and Caroline Bérard. *A Novel Parameter Varying Controller Synthesis Method for Quadrotor Control*. In AIAA Guidance, Navigation, and Control (GNC) Conference, Guidance, Navigation, and Control and Co-located Conferences. American Institute of Aeronautics and Astronautics, August 2013, DOI: 10.2514/6.2013-4534. (Cited on page 89.)

[Norouzi Ghazbi *et al.* 2016] S Norouzi Ghazbi, Y Aghli, M Alimohammadi and AA Akbari. *QUADROTORS UNMANNED AERIAL VEHICLES: A REVIEW.* International Journal on Smart Sensing & Intelligent Systems, vol. 9, no. 1, 2016. (Cited on page 1.)

[Nourmohammadi *et al.* 2018] A. Nourmohammadi, M. Jafari and T. O. Zander. *A Survey on Unmanned Aerial Vehicle Remote Control Using Brain Computer Interface*. IEEE Transactions on Human-Machine Systems, vol. 48, no. 4, pages 337–348, August 2018, DOI: 10.1109/THMS.2018.2830647. (Cited on page 1.)

[Orsag & Bogdan 2012] Matko Orsag and Stjepan Bogdan. *Influence of forward and descent flight on quadrotor dynamics*. In Recent Advances in Aircraft Technology. InTech, 2012, DOI: 10.5772/37438. (Cited on page 10.)

[Palanthandalam-Madapusi *et al.* 2008] H. J. Palanthandalam-Madapusi, A. Girard and D. S. Bernstein. *Wind-field reconstruction using flight data*. In 2008 American Control Conference, pages 1863–1868, June 2008, DOI: 10.1109/ACC.2008.4586763. (Cited on page 32.)

[Palomaki *et al.* 2017] Ross T. Palomaki, Nathan T. Rose, Michael van den Bossche, Thomas J. Sherman and Stephan F. J. De Wekker. *Wind Estimation in the Lower Atmosphere Using Multirotor Aircraft*. Journal of Atmospheric and Oceanic Technology, vol. 34, no. 5, pages 1183–1191, April 2017, DOI: 10.1175/JTECH-D-16-0177.1. (Cited on page 32.)

[Pappu *et al.* 2017] Venkatasubramani S. R. Pappu, Yande Liu, Joseph F. Horn and Jared Cooper. *Wind gust estimation on a small VTOL UAV*. In 7th AHS Technical Meeting on VTOL Unmanned Aircraft Systems and Autonomy, January 2017. (Cited on page 33.)

[Pendleton & Zhang 2017] David I. Pendleton and Wei Zhang. *Development of a New Wind Measurement Tool based on a Hovering Drone*. In 55th AIAA Aerospace Sciences Meeting, AIAA SciTech Forum. American Institute of Aeronautics and Astronautics, January 2017, DOI: 10.2514/6.2017-2006. (Cited on page 33.)

[Perruquetti *et al.* 2008] W. Perruquetti, T. Floquet and E. Moulay. *Finite-Time Observers: Application to Secure Communication*. IEEE Transactions on Automatic Control, vol. 53, no. 1, pages 356–360, February 2008, DOI: 10.1109/TAC.2007.914264. (Cited on pages 29 and 87.)

[Planckaert & Coton 2015] Laurent Planckaert and Patricia Coton. *Quadrotor UAV aerodynamic model identification using indoor flight experiment and feasibility of UAV as wind gust sensor*. In International Micro Air Vehicles Conference and Flight Competition IMAV 2015, Aachen, Germany, September 2015. (Cited on pages 12, 16, 43 and 47.)

[Polyakov & Fridman 2014] Andrey Polyakov and Leonid Fridman. *Stability notions and Lyapunov functions for sliding mode control systems*. Journal of the Franklin Institute, vol. 351, no. 4, pages 1831–1865, April 2014, DOI: 10.1016/j.jfranklin.2014.01.002. (Cited on page 19.)

[Pounds *et al.* 2004] Paul Pounds, Robert Mahony, Joel Gresham, Peter Corke and Jonathan M Roberts. *Towards dynamically-favourable quad-rotor aerial robots*. In Proceedings of the 2004 Australasian Conference on Robotics & Automation. Australian Robotics & Automation Association, 2004. (Cited on page 10.)

[Pounds *et al.* 2010] P. Pounds, R. Mahony and P. Corke. *Modelling and control of a large quadrotor robot*. Control Engineering Practice, vol. 18, no. 7, pages 691–699, July 2010, DOI: 10.1016/j.conengprac.2010.02.008. (Cited on page 10.)

[Prayitno *et al.* 2016] Agung Prayitno, Veronica Indrawati and Clark Arron. *H-infinity control for pitch-roll AR.Drone*. TELKOMNIKA Indonesian Journal of Electrical Engineering, vol. 14, pages 963–973, September 2016. (Cited on page 90.)

[Promkajin & Parnichkun 2018] Nicom Promkajin and Manukid Parnichkun. *Development of a robust attitude control for nonidentical rotor quadrotors using sliding mode control*. International Journal of Advanced Robotic Systems, vol. 15, no. 1, January 2018, DOI: 10.1177/1729881417753554. (Cited on page 19.)

[Prudden *et al.* 2018] S. Prudden, A. Fisher, M. Marino, A. Mohamed, S. Watkins and G. Wild. *Measuring wind with Small Unmanned Aircraft Systems*. Journal of Wind Engineering and Industrial Aerodynamics, vol. 176, pages 197–210, May 2018, DOI: 10.1016/j.jweia.2018.03.029. (Cited on page 32.)

[Qi *et al.* 2015] Juntong Qi, Dalei Song, Hong Shang, Nianfa Wang, Chunsheng Hua, Chong Wu, Xin Qi and Jianda Han. *Search and Rescue Rotary-Wing UAV and Its Application to the Lushan Ms 7.0 Earthquake*. Journal of Field Robotics, vol. 33, no. 3, pages 290–321, 2015, DOI: 10.1002/rob.21615. (Cited on page 1.)

[Qu *et al.* 2016a] Y. Qu, J. Duan and Y. Zhang. *An algorithm of online wind field estimation for small fixed-wing UAVs*. In 2016 35th Chinese Control Conference (CCC), pages 10645–10650, July 2016, DOI: 10.1109/ChiCC.2016.7555044. (Cited on page 33.)

[Qu *et al.* 2016b] Y. Qu, Z. Xing and Y. Zhang. *Wind estimation using the position information from a hovering quadrotor*. In 2016 IEEE Chinese Guidance, Navigation and Control Conference (CGNCC), pages 1345–1350, August 2016, DOI: 10.1109/CGNCC.2016.7828984. (Cited on page 33.)

[Qu *et al.* 2017] Y. Qu, Z. Xing, Y. Zhang and Z. Yu. *Real-time wind vector estimation for a micro UAV*. In 2017 International Conference on Unmanned Aircraft Systems (ICUAS), pages 1716–1721, June 2017, DOI: 10.1109/ICUAS.2017.7991356. (Cited on page 33.)

[Raffo *et al.* 2008a] G. V. Raffo, M. G. Ortega and F. R. Rubio. *Backstepping/nonlinear H_∞ control for path tracking of a quadrotor unmanned aerial vehicle*. In 2008 American Control Conference, pages 3356–3361, June 2008, DOI: 10.1109/ACC.2008.4587010. (Cited on page 90.)

[Raffo *et al.* 2008b] Guilherme V. Raffo, Manuel G. Ortega and Francisco R. Rubio. *MPC with Nonlinear H_∞ Control for Path Tracking of a Quad-Rotor Helicopter*. IFAC Proceedings Volumes, vol. 41, no. 2, pages 8564–8569, January 2008, DOI: 10.3182/20080706-5-KR-1001.01448. (Cited on page 90.)

[Raffo *et al.* 2010] Guilherme V. Raffo, Manuel G. Ortega and Francisco R. Rubio. *An integral predictive/nonlinear H_∞ control structure for a quadrotor helicopter*. Automatica, vol. 46, no. 1, pages 29–39, January 2010, DOI: 10.1016/j.automatica.2009.10.018. (Cited on page 90.)

[Raffo *et al.* 2011] Guilherme V. Raffo, Manuel G. Ortega and Francisco R. Rubio. *Nonlinear H_∞ Controller for the Quad-Rotor Helicopter with Input Coupling*. IFAC Proceedings Volumes, vol. 44, no. 1, pages 13834–13839, January 2011, DOI: 10.3182/20110828-6-IT-1002.02453. (Cited on page 90.)

[Ramirez-Rodriguez *et al.* 2014] Heriberto Ramirez-Rodriguez, Vicente Parra-Vega, Anand Sanchez-Orta and Octavio Garcia-Salazar. *Robust Backstepping Control Based on Integral Sliding Modes for Tracking of Quadrotors*. Journal of Intelligent & Robotic Systems, vol. 73, no. 1-4, pages 51–66, January 2014, DOI: 10.1007/s10846-013-9909-4. (Cited on page 20.)

[Raza & Etele 2016] Syed Ali Raza and Jason Etele. *Autonomous Position Control Analysis of Quadrotor Flight in Urban Wind Gust Conditions*. In AIAA Guidance, Navigation, and Control Conference, AIAA SciTech Forum. American Institute of Aeronautics and Astronautics, January 2016, DOI: 10.2514/6.2016-1385. (Cited on page 2.)

[Raza *et al.* 2017] Syed Ali Raza, M. Sutherland, J. Etele and Giovanni Fusina. *Experimental validation of quadrotor simulation tool for flight within building wakes*. Aerospace Science and Technology, vol. 67, pages 169–180, August 2017, DOI: 10.1016/j.ast.2017.03.043. (Cited on page 2.)

[Raza *et al.* 2018] Syed Ali Raza, Jason Etele and Giovanni Fusina. *Hybrid Controller for Improved Position Control of Quadrotors in Urban Wind Conditions*. Journal of Aircraft, vol. 55, no. 3, pages 1014–1023, 2018, DOI: 10.2514/1.C034573. (Cited on page 2.)

[Rhudy *et al.* 2015] M. B. Rhudy, M. L. Fravolini, Y. Gu, M. R. Napolitano, S. Gururajan and H. Chao. *Aircraft model-independent airspeed estimation without pitot tube measurements*. IEEE Transactions on Aerospace and Electronic Systems, vol. 51, no. 3, pages 1980–1995, July 2015, DOI: 10.1109/TAES.2015.130631. (Cited on page 33.)

[Rhudy *et al.* 2017] M. B. Rhudy, Y. Gu, J. N. Gross and H. Chao. *Onboard Wind Velocity Estimation Comparison for Unmanned Aircraft Systems*. IEEE Transactions on Aerospace and Electronic Systems, vol. 53, no. 1, pages 55–66, February 2017, DOI: 10.1109/TAES.2017.2649218. (Cited on page 33.)

[Rios *et al.* 2017] H. Rios, D. Efimov, J. A. Moreno, W. Perruquetti and J. G. Rueda-Escobedo. *Time-Varying Parameter Identification Algorithms: Finite and Fixed-Time Convergence*. IEEE Transactions on Automatic Control, vol. 62, no. 7, pages 3671–3678, July 2017, DOI: 10.1109/TAC.2017.2673413. (Cited on pages 36, 37 and 38.)

[Rios *et al.* 2018] H. Rios, R. Falcon, O. A. Gonzalez and A. E. Dzul. *Continuous Sliding-Modes Control Strategies for Quad-Rotor Robust Tracking: Real-Time Application*. IEEE Transactions on Industrial Electronics, 2018, DOI: 10.1109/TIE.2018.2831191. (Cited on page 20.)

[Roos *et al.* 2014] C. Roos, G. Hardier and J. M. Biannic. *Polynomial and rational approximation with the APRICOT Library of the SMAC toolbox*. In 2014 IEEE Conference on Control Applications (CCA), pages 1473–1478, Antibes, France, October 2014. (Cited on page 93.)

[Rysdyk 2006] Rolf Rysdyk. *Unmanned Aerial Vehicle Path Following for Target Observation in Wind*. Journal of Guidance, Control, and Dynamics, vol. 29, no. 5, pages 1092–1100, September 2006, DOI: 10.2514/1.19101. (Cited on page 33.)

[Ríos *et al.* 2017] Héctor Ríos, Jaime González-Sierra and Alejandro Dzul. *Robust tracking output-control for a quad-rotor: A continuous sliding-mode approach*. Journal of the Franklin Institute, vol. 354, no. 15, pages 6672–6691, October 2017, DOI: 10.1016/j.jfranklin.2017.08.024. (Cited on page 20.)

[Saeed *et al.* 2018] Adnan S. Saeed, Ahmad Bani Younes, Chenxiao Cai and Guowei Cai. *A survey of hybrid Unmanned Aerial Vehicles*. Progress in Aerospace Sciences, vol. 98, pages 91–105, April 2018, DOI: 10.1016/j.paerosci.2018.03.007. (Cited on page 1.)

[Sánchez-García *et al.* 2018] J. Sánchez-García, J. M. García-Campos, M. Arzamendia, D. G. Reina, S. L. Toral and D. Gregor. *A survey on unmanned aerial and aquatic vehicle multi-hop networks: Wireless communications, evaluation tools and applications*. Computer Communications, vol. 119, pages 43–65, April 2018, DOI: 10.1016/j.comcom.2018.02.002. (Cited on page 1.)

[Seddon & Newman 2011] John M Seddon and Simon Newman. Basic helicopter aerodynamics, volume 40. John Wiley & Sons, 2011. (Cited on page 10.)

[Shim *et al.* 2005] David Shim, Hoam Chung, Hyoun Jin Kim and Shankar Sastry. *Autonomous Exploration In Unknown Urban Environments For Unmanned Aerial Vehicles*. In AIAA Guidance, Navigation, and Control Conference and Exhibit, Guidance, Navigation, and Control and Co-located Conferences. American Institute of Aeronautics and Astronautics, August 2005, DOI: 10.2514/6.2005-6478. (Cited on page 2.)

[Shraim *et al.* 2018] H. Shraim, A. Awada and R. Youness. *A survey on quadrotors: Configurations, modeling and identification, control, collision avoidance, fault diagnosis and tolerant control*. IEEE Aerospace and Electronic Systems Magazine, vol. 33, no. 7, pages 14–33, July 2018, DOI: 10.1109/MAES.2018.160246. (Cited on pages 1 and 10.)

[Sikkel *et al.* 2016] L. N. C. Sikkel, G. C. H. E. de Croon, C. De Wagter and Q. P. Chu. *A novel online model-based wind estimation approach for quadrotor micro air vehicles using low cost MEMS IMUs*. In 2016 IEEE/RSJ International Conference on Intelligent Robots and Systems (IROS), pages 2141–2146, October 2016, DOI: 10.1109/IROS.2016.7759336. (Cited on page 33.)

[Song *et al.* 2015] Yinglin Song, Bin Xian, Yao Zhang, Xinran Jiang and Xu Zhang. *Towards autonomous control of quadrotor unmanned aerial vehicles in a GPS-denied urban area via laser ranger finder*. Optik - International Journal for Light and Electron Optics, vol. 126, no. 23, pages 3877–3882, December 2015, DOI: 10.1016/j.ijleo.2015.07.058. (Cited on page 2.)

[Song *et al.* 2016] Y. Song, Q. H. Meng, B. Luo, M. Zeng, S. G. Ma and P. F. Qi. *A wind estimation method for quadrotors using inertial measurement units*. In 2016 IEEE International Conference on Robotics and Biomimetics (ROBIO), pages 426–431, December 2016, DOI: 10.1109/ROBIO.2016.7866359. (Cited on page 33.)

[Stotsky & Kolmanovsky 2001] A. Stotsky and I. Kolmanovsky. *Simple unknown input estimation techniques for automotive applications*. In American Control Conference, volume 5, pages 3312–3317, 2001, DOI: 10.1109/ACC.2001.946139. (Cited on page 36.)

[Sumantri *et al.* 2016] Bambang Sumantri, Naoki Uchiyama and Shigenori Sano. *Least square based sliding mode control for a quad-rotor helicopter and energy saving by chattering reduction*. Mechanical Systems and

Signal Processing, vol. 66–67, pages 769–784, January 2016, DOI: 10.1016/j.ymssp.2015.05.013. (Cited on page 20.)

[Sun *et al.* 2018] K. c Sun, Q. h Zeng, J. y Liu, Y. j Zhou and Y. t Dai. *Real-time estimation of atmospheric disturbance for unmanned helicopter based on multi-source navigation data*. In 2018 IEEE/ION Position, Location and Navigation Symposium (PLANS), pages 1191–1196, April 2018, DOI: 10.1109/PLANS.2018.8373504. (Cited on page 33.)

[Taamallah 2010] Skander Taamallah. *A Qualitative Introduction to the Vortex-Ring-State, Autorotation, and Optimal Autorotation*. In 36th European Rotorcraft Forum, Paris, France, September 2010. (Cited on page 79.)

[Tomić & Haddadin 2014] T. Tomić and S. Haddadin. *A unified framework for external wrench estimation, interaction control and collision reflexes for flying robots*. In 2014 IEEE/RSJ International Conference on Intelligent Robots and Systems, pages 4197–4204, September 2014, DOI: 10.1109/IROS.2014.6943154. (Cited on page 33.)

[Tomić *et al.* 2016] T. Tomić, K. Schmid, P. Lutz, A. Mathers and S. Haddadin. *The flying anemometer: Unified estimation of wind velocity from aerodynamic power and wrenches*. In 2016 IEEE/RSJ International Conference on Intelligent Robots and Systems (IROS), pages 1637–1644, October 2016, DOI: 10.1109/IROS.2016.7759264. (Cited on page 33.)

[Ware & Roy 2016] J. Ware and N. Roy. *An analysis of wind field estimation and exploitation for quadrotor flight in the urban canopy layer*. In 2016 IEEE International Conference on Robotics and Automation (ICRA), pages 1507–1514, May 2016, DOI: 10.1109/ICRA.2016.7487287. (Cited on page 2.)

[Ware 2016] John (John Welling) Ware. An analysis of quadrotor flight in the urban canopy layer. Master's thesis, Massachusetts Institute of Technology, 2016. (Cited on page 2.)

[Waslander & Wang 2009] Steven Waslander and Carlos Wang. *Wind Disturbance Estimation and Rejection for Quadrotor Position Control*. In AIAA Infotech@Aerospace Conference, (AIAA 2009-1983). American Institute of Aeronautics and Astronautics, April 2009, DOI: 10.2514/6.2009-1983. (Cited on page 33.)

[Wenz & Johansen 2017] A. Wenz and T. A. Johansen. *Estimation of wind velocities and aerodynamic coefficients for UAVs using standard autopilot sensors and a Moving Horizon Estimator*. In 2017 International Conference on Unmanned Aircraft Systems (ICUAS), pages 1267–1276, June 2017, DOI: 10.1109/ICUAS.2017.7991443. (Cited on page 33.)

[Witte *et al.* 2016] Brandon M. Witte, Cornelia Schlagenhauf, Jon Mullen, Jacob P. Helvey, Michael A. Thamann and Sean Bailey. *Fundamental Turbulence Measurement with Unmanned Aerial Vehicles (Invited)*. In 8th AIAA Atmospheric and Space Environments Conference, AIAA AVIATION Forum. American Institute of Aeronautics and Astronautics, June 2016, DOI: 10.2514/6.2016-3584. (Cited on page 33.)

[Xiang *et al.* 2016] X. Xiang, Z. Wang, Z. Mo, G. Chen, K. Pham and E. Blasch. *Wind field estimation through autonomous quadcopter avionics*. In 2016 IEEE/AIAA 35th Digital Avionics Systems Conference (DASC), September 2016, DOI: 10.1109/DASC.2016.7778071. (Cited on page 33.)

[Xing *et al.* 2017] Z. Xing, Y. Qu and Y. Zhang. *Shear wind estimation with quadrotor UAVs using Kalman filtering regressing method*. In 2017 International Conference on Advanced Mechatronic Systems (ICAMechS), pages 196–201, December 2017, DOI: 10.1109/ICAMechS.2017.8316534. (Cited on page 33.)

[Xiong & Zhang 2017] Jing-Jing Xiong and Guo-Bao Zhang. *Global fast dynamic terminal sliding mode control for a quadrotor UAV*. ISA Transactions, vol. 66, pages 233–240, January 2017, DOI: 10.1016/j.isatra.2016.09.019. (Cited on page 20.)

[Xiong & Zheng 2014] Jing-Jing Xiong and En-Hui Zheng. *Position and attitude tracking control for a quadrotor UAV*. ISA Transactions, vol. 53, no. 3, pages 725–731, May 2014, DOI: 10.1016/j.isatra.2014.01.004. (Cited on page 20.)

[Xu & Ozguner 2006] R. Xu and U. Ozguner. *Sliding Mode Control of a Quadrotor Helicopter*. In Proceedings of the 45th IEEE Conference on Decision and Control, pages 4957–4962, December 2006, DOI: 10.1109/CDC.2006.377588. (Cited on page 19.)

[Xu & Özgüner 2008] Rong Xu and Ümit Özgüner. *Sliding mode control of a class of underactuated systems*. Automatica, vol. 44, no. 1, pages 233–241, January 2008, DOI: 10.1016/j.automatica.2007.05.014. (Cited on page 19.)

[Xu *et al.* 2017] Jing Xu, Cheng-Chew Lim and Peng Shi. *Sliding mode control of singularly perturbed systems and its application in quad-rotors*. International Journal of Control, October 2017, DOI: 10.1080/00207179.2017.1393102. (Cited on page 19.)

[Yüksel *et al.* 2014] B. Yüksel, C. Secchi, H. H. Bülthoff and A. Franchi. *A nonlinear force observer for quadrotors and application to physical interactive tasks*. In 2014 IEEE/ASME International Conference on Advanced Intelligent Mechatronics, pages 433–440, July 2014, DOI: 10.1109/AIM.2014.6878116. (Cited on page 33.)

[Zhang *et al.* 2014] Xiaodong Zhang, Xiaoli Li, Kang Wang and Yanjun Lu. *A Survey of Modelling and Identification of Quadrotor Robot*. Abstract and Applied Analysis, Article ID 320526, 16 pages, 2014, DOI: 10.1155/2014/320526. (Cited on page 10.)

[Zheng *et al.* 2014] En-Hui Zheng, Jing-Jing Xiong and Ji-Liang Luo. *Second order sliding mode control for a quadrotor UAV*. ISA Transactions, vol. 53, no. 4, pages 1350–1356, July 2014, DOI: 10.1016/j.isatra.2014.03.010. (Cited on page 20.)

Safe exploration of an aerodynamic field by a mini drone

Abstract: This thesis is part of the project "Small drones in the wind" carried by the ONERA center of Lille. This project aims to use the drone as a "wind sensor" to manage a UAV quadrotor in disturbed wind conditions using wind field prediction. In this context, the goal of the thesis is to make the quadrotor a wind sensor to provide local information to update the navigation system. With real-time on-board wind estimation, the quadrotor can compute a trajectory planning avoiding dangerous areas and the corresponding trajectory control, based on an existing cartography and information on the aerodynamic behavior of airflow close to obstacles. Thus, the results of this thesis, whose main objectives are to estimate *instant* wind and position control, will be merged with another study dealing with trajectory planning. An important problem is that pressure sensors, such as the aeroclinometer and the Pitot tube, are not usable in rotary-wing vehicles because rotors air inflow interferes with the atmospheric flow and lightweight LIDAR sensors generally are not available. Another approach to estimate the wind is to implement an estimation software (or an intelligent sensor). In this thesis, three estimators are developed using the sliding mode approach, based on an adequate drone model, available measurements on the quadrotor and inertial tracking position systems. We are then interested in the control of the trajectory also by sliding mode considering the nonlinear model of the quadrotor. In addition, we are still studying quite an early alternative solution based on the H_∞ control, considering the linearized model for different equilibrium points as a function of the wind speed. The control and estimation algorithms are strictly based on the detailed model of the quadrotor, which highlights the influence of the wind.

Keywords: Quadrotor, modeling, sliding mode control, wind estimation.

Exploration sécurisée d'un champ aérodynamique par un mini drone

Résumé Général: Cette thèse s'inscrit dans le cadre du projet "Petits drones dans le vent" porté par le centre ONERA de Lille. Ce projet vise à utiliser le drone comme "capteur du vent" pour gérer un quadcopter UAV dans des conditions aérologiques perturbées en utilisant une prédiction du champ de vent. Dans ce contexte, le but de la thèse est de faire du quadcopter un capteur de vent pour fournir des informations locales afin de mettre à jour le système de navigation. Grâce à l'estimation du vent à bord en temps réel, le quadcopter peut calculer une planification de trajectoire évitant les zones dangereuses et le contrôle de trajectoire correspondant basé sur une cartographie existante et doté des informations relatives au concernant le comportement aérodynamique de l'écoulement d'air à proximité des obstacles. Ainsi, les résultats de cette thèse, dont les objectifs principaux portent sur l'estimation du vent *instantanée* et le contrôle de position, seront fusionnés avec une autre étude traitant de la planification de trajectoire. Un problème important est que les capteurs de pression, tels que l'aéroclinomètre et le tube de Pitot, ne sont pas facilement utilisables à bord des véhicules à voilure tournante car l'entrée des rotors interfère avec le flux atmosphérique et les capteurs LIDAR légers généralement ne sont pas disponibles. Une autre approche pour estimer le vent consiste à mettre en œuvre un logiciel d'estimation (ou un capteur intelligent). Dans cette thèse, trois estimateurs de ce type sont développés en utilisant l'approche du mode glissant, basée sur un modèle de drone adéquat et des mesures disponibles sur le quadcopter et sur des systèmes de position de suivi inertiel. Nous nous intéressons ensuite au contrôle de la trajectoire également par mode glissant en considérant le modèle non linéaire du quadcopter. Nous étudions par ailleurs de façon encore assez préliminaire une solution alternative fondée sur la commande H_∞, en considérant le modèle linéarisé pour différents points d'équilibre en fonction de la vitesse du vent. Les algorithmes de contrôle et d'estimation sont strictement basés sur le modèle détaillé du quadcopter, qui met en évidence l'influence du vent.

Mots clés: Quadcopter, modélisation, contrôle par mode glissant, estimation du vent.